

**Nitric Oxide Reactions of Bio-Inspired Zinc and Cobalt Complexes**

by

Julia Kozhukh

B.S., Chemistry  
University of California, Berkeley, 2007

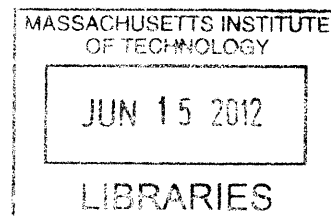
Submitted to the Department of Chemistry in Partial Fulfillment of the  
Requirements for the Degree of

DOCTOR OF PHILOSOPHY IN INORGANIC CHEMISTRY

at the  
Massachusetts Institute of Technology

June 2012

© Massachusetts Institute of Technology, 2012  
All Rights Reserved



**ARCHIVES**

Signature of Author: \_\_\_\_\_

Department of Chemistry  
May 4, 2012

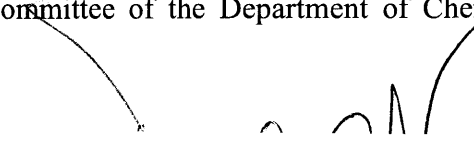
Certified by: \_\_\_\_\_

Stephen J. Lippard  
Arthur Amos Noyes Professor of Chemistry  
Thesis Supervisor

Accepted by: \_\_\_\_\_

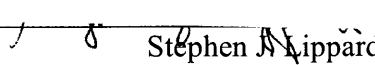
Robert W. Field  
Chairman, Departmental Committee on Graduate Students

This doctoral thesis has been examined by a committee of the Department of Chemistry as follows:




---

Daniel G. Nocera  
Henry Dreyfus Professor of Energy and Professor of Chemistry  
Committee Chairperson



---

Stephen A. Nippard  
Arthur Amos Noyes Professor of Chemistry  
Thesis Supervisor



---

Christopher C. Cummins  
Professor of Chemistry

# Nitric Oxide Reactions of Bio-Inspired Zinc and Cobalt Complexes

by

Julia Kozhukh

Submitted to the Department of Chemistry in Partial Fulfillment of the Requirements for the Degree of Doctor of Philosophy in Inorganic Chemistry

## Abstract

### Chapter 1. Bioinorganic Chemistry of Nitric Oxide and of Some of Its Targets

The redox-active nature of nitric oxide (NO) regulates the chemistry and roles of NO in biology. The interactions of NO with nitric oxide synthases, metallothioneins, and cobalamin-containing enzymes are discussed. Bioinspired small molecule models for metalloprotein active sites are introduced, and the ability of ligands to control the steric and electronic properties of coordinated metal centers is demonstrated. The bioinorganic chemistry of NO and its targets is described in the context of the investigations presented in this thesis.

### Chapter 2. Zinc Thiolate Reactivity toward Nitrogen Oxides: Insights into the Interaction of $Zn^{2+}$ with *S*-Nitrosothiols and Implications for Nitric Oxide Synthase

Zinc thiolate complexes containing  $N_2S$  tridentate ligands were prepared to investigate their reactivity toward reactive nitrogen species. This type of chemistry is proposed to occur at the zinc tetracysteine thiolate site of nitric oxide synthase (NOS). The complexes are unreactive toward nitric oxide in the absence of dioxygen, strongly indicating that NO cannot be the species directly responsible for *S*-nitrosothiol formation and loss of  $Zn^{2+}$  at the NOS dimer interface in vivo. *S*-Nitrosothiol formation does occur upon exposure of zinc thiolate solutions to NO in the

presence of air, however, or to NO<sub>2</sub> or NOBF<sub>4</sub>, indicating that these reactive nitrogen/oxygen species are capable of generating the *S*-nitrosothiol. Interaction between simple Zn<sup>2+</sup> salts and pre-formed *S*-nitrosothiols leads to decomposition of the –SNO moiety, resulting in release of gaseous NO and N<sub>2</sub>O. The potential biological relevance of this chemistry is discussed.

### **Chapter 3. Reactions of Organozinc Thiolates with Nitrosonium Ion: C-Nitroso Formation by Intramolecular Transnitrosation**

The organometallic species [ZnPAThEt] and [ZnPAThMes] are prepared, and their reactions with NOBF<sub>4</sub> are characterized. The formation of *C*-nitrosoethane and *C*-nitrosomesitylene is confirmed, and structural characterization of *C*-nitrosomesitylene conclusively establishes the dimeric nature of the molecule in the solid state. An intramolecular transnitrosation reaction pathway for *C*-nitroso formation is proposed based on theoretical calculations.

### **Chapter 4. Influence of Ligand Constraints on the Reactivity of Co(II) Complexes of Tetraazamacrocyclic Tropocoronand Ligands with Nitric Oxide**

Previous work on the reactivity of cobalt(II) complexes of tetraazamacrocyclic tropocoronand ligands with nitric oxide (NO) was extended to include the [Co(TC-5,5)] and [Co(TC-6,6)] derivatives. The cobalt mononitrosyl [Co(NO)(TC-5,5)] is isolated and structurally characterized from the reaction of [Co(TC-5,5)] and NO (g). In contrast, a {Co(NO)<sub>2</sub>}<sup>10</sup> species is observed when [Co(TC-6,6)] is exposed to NO (g) and the nitrite complex [Co(NO<sub>2</sub>)(TC-6,6)] is structurally and spectroscopically characterized from reaction mixtures. The di(cobalt dinitrosyl) [Co<sub>2</sub>(NO)<sub>4</sub>(TC-6,6)] is independently synthesized for spectroscopic comparison with reaction



mixtures. This Chapter describes the first characterization of the dependence of cobalt(II) tropocoronand reactivity on linker chain length.

## **Chapter 5. Reactivity of Tropocoronand-Bound Cobalt(III) Nitrite with Nitric Oxide as a Function of Polymethylene Linker Chain Length**

The studies on the dependence of cobalt(II) tropocoronand reactivity with nitric oxide (NO) on linker chain length, described in Chapter 4, were expanded to include the chemistry of the cobalt(III) nitrites  $[\text{Co}(\text{NO}_2)(\text{TC-}n,n)]$  ( $n = 4 - 6$ ) with NO. Complete conversion from the cobalt(III) nitrite to the cobalt mononitrosyl  $[\text{Co}(\text{NO})(\text{TC-}4,4)]$  is demonstrated upon exposure to NO (g). In contrast, exposure of  $[\text{Co}(\text{NO}_2)(\text{TC-}5,5)]$  and  $[\text{Co}(\text{NO}_2)(\text{TC-}6,6)]$  to NO (g) results in conversion to a cobalt dinitrosyl adduct. This Chapter aims to broaden the field of cobalt(III) chemistry with NO.

## **Chapter 6. Nitric Oxide Reactivity of Cobalt(III) Triflate and Cobalt(III) Thiolate Tropocoronand Complexes**

The reactivity of two cobalt(III) tropocoronands with NO (g) is described.  $[\text{Co}(\text{TC-}4,4)](\text{OTf})$  undergoes reductive nitrosylation in the presence of NO (g), forming  $[\text{Co}(\text{NO})(\text{TC-}4,4)]$ ,  $\text{N}_2\text{O}$ , and additional reactive species. The reaction releases one equivalent of protons for every equivalent of  $[\text{Co}(\text{TC-}4,4)](\text{OTf})$  consumed.  $[\text{Co}(\text{SC}_6\text{F}_5)(\text{TC-}4,4)]$  forms  $[\text{Co}(\text{NO})(\text{TC-}4,4)]$  and the disulfide  $\text{F}_5\text{C}_6\text{SSC}_6\text{F}_5$  in the presence of NO (g). We hypothesize that disulfide formation is followed by electrophilic aromatic substitution of  $\text{F}_5\text{C}_6\text{S}^+$  onto the tropocoronand aromatic ring. Efforts to prepare substituted tropocoronand ligands and test the electrophilic aromatic substitution hypothesis are described.

## **Chapter 7. Synthesis and Characterization of Mononuclear, Pseudotetrahedral Cobalt(III) Compounds**

The synthesis and characterization of two mononuclear cobalt(III) tropocoronand complexes, [Co(TC-5,5)](BF<sub>4</sub>) and [Co(TC-6,6)](BPh<sub>4</sub>), are reported. The cobalt(III) centers exist in rare pseudotetrahedral conformations, with twist angles of 65° and 74° for the [Co(TC-5,5)]<sup>+</sup> and [Co(TC-6,6)]<sup>+</sup> species, respectively. Structural and electrochemical characteristics are compared with those of newly synthesized [Ga(TC-5,5)](GaCl<sub>4</sub>) and [Ga(TC-6,6)](GaCl<sub>4</sub>) analogs.

Thesis Supervisor: Stephen J. Lippard

Title: Arthur Amos Noyes Professor of Chemistry

*To my family and Joel, for so very much love and support, and especially to Momma, for teaching me that “жизнь полосатая.”*

## Acknowledgements

I am immensely grateful to a number of people for their support and encouragement throughout the last five years, for celebrating the small victories and making the rough parts fewer and farther in between.

Thank you first to Professor Steve Lippard, for instilling in me a more structured way of thinking about science. It surprises me still how much quicker setbacks resolve themselves from this more methodical perspective. I am also grateful to have learned that there is a thin line between stubbornness and perseverance, and that sometimes it is better to let a project go. Many thanks to Steve for bearing with me while I toed that line, and for giving me the independence to explore its boundaries.

Thank you to Professor Dan Nocera for the motivating thesis chair meetings, and for the enthusiasm in discussing science. I am grateful for the insightful feedback and the big picture perspective. Thank you both to Dan and Professor Kit Cummins for thoughtful and much-appreciated comments on this thesis.

Much gratitude goes out to former members of the Lippard lab. Loi Do, Andy Tennyson, and Zach Tonzetich helped me find my way around the lab my first year, and Zach was always helpful with his extensive knowledge of the metal nitrosyl literature. Thanks to Brian Wong for a friendly ear and to Simone Friedle for teaching me to use the glovebox and grow crystals. Lindsey McQuade gave helpful advice about oral exams, and former postdocs Nora Graf, Monika Kaczmarek and Nakédia Carvalho were always supportive and ready with friendly smiles. Thank you to Juliana Fedoce Lopes for being a wonderful friend and for teaching me computational chemistry, and to Yang Li for taking care of the glovebox. I am especially fortunate to have overlapped with Mike Pluth and Daniela Buccella, two of the most helpful, thorough, thoughtful, and creative postdocs I have met in the Lippard lab. I am overwhelmingly grateful to both of them – to Mike for his willingness to discuss difficult chemistry, his realism, and his calm, and to Daniela for help with crystallography and her honesty and directness. Many thanks to both Mike and Daniela for their ability to shine a rational light on nearly any situation.

The current graduate student members of the Lippard lab have been incredible sources of helpfulness, friendship, and general hilarity. Semi Park has been a great classmate and a source of both historical and cultural perspective. Justin Wilson's depth and breadth of knowledge of chemistry has been an incredible resource for the whole group. I'm grateful for his willingness to lend a hand and his chemical insights, which were always thoughtful and frequently delivered with a dry sense of humor. Justin's stealth at the Museum of Science will remain memorable for years to come. Eric Victor has been a supportive subgroup-mate and is always ready with a joke, or a trip for coffee, or a "quick question." Thank you for bringing the cookie maker to school. I hope Tim Johnstone's genial and unassuming personality has rubbed off just a little bit, as the Lippard lab is unquestionably a better place for it. Thank you to Meiyi Li for the friendly chats in the tea room and to Mik Minier for taking over the group safety officer job and inspiring trips to Chinatown for phở. Thank you most of all to Ali Liang for being an incredibly supportive friend and labmate. I'm grateful for lunches, coffees, dinners, and chats in the lab, and all the laughter that went with them. There's always money in the banana stand!

I would like to thank current postdocs Ulf Apfel and Amit Majumdar for valuable discussions about chemistry and relentless banter in the synthetic bay, and in the offices, and at the CBC. Thanks to Shawn Lu for being the model of patience, to Max Royzen for a ready helping hand and a dose of the Russian way, and to Robert Radford for being the sensing bay DJ. Also thanks to Zhen Huang and Wei Lin for being friendly bay-mates. Thank you to Patricia Marques for steady encouragement, and to Ying Song, Ga Young Park, and Yaorong Zhen for helping making the lab an amicable place. Also thanks to Lippard lab UROPs Tara Mokhtari, Angela Ma, Maria Chan, and Suan Tuang being so very enthusiastic and outgoing.

Yogi Surendranath and Dan Graham provided a lot of help with the EI-MS studies, Danny Lutterman was always willing to discuss computational chemistry, and Danna Freedman advised about magnetism and the SQUID instruments in the CMSE.

Many thanks to Rich Girardi and Allison Kelsey for help with all kinds of forms, for organizing and coordinating meetings, and for keeping things and people running smoothly. Thank you to Bob Kennedy, Anne Rachupka, Jeff Simpson and Deb Bass in the DCIF for NMR and EPR help, and to Peter Müller for teaching me crystallography and patiently helping me work through some difficult structures.

I am incredibly thankful to my undergraduate mentors Kris Saha and Eric Werner in the Schaffer and Raymond groups at Cal, who taught me to love research and inspired me to go to graduate school. Thanks to Professors Dave Schaffer and Ken Raymond for taking in an excited undergrad, and countless thanks to former Raymond group members Géza Szigethy, Christoph Jocher, Evan Moore, Michael Seitz, Mike Pluth, and Ingrid Castro for being my Berkeley family.

Charlene Tsay, José Lobe, Nicole Davis, Jan Schnorr, and Ayumi Takaoka have been wonderful friends and classmates, and I've loved our adventures around the Boston area. Thank you also to Priam Pillai for being a great rock climbing pal. I miss the Sunday trips to Metrorock and Chipotle. Kelly Thaker, Jon Hsieh, and Jessie Black have been incredible friends from across the country and the world, and I'm thankful for their unconditional patience, understanding, and love. Also thanks to Nikolai Schweingruber for spontaneous adventures in Boston and in California.

My family has been a ceaseless source of love, support, and encouragement. I am especially indebted to my parents, Michael Kozhukh and Raisa Pavlyuchkova, for instilling in me the importance of hard work, and for teaching by example. My mother also taught me strength and perseverance, and has been the steady voice of reason without which graduate school would have been much less surmountable. I could not wish for a better advocate.

Lastly, I would like to thank Joel Rosenthal for his unconditional love and belief in me, for being an encouraging labmate and caring friend, and for reminding me of the big picture when I would forget. I love you.

## Table of Contents

Abstract	3
Dedication	7
Acknowledgements	8
Tables of Contents	10
List of Figures	15
List of Charts	19
List of Schemes	19
List of Tables	20
List of Equations	22
<b>Chapter 1. Bioinorganic Chemistry of Nitric Oxide and Some of Its Targets</b>	<b>23</b>
1.1. Introduction	24
1.2. Nitric Oxide Synthase and Metallothioneins	25
1.3. Small Molecule Models Containing Thiolate Ligands	27
1.4. Redox Active Metal Centers and RNOS	29
1.5. Cobalamins and Nitric Oxide	30
1.6. The Entatic State	31
1.7. Tropocoronands	32
1.8. Reactions of Cobalt Tropocoronands with Nitric Oxide	35
1.9. Entatic States of Cobalt(III)	36
1.10. References	39
<b>Chapter 2. Zinc Thiolate Reactivity toward Nitrogen Oxides: Insights into the Interaction of Zn<sup>2+</sup> with <i>S</i>-Nitrosothiols and Implications for Nitric Oxide Synthase</b>	<b>46</b>
2.1. Introduction	47
2.2. Experimental Methods	48
Synthesis Materials and Methods	48
Spectroscopic and Spectrometric Studies	53
2.3. Results and Discussion	58

Preparation of Compounds	58
Exposure of Zinc PATH and APATH Complexes to Nitric Oxide under Various Conditions	60
Reactions of Zinc PATH and APATH Complexes with NOBF <sub>4</sub>	62
Reactions of S-Nitrosothiols with Zinc(II) Salts	65
Reactions of Zinc PATH and APATH Complexes with NO <sub>2</sub>	73
Potential Biological Relevance	74
2.4. Summary and Conclusions	74
2.5. References	75
<b>Chapter 3. Reactions of Organozinc Thiolates with Nitrosonium Ion: C-Nitroso Formation by Intramolecular Transnitrosation</b>	<b>78</b>
3.1. Introduction	79
3.2. Experimental Methods	80
Synthesis Materials and Methods	80
Spectroscopic and Spectrometric Studies	83
Theoretical Calculations	85
3.3. Results	85
Preparation of Compounds	85
Reactions of [ZnPATHet] and [ZnPATHmes] with NOBF <sub>4</sub>	88
Computational Geometry Optimization and Orbital Analysis of [ZnPATHet]	93
Intrinsic Reaction Coordinate Calculations of [ZnPATHet] and NO <sup>+</sup>	95
3.4. Discussion	97
Reactions of [ZnPATHet] with NOBF <sub>4</sub>	97
Reactions of [ZnPATHmes] with NOBF <sub>4</sub>	98
Historical Perspective on the Structural Characterization of [MesNO] <sub>2</sub>	99
Proposed Pathway for the Reaction of [ZnPATHmes] with NOBF <sub>4</sub>	99
Proposed C-Nitroso Formation by Intramolecular Transnitrosation	101
3.5. Summary and Conclusions	102
3.6. Tables of XYZ Matrices of Computationally Determined Species	102
3.7. References	107

<b>Chapter 4. Influence of Ligand Constraints on the Reactivity of Co(II)</b>	
<b>Complexes of Tetraazamacrocyclic Tropocoronand Ligands with Nitric Oxide</b>	<b>112</b>
4.1. Introduction	113
4.2. Experimental Methods	114
Synthesis Materials and Methods	114
Spectroscopic and Spectrometric Studies	116
4.3. Results and Discussion	118
Reactions of [Co(TC-5,5)] with NO (g)	118
Reactions of [Co(TC-6,6)] with NO (g)	122
Preparation and Characterization of [Co <sub>2</sub> (NO) <sub>4</sub> (TC-6,6)]	125
4.4. Summary and Conclusions	129
4.5. References	130
<b>Chapter 5. Reactivity of Tropocoronand-Bound Cobalt(III) Nitrite with Nitric Oxide as a Function of Polymethylene Linker Chain Length</b>	<b>132</b>
5.1. Introduction	133
5.2. Experimental Methods	134
Synthesis Materials and Methods	134
Spectroscopic Studies with NO (g)	136
5.3. Results	137
Preparation of [Co(NO <sub>2</sub> )(TC-4,4)], [Co(NO <sub>2</sub> )(TC-5,5)], and [Co(NO <sub>2</sub> )(TC-6,6)]	137
Reactions of [Co(NO <sub>2</sub> )(TC-4,4)] with NO (g)	140
Reactions of [Co(NO <sub>2</sub> )(TC-5,5)] with NO (g)	142
Reactions of [Co(NO <sub>2</sub> )(TC-6,6)] with NO (g)	143
5.4. Discussion	145
Steric Properties of [Co(NO <sub>2</sub> )(TC-4,4)], [Co(NO <sub>2</sub> )(TC-5,5)], and [Co(NO <sub>2</sub> )(TC-6,6)]	145
Cobalt Nitrosyl Formation from Exogenous NO	147
Redox Nature of Cobalt Nitrosyl Formation	147
5.5. Conclusions	148



5.6. References	148
-----------------	-----

**Chapter 6. Nitric Oxide Reactivity of Cobalt(III) Triflate and Cobalt(III) Thiolate Tropocoronand Complexes** **150**

6.1. Introduction	151
6.2. Experimental Methods	151
Synthesis Materials and Methods	151
Spectroscopic and Spectrometric Studies	154
Computational Methods	158
6.3. Results and Discussion	158
Preparation of [Co(TC-4,4)](OTf)	158
Reactions of [Co(TC-4,4)](OTf) with NO (g)	160
Reactions of [Co(TC-4,4)](OTf) with NO (g) and Proton Sponge	162
Reactions of [Co(TC-4,4)](OTf) with NO (g) and Cs <sub>2</sub> CO <sub>3</sub>	164
Titration of Nitric Oxide into Solutions of [Co(TC-4,4)](OTf) and Proton Sponge	166
Molecular Orbital Analysis of [Co(NO)(TC-4,4)]	167
Reactions of [Co(SC <sub>6</sub> F <sub>5</sub> )(TC-4,4)] with NO (g)	167
Proposed Pathway for the Reaction of [Co(SC <sub>6</sub> F <sub>5</sub> )(TC-4,4)] with NO (g)	172
Aromatic Substitution Reactions of Tropocoronands and Tropolones	173
6.4. Summary and Conclusions	178
6.5. References	179

**Chapter 7. Synthesis and Characterization of Mononuclear, Pseudotetrahedral Cobalt(III) Compounds** **181**

7.1. Introduction	182
7.2. Experimental Methods	183
Synthesis Materials and Methods	183
7.3. Results	186
Preparation of [Co(TC-5,5)](BF <sub>4</sub> )	186
Preparation of [Co(TC-6,6)](BPh <sub>4</sub> )	188

Preparation of [Ga(TC-5,5)](GaCl <sub>4</sub> ) and [Ga(TC-6,6)](GaCl <sub>4</sub> )	189
Spectroscopic Characterization of [Co(TC-5,5)](BF <sub>4</sub> ) and [Co(TC-6,6)](BPh <sub>4</sub> )	190
7.4. Discussion	191
Comparison of Structural Properties for [Co(TC-5,5)](BF <sub>4</sub> ) and [Ga(TC-5,5)](GaCl <sub>4</sub> )	191
Comparison of Structural Properties for [Co(TC-6,6)](BPh <sub>4</sub> ) and [Ga(TC-6,6)](GaCl <sub>4</sub> )	192
Electrochemical Studies	193
Optical Spectroscopy	195
7.5. Summary and Conclusions	196
7.6. References	196
Biographical Note	198
Curriculum Vitae	199

## List of Figures

### Chapter 1

Figure 1.1.	Crystal structure of the oxygenase domain of nitric oxide synthase	26
Figure 1.2.	The cobalamin architecture	30
Figure 1.3.	Definition of twist angle for tropocoronand metal complexes	34
Figure 1.4.	Correlation of tropocoronand linker chain length with twist angle for cobalt(II), nickel(II) and copper(II) complexes	35
Figure 1.5.	Orbital correlation diagram for the transition from square-planar to tetrahedral geometry	38

### Chapter 2

Figure 2.1.	Infrared spectral comparison of Zn(OTf) <sub>2</sub> , PThH, PThNO, PThNO + Zn(OTf) <sub>2</sub> , APThH and APThNO	59
Figure 2.2.	UV-Vis reactivity profile for [ZnPThCl] + NO, and [ZnPThCl] + NO + air	61
Figure 2.3.	UV-Vis reactivity profile for [ZnPThOTf] + NO, and [ZnPThOTf] + NO + air	61
Figure 2.4.	UV-Vis reactivity profile for [ZnAPThCl] + NO, and [ZnAPThCl] + NO + air	62
Figure 2.5.	UV-Vis reactivity profiles for [ZnPThCl], [ZnPThOTf], and [ZnAPThCl] with NOBF <sub>4</sub>	63
Figure 2.6.	ESI-MS spectrum of [ZnAPThCl] + 0.9 equiv NOBF <sub>4</sub> + PPh <sub>2</sub> R	64
Figure 2.7.	UV-Vis reactivity profile for PThNO + Zn(OTf) <sub>2</sub> and APThNO + Zn(OTf) <sub>2</sub>	65
Figure 2.8.	Solution IR spectral timecourse for APThNO + ZnCl <sub>2</sub> and APThNO + Zn(OTf) <sub>2</sub>	66
Figure 2.9.	Infrared spectral comparison of APThNO + ZnX <sub>2</sub> vs. APTh <sup>15</sup> NO + ZnX <sub>2</sub> (X = Cl, OTf)	67
Figure 2.10.	Comparison of <sup>1</sup> H NMR spectra for [ZnPThOTf]/NOBF <sub>4</sub> vs. PThNO/Zn(OTf) <sub>2</sub> reactions	68

Figure 2.11.	$^1\text{H}$ NMR spectral comparison of $\text{PAtH}_2$ solutions containing variable amounts of $\text{Zn}(\text{OTf})_2$	70
Figure 2.12.	$^1\text{H}$ NMR comparison of a $\text{PAtH}_2/\text{Zn}(\text{OTf})_2$ solution with reaction spectra of $[\text{ZnPAtH}\text{OTf}]$ with $\text{NOBF}_4$ and $\text{PAtHNO}$ with $\text{Zn}(\text{OTf})_2$	71
Figure 2.13.	EI-MS analysis of the reaction headspaces for $[\text{ZnAPAtHCl}]/\text{NOBF}_4$ , $\text{APAtHNO}/\text{ZnCl}_2$ , $\text{APAtHNO}/\text{Zn}(\text{OTf})_2$ , and $\text{APAtHNO}$	72
Figure 2.14.	UV-Vis reactivity profiles for $[\text{ZnPAtHCl}]$ , $[\text{ZnPAtH}\text{OTf}]$ , and $[\text{ZnAPAtHCl}]$ with $\text{NO}_2$ (g)	73
<b>Chapter 3</b>		
Figure 3.1.	Thermal ellipsoid plots for $[\text{ZnPAtHEt}]$ and $[\text{ZnPAtHMes}]$	86
Figure 3.2.	UV-Vis reactivity profiles for $[\text{ZnPAtHEt}]$ and $[\text{ZnPAtHMes}]$ with $\text{NOBF}_4$	88
Figure 3.3.	EI-MS analysis of the headspace of the reaction between $[\text{ZnPAtHEt}]$ and $\text{NOBF}_4$	88
Figure 3.4.	Thermal ellipsoid plot of the <i>C</i> -nitrosomesitylene dimer	89
Figure 3.5.	Thermal ellipsoid plot of the <i>C</i> -nitrosomesitylene dimer depicting the whole molecule disorder	91
Figure 3.6.	Thermal ellipsoid plot for $[\text{ZnPAtHCl}]$ , obtained from the $[\text{ZnPAtHMes}]/\text{NOBF}_4$ reaction mixture	92
Figure 3.7.	$^1\text{H}$ NMR spectroscopic yield analysis for conversion of $[\text{ZnPAtHMes}]$ to $[\text{ZnPAtHCl}]$	93
Figure 3.8.	Highest occupied molecular orbitals for the geometry optimized ( <i>S,R</i> ) and ( <i>R,S</i> ) configurations of $[\text{ZnPAtHEt}]$	95
Figure 3.9.	Intrinsic reaction coordinate for the interaction of $[\text{ZnPAtHEt}]$ with $\text{NO}^+$	96
Figure 3.10.	Highest occupied molecular orbital for $[\text{ZnPAtHEt}]$	101
<b>Chapter 4</b>		
Figure 4.1.	Thermal ellipsoid plot for $[\text{Co}(\text{NO})(\text{TC-5,5})]$	119
Figure 4.2.	Infrared spectroscopic comparison of $[\text{Co}(\text{TC-4,4})]$ and $[\text{Co}(\text{TC-5,5})]$ reactions with $\text{NO}$ (g) and $^{15}\text{NO}$ (g)	121
Figure 4.3.	EI-MS analysis of $^{15}\text{NO}$ (g) and the headspace of the $[\text{Co}(\text{TC-5,5})]/^{15}\text{NO}$ reaction	122

Figure 4.4.	Thermal ellipsoid plot for [Co(NO <sub>2</sub> )(TC-6,6)]	122
Figure 4.5.	Infrared spectroscopic comparison of [Co(NO <sub>2</sub> )(TC-6,6)], [Co(TC-6,6)] + NO (g), and [Co(TC-6,6)] + <sup>15</sup> NO (g)	124
Figure 4.6.	Solution IR timecourse for the [Co(TC-6,6)]/NO reaction	125
Figure 4.7.	Infrared spectroscopic comparison of [Co <sub>2</sub> (NO) <sub>4</sub> (TC-6,6)] and the [Co(TC-6,6)]/NO reaction mixture	125
Figure 4.8.	Thermal ellipsoid plot for [Co <sub>2</sub> (NO) <sub>4</sub> (TC-6,6)]	126
Figure 4.9.	EI-MS analysis of the headspace of the [Co(TC-6,6)]/ <sup>15</sup> NO reaction	129

## Chapter 5

Figure 5.1.	Thermal ellipsoid plots for [Co(NO <sub>2</sub> )(TC-4,4)], [Co(NO <sub>2</sub> )(TC-5,5)], and [Co(NO <sub>2</sub> )(TC-6,6)]	137
Figure 5.2.	Infrared spectroscopic comparisons of the reactions of [Co(NO <sub>2</sub> )(TC-4,4)] with NO (g) and <sup>15</sup> NO (g)	141
Figure 5.3.	<sup>1</sup> H NMR spectrum of the reaction of [Co(NO <sub>2</sub> )(TC-4,4)] with NO (g)	142
Figure 5.4.	Infrared spectroscopic comparisons of the reactions of [Co(NO <sub>2</sub> )(TC-5,5)] with NO (g) and <sup>15</sup> NO (g)	142
Figure 5.5.	<sup>1</sup> H NMR spectrum of the reaction of [Co(NO <sub>2</sub> )(TC-5,5)] with NO (g)	143
Figure 5.6.	Infrared spectroscopic comparisons of the reactions of [Co(NO <sub>2</sub> )(TC-6,6)] with NO (g) and <sup>15</sup> NO (g)	144
Figure 5.7.	<sup>1</sup> H NMR spectrum of the reaction of [Co(NO <sub>2</sub> )(TC-6,6)] with NO (g)	145
Figure 5.8.	Space filling models of [Co(NO <sub>2</sub> )(TC-4,4)], [Co(NO <sub>2</sub> )(TC-5,5)], and [Co(NO <sub>2</sub> )(TC-6,6)]	146

## Chapter 6

Figure 6.1.	Thermal ellipsoid plot for [Co(TC-4,4)](OTf)	159
Figure 6.2.	Solution infrared spectrum of the reaction between [Co(TC-4,4)](OTf) and NO (g)	160
Figure 6.3.	<sup>1</sup> H NMR spectrum of the reaction of [Co(TC-4,4)](OTf) with NO (g)	161
Figure 6.4.	EI-MS analysis of NO (g) and the headspace of the [Co(TC-4,4)](OTf)/NO reaction	162
Figure 6.5.	<sup>1</sup> H NMR spectrum of [Co(TC-4,4)](OTf) with NO (g) and proton sponge	163

Figure 6.6.	$^1\text{H}$ NMR spectra for the titration of proton sponge into [Co(TC-4,4)](OTf)/NO	164
Figure 6.7.	$^1\text{H}$ NMR spectrum of the [Co(TC-4,4)](OTf)/NO reaction in the presence of $\text{Cs}_2\text{CO}_3$	165
Figure 6.8.	$^1\text{H}$ NMR spectra of the [Co(TC-4,4)](OTf)/NO reaction spiked with [Co(NO)(TC-4,4)]	165
Figure 6.9.	$^1\text{H}$ NMR spectroscopic titration of NO (g) into solutions of [Co(TC-4,4)](OTf)	166
Figure 6.10.	Highest occupied molecular orbital for [Co(NO)(TC-4,4)]	167
Figure 6.11.	Isotope labeling comparison of the reactions of [Co(SC <sub>6</sub> F <sub>5</sub> )(TC-4,4)] with NO (g) or $^{15}\text{NO}$ (g)	168
Figure 6.12.	$^1\text{H}$ NMR spectroscopic analysis of the [Co(SC <sub>6</sub> F <sub>5</sub> )(TC-4,4)]/NO reaction	168
Figure 6.13.	COSY spectrum of the [Co(SC <sub>6</sub> F <sub>5</sub> )(TC-4,4)]/NO reaction mixture	169
Figure 6.14.	$^1\text{H}$ NMR spectrum of the [Co(SC <sub>6</sub> F <sub>5</sub> )(TC-4,4)]/NO reaction after 10 min	170
Figure 6.15.	$^{19}\text{F}$ NMR spectrum of the [Co(SC <sub>6</sub> F <sub>5</sub> )(TC-4,4)]/NO reaction after 10 min	170
Figure 6.16.	$^1\text{H}$ NMR spectrum of the [Co(SC <sub>6</sub> F <sub>5</sub> )(TC-4,4)]/NO reaction after 1 day	171
Figure 6.17.	$^{19}\text{F}$ NMR spectrum of the [Co(SC <sub>6</sub> F <sub>5</sub> )(TC-4,4)]/NO reaction after 1 day	171
Figure 6.18.	ESI-MS analysis of the [Co(SC <sub>6</sub> F <sub>5</sub> )(TC-4,4)]/NO reaction mixture	173
Figure 6.19.	Thermal ellipsoid plot for $\text{H}_2\text{TC-4,4}^{2\text{Br}}$	174
Figure 6.20.	Thermal ellipsoid plot for [Co(TC-4,4 <sup>2Br</sup> )]	175
Figure 6.21.	Thermal ellipsoid plot of [Co(Br)(TC-4,4 <sup>2Br</sup> )]	176

## Chapter 7

Figure 7.1.	Thermal ellipsoid plots for [Co(TC-5,5)](BF <sub>4</sub> ) and [Co(TC-6,6)](BPh <sub>4</sub> )	186
Figure 7.2.	Crystal packing diagram for [Co(TC-6,6)](BPh <sub>4</sub> ), showing $\pi$ - $\pi$ interactions	188
Figure 7.3.	Thermal ellipsoid plots for [Ga(TC-5,5)](GaCl <sub>4</sub> ) and [Ga(TC-6,6)](GaCl <sub>4</sub> )	189
Figure 7.4.	Comparison of structural parameters for [Co(TC-5,5)](BF <sub>4</sub> ) and [Ga(TC-5,5)](GaCl <sub>4</sub> )	192
Figure 7.5.	Comparison of structural parameters for [Co(TC-6,6)](BPh <sub>4</sub> ) and [Ga(TC-6,6)](GaCl <sub>4</sub> )	192

Figure 7.6.	Cyclic voltammograms of [Co(TC-5,5)], [Co(TC-6,6)], [Ga(TC-5,5)](GaCl <sub>4</sub> ) and [Ga(TC-6,6)](GaCl <sub>4</sub> )	194
-------------	--	-----

## List of Charts

### Chapter 1

Chart 1.1.	Biologically important <i>S</i> -nitrosothiols	25
Chart 1.2.	The pyridyl aminothiols ligand, PAThH	28
Chart 1.3.	The tropocoronand metal complex scaffold	29

### Chapter 2

Chart 2.1.	<i>N</i> <sub>2</sub> <i>S</i> tridentate chelating ligands and related Zn <sup>2+</sup> complexes	48
------------	--	----

### Chapter 3

Chart 3.1.	<i>N</i> <sub>2</sub> <i>S</i> -coordinated Zn <sup>2+</sup> species of interest	79
Chart 3.2.	PAThNO and APAThNO	79

### Chapter 4

Chart 4.1.	The tropocoronand metal complex scaffold	113
------------	--	-----

### Chapter 6

Chart 6.1.	Proposed product for the reaction of [Co(SC <sub>6</sub> F <sub>5</sub> )(TC-4,4)] and NO (g)	172
------------	---	-----

## List of Schemes

### Chapter 1

Scheme 1.1.	Synthetic route toward tropocoronand ligands and metal complexes	33
-------------	--	----

### Chapter 2

Scheme 2.1.	Synthesis of PATh species	59
Scheme 2.2.	Synthesis of APATh species	60
Scheme 2.3.	APAThNO ligation by phosphine-mediated N=O bond scission	64

### Chapter 3

Scheme 3.1.	Formation and autodecomposition pathway for EtNO	98
Scheme 3.2.	Proposed reaction pathway for the nitrosation of [ZnPAThMes]	100

Scheme 3.3.	Proposed reaction pathway for <i>C</i> -nitroso formation by intramolecular transnitrosation	101
-------------	---	-----

## Chapter 6

Scheme 6.1.	The [Co(TC-4,4)](OTf)/NO reaction in the presence of proton sponge and 1,2-dimethoxybenzene	162
Scheme 6.2.	The [Co(TC-4,4)](OTf)/NO reaction in the presence of proton sponge	163
Scheme 6.3.	Synthesis of substituted tropolone derivatives	177
Scheme 6.4.	Attempted substitution of trifluoroacetate onto the tropocoronand scaffold	178

## List of Tables

### Chapter 3

Table 3.1.	Crystallographic parameters for [ZnPAThEt] and [ZnPAThMes]	86
Table 3.2.	Summary of bond lengths and angles of interest for [ZnPAThEt]	87
Table 3.3.	Summary of bond lengths and angles of interest for [ZnPAThMes]	87
Table 3.4.	Crystallographic parameters for [MesNO] <sub>2</sub>	90
Table 3.5.	Summary of bond lengths (Å) and angles (deg) of interest for [MesNO] <sub>2</sub>	90
Table 3.6.	Comparison of bond distances for experimentally and computationally characterized isomers of [ZnPAThEt]	95
Table 3.7.	Bond distances for species obtained from the IRC calculation, compared with experimentally determined values for [ZnPAThEt]	97
Table 3.8.	XYZ coordinates, energy, and lowest calculated frequency for the ( <i>S,R</i> ) enantiomer of [ZnPAThEt]	102
Table 3.9.	XYZ coordinates, energy, and lowest calculated frequency for the ( <i>R,S</i> ) enantiomer of [ZnPAThEt]	103
Table 3.10.	XYZ coordinates, energy, and lowest calculated frequency for the reactant determined from the IRC calculation	104
Table 3.11.	XYZ coordinates, energy, and lowest calculated frequency for the transition state for NO <sup>+</sup> attack at the sulfur atom of [ZnPAThEt]	105



Table 3.12.	XYZ coordinates, energy, and lowest calculated frequency for the product determined from the IRC calculation	106
<b>Chapter 4</b>		
Table 4.1.	Crystallographic parameters for [Co(NO)(TC-5,5)], 2 [Co(TC-6,6)] · [Co(NO <sub>2</sub> )(TC-6,6)], and [Co <sub>2</sub> (NO) <sub>2</sub> (TC-6,6)]	119
Table 4.2.	Summary of bond lengths and angles of interest for [Co(NO)(TC-5,5)]	120
Table 4.3.	Summary of bond lengths and angles of interest for 2 [Co(TC-6,6)] · [Co(NO <sub>2</sub> )(TC-6,6)]	123
Table 4.4.	Summary of bond lengths and angles of interest for [Co <sub>2</sub> (NO) <sub>2</sub> (TC-6,6)]	126
<b>Chapter 5</b>		
Table 5.1.	Crystallographic parameters for [Co(NO <sub>2</sub> )(TC-4,4)] , [Co(NO <sub>2</sub> )(TC-5,5)], and [Co(NO <sub>2</sub> )(TC-6,6)]	139
Table 5.2.	Summary of bond lengths and angles of interest for [Co(NO <sub>2</sub> )(TC-4,4)]	139
Table 5.3.	Summary of bond lengths and angles of interest for [Co(NO <sub>2</sub> )(TC-5,5)]	140
Table 5.4.	Summary of bond lengths and angles of interest for [Co(NO <sub>2</sub> )(TC-6,6)]	140
<b>Chapter 6</b>		
Table 6.1.	Summary of crystallographic parameters for [Co(TC-4,4)](OTf)	159
Table 6.2.	Summary of bond lengths and angles of interest for [Co(TC-4,4)](OTf)	160
Table 6.3.	Crystallographic parameters for H <sub>2</sub> TC-4,4 <sup>2Br</sup> and [Co(TC-4,4 <sup>2Br</sup> )]	174
Table 6.4.	Summary of bond lengths and angles of interest for [Co(TC-4,4 <sup>2Br</sup> )]	175
<b>Chapter 7</b>		
Table 7.1.	Crystallographic parameters for [Co(TC-5,5)](BF <sub>4</sub> ) and [Co(TC-6,6)](BPh <sub>4</sub> )	187
Table 7.2.	Summary of bond lengths and angles of interest for [Co(TC-5,5)](BF <sub>4</sub> )	187
Table 7.3.	Summary of bond lengths and angles of interest for [Co(TC-6,6)](BPh <sub>4</sub> )	188
Table 7.4.	Crystallographic parameters for [Ga(TC-5,5)](GaCl <sub>4</sub> ) and [Ga(TC-6,6)](GaCl <sub>4</sub> )	189
Table 7.5.	Summary of bond lengths and angles of interest for [Ga(TC-5,5)](GaCl <sub>4</sub> )	190

Table 7.6.	Summary of bond lengths and angles of interest for [Ga(TC-6,6)](GaCl <sub>4</sub> )	190
Table 7.7.	Optical properties of Co(II), Co(III), and Ga(III) tropocoronands	191

## List of Equations

### Chapter 1

Equation 1.1.	Oxidation of NO by O <sub>2</sub> .	24
---------------	-------------------------------------	----

### Chapter 2

Equation 2.1.	Interconversion of Henry's law coefficients	54
Equation 2.2	Reaction of NO with RS <sup>-</sup>	62
Equation 2.3.	Formation of NO <sub>2</sub> from NO and O <sub>2</sub>	62
Equation 2.4.	Reaction of RS <sup>-</sup> with NO <sub>2</sub>	62
Equation 2.5.	Interaction of RSNO with Zn <sup>2+</sup>	73
Equation 2.6.	Reaction of RSNO with N <sub>2</sub> O <sub>4</sub>	73

### Chapter 6

Equation 6.1.	Proposed reaction between [Co(TC-4,4)](OTf) and NO	162
Equation 6.2.	Protonation of carbonate	164
Equation 6.3.	Reaction of carbonate and nitronium	164
Equation 6.4.	Reaction of [Co(SC <sub>6</sub> F <sub>5</sub> )(TC-4,4)] with NO	172
Equation 6.5.	Reaction of [Co(NO)(TC-4,4)] with F <sub>5</sub> C <sub>6</sub> SSC <sub>6</sub> F <sub>5</sub>	172

# **Chapter 1. Bioinorganic Chemistry of Nitric Oxide and of Some of Its Targets**

## 1.1. Introduction

Nitric oxide (NO) serves regulatory roles in diverse biological processes, including vital contributions to the function of the immune, circulatory, and nervous systems. Although initially considered a pollutant, NO gained increasing popularity as a physiological messenger and was named Molecule of the Year in 1992.<sup>1</sup> The 1998 Nobel Prize in Physiology and Medicine was awarded to Furchgott, Ignarro, and Murad for their discoveries of the role of nitric oxide as a signaling molecule in the cardiovascular system.<sup>2-4</sup> NO contributes to the regulation of macrophage cytotoxicity, neuronal signaling, and vasodilation, and it was determined to be the endothelium-derived relaxation factor (EDRF).<sup>5-7</sup>

Nitric oxide is redox active and experiences a brief lifetime in the cell. Half-life values for NO under physiological conditions have been reported to be 0.1 – 5 s.<sup>8</sup> Oxidation of NO to NO<sup>+</sup> occurs at 1.52 V vs. NHE in acetonitrile,<sup>9</sup> and reduction to the triplet ground state of NO<sup>-</sup> takes place at -0.8 V vs. NHE, or -1.042 V vs. SCE, in aqueous solutions.<sup>10-11</sup> NO is susceptible to attack by dioxygen, which ultimately leads to the formation of NO<sub>2</sub> (eq. 1.1).



Nitrogen dioxide is a good nitrosating and nitrating agent<sup>12</sup> and a powerful oxidant, which becomes readily reduced at 1 V vs. NHE.<sup>13</sup> The biochemistry of NO and its redox forms has been the subject of previous reviews.<sup>14-15</sup>

NO and its derivatives target a varied spectrum of biological functionalities, both organic and inorganic. Organic targets include primary and secondary amines and alcohols, which may react with reactive nitrogen and oxygen species (RNOS) to form *N*-nitrosamines and organic nitrites, respectively. Two examples of these species include the hepatocarcinogen *N*-nitrosodimethylamine,<sup>16-17</sup> and amyl nitrite, which is used as a detoxicant against cyanide

poisoning and as a vasodilator in the treatment of angina pectoris.<sup>18</sup> Thiolates may also react with RNOS to form *S*-nitrosothiols such as *S*-nitrosoglutathione and *S*-nitrosocysteine (Chart 1.1), which may then donate  $\cdot\text{NO}$  or  $\text{NO}^+$  to

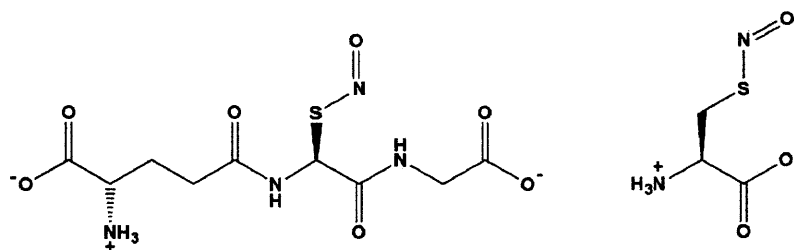


**Chart 1.1.** *S*-Nitrosoglutathione (*left*) and *S*-nitrosocysteine (*right*) are two examples of biologically important *S*-nitrosothiols.

subsequent substrates, and thereby function to store and transport an otherwise short-lived NO molecule.<sup>15,19-27</sup> Zinc-bound thiolates in nitric oxide synthase<sup>28-34</sup> and metallothioneins<sup>35-53</sup> undergo *S*-nitrosylation by RNOS with subsequent dissociation of the zinc(II) ion as a means of effecting enzyme regulation and inducing or propagating signaling pathways.

Zinc thiolate sites are ubiquitous in biology, and common coordination motifs of biological  $\text{Zn}^{2+}$  include cysteine, histidine, aspartate and glutamate ligands.<sup>43,54-59</sup> Transition metal substrates for biological RNOS include the cobalt center of cobalamin,<sup>60-69</sup> as well as numerous heme and non-heme iron centers.<sup>70-83</sup> Of particular interest and relevance to the work described in this thesis are the transformations of zinc thiolate and cobalamin centers of biomolecules in the presence of RNOS.

## 1.2. Nitric Oxide Synthase and Metallothioneins

Biological NO is synthesized by five-electron oxidation of L-arginine in nitric oxide synthases (NOSs), of which there are neuronal, endothelial, and inducible NOS isoforms.<sup>70,84-86</sup> These enzymes are head-to-head homodimers,<sup>87</sup> with a tetrahydrobiopterin binding pocket and a

tetracysteine thiolate coordination site for zinc at the interface of the oxygenase domains (Fig. 1.1). There are also sites for binding FMN, FAD, and NADH in the reductase domain. The oxygenase and reductase are joined by a linker that binds  $\text{Ca}^{2+}$ /calmodulin, and reductase activity is regulated by this binding.<sup>88-89</sup> NOS dimer formation and activity require binding of tetrahydrobiopterin.<sup>87,90-91</sup> The absence of zinc destabilizes the NOS dimer and strongly favors dissociation of the enzyme into its composite monomers.<sup>30-32,34</sup> NOS activity therefore relies on zinc binding to the tetra-cysteine thiolate site, and the enzyme utilizes this structural feature to enable a feedback mechanism for regulating NO production.<sup>30-32,34</sup>

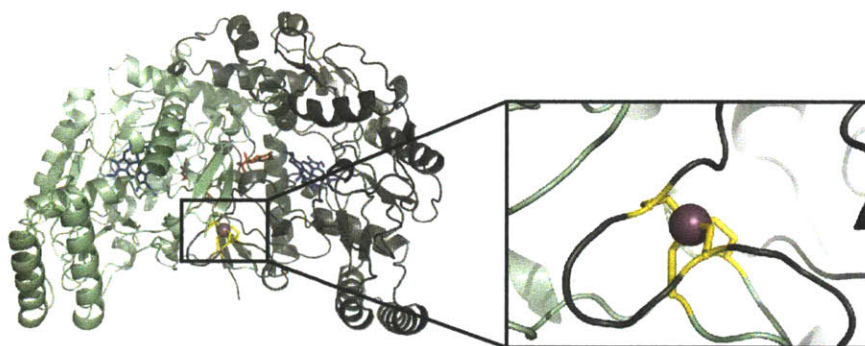


**Figure 1.1.** Crystal structure of the oxygenase domain of human inducible nitric oxide synthase, PDB ID 1NSI.<sup>31</sup> The heme units are shown in blue and tetrahydrobiopterin in orange. The zinc ion, bound by four cysteine thiolates, is shown in purple, and appears at the interface of the two monomer units.

Exposure of nitric oxide synthase to NO in aerobic aqueous solutions leads to *S*-nitrosylation of the zinc-binding cysteine residues with concomitant dissociation of the metal ion from the tetrathiolate site.<sup>28-34</sup> This chemistry destabilizes the NOS homodimer, which dissociates into monomers and halts NO production.<sup>30-32</sup> Metallothioneins exposed to either aerobic nitric oxide or biologically relevant *S*-nitrosothiols also lose  $\text{Zn}^{2+}$  from tetracysteine thiolate coordination sites with concomitant formation of *S*-nitrosothiol.<sup>35-53</sup> Similar behavior is observed for the zinc thiolate site of alcohol dehydrogenase in the presence of RNOS.<sup>92-93</sup> The

release of  $Zn^{2+}$  upon *S*-nitros(yl)ation of metallothionein cysteine residues contributes to the available pool of labile zinc(II), which has been characterized in pulmonary epithelial tissue and in the hippocampus.<sup>37,44,47,49-50,94</sup> Moreover, *S*-nitros(yl)ation-related mobilization of  $Zn^{2+}$  contributes to the up- or down-regulation of transcription factors.<sup>41,43-44,48,95-99</sup> NO-mediated  $Zn^{2+}$  release from metallothioneins induces nuclear translocation of the metallothionein transcription factor MTF-1, for example.<sup>43-44,97</sup> Transcription factors containing zinc finger domains may undergo demetallation upon *S*-nitros(yl)ation of coordinating cysteine residues.<sup>38,44,98-99</sup> The transcription activator LAC9, which regulates genes involved in lactose and galactose metabolism in *Kluyveromyces lactis*, suffers demetallation of its  $[Zn_2S_6]$  zinc finger domain upon *S*-nitros(yl)ation by RNOS.<sup>95</sup> Comparison of studies conducted aerobically and anaerobically reveals that it is not NO itself, but an oxidation product thereof, that is responsible for thiolate nitrosation in these systems.<sup>36,53,100</sup>

### 1.3. Small Molecule Models Containing Thiolate Ligands

These numerous reports of zinc dissociation upon *S*-nitrosylation of coordinating sulfur residues spurred our interest in understanding the interaction of  $Zn^{2+}$  with *S*-nitrosothiols. Whereas a review of the literature revealed detailed studies of metal-*S*-nitrosothiol interactions for copper,<sup>101-103</sup> iron,<sup>104-106</sup> iridium,<sup>107-108</sup> and others,<sup>24,109</sup> a gap was evident in the chemistry of *S*-nitrosothiol interactions with  $Zn^{2+}$ . Previous studies of the *S*-nitrosation of zinc-bound thiolate ligands were performed with monodentate thiolates, which undergo dissociation from the metal center upon conversion to *S*-nitrosothiols.<sup>110</sup> We sought to fill the void by preparing small molecule models of zinc thiolates and examining their reactivities with RNOS, and we also undertook the preparation of the *S*-nitros(yl)ated ligand analogues and studied their interactions

with  $\text{Zn}^{2+}$ . Model chemistry provides the benefit of large-scale preparations of zinc thiolate complexes with easily tunable properties in relatively short periods of time, allowing studies to be focused on reactivity, as opposed to protein isolation and purification, or mutagenesis studies to achieve the desired tuning effects. Well-characterized model compounds of peptide deformylase utilized the pyridyl aminothioliolate ligand PATHH to bind  $\text{Zn}^{2+}$ ,  $\text{Co}^{2+}$ ,  $\text{Fe}^{2+}$ ,  $\text{Cu}^{2+}$ , and  $\text{Pb}^{2+}$  metal centers,<sup>111-118</sup> and these studies were reported shortly before we became interested in this field (Chart 1.2).

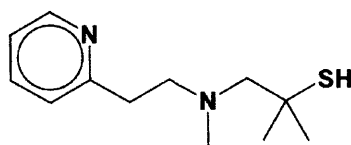


**Chart 1.2.** The tridentate coordinating pyridyl aminothioliolate ligand, PATHH.

The tridentate chelating [PATH]<sup>-</sup> scaffold provides an  $N_2S$  donor set to the metal center, leaving a fourth binding site available for exchangeable monodentate coordination. The reported metal complexes [MPATHX] are amenable to structural characterization by X-ray crystallography,<sup>111,113-118</sup> and thus provide a well-defined starting point for reactivity studies with RNOS. The binding interaction for  $\text{Zn}^{2+}$  and [PATH]<sup>-</sup> had been previously examined in aqueous 0.1 M  $\text{NaNO}_3$ , and the  $\log K([\text{ZnPATH}]^-)$  was determined to be 10.35(2).<sup>116</sup> The study indicates a tight binding of  $\text{Zn}^{2+}$  by the tridentate coordinating ligand, although we recognize that the binding is likely to change somewhat in a non-aqueous solvent. A strong interaction between the ligand and  $\text{Zn}^{2+}$  was essential to our endeavors, for it offered the possibility that the complex would remain intact upon *S*-nitros(yl)ation of the ligand, allowing us to probe the interaction between the *S*-nitrosothiol moiety and  $\text{Zn}^{2+}$ . Moreover, the [ZnPATHX] architecture facilitated studies of RNOS reactivity at a unique zinc thiolate site, providing a simplified scaffold for establishing basic  $\text{Zn}^{2+}/S$ -nitrosothiol reactivity principles. The system has the potential to



become more complex by substitution of additional thiolates at the exchangeable fourth coordination site to mimic the biological coordination spheres more closely.

Chapters 2 and 3 of this thesis describe the chemistry of small molecule models containing zinc thiolate centers and their reactivities with RNOS. Chapter 2 focuses on the formation of *S*-nitrosothiols from zinc thiolates as well as the interaction of independently prepared *S*-nitrosothiols with  $\text{Zn}^{2+}$ . Chapter 3 explores the interaction between  $\text{NO}^+$  with two organozinc [PATH]<sup>-</sup> complexes, and describes an unexpected intramolecular transnitrosation reaction.

#### 1.4. Redox Active Metal Centers and RNOS

In addition to studies of RNOS reactivity with redox-inactive zinc centers, we pursued the chemistry of systems in which NO plays bioregulatory roles by interaction with redox-active metal sites. Specifically, we explored the nitric oxide chemistry of cobalamin-inspired small molecule coordination compounds bound to tropocoronand ligands (Chart 1.3). These complexes

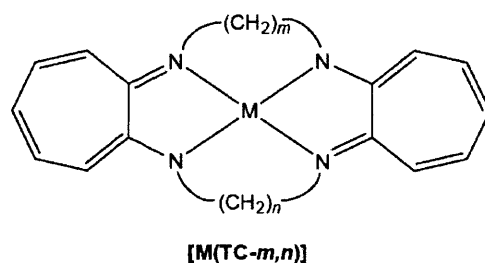


**Chart 1.3.** The tropocoronand metal complex scaffold.

employ a macrocyclic ligand scaffold that can be manipulated to tune the steric and electronic properties of a coordinated metal center. Changes to the ligand can be made without affecting the nature of the donor atoms that coordinate to the metal ions. This control of the metal coordination geometry through changes in ligand size, but not donor atom character, mimics the



The characteristics of these “base-on” and “base-off” states contribute to the reactivity of the cobalamin.<sup>124</sup> The cobalt center has been characterized in the  $d^6$ ,  $d^7$  and  $d^8$  electronic states in biology.<sup>126-127</sup> Methylcobalamin (MeCbl) and adenosylcobalamin (AdoCbl) are the cofactors for isomerases, methyltransferases, and dehalogenases,<sup>124,128-129</sup> and glutathionylcobalamin (GsCbl) is a proposed precursor to MeCbl and AdoCbl.<sup>125,130</sup> The alkyl derivatives are the only cobalamin cofactors observed in physiological systems.<sup>124,128-129</sup> Cyanocobalamin is synonymous with vitamin B<sub>12</sub>, which is physiologically important as a nutritional supplement, but is only naturally observed in trace quantities in the lungs of smokers.<sup>131</sup> Physiological deficiencies of cobalamins may result in pernicious anemia.<sup>132-134</sup>

The interaction between NO and cobalamins, both in the  $\text{Co}^{2+}$  and  $\text{Co}^{3+}$  states, has been studied extensively. Cbl(II) reacts with NO to form nitrosylcobalamin (NO-Cbl), formally a  $\{\text{Co}^{\text{III}}\text{-NO}^-\}$  species that has been characterized both structurally and spectroscopically.<sup>135-139</sup> The reactivity of Cbl(III) species such as aquacobalamin ( $[\text{H}_2\text{O-Cbl(III)}]^+$ ) with NO remains controversial, however.<sup>61,69,137,140-144</sup> Reports of pH-dependent NO-Cbl formation from  $[\text{H}_2\text{O-Cbl(III)}]^+$  exposure to nitric oxide exist alongside claims that  $[\text{H}_2\text{O-Cbl(III)}]^+$  is inert to NO, regardless of pH. MeCbl and AdoCbl do not react with nitric oxide in the dark, but under photolysis conditions and in the presence of NO MeCbl and AdoCbl react to form nitrosylcobalamin.<sup>60</sup> GsCbl exposure to NO also leads to NO-Cbl formation, with concomitant formation of glutathione disulfide (GSSG).<sup>145</sup>

## 1.6. The Entatic State

The arrangement of ligands in the cofactor binding sites of metalloproteins may force unusual coordination geometries about the metal centers.<sup>146</sup> Such protein-metal interactions are

said to be entatic states,<sup>147</sup> whereby the strained coordination environment destabilizes the metal center in order to elicit elevated reactivity. Blue copper proteins, also called cupredoxins, facilitate electron transfer over distances of  $\sim 13 \text{ \AA}$ <sup>148</sup> and serve as the mostly commonly cited examples of entasis. Plastocyanins, azurins, stellacyanin, laccase, ascorbate oxidase, nitrite reductase, and ceruloplasmin all contain the Type 1 copper, or blue copper, centers.<sup>148</sup> The copper binding sites of cupredoxins contain at least one cysteine thiolate residue coordinated to the metal, and blue copper proteins derive their name from the intense  $S_{\text{Cys}} \rightarrow \text{Cu}^{2+}$  charge transfer band that appears at  $\sim 600 \text{ nm}$  in the optical spectrum.<sup>148-149</sup> The protein enforces a tetrahedral coordination environment about the copper, which is a favorable geometry for copper(I), but not copper(II) coordination. The imposed geometric constraints result in high reduction potentials for the copper(II)/(I) couple,<sup>149</sup> and simultaneously allow the metal to cycle between the copper(II) and copper(I) oxidation states with minimal reorganizational energy during electron transfer.<sup>150-</sup>

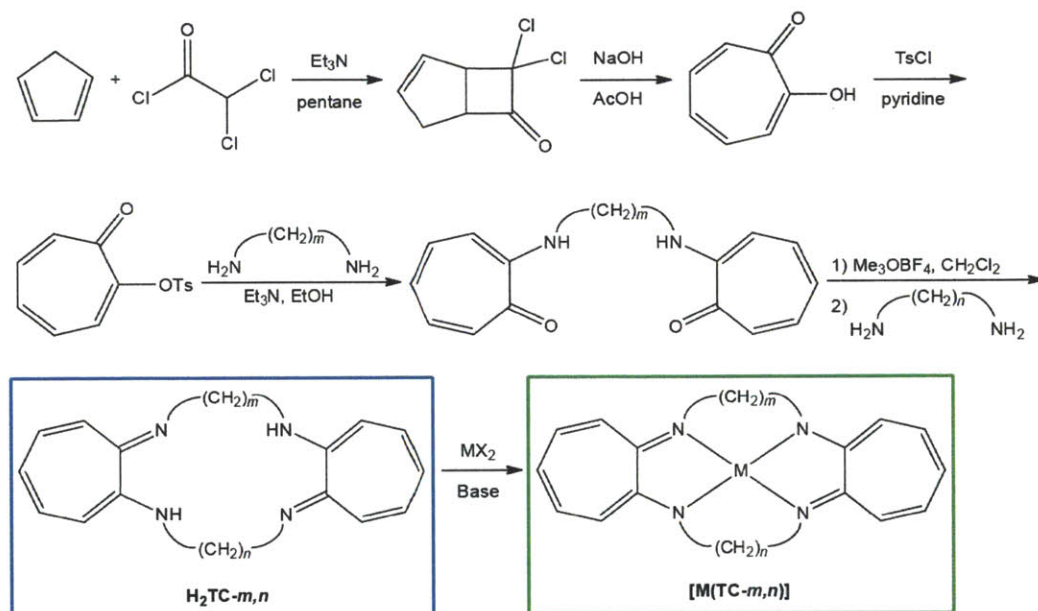
151

Entatic states have been both observed and intentionally induced in small molecule, peptide, and biosynthetic protein models of cupredoxins,<sup>152-159</sup> iron hydrogenase,<sup>160-161</sup> and alcohol dehydrogenase,<sup>162</sup> as well as in metal-organic frameworks.<sup>163-165</sup> Our group has explored the coordination chemistry of a series of macrocyclic  $N_4$ -donor ligands, collectively named tropocoronands, which are capable of enforcing and supporting unconventional geometries about coordinated metal centers.

## 1.7. Tropocoronands

The tropocoronand ligands were developed by Nozoe and coworkers,<sup>119,121</sup> and utilized by our group as bioinspired models of the cobalamin ligand scaffold. The ligands are

tetraazamacrocycles that are characterized by two aminotropones linked by alkyl or polyethylene glycol chains. They have been prepared with chains of 2 – 12 atoms in length (Scheme 1.1).<sup>119,121,166-167</sup>



**Scheme 1.1.** Synthesis of the tropocoronand ligands (*blue*) and metal complexes (*green*).<sup>119,121,168</sup>

Tropocoronand metal complexes have been synthesized and characterized with manganese,<sup>169-171</sup> iron,<sup>170,172-173</sup> cobalt,<sup>122,174-177</sup> nickel,<sup>119,121,178</sup> copper,<sup>179-184</sup> zinc,<sup>123</sup> zirconium,<sup>185-188</sup> rhodium,<sup>189</sup> cadmium,<sup>123</sup> and hafnium<sup>185-188,190</sup> metal centers, using macrocycle chain lengths ranging from 3 to 7 atoms.<sup>120</sup> Variations in tropocoronand linker chain lengths allow control of steric and electronic properties at the metal centers. That is, an increase in linker chain length induces a twist at the metal center from idealized square-planar to tetrahedral geometry, until the number of methylene groups becomes too large to fit the tetradentate ligand about a single metal center without destabilizing steric interactions (Fig. 1.3). The extent of this torsional effect is described by the twist angle, defined as the angle between the planes of the aminotroponimine nitrogen

atoms and the metal centers. A twist angle of  $0^\circ$  thus describes an idealized square-planar geometry, and an angle of  $90^\circ$  describes an idealized tetrahedron.

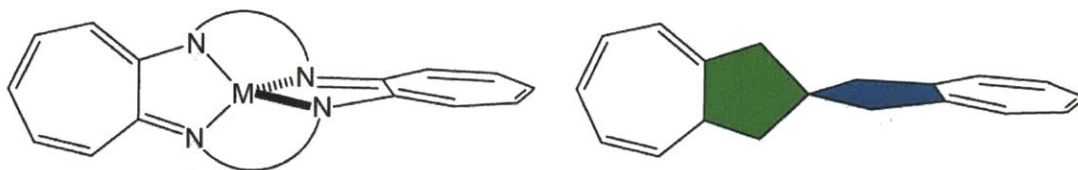


**Figure 1.3.** The twist angle of tropocoronand metal complexes is defined as the angle between the planes of the aminotroponimine nitrogen atoms and the metal center. These two planes are depicted above in green and blue.

The striking effect of tropocoronand size on the steric and electronic characteristics of the metal center is exemplified by the nickel(II),<sup>119,121,178</sup> cobalt(II),<sup>122</sup> and copper(II)<sup>179-180</sup> complexes (Fig. 1.4). Structural characterization of nickel tropocoronands ranging from [Ni(TC-3,3)] to [Ni(TC-6,6)] reveals a non-linear progression from square-planar to tetrahedral geometry and a corresponding change in spin state from  $S = 0$  to  $S = 1$  that occurs at the transition of macrocycle size from [Ni(TC-4,5)] to [Ni(TC-5,5)].<sup>119,121,178</sup> The non-linear nature of the increase in the twist angle reflects the resistance of nickel(II) to undergo the change from low- to high-spin as the coordination about the metal approaches tetrahedral geometry, which is a less favorable environment for nickel(II).<sup>119,121,178</sup> In contrast, the cobalt(II) analogues exhibit a nearly linear change in twist angle with increasing tropocoronand size, and undergo the corresponding change in spin state between [Co(TC-4,4)] ( $S = 1/2$ ) and [Co(TC-4,5)] ( $S = 3/2$ ).<sup>122</sup> The differing behaviors of the nickel(II) and cobalt(II) tropocoronand series may be attributed to a greater preference of cobalt(II) for tetrahedral geometry in comparison to the nickel(II) derivatives. Structural characterization of the mononuclear copper(II) tropocoronand complexes [Cu(TC-3,3)], [Cu(TC-4,4)], and [Cu(TC-5,5)] revealed behavior similar to that of the cobalt(II) species, with a linear increase in twist angle in the progression from [Cu(TC-3,3)] to [Cu(TC-

5,5)].<sup>180</sup> As expected, based on the nature of copper(II), the spin state of the metal center remains  $S = 1/2$  throughout.<sup>180</sup> Mononuclear [Cu(TC-6,6)] could not be synthesized. Instead, the acetate- and methoxide-bridged [Cu<sub>2</sub>(OMe)(OAc)(TC-6,6)] complex was isolated and structurally characterized.<sup>179</sup> The authors suggest that [Cu(TC-6,6)] may form and then undergo reduction of copper(II) with concomitant oxidation of the tropocoronand ligand, ultimately contributing to intractable material observed in the reaction mixture.<sup>179</sup> This hypothesis is supported by the electronic preference of copper(II) centers to form Jahn-Teller distorted square-planar geometries, as well as the preference of copper(I) for tetrahedral coordination environments.<sup>191</sup>

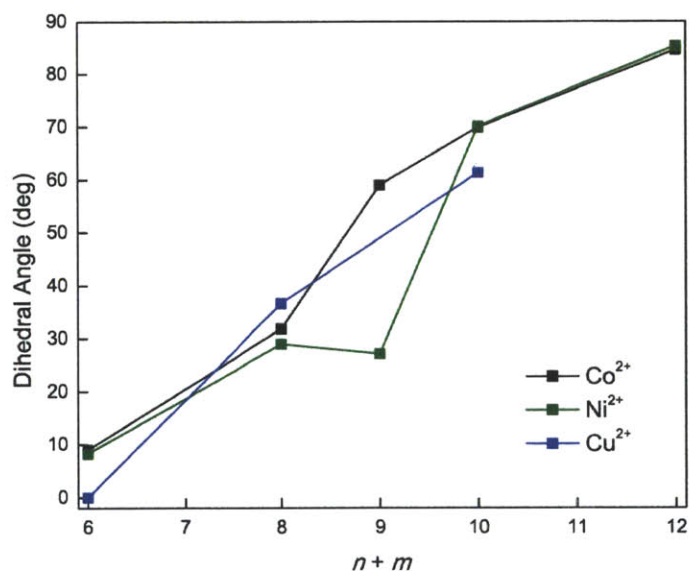


**Figure 1.4.** Correlation of tropocoronand linker chain length ( $n + m$ ) with the corresponding twist angle at the metal center, shown for Co<sup>2+</sup>, Ni<sup>2+</sup>, and Cu<sup>2+</sup>.<sup>119,121-122,178,180</sup>

### 1.8. Reactions of Cobalt Tropocoronands with Nitric Oxide

Nitric oxide chemistry has been examined for [Co(TC-3,3)],<sup>176</sup> [Co(TC-4,4)],<sup>176</sup> [Mn(THF)(TC-5,5)],<sup>169-170</sup> and [Fe(TC-5,5)],<sup>170,172</sup> as well as for the cobalt(II) bis-aminotroponeiminate derivatives [Co(*i*-PrDATI)<sub>2</sub>], [Co(*t*-BuDATI)<sub>2</sub>], [Co(BzDATI)<sub>2</sub>], [Co(*i*-Pr<sub>2</sub>ATI)<sub>2</sub>], and [Co(DATI-4)] and the cobalt(II) complexes of linked aminotroponeiminate-



salicylaldimine ligands, [Co(<sup>i</sup>PrSATI-3)], [Co<sub>2</sub>(<sup>i</sup>PrSATI-4)<sub>2</sub>], [Co(<sup>i</sup>PrFATI-3)], [Co(<sup>i</sup>PrFATI-4)].<sup>192-195</sup> Mononitrosyl complex formation occurs upon exposure of [Co(TC-3,3)] and [Co(TC-4,4)] to NO (g), and N<sub>2</sub>O is detected by solution react-IR spectroscopy.<sup>176</sup> [Mn(THF)(TC-5,5)] and [Fe(TC-5,5)] form mononitrosyl complexes in the presence of stoichiometric amounts of NO (g).<sup>169,172</sup> Exposure to excess NO (g) results in nitric oxide disproportionation, forming of NO<sub>2</sub> and N<sub>2</sub>O.<sup>169-170,172</sup> The cobalt(II) bis-aminotroponeimine derivatives form cobalt dinitrosyl adducts in the presence of NO (g).<sup>192-194</sup>

In this thesis, we strove to exploit the ability to tune the steric and electronic properties of metal centers and to examine the capability of tropocoronand ligands to control the reactivity of cobalt(II) complexes with NO (g). We extended the known Co<sup>2+</sup>/NO chemistry to include reactions of the [Co(TC-5,5)] and [Co(TC-6,6)] derivatives. This work is described in Chapter 4. The ability of ligand size to tune the NO reactivity of cobalt(III) nitrite complexes was examined by extension of the cobalt(II) work. The preparation and NO reactivity of [Co(NO<sub>2</sub>)(TC-4,4)], [Co(NO<sub>2</sub>)(TC-5,5)], and [Co(NO<sub>2</sub>)(TC-6,6)] are described in Chapter 5. Chapter 6 describes the nitric oxide chemistry of tropocoronand complexes of cobalt(III) triflate and cobalt(III) pentafluorobenzene thiolate, [Co(TC-4,4)](OTf) and [Co(SC<sub>6</sub>F<sub>5</sub>)(TC-4,4)].

### **1.9. Entatic States of Cobalt(III)**

In the absence of entatic tuning, cobalt(II) metal centers display a proclivity toward high-spin octahedral or tetrahedral configurations, and cobalt(III) centers prefer low-spin octahedral geometries.<sup>191</sup> Square-planar coordination environments are also readily observed for four-coordinate cobalt(III) complexes, but small molecules with cobalt(III) centers in tetrahedral environments are significantly scarce. The cobalt(III) center in [CoW<sub>12</sub>O<sub>40</sub>]<sup>5-</sup> exists in a



tetrahedral environment,<sup>191</sup> as does cobalt(III) in  $[\text{Co}(\text{nor})_4]^-$ ,<sup>196-197</sup> where nor is the norbornyl anion. In the former case, the polyoxometallate scaffold hardly constitutes a small molecule construct, and in the latter, the geometry of the metal center was assigned based on spectroscopic characteristics, and structural characterization of the tetranorbornyl cobalt(III) complex was unattainable.<sup>196-197</sup> A small number of mononuclear cobalt(III) imides have been prepared and structurally characterized, and in these species the multiple bond character of the metal-imide interaction stabilizes the pseudotetrahedral geometry of cobalt(III).<sup>198-203</sup> The reason for the rarity of cobalt(III) in tetrahedral environments becomes clear upon comparison of orbital splitting diagrams for a  $d^6$  metal center in square-planar versus tetrahedral geometries. The orbital filling diagram for a square-planar  $d^6$  center is shown in Figure 1.5 for an  $S = 1$  electronic configuration.<sup>204</sup> The allocation of electrons corresponds to minimization of electron repulsion interactions and is the observed electronic distribution in  $[\text{Co}(\text{TC-4,4})]^+$  complexes. In contrast, the orbital distribution in a  $d^6$  tetrahedral orbital splitting diagram results in the partial occupancy of two destabilized  $t_2$  molecular orbitals, with no contribution to minimization of electron repulsion interactions. That is, the transition from square-planar to tetrahedral geometry results in partial filling of orbitals that are destabilized in the tetrahedral configuration relative to the square-planar one, without minimizing electron repulsion. The square-planar geometry is consequently favored over the tetrahedral configuration in  $d^6$  transition metal ions.

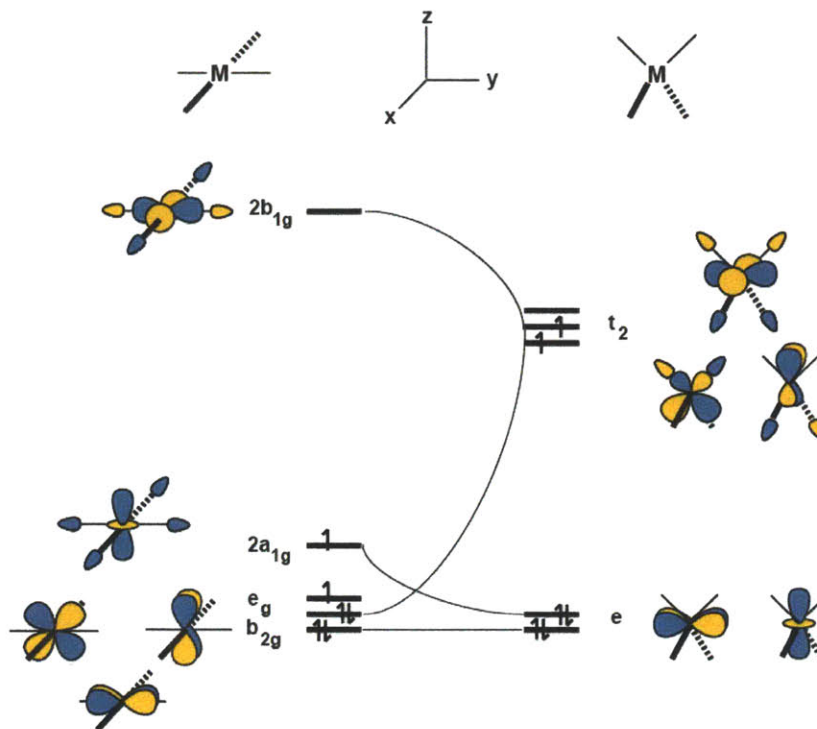


**Figure 1.5.** Orbital correlation diagram for the transition from square-planar to tetrahedral geometry, shown for the electron occupancy corresponding to a  $d^6$  metal center. Modified from Albright, Burdett, and Whangbo.<sup>204</sup>

Having the ability to control the environment at the metal center simply by changing tropocoronand linker chain length places us in a unique situation to examine unusual coordination environments. The previously established tropocoronand series of cobalt(III) complexes comprises  $[\text{Co}(\text{R})(\text{TC-3,3})]$  ( $\text{R} = \text{Me}, \text{Et}, n\text{-Pr}, \text{Cl}$ ),  $[\text{Co}(\text{THF})(\text{TC-3,3})](\text{BPh}_4)$  and  $[\text{Co}(\text{TC-3,3})](\text{X})$  ( $\text{X} = \text{BPh}_4, \text{BAr}_4'$ ),  $[\text{Co}(n\text{-Pr})(\text{TC-3,4})]$ ,  $[\text{Co}(\text{R})(\text{TC-4,4})]$  ( $\text{R} = \text{Me}, \text{COMe}, \text{Cl}$ ) and  $[\text{Co}(\text{TC-4,4})](\text{BPh}_4)$  derivatives.<sup>174-175,177</sup> These species exist in square pyramidal or distorted square-planar geometries, with twist angles of  $8^\circ$  and  $41^\circ$  for the four-coordinate complexes. In our pursuit to examine the size dependence of cobalt(II) and cobalt(III) tropocoronands on their ability to tune reactivity with nitric oxide, we fortuitously prepared and structurally characterized two pseudo-tetrahedral cobalt(III) complexes,  $[\text{Co}(\text{TC-5,5})](\text{BF}_4)$  and  $[\text{Co}(\text{TC-6,6})](\text{BPh}_4)$ . This work is described in Chapter 7 of this thesis.

## 1.10. References

- (1) Culotta, E.; Koshland, D. *Science* **1992**, *258*, 1862-1865.
- (2) Furchgott, R. F. *Angew. Chem. Int. Ed.* **1999**, *38*, 1870-1880.
- (3) Ignarro, L. J. *Angew. Chem. Int. Ed.* **1999**, *38*, 1882-1892.
- (4) Murad, F. *Angew. Chem. Int. Ed.* **1999**, *38*, 1856-1868.
- (5) Furchgott, R.; Vanhoutte, P. *FASEB J.* **1989**, *3*, 2007-2018.
- (6) Ignarro, L. J.; Buga, G. M.; Wood, K. S.; Byrns, R. E.; Chaudhuri, G. *Proc. Natl. Acad. Sci. USA* **1987**, *84*, 9265-9269.
- (7) Rapoport, R. M.; Draznin, M. B.; Murad, F. *Nature* **1983**, *306*, 174-176.
- (8) Nagano, T.; Yoshimura, T. *Chem. Rev.* **2002**, *102*, 1235-1270.
- (9) Lee, K. Y.; Kuchynka, D. J.; Kochi, J. K. *Inorg. Chem.* **1990**, *29*, 4196-4204.
- (10) Bartberger, M. D.; Liu, W.; Ford, E.; Miranda, K. M.; Switzer, C.; Fukuto, J. M.; Farmer, P. J.; Wink, D. A.; Houk, K. N. *Proc. Natl. Acad. Sci. USA* **2002**, *99*, 10958-10963.
- (11) Shafirovich, V.; Lymar, S. V. *Proc. Natl. Acad. Sci. USA* **2002**, *99*, 7340-7345.
- (12) Shiri, M.; Zolfigol, M. A.; Kruger, H. G.; Tanbakouchian, Z. *Tetrahedron* **2010**, *66*, 9077-9106.
- (13) Stanbury, D. M. In *Adv. Inorg. Chem.*; Sykes, A. G., Ed.; Academic Press, Inc.: San Diego, CA, 1989; Vol. 33.
- (14) Stamler, J.; Singel, D.; Loscalzo, J. *Science* **1992**, *258*, 1898-1902.
- (15) Tennyson, Andrew G.; Lippard, Stephen J. *Chem. Biol.* **2011**, *18*, 1211-1220.
- (16) Hecht, S. S. *Chem. Res. Toxicol.* **1998**, *11*, 559-603.
- (17) Peto, R.; Gray, R.; Brantom, P.; Grasso, P. *Cancer Res.* **1991**, *51*, 6452-6469.
- (18) Haley, T. J. *Clin. Toxicol.* **1980**, *16*, 317-329.
- (19) Al-Sa'doni, H.; Ferro, A. *Clinical Science* **2000**, *98*, 507-520.
- (20) Broillet, M. C. *Cell. Mol. Life Sci.* **1999**, *55*, 1036-1042.
- (21) Butler, A. R.; Rhodes, P. *Anal. Biochem.* **1997**, *249*, 1-9.
- (22) Gaston, B. *BBA Bioenergetics* **1999**, *1411*, 323-333.
- (23) Hogg, N. *Free Radical Biol. Med.* **2000**, *28*, 1478-1486.
- (24) Szaciłowski, K.; Stasicka, Z. *Prog. React. Kinet. Mech.* **2001**, *26*, 1-58.
- (25) Wang, K.; Zhang, W.; Xian, M.; Hou, Y. C.; Chen, X. C.; Cheng, J. P.; Wang, P. G. *Curr. Med. Chem.* **2000**, *7*, 821-834.
- (26) Wang, P. G.; Xian, M.; Tang, X.; Wu, X.; Wen, Z.; Cai, T.; Janczuk, A. J. *Chem. Rev.* **2002**, *102*, 1091-1134.
- (27) Williams, D. L. H. *Acc. Chem. Res.* **1999**, *32*, 869-876.
- (28) Erwin, P. A.; Lin, A. J.; Golan, D. E.; Michel, T. *J. Biol. Chem.* **2005**, *280*, 19888-19894.
- (29) Erwin, P. A.; Mitchell, D. A.; Sartoretto, J.; Marletta, M. A.; Michel, T. *J. Biol. Chem.* **2006**, *281*, 151-157.
- (30) Hemmens, B.; Goessler, W.; Schmidt, K.; Mayer, B. *J. Biol. Chem.* **2000**, *275*, 35786-35791.
- (31) Mitchell, D. A.; Erwin, P. A.; Michel, T.; Marletta, M. A. *Biochemistry* **2005**, *44*, 4636-4647.
- (32) Ravi, K.; Brennan, L. A.; Levic, S.; Ross, P. A.; Black, S. M. *Proc. Natl. Acad. Sci. USA* **2004**, *101*, 2619-2624.
- (33) Smith, B. C.; Fernhoff, N. B.; Marletta, M. A. *Biochemistry* **2012**, *51*, 1028-1040.
- (34) Tummala, M.; Ryzhov, V.; Ravi, K.; Black, S. M. *DNA Cell Biol.* **2008**, *27*, 25-33.

- (35) Aravindakumar, C. T.; Ceulemans, J.; De Ley, M. *Biophys. Chem.* **2000**, *85*, 1-6.
- (36) Aravindakumar, C. T.; Ceulemans, J.; deLey, M. *Biochem. J* **1999**, *344*
- (37) Bernal, P. J.; Leelavanichkul, K.; Bauer, E.; Cao, R.; Wilson, A.; Wasserloos, K. J.; Watkins, S. C.; Pitt, B. R.; St. Croix, C. M. *Circul. Res.* **2008**, *102*, 1575-1583.
- (38) Binet, M. R. B.; Cruz-Ramos, H.; Laver, J.; Hughes, M. N.; Poole, R. K. *FEMS Microbiol. Lett.* **2002**, *213*, 121-126.
- (39) Casero, E.; Martin-Gago, J. A.; Pariente, F.; Lorenzo, E. *Eur. Biophys. J.* **2004**, *33*, 726-731.
- (40) Chen, Y.; Irie, Y.; Keung, W. M.; Maret, W. *Biochemistry* **2002**, *41*, 8360-8367.
- (41) Gow, A.; Ischiropoulos, H. *Am. J. Physiol. Lung Cell. Mol. Physiol.* **2002**, *282*, L183-L184.
- (42) Khatai, L.; Goessler, W.; Lorencova, H.; Zangger, K. *Eur. J. Biochem.* **2004**, *271*, 2408-2416.
- (43) Kröncke, K. D. *Arch. Biochem. Biophys.* **2007**, *463*, 183-187.
- (44) Li, H.; Cao, R.; Wasserloos, K. J.; Bernal, P.; Liu, Z.-Q.; Pitt, B. R.; St. Croix, C. M. *Ann. N.Y. Acad. Sci.* **2010**, *1203*, 73-78.
- (45) Montoliu, C.; Monfort, P.; Carrasco, J.; Palacios, Ó.; Capdevila, M.; Hidalgo, J.; Felipo, V. *J. Neurochem.* **2000**, *75*, 266-273.
- (46) Pearce, L. L.; Gandley, R. E.; Han, W.; Wasserloos, K.; Stitt, M.; Kanai, A. J.; McLaughlin, M. K.; Pitt, B. R.; Levitan, E. S. *Proc. Natl. Acad. Sci. USA* **2000**, *97*, 477-482.
- (47) Pearce, L. L.; Wasserloos, K.; St. Croix, C. M.; Gandley, R.; Levitan, E. S.; Pitt, B. R. *J. Nutr.* **2000**, *130*, 1467S-1470S.
- (48) Spahl, D. U.; Berendji-Grün, D.; Suschek, C. V.; Kolb-Bachofen, V.; Kröncke, K.-D. *Proc. Natl. Acad. Sci. USA* **2003**, *100*, 13952-13957.
- (49) St. Croix, C. M.; Leelavaninchkul, K.; Watkins, S. C.; Kagan, V. E.; Pitt, B. R. *Proc. Am. Thorac. Soc.* **2005**, *2*, 236-242.
- (50) St. Croix, C. M.; Wasserloos, K. J.; Dineley, K. E.; Reynolds, I. J.; Levitan, E. S.; Pitt, B. R. *American Journal of Physiology: Lung Cellular and Molecular Physiology* **2002**, *282*, L185-L192.
- (51) Wang, H.; Li, H.; Cai, B.; Huang, Z. X.; Sun, H. *J. Biol. Inorg. Chem.* **2008**, *13*, 411-419.
- (52) Zangger, K.; Öz, G.; Haslinger, E.; Kunert, O.; Armitage, I. M. *FASEB J.* **2001**, *15*, 1303-1305.
- (53) Zhu, J.; Meeusen, J.; Krezoski, S.; Petering, D. H. *Chem. Res. Toxicol.* **2010**, *23*, 422-431.
- (54) Dudev, T.; Lin; Dudev, M.; Lim, C. *J. Am. Chem. Soc.* **2003**, *125*, 3168-3180.
- (55) Karlin, S.; Zhu, Z.-Y. *Proc. Natl. Acad. Sci. USA* **1997**, *94*, 14231-14236.
- (56) Maret, W. *Antioxid. Redox Signal.* **2006**, *8*, 1419-1441.
- (57) Maret, W.; Li, Y. *Chem. Rev.* **2009**, *109*, 4682-4707.
- (58) Parkin, G. *Chem. Rev.* **2004**, *104*, 699-768.
- (59) Vallee, B. L.; Auld, D. S. *FEBS Lett.* **1989**, *257*, 138-140.
- (60) Brouwer, M.; Chamulitrat, W.; Ferruzzi, G.; Sauls, D. L.; Weinberg, J. B. *Blood* **1996**, *88*, 1857-1864.
- (61) Brown, K. L. *Chem. Rev.* **2005**, *105*, 2075-2150.
- (62) Danishpajooh, I. O.; Gudi, T.; Chen, Y.; Kharitonov, V. G.; Sharma, V. S.; Boss, G. R. *J. Biol. Chem.* **2001**, *276*, 27296-27303.

- (63) Jenkinson, K. M.; Reid, J. J.; Rand, M. J. *Eur. J. Pharmacol.* **1995**, *275*, 145-152.
- (64) Li, C. G.; Rand, M. J. *Clin. Exp. Pharmacol. Physiol.* **1993**, *20*, 633-640.
- (65) Nicolaou, A.; Kenyon, S. H.; Gibbons, J. M.; Ast, T.; Gibbons, W. A. *Eur. J. Clin. Invest.* **1996**, *26*, 167-170.
- (66) Nicolaou, A.; Waterfield, C. J.; Kenyon, S. H.; Gibbons, W. A. *Eur. J. Biochem.* **1997**, *244*, 876-882.
- (67) Rajanayagam, M. A.; Li, C. G.; Rand, M. J. *Br. J. Pharmacol.* **1993**, *108*, 3-5.
- (68) Rand, M. J.; Li, C. G. *Eur. J. Pharmacol.* **1993**, *241*, 249-254.
- (69) Rochelle, L. G.; Morana, S. J.; Kruszyna, H.; Russell, M. A.; Wilcox, D. E.; Smith, R. P. *J. Pharmacol. Exp. Ther.* **1995**, *275*, 48-52.
- (70) Brecht, D. S.; Snyder, S. H. *Annu. Rev. Biochem.* **1994**, *63*, 175-195.
- (71) Butler, A. R.; Flitney, F. W.; Williams, D. L. H. *Trends Pharmacol. Sci.* **1995**, *16*, 18-22.
- (72) Butler, A. R.; Megson, I. L. *Chem. Rev.* **2002**, *102*, 1155-1166.
- (73) Clarke, M.; Gaul, J.; Springer Berlin / Heidelberg: 1993; Vol. 81, p 147-181.
- (74) McCleverty, J. A. *Chem. Rev.* **2004**, *104*, 403-418.
- (75) Tonzetich, Z. J.; McQuade, L. E.; Lippard, S. J. *Inorg. Chem.* **2010**, *49*, 6338-6348.
- (76) Williams, R. J. P. *Chem. Soc. Rev.* **1996**, *25*, 77-83.
- (77) Yonetani, T.; Tsuneshige, A.; Zhou, Y.; Chen, X. *J. Biol. Chem.* **1998**, *273*, 20323-20333.
- (78) Yonetani, T.; Yamamoto, H.; Erman, J. E.; Leigh, J. S.; Reed, G. H. *J. Biol. Chem.* **1972**, *247*, 2447-2455.
- (79) Walker, F. A. *J. Inorg. Biochem.* **2005**, *99*, 216-236.
- (80) Hickok, J. R.; Sahni, S.; Shen, H.; Arvind, A.; Antoniou, C.; Fung, L. W. M.; Thomas, D. D. *Free Radical Biol. Med.* **2011**, *51*, 1558-1566.
- (81) Toledo, J. C.; Bosworth, C. A.; Hennon, S. W.; Mahtani, H. A.; Bergonia, H. A.; Lancaster, J. R. *J. Biol. Chem.* **2008**, *283*, 28926-28933.
- (82) Cheng, L.; Richter-Addo, G. B. In *The Porphyrin Handbook*; Kadish, K. M., Smith, K. M., Guilard, R., Eds.; Academic Press, Inc.: San Diego, CA, 2000; Vol. 4.
- (83) Richter-Addo, G. B.; Legzdins, P. In *Metal Nitrosyls*; Oxford University Press, Inc.: New York, NY, 1992.
- (84) Moncada, S.; Palmer, R. M. J.; Higgs, E. A. *Pharmacol. Rev.* **1991**, *43*, 109-142.
- (85) Lehninger, A. L.; Nelson, D. L.; Cox, M. M. *Lehninger Principles of Biochemistry*; 4 ed.; W. H. Freeman & Co., 2004.
- (86) Nathan, C.; Xie, Q.-w. *Cell* **1994**, *78*, 915-918.
- (87) Ghosh, D. K.; Stuehr, D. J. *Biochemistry* **1995**, *34*, 801-807.
- (88) Roman, L. J.; Martasek, P.; Masters, B. S. S. *Chem. Rev.* **2002**, *102*, 1179 - 1189.
- (89) Stuehr, D. J. *Biochim. Biophys. Acta* **1999**, *1411*, 217 - 230.
- (90) Crane, B. R.; Rosenfeld, R. J.; Arvai, A. S.; Ghosh, D. K.; Ghosh, S.; Tainer, J. A.; Stuehr, D. J.; Getzoff, E. D. *EMBO J.* **1999**, *18*, 6271-6281.
- (91) Ghosh, D. K.; Wu, C.; Pitters, E.; Moloney, M.; Werner, E. R.; Mayer, B.; Stuehr, D. J. *Biochemistry* **1997**, *36*, 10609-10619.
- (92) Daiber, A.; Frein, D.; Namgaladze, D.; Ullrich, V. *J. Biol. Chem.* **2002**, M111988200.
- (93) Gergel, D.; Cederbaum, A. I. *Biochemistry* **1996**, *35*, 16186-16194.
- (94) Cuajungco, M. P.; Lees, G. J. *Brain Res.* **1998**, *799*, 118-129.

- (95) Kröncke, K. D.; Fehsel, K.; Schmidt, T.; Zenke, F. T.; Dasting, I.; Wesener, J. R.; Bettermann, H.; Breunig, K. D.; Kolb-Bachofen, V. *Biochem. Biophys. Res. Commun.* **1994**, *200*, 1105-1110.
- (96) Kröncke, K.-D.; Klotz, L.-O.; Suschek, C. V.; Sies, H. *J. Biol. Chem.* **2002**, *277*, 13294-13301.
- (97) Ogra, Y.; Onishi, S.; Kajiwara, A.; Hara, A.; Suzuki, K. T. *J. Health Sci.* **2008**, *54*, 339-342.
- (98) Kröncke, K. D.; Kolb-Bachofen, V. In *Methods Enzymol.*; Lester, P., Ed.; Academic Press: 1999; Vol. 301, p 126-135.
- (99) Kröncke, K.-D.; Carlberg, C. *FASEB J.* **2000**, *14*, 166-173.
- (100) Williams, D. L. H. *Chem. Soc. Rev.* **1985**, *14*, 171-196.
- (101) Baciú, C.; Cho, K.-B.; Gault, J. W. *J. Phys. Chem. B* **2005**, *109*, 1334-1336.
- (102) Stubauer, G.; Giuffrè, A.; Sarti, P. *J. Biol. Chem.* **1999**, *274*, 28128-28133.
- (103) Williams, D. L. H. *Chem. Commun.* **1996**, 1085-1091.
- (104) Harrop, T. C.; Tonzetich, Z. J.; Reisner, E.; Lippard, S. J. *J. Am. Chem. Soc.* **2008**, *130*, 15602-15610.
- (105) Szaciłowski, K.; Chmura, A.; Stasicka, Z. *Coord. Chem. Rev.* **2005**, *249*, 2408-2436.
- (106) Vanin, A. F.; Papina, A. A.; Serezhenkov, V. A.; Koppenol, W. H. *Nitric Oxide* **2004**, *10*, 60-73.
- (107) Perissinotti, L. L.; Estrin, D. A.; Leitus, G.; Doctorovich, F. *J. Am. Chem. Soc.* **2006**, *128*, 2512-2513.
- (108) Perissinotti, L. L.; Leitus, G.; Shimon, L.; Estrin, D.; Doctorovich, F. *Inorg. Chem.* **2008**, *47*, 4723-4733.
- (109) Lee, J.; Chen, L.; West, A. H.; Richter-Addo, G. B. *Chem. Rev.* **2002**, *102*, 1019-1066.
- (110) Varonka, M. S.; Warren, T. H. *Inorg. Chem.* **2009**, *48*, 5605-5607.
- (111) Andersen, R. J.; diTargiani, R. C.; Hancock, R. D.; Stern, C. L.; Goldberg, D. P.; Godwin, H. A. *Inorg. Chem.* **2006**, *45*, 6574-6576.
- (112) Brinkerhoff, C. J.; Podsiadlo, P.; Komiyama, T.; Fuller, R. S.; Blum, O. *ChemBioChem* **2002**, *3*, 1141-1143.
- (113) Chang, S.; Karambelkar, V. V.; diTargiani, R. C.; Goldberg, D. P. *Inorg. Chem.* **2001**, *40*, 194-195.
- (114) Chang, S.; Karambelkar, V. V.; Sommer, R. D.; Rheingold, A. L.; Goldberg, D. P. *Inorg. Chem.* **2002**, *41*, 239-248.
- (115) Chang, S.; Sommer, R. D.; Rheingold, A. L.; Goldberg, D. P. *Chem. Commun.* **2001**, 2396-2397.
- (116) diTargiani, R. C.; Chang, S.; Salter, M. H.; Hancock, R. D.; Goldberg, D. P. *Inorg. Chem.* **2003**, *42*, 5825-5836.
- (117) Ji, M.; Vahrenkamp, H. *Eur. J. Inorg. Chem.* **2005**, *2005*, 1398-1405.
- (118) Karambelkar, V. V.; Xiao, C.; Zhang, Y.; Narducci Sarjeant, A. A.; Goldberg, D. P. *Inorg. Chem.* **2006**, *45*, 1409-1411.
- (119) Imajo, S.; Nakanishi, K.; Roberts, M.; Lippard, S. J.; Nozoe, T. *J. Am. Chem. Soc.* **1983**, *105*, 2071-2073.
- (120) Villacorta, G. M.; Lippard, S. J. *Pure Appl. Chem.* **1986**, *58*, 1474 - 1477.
- (121) Zask, A.; Gonnella, N.; Nakanishi, K.; Turner, C. J.; Imajo, S.; Nozoe, T. *Inorg. Chem.* **1986**, *25*, 3400-3407.
- (122) Jaynes, B. S.; Doerrler, L. H.; Liu, S.; Lippard, S. J. *Inorg. Chem.* **1995**, *34*, 5735-5744.

- (123) Doerrler, L. H.; Lippard, S. J. *Inorg. Chem.* **1997**, *36*, 2554-2563.
- (124) Banerjee, R.; Ragsdale, S. W. *Annu. Rev. Biochem.* **2003**, *72*, 209-247.
- (125) Suarez-Moreira, E.; Hannibal, L.; Smith, C. A.; Chavez, R. A.; Jacobsen, D. W.; Brasch, N. E. *Dalton Trans.* **2006**, 5269-5277.
- (126) Ragsdale, S. W. *Chem. Rev.* **2006**, *106*, 3317-3337.
- (127) Kräutler, B. *Biochem. Soc. Trans.* **2005**, *33*, 806-810.
- (128) Butler, P.; Kräutler, B. In *Bioorganometallic Chemistry*; Simonneaux, G., Ed.; Springer Berlin / Heidelberg: 2006; Vol. 17, p 1-55.
- (129) Kräutler, B. In *Metal Ions in Life Sciences*; Sigel, A., Sigel, H., Sigel, R. K. O., Eds. 2009; Vol. 6, p 1-51.
- (130) Pezacka, E.; Green, R.; Jacobsen, D. W. *Biochem. Biophys. Res. Commun.* **1990**, *169*, 443-450.
- (131) Linnell, J. C.; Smith, A. D.; Smith, C. L.; Wilson, J.; Matthews, D. M. *Br. Med. J.* **1968**, *2*, 215-216.
- (132) Rickes, E. L.; Brink, N. G.; Koniuszy, F. R.; Wood, T. R.; Folkers, K. *Science* **1948**, *107*, 396-397.
- (133) Smith, E. L. *Nature* **1948**, *162*, 144-145.
- (134) Smith, E. L. *Nature* **1948**, *161*, 638-639.
- (135) Hannibal, L.; Smith, C. A.; Jacobsen, D. W.; Brasch, N. E. *Angew. Chem. Int. Ed.* **2007**, *46*, 5140-5143.
- (136) Hassanin, H. A.; Hannibal, L.; Jacobsen, D. W.; Brown, K. L.; Marques, H. M.; Brasch, N. E. *Dalton Trans.* **2009**, 424-433.
- (137) Sharma, V. S.; Pilz, R. B.; Boss, G. R.; Magde, D. *Biochemistry* **2003**, *42*, 8900-8908.
- (138) Wolak, M.; Zahl, A.; Schnepf, T.; Stochel, G.; van Eldik, R. *J. Am. Chem. Soc.* **2001**, *123*, 9780-9791.
- (139) Zheng, D.; Birke, R. L. *J. Am. Chem. Soc.* **2001**, *123*, 4637-4638.
- (140) Wolak, M.; Stochel, G.; Hamza, M.; van Eldik, R. *Inorg. Chem.* **2000**, *39*, 2018-2019.
- (141) Zheng, D.; Yan, L.; Birke, R. L. *Inorg. Chem.* **2002**, *41*, 2548-2555.
- (142) Vilakazi, S. L.; Nyokong, T. *Electrochim. Acta* **2000**, *46*, 453-461.
- (143) Selçuki, C.; van Eldik, R.; Clark, T. *Inorg. Chem.* **2004**, *43*, 2828-2833.
- (144) Franke, A.; Roncaroli, F.; van Eldik, R. *Eur. J. Inorg. Chem.* **2007**, *2007*, 773-798.
- (145) Zheng, D.; Birke, R. L. *J. Am. Chem. Soc.* **2002**, *124*, 9066-9067.
- (146) Lippard, S. J.; Berg, J. M. *Principles of Bioinorganic Chemistry*; University Science Books: Mill Valley, CA, 1994.
- (147) Vallee, B. L.; Williams, R. J. P. *Proc. Natl. Acad. Sci. USA* **1968**, *59*, 498-505.
- (148) Solomon, E. I.; LaCroix, L. B.; Randall, D. W. *Pure Appl. Chem.* **1998**, *70*, 799-808.
- (149) Holm, R. H.; Kennepohl, P.; Solomon, E. I. *Chem. Rev.* **1996**, *96*, 2239-2314.
- (150) Comba, P. *Coord. Chem. Rev.* **2000**, *200-202*, 217-245.
- (151) Gray, H. B.; Malmström, B. G.; Williams, R. J. P. *J. Biol. Inorg. Chem.* **2000**, *5*, 551-559.
- (152) Comba, P.; Schiek, W. *Coord. Chem. Rev.* **2003**, *238-239*, 21-29.
- (153) Andrew, C. R.; Lappalainen, P.; Saraste, M.; Hay, M. T.; Lu, Y.; Dennison, C.; Canters, G. W.; Fee, J. A.; Nakamura, N.; Sanders-Loehr, J. *J. Am. Chem. Soc.* **1995**, *117*, 10759-10760.
- (154) Clark, K. M.; Yu, Y.; Marshall, N. M.; Sieracki, N. A.; Nilges, M. J.; Blackburn, N. J.; van der Donk, W. A.; Lu, Y. *J. Am. Chem. Soc.* **2010**, *132*, 10093-10101.

- (155) Hwang, H. J.; Berry, S. M.; Nilges, M. J.; Lu, Y. *J. Am. Chem. Soc.* **2005**, *127*, 7274-7275.
- (156) Marshall, N. M.; Garner, D. K.; Wilson, T. D.; Gao, Y.-G.; Robinson, H.; Nilges, M. J.; Lu, Y. *Nature* **2009**, *462*, 113-116.
- (157) Ralle, M.; Berry, S. M.; Nilges, M. J.; Gieselmann, M. D.; van der Donk, W. A.; Lu, Y.; Blackburn, N. J. *J. Am. Chem. Soc.* **2004**, *126*, 7244-7256.
- (158) Savelieff, M. G.; Wilson, T. D.; Elias, Y.; Nilges, M. J.; Garner, D. K.; Lu, Y. *Proc. Natl. Acad. Sci. USA* **2008**, *105*, 7919-7924.
- (159) Wilson, T. D.; Savelieff, M. G.; Nilges, M. J.; Marshall, N. M.; Lu, Y. *J. Am. Chem. Soc.* **2011**, *133*, 20778-20792.
- (160) Darensbourg, M. Y.; Lyon, E. J.; Zhao, X.; Georgakaki, I. P. *Proc. Natl. Acad. Sci. USA* **2003**, *100*, 3683-3688.
- (161) Georgakaki, I. P.; Thomson, L. M.; Lyon, E. J.; Hall, M. B.; Darensbourg, M. Y. *Coord. Chem. Rev.* **2003**, *238-239*, 255-266.
- (162) Bergman, T.; Zhang, K.; Palmberg, C.; Jörnvall, H.; Auld, D. *Cell. Mol. Life Sci.* **2008**, *65*, 4019-4027.
- (163) Ma, S.; Yuan, D.; Chang, J.-S.; Zhou, H.-C. *Inorg. Chem.* **2009**, *48*, 5398-5402.
- (164) Ma, S.; Zhou, H.-C. *J. Am. Chem. Soc.* **2006**, *128*, 11734-11735.
- (165) Tonigold, M.; Lu, Y.; Mavrandonakis, A.; Puls, A.; Staudt, R.; Möllmer, J.; Sauer, J.; Volkmer, D. *Chem. Eur. J.* **2011**, *17*, 8671-8695.
- (166) Nozoe, T.; Okai, H.; Someya, T. *Bull. Chem. Soc. Jpn.* **1978**, *51*, 2185-2186.
- (167) Shindo, K.; Wakabayashi, H.; Ishikawa, S.; Nozoe, T. *Bull. Chem. Soc. Jpn.* **1993**, *66*, 2941-2948.
- (168) Minns, R. A. *Org. Synth.* **1977**, *57*, 1117.
- (169) Franz, K. J.; Lippard, S. J. *J. Am. Chem. Soc.* **1998**, *120*, 9034-9040.
- (170) Franz, K. J.; Lippard, S. J. *Inorg. Chem.* **2000**, *39*, 3722-3723.
- (171) Tangen, E.; Conradie, J.; Franz, K.; Friedle, S.; Telsler, J.; Lippard, S. J.; Ghosh, A. *Inorg. Chem.* **2010**, *49*, 2701-2705.
- (172) Franz, K. J.; Lippard, S. J. *J. Am. Chem. Soc.* **1999**, *121*, 10504-10512.
- (173) Tangen, E.; Conradie, J.; Ghosh, A. *Inorg. Chem.* **2005**, *44*, 8699-8706.
- (174) Jaynes, B. S.; Ren, T.; Liu, S.; Lippard, S. J. *J. Am. Chem. Soc.* **1992**, *114*, 9670-9671.
- (175) Jaynes, B. S.; Ren, T.; Masschelein, A.; Lippard, S. J. *J. Am. Chem. Soc.* **1993**, *115*, 5589-5599.
- (176) Franz, K. J.; Doerrler, L. H.; Spingler, B.; Lippard, S. J. *Inorg. Chem.* **2001**, *40*, 3774-3780.
- (177) Doerrler, L. H.; Bautista, M. T.; Lippard, S. J. *Inorg. Chem.* **1997**, *36*, 3578-3579.
- (178) Davis, W. M.; Roberts, M. M.; Zask, A.; Nakanishi, K.; Nozoe, T.; Lippard, S. J. *J. Am. Chem. Soc.* **1985**, *107*, 3864-3870.
- (179) Davis, W. M.; Lippard, S. J. *Inorg. Chem.* **1985**, *24*, 3688-3691.
- (180) Davis, W. M.; Zask, A.; Nakanishi, K.; Lippard, S. J. *Inorg. Chem.* **1985**, *24*, 3737-3743.
- (181) Villacorta, G. M.; Gibson, D.; Williams, I. D.; Lippard, S. J. *J. Am. Chem. Soc.* **1985**, *107*, 6732-6734.
- (182) Villacorta, G. M.; Gibson, D.; Williams, I. D.; Whang, E.; Lippard, S. J. *Organometallics* **1987**, *6*, 2426-2431.
- (183) Villacorta, G. M.; Lippard, S. J. *Inorg. Chem.* **1987**, *26*, 3672-3676.
- (184) Villacorta, G. M.; Rao, C. P.; Lippard, S. J. *J. Am. Chem. Soc.* **1988**, *110*, 3175-3182.



- (185) Scott, M. J.; Lippard, S. J. *J. Am. Chem. Soc.* **1997**, *119*, 3411-3412.
- (186) Scott, M. J.; Lippard, S. J. *Organometallics* **1997**, *16*, 5857-5868.
- (187) Scott, M. J.; Lippard, S. J. *Inorg. Chim. Acta* **1997**, *263*, 287-299.
- (188) Scott, M. J.; Lippard, S. J. *Organometallics* **1998**, *17*, 1769-1773.
- (189) Villacorta, G. M.; Lippard, S. J. *Inorg. Chem.* **1988**, *27*, 144-149.
- (190) Scott, M. J.; Lippard, S. J. *Organometallics* **1998**, *17*, 466-474.
- (191) Greenwood, N. N.; Earnshaw, A. *Chemistry of the Elements*; Pergamon Press Ltd.: Oxford, England, 1984.
- (192) Franz, K. J.; Singh, N.; Lippard, S. J. *Angew. Chem. Int. Ed.* **2000**, *39*, 2120-2122.
- (193) Franz, K. J.; Singh, N.; Spingler, B.; Lippard, S. J. *Inorg. Chem.* **2000**, *39*, 4081-4092.
- (194) Lim, M. H.; Kuang, C.; Lippard, S. J. *ChemBioChem* **2006**, *7*, 1571-1576.
- (195) Hilderbrand, S. A.; Lippard, S. J. *Inorg. Chem.* **2004**, *43*, 4674-4682.
- (196) Byrne, E. K.; Theopold, K. H. *J. Am. Chem. Soc.* **1987**, *109*, 1282-1283.
- (197) Byrne, E. K.; Theopold, K. H. *J. Am. Chem. Soc.* **1989**, *111*, 3887-3896.
- (198) Cowley, R. E.; Bontchev, R. P.; Sorrell, J.; Sarracino, O.; Feng, Y.; Wang, H.; Smith, J. M. *J. Am. Chem. Soc.* **2007**, *129*, 2424-2425.
- (199) Hu, X.; Meyer, K. *J. Am. Chem. Soc.* **2004**, *126*, 16322-16323.
- (200) Jenkins, D. M.; Betley, T. A.; Peters, J. C. *J. Am. Chem. Soc.* **2002**, *124*, 11238-11239.
- (201) Mehn, M. P.; Brown, S. D.; Jenkins, D. M.; Peters, J. C.; Que, L. *Inorg. Chem.* **2006**, *45*, 7417-7427.
- (202) Shay, D. T.; Yap, G. P. A.; Zakharov, L. N.; Rheingold, A. L.; Theopold, K. H. *Angew. Chem. Int. Ed.* **2005**, *44*, 1508-1510.
- (203) Wasbotten, I. H.; Ghosh, A. *Inorg. Chem.* **2007**, *46*, 7890-7898.
- (204) Albright, T. A.; Burdett, J. K.; Whangbo, M.-H. *Orbital Interactions in Chemistry*; John Wiley & Sons: New York, NY, 1985.

# **Chapter 2. Zinc Thiolate Reactivity toward Nitrogen Oxides: Insights into the Interaction of $Zn^{2+}$ with *S*-Nitrosothiols and Implications for Nitric Oxide Synthase**

*The work presented in this Chapter has been submitted for publication:*

Kozhukh, J.; Lippard, S.J. *Inorg. Chem.* Submitted.

## 2.1. Introduction

Nitric oxide (NO) contributes to the functions of the immune, circulatory, and nervous systems. NO may induce a physiological response directly, as in the case of NO release by macrophages as part of the immune response, or may serve the role of a signaling molecule by activating downstream pathways.<sup>1</sup> One target of NO-derived species, such as NO<sub>2</sub>, N<sub>2</sub>O<sub>3</sub>, and *S*-nitrosothiols, is the metallothionein family of proteins.<sup>2-20</sup> These cysteine-rich proteins bind Zn<sup>2+</sup> in an assortment of coordination environments.<sup>10,21-25</sup> *S*-nitros(yl)ation of the zinc thiolate sites by aerobic NO and some biologically relevant *S*-nitrosothiols causes demetallation.<sup>2-20</sup> The Zn<sup>2+</sup> that is released upon *S*-nitros(yl)ation continues a signaling cascade, and ultimately may mediate effects that range from vasodilation<sup>4,11,14,16-17,26</sup> to regulation of transcription factors.<sup>8,10-11,15,27-31</sup>

A similar labilization of coordinated Zn<sup>2+</sup> occurs in nitric oxide synthases (NOSs). The functional NOS homodimer employs NO-mediated feedback inhibition.<sup>32-34</sup> In the presence of high concentrations of NO, which is usually produced endogenously by the NOS itself, NO-derived RNOS may react with a zinc tetracysteine thiolate site that exists at the interface of the two NOS monomer units. The reaction with RNOS results in *S*-nitrosylation and concomitant loss of Zn<sup>2+</sup> due to demetallation.<sup>32-38</sup>

The work described in this Chapter explores the reactivity of tightly bound zinc thiolates toward reactive nitrogen species. This work was inspired by the aforementioned studies of NOS, metallothioneins, and transcription factors possessing zinc finger domains with NO, which expose a need to uncover principles that underlie the chemistry of NO-containing compounds with zinc cysteine thiolates. Although many of the relevant biological targets of NO contain polythiolate zinc centers, we restrict our studies to zinc complexes containing a single thiolate ligand in order to interrogate a unique site.

We selected for study the previously described ligand PAtH,<sup>39-41</sup> and an alkyl analog APAtH (Chart 2.1) to generate mononuclear zinc thiolates. Geminal dimethyl groups at the *ipso* carbon provide steric bulk at the sulfur atom, blocking formation of thiolate-bridged metal dimers or oligomers. In addition, *gem*-dimethyl groups may stabilize tertiary *S*-nitrosothiol species that can form upon exposure of the zinc thiolates to RNOS.<sup>42</sup> The tridentate coordination mode of the PAtH and APAtH ligands assures tight binding of zinc,<sup>41,43</sup> a feature that favors its retention following exposure to RNOS and facilitates analysis of the products of zinc/*S*-nitrosothiol reactions. We herein describe the preparation and characterization of the desired zinc thiolates and their reactivity toward biologically relevant nitrogen oxides, specifically NO, NO<sup>+</sup>, and NO<sub>2</sub>. Reactions of zinc salts with pre-formed *S*-nitrosothiols are also presented.

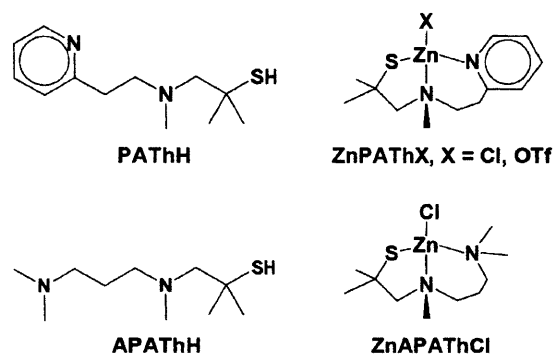


**Chart 2.1.** *N*<sub>2</sub>*S* tridentate chelating ligands and the related Zn<sup>2+</sup> coordination compounds.

## 2.2. Experimental Methods

**General Procedures and Starting Materials.** Air- and moisture-sensitive materials were handled in an MBraun glovebox under a nitrogen atmosphere. 2-(2-Methylaminoethyl)-pyridine and *N,N,N'*-trimethyl-1,3-propanediamine were purchased from Sigma-Aldrich and used without further purification. Nitrosonium tetrafluoroborate (97%) was obtained from Strem and used as received. Isobutylene sulfide<sup>44</sup> and trityl *S*-nitrosothiol<sup>45</sup> were prepared according to published

methods. PAtH was synthesized as described<sup>39-40</sup> and purified by Al<sub>2</sub>O<sub>3</sub> column chromatography using 2:1 ethyl acetate: pentane to give the desired product as a colorless oil. [ZnPAtHCl] was prepared by a method analogous to the published procedure and characterized by <sup>1</sup>H and <sup>13</sup>C NMR spectroscopy, as well as X-ray crystallography.<sup>46</sup> Nitric oxide was obtained from Airgas and purified according to published methods.<sup>45,47</sup> Briefly, NO was passed through an Ascarite column and a 6 ft coil containing silica gel at -78 °C to remove impurities, and NO was then collected and stored under nitrogen in a gas storage bulb. N<sub>2</sub>O<sub>4</sub> was obtained from Sigma-Aldrich and collected in a gas bulb under nitrogen. Purification by successive freeze-pump-thaw steps at -78 °C facilitated the removal of NO<sub>2</sub>, N<sub>2</sub>O and N<sub>2</sub>O<sub>3</sub> impurities. Na<sup>15</sup>NO<sub>2</sub> was purchased from Cambridge Isotope Laboratories and used without purification. *n*-Butanol was obtained from Alfa Aesar and also used as received. *n*-Butyl nitrite was prepared by modification of a published procedure,<sup>48</sup> in which the reaction scale was 1/40<sup>th</sup> the size of that reported. PAtH<sup>15</sup>NO was prepared in a manner analogous to that reported for PAtHNO below, using <sup>15</sup>N *n*-butyl nitrite to nitrosate the thiol. All gas transfers were performed using gas-tight syringes under an inert atmosphere, unless otherwise noted. Acetonitrile (MeCN), tetrahydrofuran (THF), methylene chloride (DCM), pentane, and diethyl ether were saturated with argon, purified by passage through activated alumina, and stored over 4 Å molecular sieves under a nitrogen atmosphere prior to use. Deuterated NMR solvents were obtained from Cambridge Isotope Laboratories and used without further purification. Acetonitrile-*d*<sub>3</sub> and methylene chloride-*d*<sub>2</sub> were brought into the glovebox and stored over 4 Å molecular sieves under a nitrogen atmosphere. CHN analyses were performed by Intertek-QTI (Whitehouse, NJ, USA) and Midwest Microlab, LLC (Indianapolis, IN, USA).

**Synthesis of [ZnPAThOTf].** To a solution of [ZnPAThCl] (1.0 g, 3.1 mmol, 1 equiv) in ~10 mL of acetonitrile was added thallium triflate (1.10 g, 3.11 mmol, 1 equiv). The resultant suspension was allowed to stir overnight, after which the reaction mixture was filtered. The solvent was removed from the filtrate and the solid was washed with diethyl ether. The material was dried under vacuum, yielding 0.499 g (36.6%) of the desired product as an off-white powder.  $^1\text{H}$  NMR (MeCN- $d_3$ )  $\delta$  1.32 (s, 3H,  $\text{CH}_3$ ), 1.52 (s, 3H,  $\text{CH}_3$ ), 2.64 (d,  $J = 13.4$  Hz, 1H,  $\text{CH}_2$ ), 2.73 (s, 3H,  $\text{CH}_3$ ), 2.89 (d,  $J = 13.4$  Hz, 1H,  $\text{CH}_2$ ), 2.95 – 3.26 (m, 4H,  $\text{CH}_2$ ), 7.52 – 7.56 (m, 2H, py- $H_\beta$  + py- $H_\delta$ ), 8.05 (td,  $J = 8$  Hz, 1.2 Hz, 1H, py- $H_\gamma$ ), 8.50 (d,  $J = 4.8$  Hz, 1H, py- $H_\epsilon$ ).  $^{13}\text{C}$  NMR (MeCN- $d_3$ )  $\delta$  33.39, 33.89, 34.99, 49.14, 49.92, 60.67, 73.89, 125.31, 127.45, 142.97, 150.06, 161.65.  $^{19}\text{F}$  NMR (MeCN- $d_3$ )  $\delta$  -79.41. IR (MeCN,  $\text{cm}^{-1}$ ) 1612, 1571, 1271. Anal. Calc'd. for  $\text{C}_{13}\text{H}_{19}\text{F}_3\text{N}_2\text{O}_3\text{S}_2\text{Zn}$ : C, 35.66; H, 4.37; N, 6.40. Found: C, 35.33; H, 4.23; N, 6.42.

**Synthesis of PAThNO.** To a solution of PAThH (1.0 g, 4.5 mmol, 1 equiv) in methylene chloride (~10 mL) was added *iso*-amyl nitrite (0.6 mL, 4.5 mmol, 1 equiv). The reaction mixture was allowed to stir overnight in the dark and the solvent was removed. Silica gel chromatography (1:1 ethyl acetate: pentane) allowed isolation of the pure product as a dark-green oil (0.518 g, 45.9%). Care was taken to minimize exposure of the reaction mixture and product to light.  $^1\text{H}$  NMR (MeCN- $d_3$ )  $\delta$  1.80 (s, 6H,  $\text{CH}_3$ ), 2.40 (s, 3H,  $\text{CH}_3$ ), 2.87 (s, 4H,  $\text{CH}_2$ ), (s, 2H,  $\text{CH}_2$ ), 7.10 – 7.14 (m, 1H, py- $H_\beta$ ), 7.18 (d,  $J = 8.8$  Hz, 1H, py- $H_\delta$ ), 7.60 (t,  $J = 5.6$  Hz, 1H, py- $H_\gamma$ ), 8.44 (d,  $J = 4.8$  Hz, 1H, py- $H_\epsilon$ ).  $^{13}\text{C}$  NMR (MeCN- $d_3$ )  $\delta$  27.32, 36.83, 44.83, 60.41, 60.98, 69.01, 122.08, 124.27, 137.07, 150.05, 161.43. IR (MeCN- $d_3$ ,  $\text{cm}^{-1}$ ) 1591, 1569, 1484, 1476. Anal. Calc'd. for  $\text{C}_{12}\text{H}_{19}\text{N}_3\text{OS}$ : C, 56.89; H, 7.56; N, 16.58. Found: C, 57.01; H, 7.39; N, 16.48.

**Synthesis of PAtH<sub>2</sub>.** Sodium hydride (0.214 g, 8.92 mmol, 1 equiv) was added as a solid to a solution of PAtH (2.0 g, 8.9 mmol, 1 equiv) in ~40 mL of tetrahydrofuran and the mixture was allowed to stir overnight. The resulting suspension was left to stand at -30 °C to precipitate unreacted NaH. The solution was decanted by pipette into an aluminum foil-covered flask and iodine (1.36 g, 5.35 mmol, 0.65 equiv) was added to the stirring solution. After 24 h of stirring the solvent was removed and the oily residue was partitioned between diethyl ether and saturated an aqueous sodium thiosulfate solution. The desired product was extracted into the ether layer and the organics were washed with water and dried (MgSO<sub>4</sub>). The solvent was removed to yield the desired product as a viscous, bright yellow oil (1.38 g, 69.2%). <sup>1</sup>H NMR (CD<sub>2</sub>Cl<sub>2</sub>) δ 1.18 (s, 12H, CH<sub>3</sub>), 2.40 (s, 6H, CH<sub>3</sub>), 2.47 (s, 4H, CH<sub>2</sub>), 2.81 – 2.85 (m, 4H, CH<sub>2</sub>), 2.88 – 2.92 (m, 4H, CH<sub>2</sub>), 7.08 (dd, *J* = 7.2 Hz, 5.6 Hz, 1H, py-*H*<sub>β</sub>), 7.17 (d, *J* = 8.0 Hz, 1H, py-*H*<sub>δ</sub>), 7.53 – 7.61 (m, 1H, py-*H*<sub>γ</sub>), 8.47 (d, *J* = 4.8 Hz, 1H, py-*H*<sub>ε</sub>). <sup>13</sup>C NMR (CD<sub>2</sub>Cl<sub>2</sub>) δ 26.52, 36.83, 45.02, 51.53, 60.84, 68.70, 121.44, 123.74, 136.47, 149.64, 161.26. IR (MeCN-*d*<sub>3</sub>, cm<sup>-1</sup>) 1591, 1569, 1475, 1463, 1436. Anal. Calc'd for C<sub>24</sub>H<sub>38</sub>N<sub>4</sub>S<sub>2</sub>: C, 64.53; H, 8.57; N, 12.54. Found: C, 64.58; H, 8.70; N, 12.58.

**Synthesis of APAtH.** To a stirring solution of *N,N,N'*-trimethyl-1,3-propanediamine (10 g, 86 mmol, 1 equiv) in approximately 500 mL of MeCN was added dropwise a solution of isobutylene sulfide (10.2 mL, 103 mmol, 1.2 equiv) in 100 mL MeCN at room temperature. The reaction mixture was heated to 45 °C for 16.5 h. The solvent was removed in vacuo and the residue was purified by column chromatography (Al<sub>2</sub>O<sub>3</sub>, 2:1 pentane: EtOAc, *R*<sub>f</sub> ~ 0.55) to yield the desired product as a colorless oil (6.31 g, 35.9%). <sup>1</sup>H NMR (MeCN-*d*<sub>3</sub>) δ 1.28 (s, 6H, CH<sub>3</sub>), 1.55 – 1.62 m, 2H, CH<sub>2</sub>), 2.12 (s, 6H, N-(CH<sub>3</sub>)<sub>2</sub>), 2.24 (t, *J* = 7.2 Hz, 2H, CH<sub>2</sub>), 2.30 (s, 1H, SH), 2.32 (s, 3H, N-CH<sub>3</sub>), 2.40 (s, 2H, CH<sub>2</sub>), 2.50 (t, *J* = 7.2 Hz, 2H, CH<sub>2</sub>). <sup>13</sup>C NMR (MeCN-*d*<sub>3</sub>) δ

26.89, 30.75, 45.10, 45.79, 47.03, 58.20, 59.03, 72.82. IR (MeCN-*d*<sub>3</sub>, cm<sup>-1</sup>) 1463, 1383, 1363.

Anal. Calc'd. for C<sub>10</sub>H<sub>24</sub>N<sub>2</sub>S: C, 58.77; H, 11.84; N, 13.71. Found: C, 58.22; H, 11.41; N, 13.07.

**Synthesis of [ZnAPATHCl].** To a solution of APATHH (1.0 g, 4.9 mmol, 1 equiv) in ~5 mL of tetrahydrofuran was added NaH (0.117 g, 4.89 mmol, 1 equiv) as a solid. The suspension was allowed to stir until all solid material had dissolved and gas evolution ceased. Zinc chloride (0.667 g, 4.89 mmol, 1 equiv) was suspended in 10 mL of tetrahydrofuran and the suspension was added to the deprotonated ligand solution. The reaction was allowed to stir overnight. The solvent was removed in vacuo, the residue was taken up in methylene chloride, and the solution was filtered. Solvent was evaporated from the filtrate and the resulting residue was washed with diethyl ether to remove unreacted ligand. The remaining solid was dried in vacuo, and the product was isolated as a white powder (0.858 g, 57.7%). <sup>1</sup>H NMR (MeCN-*d*<sub>3</sub>) δ 1.39 (d, *J* = 7.6 Hz, 6H, CH<sub>3</sub>), 1.66 – 1.74 (m, 1H, CH<sub>2</sub>), 1.86 – 1.95 (m, 1H, CH<sub>2</sub>), 2.28 (d, *J* = 13.0 Hz, 1H, CH<sub>2</sub>), 2.45 (bs, 6H, N-(CH<sub>3</sub>)<sub>2</sub>), 2.53 (s, 3H, N-CH<sub>3</sub>), 2.61 (d, *J* = 13.0 Hz, 1H, CH<sub>2</sub>), 2.66 – 2.80 (m, 3H, CH<sub>2</sub>), 2.95 – 3.00 (m, 1H, CH<sub>2</sub>). <sup>13</sup>C NMR (MeCN-*d*<sub>3</sub>) δ 22.96, 36.70, 37.23, 45.20, 48.72, 48.98, 49.53, 62.34, 62.83, 73.55. IR (CH<sub>2</sub>Cl<sub>2</sub>, cm<sup>-1</sup>) 1469, 1456. Anal. Calc'd. for C<sub>10</sub>H<sub>23</sub>ClN<sub>2</sub>SZn: C, 39.48; H, 7.62; N, 9.21. Found: C, 37.59; H, 7.22; N, 8.27.

**Synthesis of APATHNO.** APATHH (1.0 g, 4.9 mmol, 1 equiv) and *iso*-amyl nitrite (0.66 mL, 4.9 mmol, 1 equiv) were combined in 10 mL of methylene chloride and the solution was stirred overnight in the dark. The solvent was removed and the green residue was purified by silica gel chromatography (96:4 CH<sub>2</sub>Cl<sub>2</sub>:MeOH). The product was isolated as a dark-green oil (0.668 g, 58.4%). Care was taken to minimize exposure of the reaction mixture and product to light. <sup>1</sup>H NMR (CD<sub>2</sub>Cl<sub>2</sub>) δ 1.55 – 1.62 (m, 2H, CH<sub>2</sub>), 1.88 (s, 6H, CH<sub>3</sub>), 2.20 (s, 6H, N-(CH<sub>3</sub>)<sub>2</sub>), 2.27 (t, *J* = 7.2 Hz, 2H, CH<sub>2</sub>), 2.32 (s, 3H, N-CH<sub>3</sub>), 2.50 (t, *J* = 7.2 Hz, 2H, CH<sub>2</sub>), 3.01 (s, 2H, CH<sub>2</sub>). <sup>13</sup>C



NMR ( $CD_2Cl_2$ )  $\delta$  26.06, 27.51, 44.90, 45.46, 57.72, 58.67, 59.81, 69.41; UV-Vis (MeCN)  $\lambda$  ( $\epsilon$ ) 346 nm (554.1), 556 nm (9.2), 599 nm (16.8). IR ( $CH_2Cl_2$ ,  $cm^{-1}$ ) 1493, 1461, 1382, 1366. Anal. Calc'd. for  $C_{10}H_{23}N_3OS$ : C, 51.47; H, 9.93; N, 18.01. Found: C, 51.76; H, 9.59; N, 18.23.

**Phosphine-Mediated APAThNO Ligation.** *S*-(2-(Diphenylphosphino)phenyl)butanethioate was prepared according to published procedures.<sup>49-50</sup> To [ZnAPAThCl] (50 mg, 0.16 mmol, 1 equiv) in ~15 mL MeCN under a nitrogen atmosphere was added solid  $NOBF_4$  (17 mg, 0.15 mmol, 0.9 equiv). The mixture was allowed to stir for 2 h, at which point the phosphine reagent (120 mg, 0.329 mmol, 2 equiv) was added as a solid. An aliquot of the reaction mixture was immediately analyzed by ESI-MS with anaerobic acetonitrile as the carrier solvent. An  $[M+H]^+$  peak at  $m/z = 582.1$  (calc'd 582.27) was observed for the phosphine-ligated APAThNO.

**Physical Measurements.**  $^1H$  and  $^{13}C$  NMR spectra were recorded on a 400 MHz Bruker Avance spectrometer. Optical spectra were measured on a Varian Cary 50 Bio UV-visible spectrophotometer in 6SQ Starna cells. The Cary WinUV Scanning Kinetics software was used to record optical time-dependent spectra. FT-IR spectra were recorded on a Thermo Nicolet Avatar 360 spectrometer running the OMNIC software package. A  $CaF_2$  cell was used for solution IR spectra. ESI-MS analyses were performed on an Agilent 1100 Series LC/MSD Trap spectrometer. An Agilent Technologies 5975C Mass Selective Detector running in electron impact ionization mode was used for EI-MS studies of the reaction headspace.

**UV-Vis Studies.** All solutions were prepared under a nitrogen atmosphere. Optical spectra were recorded at 25 °C.

*Zinc Thiolate Reactions with NO(g).* Stock solutions of zinc thiolates were prepared at 10 times the desired reaction concentration. A 2.7 mL volume of acetonitrile was transferred to a cuvette and 300  $\mu$ L of the zinc thiolate solution was injected into the cell. The cell was sealed with an

air-tight Teflon cap containing a septum, and 1 mL of headspace was removed from the sealed cuvette by a gas-tight syringe. Nitric oxide (1 mL) was withdrawn from the storage bulb by a gas-tight syringe and the syringe needle was covered with a septum. The syringe and cuvette were removed from the glovebox and the cuvette was transferred to the UV-Vis spectrophotometer. After one optical scan of the zinc thiolate solution, nitric oxide was quickly injected into the cuvette. The cuvette was shaken to mix the reagents and returned to the spectrophotometer. Optical spectra were recorded at regular intervals. For studies with NO + air, a 1 mL volume of air was injected into the reaction cuvette following completion of the NO study, the cuvette was shaken, and the cell was returned to the spectrophotometer. Optical spectra were again recorded at regular intervals. A calculation utilizing Henry's law reveals that the kinetics of the reaction may be dominated by gas transport. The partitioning coefficient for nitric oxide in acetonitrile,  $K_{H,inv}^{px}$ , is 1332 atm.<sup>51</sup>  $K_{H,inv}^{px}$  may be converted to  $K_H^{cp}$  using equation 2.1,<sup>52</sup> where  $\rho$  is the density of acetonitrile and  $M$  is the molar mass of the solvent.  $K_H^{cp}$  is determined to be  $1.44 \times 10^{-2}$  M/atm, and at 1 atm, the concentration of NO in the reaction solution is calculated to be 14.4 mM.

$$K_{H,inv}^{px} = \rho / (M \times K_H^{cp}) \quad (2.1)$$

The concentration of dioxygen in acetonitrile is  $8.1 \times 10^{-3}$  M at 1 atm. We estimate that the pressure in the headspace of the cuvette is 1.5 atm after injection of air. Approximating the composition of air to contain 20% O<sub>2</sub>, we determine the partial pressure of dioxygen in the cuvette to be 0.3 atm, and further calculate the concentration of O<sub>2</sub> in the acetonitrile solution to be 2.43 mM. A Henry's law constant for NO<sub>2</sub> in acetonitrile could not be found in the literature. Reaction concentrations of 14.4 mM and 2.43 mM for NO and O<sub>2</sub>, respectively, are greater than that of 1.5 mM [ZnPAThCl], but dioxygen concentrations are lower than the 7.5 mM

concentrations of the solutions of [ZnPAThOTf] and [ZnAPAThCl]. These reactions are therefore rate-limited by gas transport into solution, and the reactions between zinc thiolates and NO in the presence of air would be expected to occur faster at greater concentrations of O<sub>2</sub> than is observed in this work. Our goal, however, is to determine whether or not nitric oxide may cause S-nitrosothiol formation in the presence or absence of dioxygen, and this objective is achieved effectively with the experimental design described herein.

*Zinc Thiolate Reactions with NOBF<sub>4</sub>.* Stock solutions of NOBF<sub>4</sub> in acetonitrile were prepared at 1.1 times the desired reaction concentration. Solutions of zinc thiolates were prepared at 10 times the desired reaction concentration. A 2.7-mL portion of the NOBF<sub>4</sub> solution was transferred to a cuvette and the cell was sealed with an air-tight Teflon cap containing a septum. A 300-μL portion of zinc thiolate solution was withdrawn by a gas-tight syringe and the needle was covered by a septum. The cuvette was transferred to the UV-Vis spectrophotometer and, after one optical scan of the nitrosonium tetrafluoroborate solution, the zinc thiolate solution was quickly injected. The cuvette was shaken to mix the reagents and returned to the spectrophotometer. Optical spectra were recorded at regular intervals.

*Zinc Thiolate Reactions with NO<sub>2</sub>(g).* The procedure and quantities used identical as those described for the reactions with nitric oxide, except that NO<sub>2</sub> (g) was added instead of NO (g).

*S-Nitrosothiol Reactions with Zn(OTf)<sub>2</sub>.* All solutions were prepared under a nitrogen atmosphere.

*PATHNO:* A 2.52 mM PATHNO solution in acetonitrile was prepared and 2.5 mL of the stock solution were sealed in a cuvette. A 1-mL solution of Zn(OTf)<sub>2</sub> (2.3 mg, 0.0063 mmol) dissolved in acetonitrile was withdrawn into a gas-tight syringe and the needle was covered by a septum. The cuvette and syringe were removed from the glovebox and the cuvette was placed

into the spectrophotometer. After one optical scan of the PAtHNO solution, the zinc solution was injected into the cuvette. The cell was shaken to mix the reagents and returned to the spectrophotometer. The final solution was 1.8 mM in both reagents. Optical spectra were recorded at regular intervals.

*APAtHNO*: The procedure was identical to that described for PAtHNO, with the following exceptions. The prepared solution of *S*-nitrosothiol was 2.1 mM in APAtHNO and the acetonitrile solution of zinc(II) salt was 5.25 mM in Zn(OTf)<sub>2</sub>. The final solution was 1.5 mM in both reagents.

**FT-IR Time Dependent Studies of *S*-Nitrosothiol Reactions with Zinc Salts.** All reactions were performed under a nitrogen atmosphere. To a stirring solution of 100 mg (0.429 mmol) of APAtHNO in ~3 mL acetonitrile-*d*<sub>3</sub> was added 1 equiv of solid ZnX<sub>2</sub> (X = Cl, OTf). Aliquots of the reaction mixtures were obtained over the duration of the study and injected into a CaF<sub>2</sub> solution IR cell under a nitrogen atmosphere. The cell was sealed, removed from the glovebox, and placed into the FT-IR spectrometer for analysis. For the study with APAtH<sup>15</sup>NO, the conditions were analogous except that 50 mg (0.21 mmol) of the *S*-nitrosothiol were used.

**<sup>1</sup>H NMR Studies.** All samples were prepared under a nitrogen atmosphere.

*Comparison of the reactivity of [ZnPAtHOTf] with NO<sup>+</sup> with that of PAtHNO with Zn(OTf)<sub>2</sub>.*

*Reactivity of [ZnPAtHOTf] with NO<sup>+</sup>.* A 1-mL portion of a 7.5 mM stock solution of [ZnPAtHOTf] (0.008 mmol) in acetonitrile-*d*<sub>3</sub> was added to 0.9 mg (0.008 mmol) of NOBF<sub>4</sub>. The solution was allowed to stir for 1 h, at which point an aliquot was analyzed by <sup>1</sup>H NMR spectroscopy. *Reactivity of PAtHNO with Zn(OTf)<sub>2</sub>.* PAtHNO (0.100 g, 0.395 mmol) in ~2 mL of acetonitrile-*d*<sub>3</sub> was added to Zn(OTf)<sub>2</sub> (0.144 g, 0.395 mmol). The solution was allowed to stir for 1 h, at which point an aliquot was analyzed by <sup>1</sup>H NMR spectroscopy.

*Disulfide titrations with Zn(OTf)<sub>2</sub>.* All samples were prepared under a nitrogen atmosphere. Stock solutions of the disulfide PAtH<sub>2</sub> (15 mM) and Zn(OTf)<sub>2</sub> (75 mM) were prepared in acetonitrile-*d*<sub>3</sub>. Samples for <sup>1</sup>H NMR spectroscopic analysis were prepared by adding 250 μL of the PAtH<sub>2</sub> stock solution and the appropriate volume of MeCN-*d*<sub>3</sub> to NMR tubes containing 0.5, 1, 2, or 5 equivalents of Zn(OTf)<sub>2</sub> in a total reaction volume of 500 μL. The final concentration of PAtH<sub>2</sub> in each NMR tube was 7.5 mM. Samples were analyzed after 1 h of mixing.

**EI-MS Studies of Zinc Thiolate with NO<sup>+</sup> and of S-Nitrosothiol with Zinc Salts.** All solutions were prepared under a nitrogen atmosphere. NOBF<sub>4</sub> (0.154 g, 1.32 mmol) was placed into a custom-made gas-tight cell in ~3 mL of methylene chloride in a glovebox under a nitrogen atmosphere. The cell was removed from the glovebox and exposed to an inert argon purge. This procedure ensured that high concentrations of nitrogen would not mask peaks in the *m/z* = 30 region. [ZnAPAtHCl] (0.40 g, 1.3 mmol) was dissolved in ~1 mL of methylene chloride under a nitrogen atmosphere and was transferred by gas-tight syringe to the reaction cell under an inert argon flow. The cell was sealed and the reaction mixture was allowed to stir for 1.5 h prior to analysis. The cell was then connected to an inert He gas flow and to the mass spectrometer, and the connecting copper tubing was purged thoroughly prior to analysis of the reaction headspace. Headspace analysis was undertaken with the mass spectrometer operating in selective ion mode. Analogous reaction conditions were employed for the reactions of APAtHNO with ZnCl<sub>2</sub> and with Zn(OTf)<sub>2</sub>. ZnCl<sub>2</sub> (58.4 mg, 0.428 mmol, 1 equiv) and acetonitrile were added to the reaction cell in the glovebox and a solution of APAtHNO (100 mg, 0.214 mmol, 1 equiv) was injected into the cell after an argon purge. A sample of Zn(OTf)<sub>2</sub> (77.9 mg, 0.214 mmol, 1 equiv) was exposed to APAtHNO (50 mg, 0.21 mmol, 1 equiv) in acetonitrile in a parallel experiment. For the control experiment with APAtHNO, a solution containing 50 mg of the S-nitrosothiol was

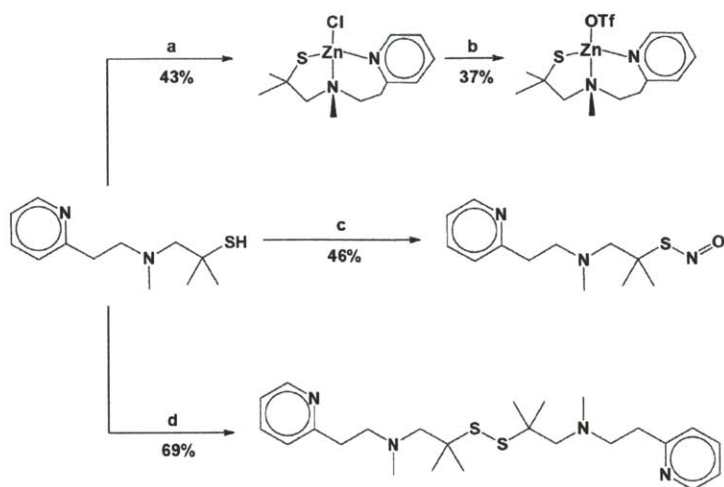
added to the reaction cell in the glovebox. The cell was then sealed, removed from the glovebox, and purged with argon. The headspace of the stirring solution was analyzed by EI-MS after 2 h. All reactions were carried out in the dark to prevent photodecomposition of S-nitrosothiol.

### 2.3. Results and Discussion

#### *Preparation of Compounds.*

To prepare for studies of the reactivity of the zinc thiolate moiety we first synthesized the PATHH ligand from isobutylene sulfide and 2-(2-methylaminoethyl)-pyridine according to previously published procedures.<sup>39-40</sup> Deprotonation of the ligand followed by ZnCl<sub>2</sub> addition afforded the chloride complex [ZnPATHCl] in decent yield (Scheme 2.1a). Structural parameters for [ZnPATHCl] match previously reported values.<sup>46</sup> Reaction of thallium triflate with an acetonitrile solution of [ZnPATHCl] gave [ZnPATHOTf], which was obtained in 37% yield (Scheme 2.1b). The S-nitrosothiol PATHNO was prepared as a green oil for spectral comparison with zinc thiolate/nitrogen oxide reaction products by treating PATHH with *iso*-amyl nitrite (Scheme 2.1c).

We also synthesized the new ligand APATHH, an alkyl propylaminothiolate, to eliminate C=C and C=N stretches that appear in the characteristic infrared N–O spectral stretching region and thereby facilitate the interpretation of IR spectroscopic studies (Fig. 2.1).



a 1. NaH, THF 2.  $\text{ZnCl}_2$ ; b TIOtF, MeCN; c *iso*-amyl nitrite,  $\text{CH}_2\text{Cl}_2$ ; d 1. NaH, THF 2.  $\text{I}_2$

**Scheme 2.1.** Synthesis of PATH species.

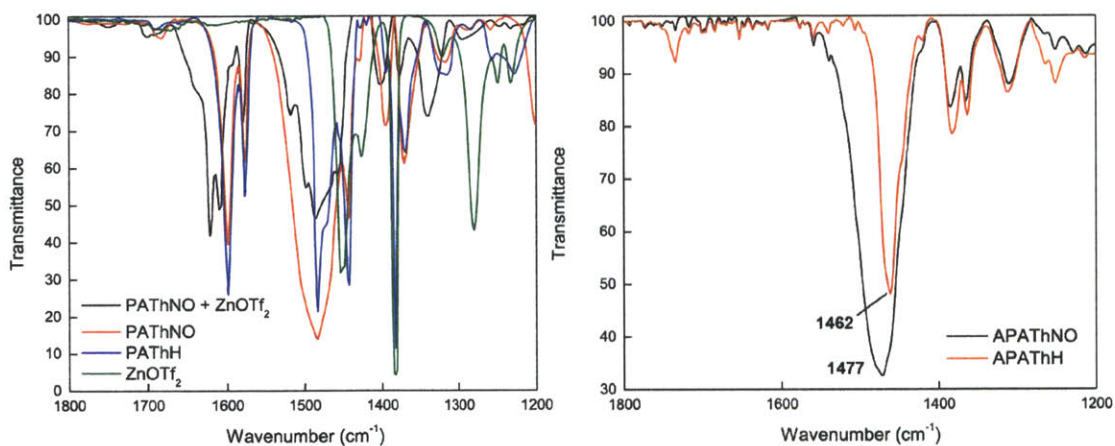
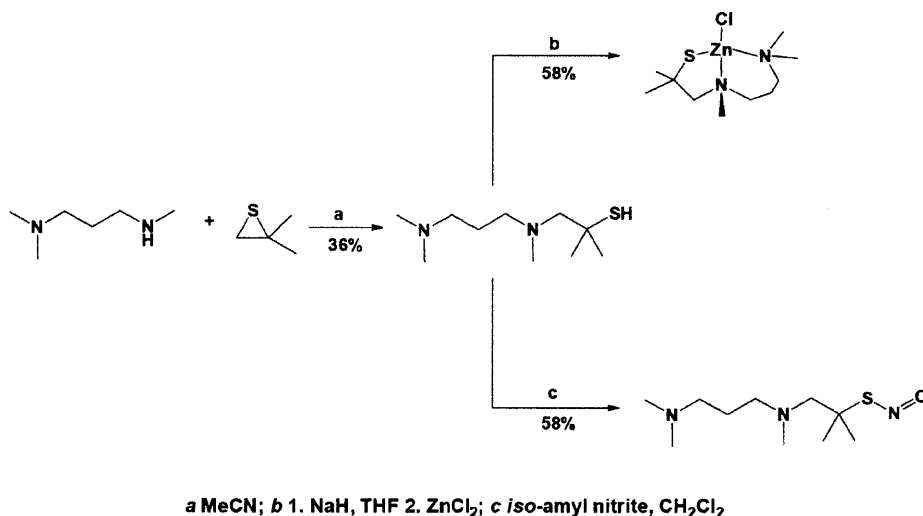


**Figure 2.1.** *Left:* Infrared spectral comparison of  $\text{Zn}(\text{OTf})_2$ , PATHH, PATHNO, and PATHNO +  $\text{Zn}(\text{OTf})_2$  in MeCN. Strong absorbance bands between  $1550\text{ cm}^{-1}$  and  $1650\text{ cm}^{-1}$  obscure features arising from the reaction products of  $\text{Zn}^{2+}$  with PATHNO. *Right:* The infrared spectra of APATHH and APATHNO are shown for comparison.

APATHH retains the coordinating atoms afforded by PATH but replaces the spectrally interfering pyridyl moiety of the latter with a tertiary amine. Condensation of *N,N,N'*-trimethyl-1,3-diaminopropane with isobutylene sulfide readily yielded APATHH (Scheme 2.2a). The zinc complex  $[\text{ZnAPATHCl}]$  was prepared by analogy to the synthesis of  $[\text{ZnPATHCl}]$  (Scheme 2.2b).

The *S*-nitrosothiol APATHNO was obtained by transnitrosation of APATHH with *iso*-amyl nitrite (Scheme 2.2c), and the disulfide PATH<sub>2</sub> (Scheme 2.1d) was prepared by iodine oxidation of [PATH]<sup>-</sup> thiolate. These compounds were synthesized for spectral comparison with the products of reactions between the zinc complexes and RNOS.



**Scheme 2.2.** Synthesis of APATH species.

*Exposure of Zinc PATH and APATH Complexes to Nitric Oxide under Various Conditions.*

No reaction was observed by UV-Vis spectroscopy upon addition of excess nitric oxide to anaerobic acetonitrile solutions of [ZnPATHCl], [ZnPATHOTf], and [ZnAPATHCl]. Injection of air into the cuvette led to the immediate appearance of peaks in the UV-Vis spectrum that are characteristic of tertiary *S*-nitrosothiols (Fig. 2.2 – 2.4).<sup>42</sup> The “0 min” trace reflects immediate appearance of a spectral band arising from the *S*-nitrosothiol, which then decays over time.

The lack of reactivity under anaerobic conditions is consistent with previous findings<sup>53</sup> and has important implications for nitric oxide in biology. Specifically, this result requires that it is not NO itself, but an oxidation product thereof, that is responsible for *S*-nitrosothiol formation



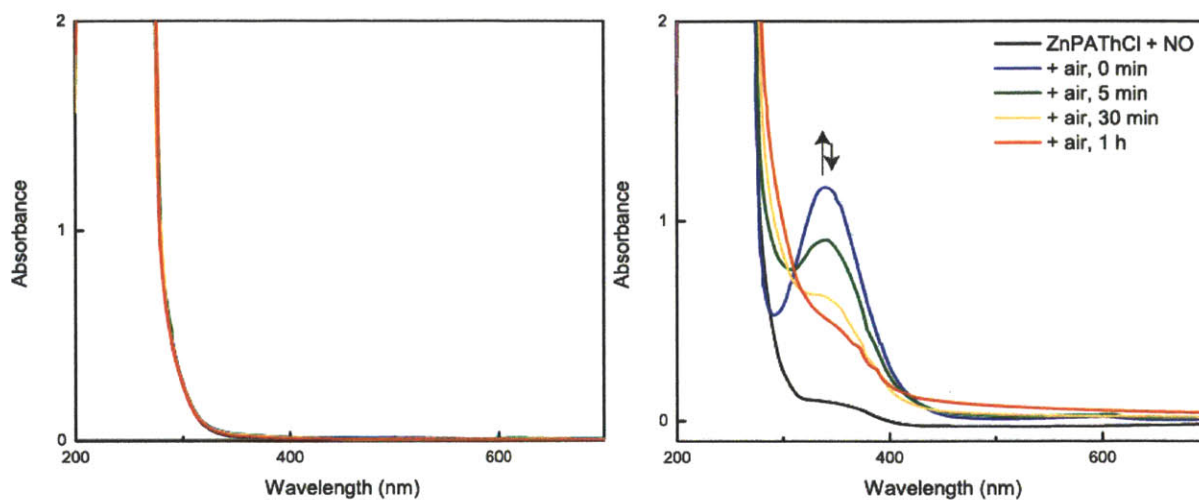


**Figure 2.2.** UV-Vis reactivity profiles for anaerobic 1.5 mM [ZnPAThCl] + excess NO (g) (*left*), and 1.5 mM [ZnPAThCl] + excess NO (g) + air (*right*). Recorded in acetonitrile.

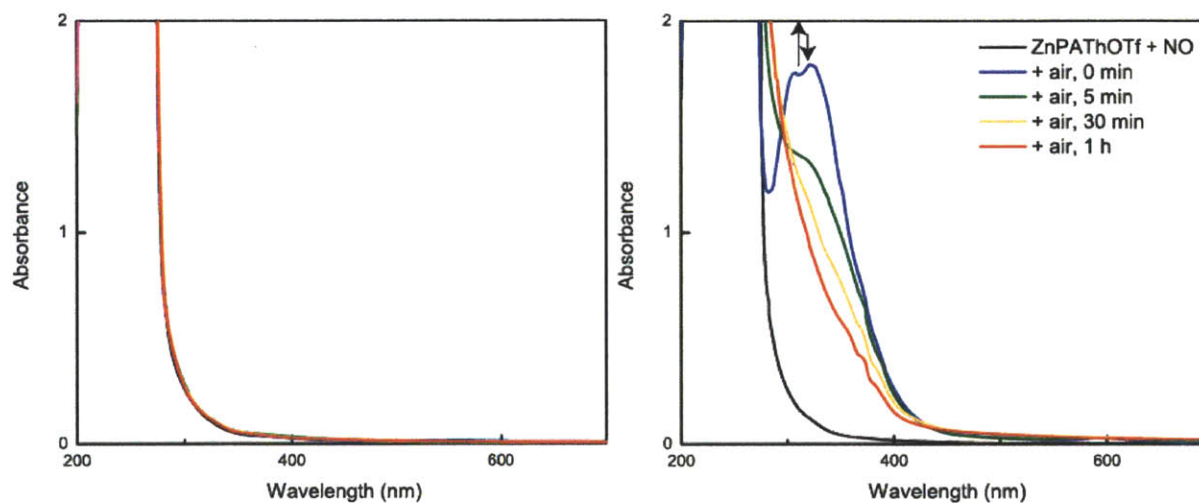


**Figure 2.3.** UV-Vis spectral profiles for reactions of anaerobic 7.5 mM [ZnPAThOTf] with excess NO (g) (*left*), and of 7.5 mM [ZnPAThOTf] with excess NO (g) + air (*right*). Recorded in acetonitrile.

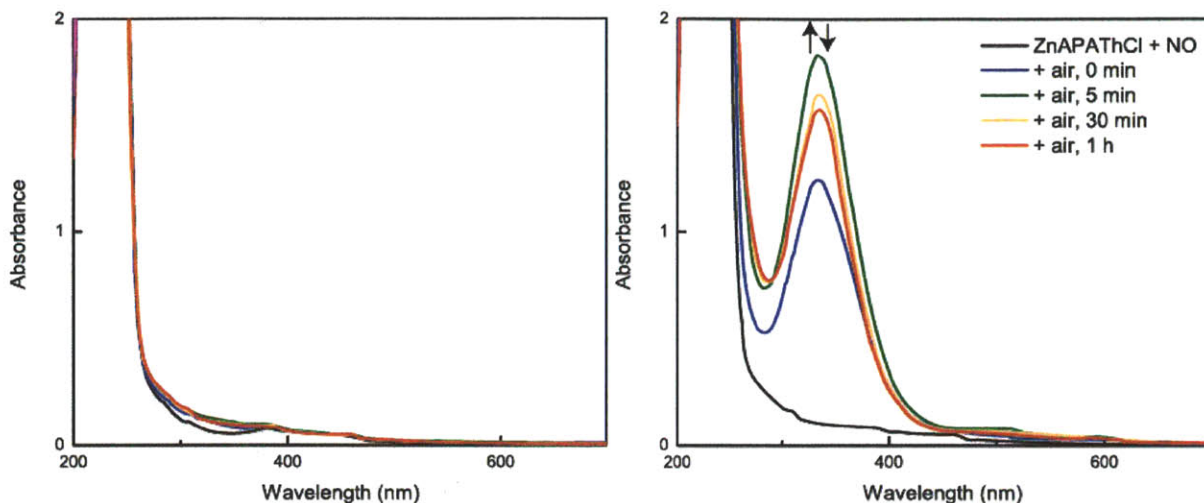


**Figure 2.4.** UV-Vis spectral profiles for reactions of anaerobic 7.5 mM [ZnAPATHCl] with excess NO (g) (*left*), and of 7.5 mM [ZnAPATHCl] with excess NO (g) + air (*right*). Recorded in acetonitrile. Optical bands corresponding to *S*-nitrosothiol formation appear and increase in intensity over the course of 5 min after injection of air, then decrease in intensity throughout the remaining 55 min of the experiment.

at biological zinc thiolate sites, such as those in NOS and metallothioneins. NO has been previously described as a poor nitrosating agent for thiols.<sup>54</sup> The nitric oxide mediated thiolate nitros(yl)ation reaction is an electron-releasing process (eq. 2.2), and, in the absence of a viable electron acceptor, no reaction is observed. In biological milieu, however, dioxygen is present to oxidize NO to NO<sub>2</sub>, for example, thereby enabling *S*-nitrosothiol formation (eq. 2.3, 2.4). Our results are consistent with this chemistry.



### Reactions of Zinc PATH and APATH Complexes with NOBF<sub>4</sub>.

We next examined the reactivity of nitrosonium tetrafluoroborate with zinc thiolates. Exposure of [ZnPATHCl], [ZnPATHOTf], and [ZnAPATHCl] to 1 equiv of NOBF<sub>4</sub> in acetonitrile led to the appearance of peaks in the optical spectra corresponding to tertiary *S*-nitrosothiols (Fig. 2.5).

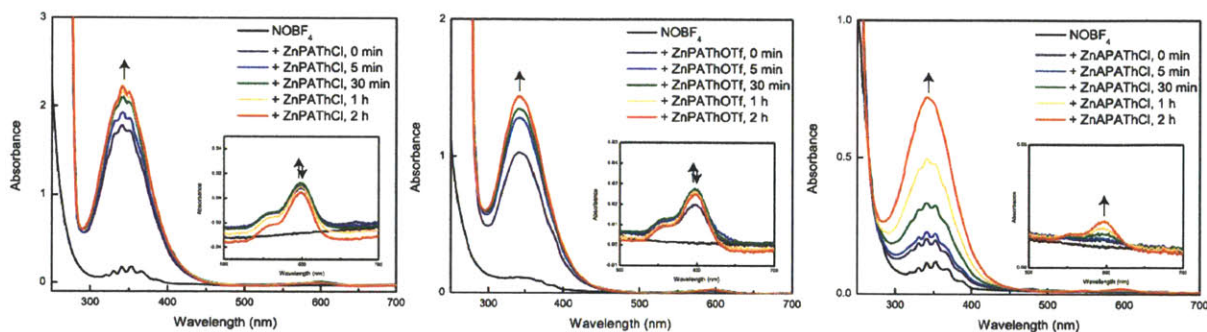
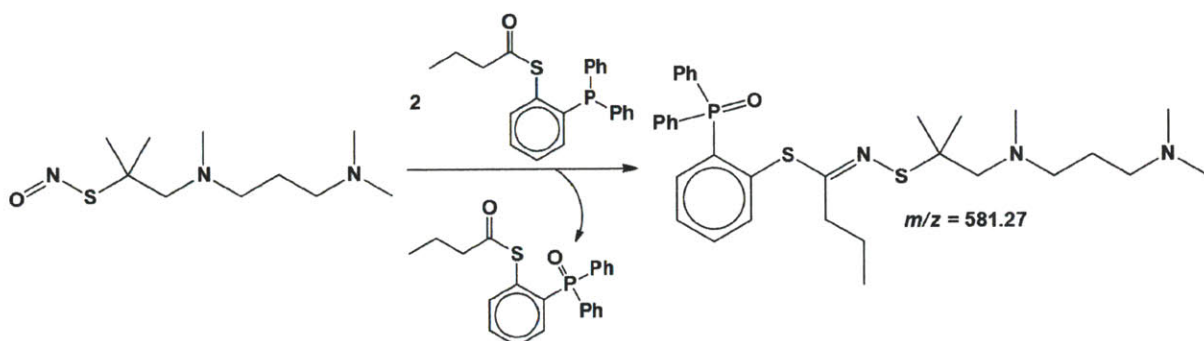


**Figure 2.5.** Spectral profiles for reactions of 1 equiv of NOBF<sub>4</sub> with 7.5 mM zinc thiolate complexes. From left to right: [ZnPATHCl], [ZnPATHOTf], and [ZnAPATHCl]. The low-intensity features observed between 300 nm and 400 nm result from NO<sub>2</sub>BF<sub>4</sub> contamination of commercially available NOBF<sub>4</sub>.

*S*-Nitrosothiol formation was demonstrated for the reaction of [ZnAPATHCl] with NO<sup>+</sup> by trapping APATHNO and studying the products by mass spectrometry (Scheme 2.3).<sup>49-50</sup> Utilization of phosphine-mediated N=O bond scission and ESI-MS analysis of products confirmed that APATHNO formed upon exposure of [ZnAPATHCl] to NO<sup>+</sup> (Fig. 2.6). We therefore conclude that optical peaks attributed to tertiary *S*-nitrosothiol formation in reactions of zinc thiolates and RNOS are correctly assigned. A number of additional peaks are observed in the ESI-MS spectrum of the APATHNO/phosphine ligation reaction and may correspond to additional reaction products. At present we have not identified them. The interaction of [ZnPATHX] (X = Cl, OTf) and [ZnAPATHCl] with NO<sup>+</sup> results in complicated reaction

mixtures, and the difficulty in determining the nature of the species in solution precludes kinetic and mechanistic studies.



**Scheme 2.3.** Traceless ligation of APATHNO by phosphine-mediated N=O bond scission.<sup>49-50</sup>

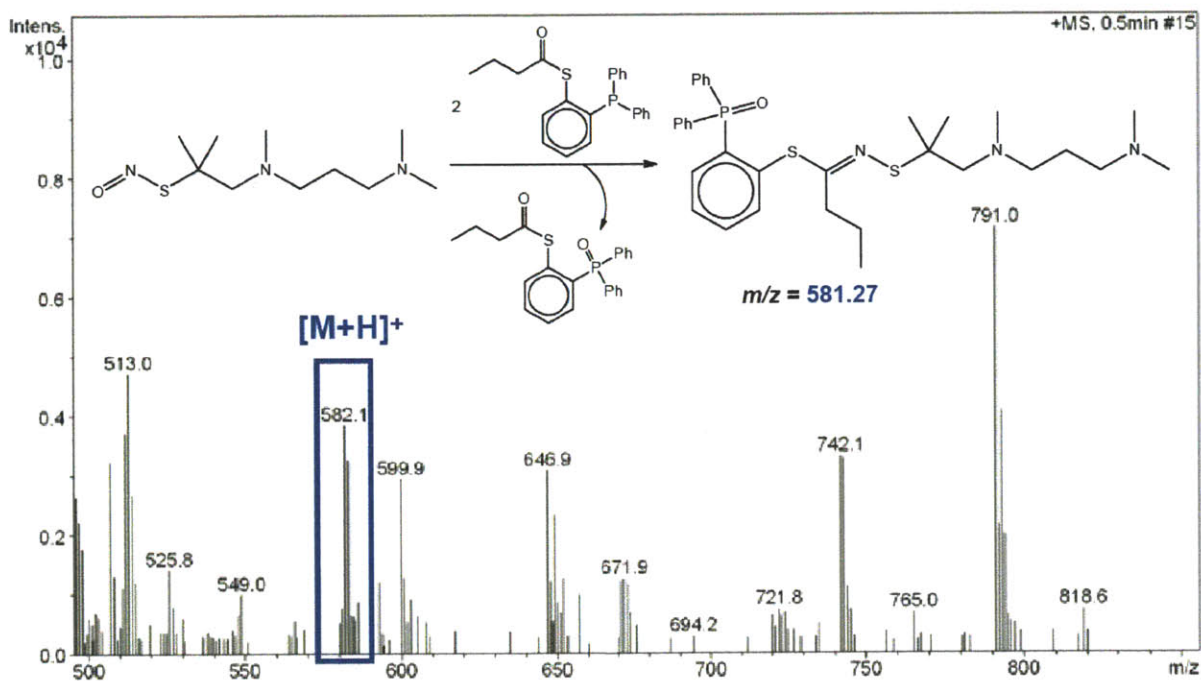


**Figure 2.6.** ESI-MS spectrum of [ZnAPATHCl] + 0.9 equiv NOBF<sub>4</sub> + PPh<sub>2</sub>R. A peak is observed for the expected species at  $m/z = 582.1$ . Additional peaks correspond to reaction products that cannot be identified at this time. The presence of these species attests to the complexity of the reaction mixture and is consistent with the difficulty in isolating and characterizing the reaction products.



### Reactions of *S*-Nitrosothiols with Zinc(II) Salts.

PATHNO and APATHNO were prepared to examine the interaction between these pre-formed tertiary *S*-nitrosothiols and  $\text{Zn}^{2+}$ . Optical spectroscopic studies of reaction mixtures containing 1 equiv of  $\text{Zn}(\text{OTf})_2$  and PATHNO or APATHNO revealed a decrease in the intensity of the peaks at  $\sim 340$  nm compared to optical spectra of *S*-nitrosothiol solutions lacking  $\text{Zn}^{2+}$  (Fig. 2.7). This spectroscopic change corresponds to decay of the  $n_{\text{O}} \rightarrow \pi^*$  transitions for each *S*-nitrosothiol<sup>42</sup> in the presence of  $\text{Zn}(\text{OTf})_2$ . Peaks at 602 nm in the spectra of PATHNO and APATHNO disappear completely upon addition of  $\text{Zn}(\text{OTf})_2$ . A new peak, corresponding to an as-of-yet unidentified species, grows in at 330 nm after 1 h in the APATHNO/ $\text{Zn}(\text{OTf})_2$  reaction spectrum (Fig. 2.7, right). IR spectroscopic analysis of the APATHNO reaction with  $\text{ZnCl}_2$  revealed the appearance of three bands in the  $1600\text{ cm}^{-1}$  region of the spectrum, and two bands were similarly observed for the reaction of APATHNO with  $\text{Zn}(\text{OTf})_2$  (Fig. 2.8, left). Concomitant disappearance of the  $\nu_{\text{NO}}$  feature of APATHNO at  $1477\text{ cm}^{-1}$  was observed for reactions with both zinc(II) salts (Fig. 2.8, right).

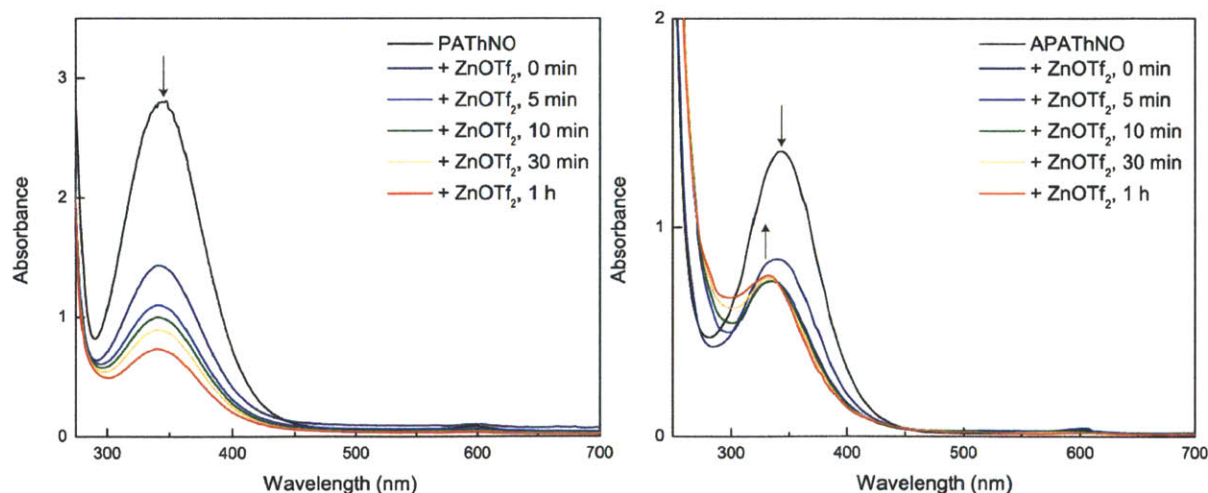


**Figure 2.7.** Disappearance of characteristic *S*-nitrosothiol peaks occurs upon exposure of 1.8 mM PATHNO (*left*) and 1.5 mM APATHNO (*right*) to 1 equiv of  $\text{Zn}(\text{OTf})_2$  in acetonitrile. Reactions were monitored for 1 h.

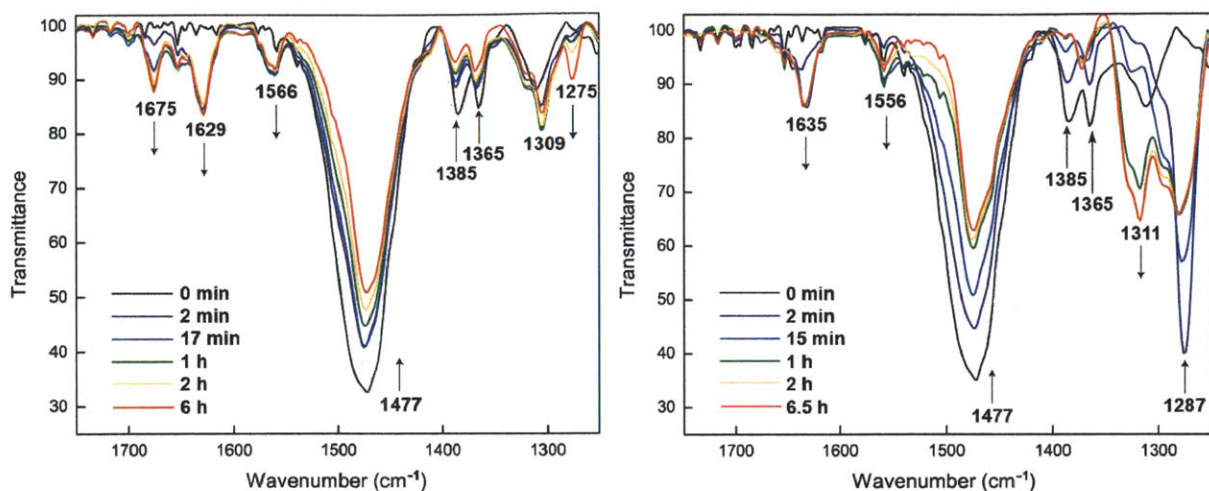


**Figure 2.8.** Solution IR spectral timecourse for the reactions of APATHNO with 1 equiv of  $\text{ZnCl}_2$  (left) and  $\text{Zn}(\text{OTf})_2$  (right) in  $\text{MeCN-}d_3$ . The  $\nu_{\text{NO}}$  band at  $1477\text{ cm}^{-1}$  for APATHNO disappears upon addition of zinc(II) salt to the nitrosothiol. Because  $\nu_{\text{NO}}$  of APATHNO overlaps the C–H rocking and/or bending modes, some intensity remains after the S-nitrosothiol N=O stretch at  $1477\text{ cm}^{-1}$  disappears. For comparison, see Figure 2.1, right.

Additionally, inner-sphere coordination of a single triflate anion was deduced for the reaction with  $\text{Zn}(\text{OTf})_2$ , judging by the appearance of a band at  $1311\text{ cm}^{-1}$ , a signature for covalent binding of the sulfonate moiety.<sup>55</sup> There is a corresponding decrease in the intensity of the asymmetric sulfonate ion stretching frequency at  $1287\text{ cm}^{-1}$  from the outer-sphere triflate anion.<sup>55</sup> Use of  $^{15}\text{N}$ -isotopically labeled APATHNO revealed that the bands in the  $1600\text{ cm}^{-1}$  infrared spectral region for reactions with  $\text{ZnCl}_2$  and  $\text{Zn}(\text{OTf})_2$  showed negligible changes compared to the unlabeled nitrosothiol, indicating that these peaks are not caused by stretches of N-containing moieties in the product(s) (Fig. 2.9).

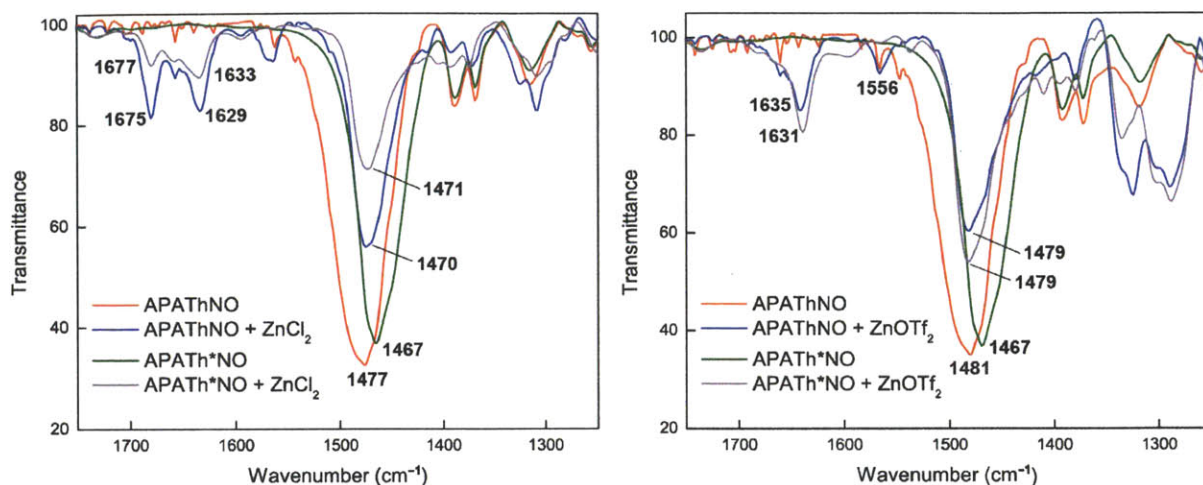


**Figure 2.9.** <sup>15</sup>N (designated \*N) vs. <sup>14</sup>N spectral comparison of reactions of APATH\*NO and APATHNO with ZnCl<sub>2</sub> (*left*) and Zn(OTf)<sub>2</sub> (*right*). Recorded in acetonitrile-*d*<sub>3</sub>.

There is a dependence on the anion in the reactions of zinc salts with the *S*-nitrosothiol, as inferred from the presence of an additional band in the IR spectra of the [ZnAPATHCl]/NOBF<sub>4</sub> and APATHNO/ZnCl<sub>2</sub> reaction mixtures that is absent in solutions containing a triflate counterion (Fig. 2.9). The better coordinating ability of chloride compared to triflate may control the availability of binding sites for the –SNO moiety on zinc, or Cl<sup>–</sup> may participate directly in the reaction.

To further explore the chemistry between Zn<sup>2+</sup> and the –SNO moiety of *S*-nitrosothiols we recorded <sup>1</sup>H NMR spectra for reactions of [ZnPATHOTf] with NOBF<sub>4</sub> and of PATHNO with Zn(OTf)<sub>2</sub> (Fig. 2.10). All of the peaks observed in the PATHNO/Zn(OTf)<sub>2</sub> reaction mixture are

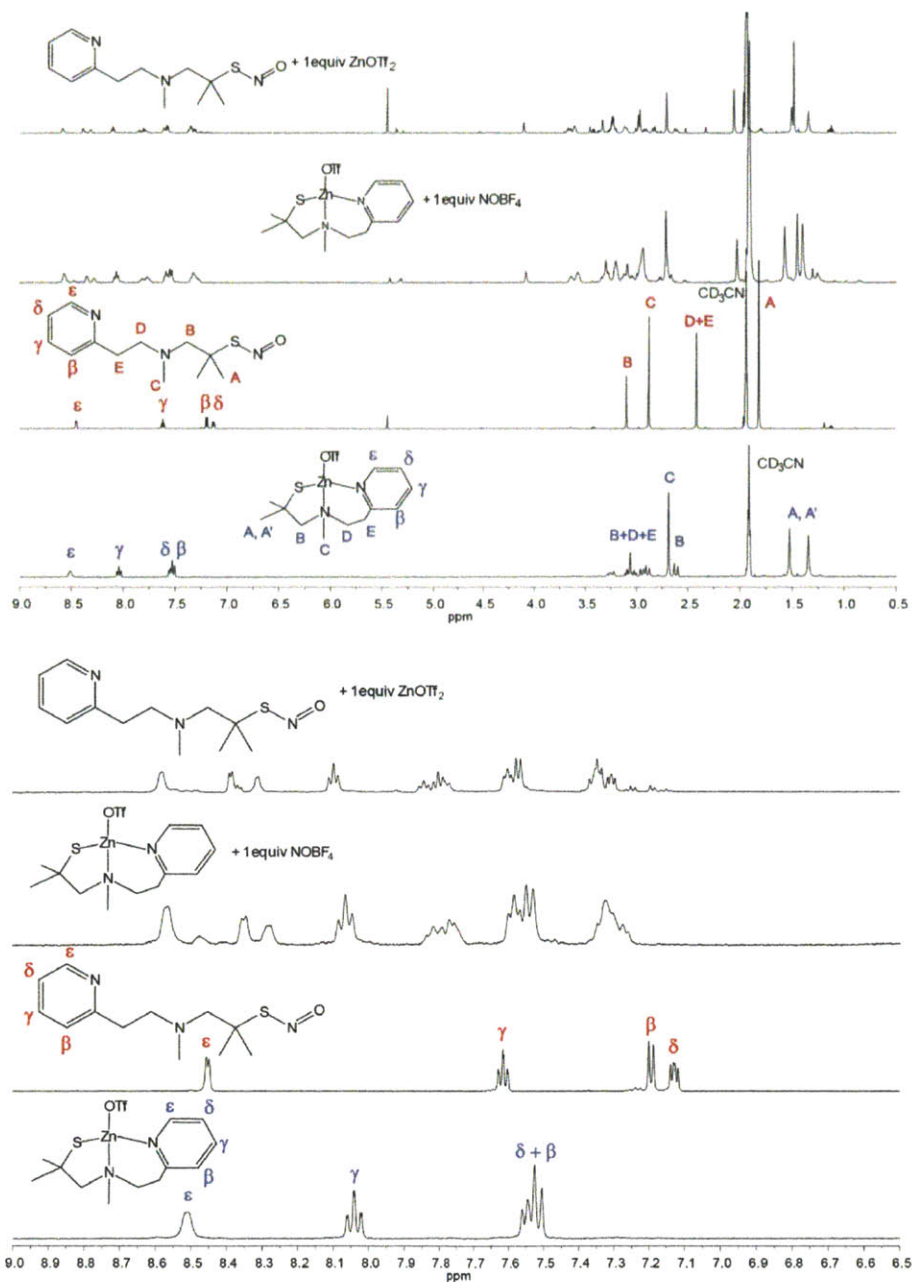


**Figure 2.10.** Comparison of  $^1\text{H}$  NMR spectra for 7.5 mM  $[\text{ZnPATHOTf}]/\text{NOBF}_4$  vs. 7.5 mM  $\text{PATHNO}/\text{Zn}(\text{OTf})_2$  reactions. Recorded in  $\text{MeCN}-d_3$ .

present in the  $[\text{ZnPATHOTf}]/\text{NOBF}_4$   $^1\text{H}$  NMR spectrum. Spectroscopic comparison of mixtures suggests that  $\text{PATHNO}$  binds zinc(II) and, based on infrared spectroscopic evidence, induces dissociation of one triflate counteranion. In the related  $[\text{ZnPATHOTf}]$  reaction with  $\text{NOBF}_4$ ,  $\text{NO}^+$



attacks the thiolate, such that the reactive species in both instances is  $[\text{Zn}(\text{P}(\text{A})\text{ThNO})(\text{OTf})]^+$ . In addition, the spectrum contains a new singlet at 2.05 ppm. This peak may arise from the *gem*-dimethyl groups of a metastable intermediate, possibly coordinated *S*-nitrosothiol. We were unable to trap and identify this species.

The complexity of the NMR spectra of these reaction mixtures precluded definitive identification of the products or kinetic studies to probe the mechanism of *S*-nitrosothiol formation and decomposition. However, being aware of the propensity of *S*-nitrosothiols to decompose to the corresponding disulfides over time,<sup>42</sup> we prepared the disulfide  $\text{P}(\text{A})\text{Th}_2$  as a control to assess whether exposure of zinc thiolates to nitrosonium ion, or of *S*-nitrosothiol to  $\text{Zn}^{2+}$ , could result in disulfide formation.  $^1\text{H}$  NMR spectral titration studies of  $\text{P}(\text{A})\text{Th}_2$  with  $\text{Zn}(\text{OTf})_2$  revealed formation of various species, depending on the ratio of zinc to disulfide in solution (Fig. 2.11). The  $^1\text{H}$  NMR spectra of neither the free disulfide nor of disulfide solutions containing  $\text{Zn}^{2+}$  matched the  $^1\text{H}$  NMR spectra of the zinc thiolate/ $\text{NOBF}_4$  or *S*-nitrosothiol/ $\text{Zn}(\text{OTf})_2$  reaction mixtures (Fig. 2.12). From these results we conclude that disulfide is not a product of *S*-nitrosothiol exposure to  $\text{Zn}^{2+}$ . It therefore appears likely that zinc promotes heterolytic, not homolytic, cleavage of the S–N bond of *S*-nitrosothiols.

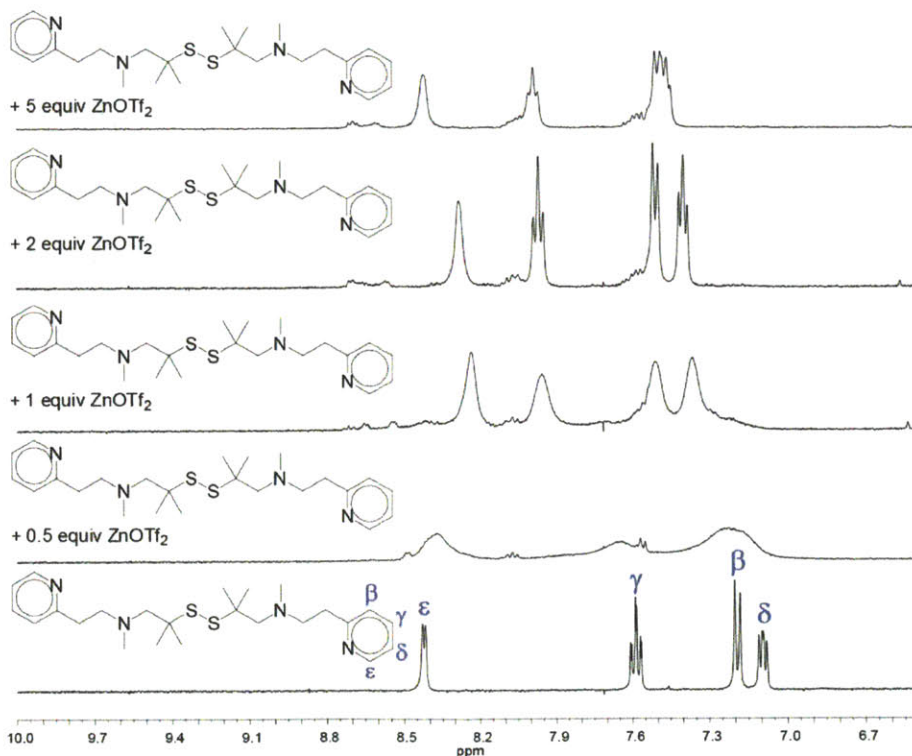
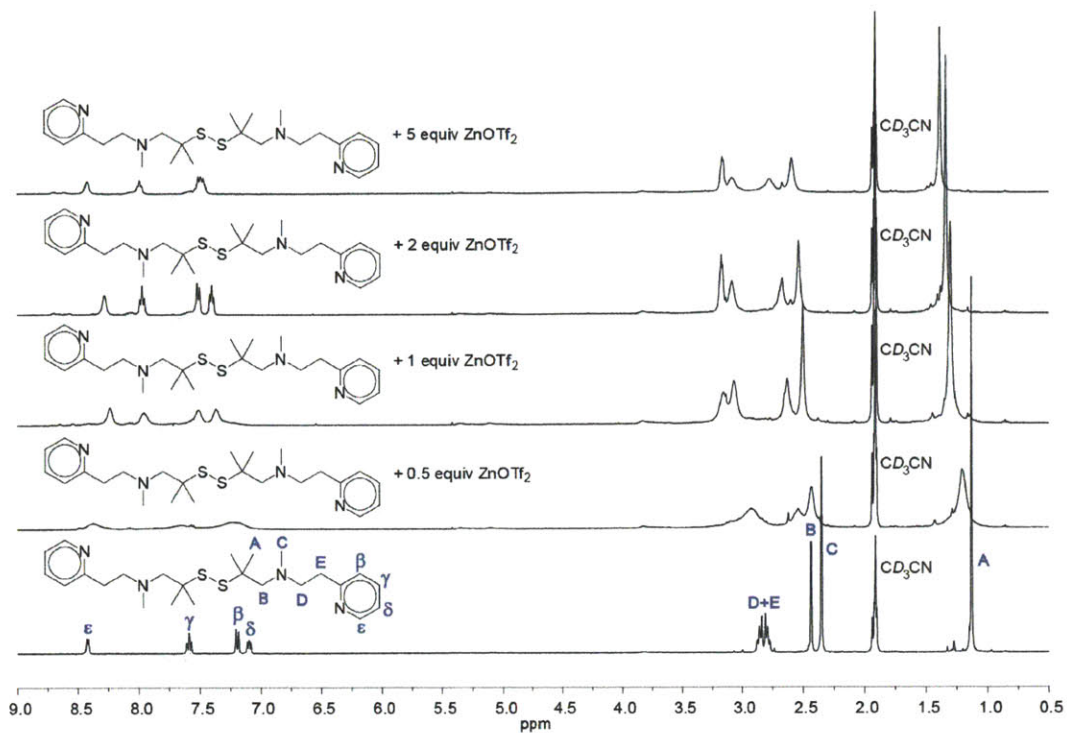


**Figure 2.11.**  $^1\text{H}$  NMR spectral comparison of  $\text{PATH}_2$  solutions in  $\text{MeCN-}d_3$  containing variable amounts of  $\text{Zn}(\text{OTf})_2$ .

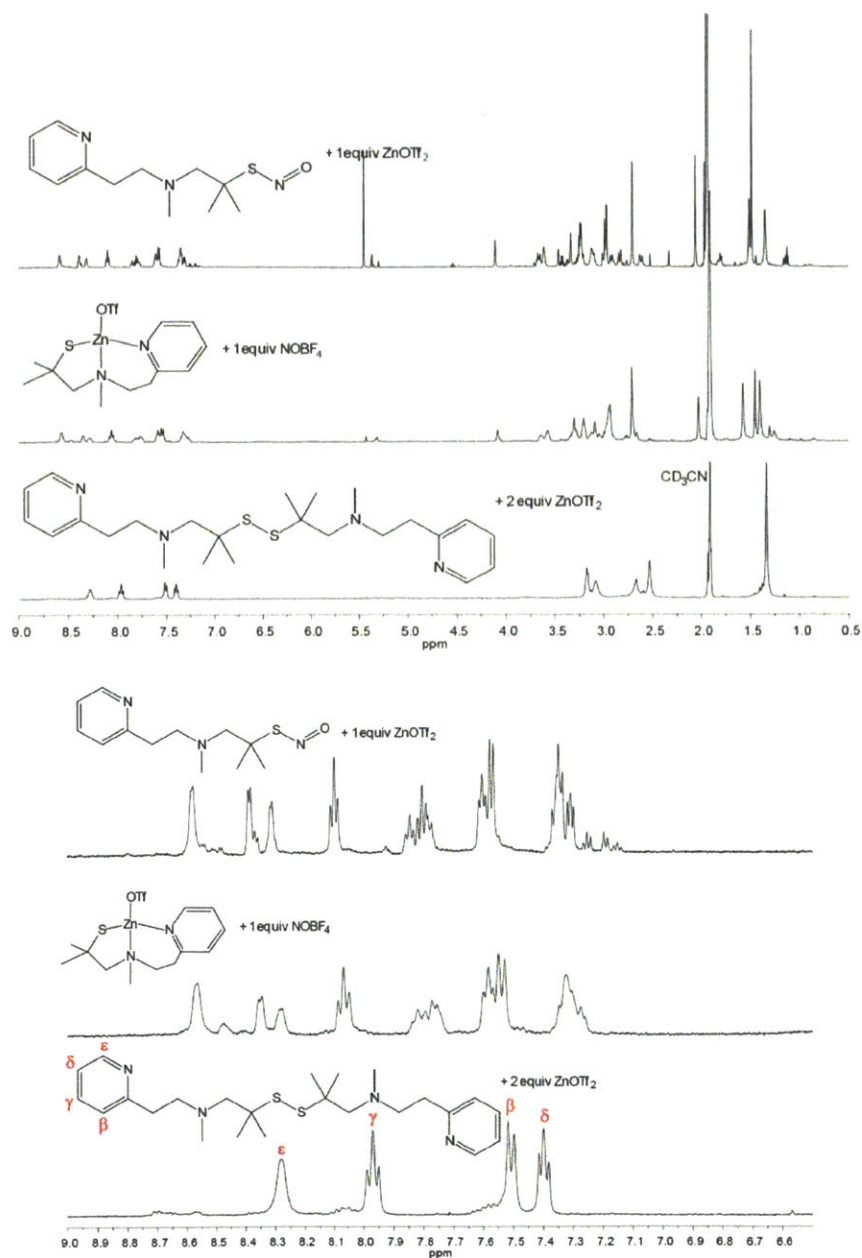


**Figure 2.12.**  $^1\text{H}$  NMR comparison of a  $\text{PATH}_2/\text{Zn}(\text{OTf})_2$  solution with reaction spectra of  $[\text{ZnPATHOTf}]$  with  $\text{NOBF}_4$  and  $\text{PATHNO}$  with  $\text{Zn}(\text{OTf})_2$ . Recorded in  $\text{MeCN-}d_3$ .

Finally, we analyzed the reaction headspace of  $[\text{ZnAPATHCl}]/\text{NOBF}_4$ ,  $\text{APATHNO}/\text{ZnCl}_2$ , and  $\text{APATHNO}/\text{Zn}(\text{OTf})_2$  reaction mixtures by EI-MS to determine whether gaseous species are generated by *S*-nitrosothiols in the presence of  $\text{Zn}^{2+}$ .  $\text{NO}$  and  $\text{N}_2\text{O}$  were

detected in all instances (Fig. 2.13, *top row and bottom left*).  $\text{NO}_2$  was not observed. The  $\text{ZnCl}_2/\text{APATHNO}$  reaction was also monitored for the possible formation of  $\text{Cl}_2$  or  $\text{NOCl}$  (Fig. 2.13, *top right*). Neither was observed, indicating that the chloride anion is unlikely to participate

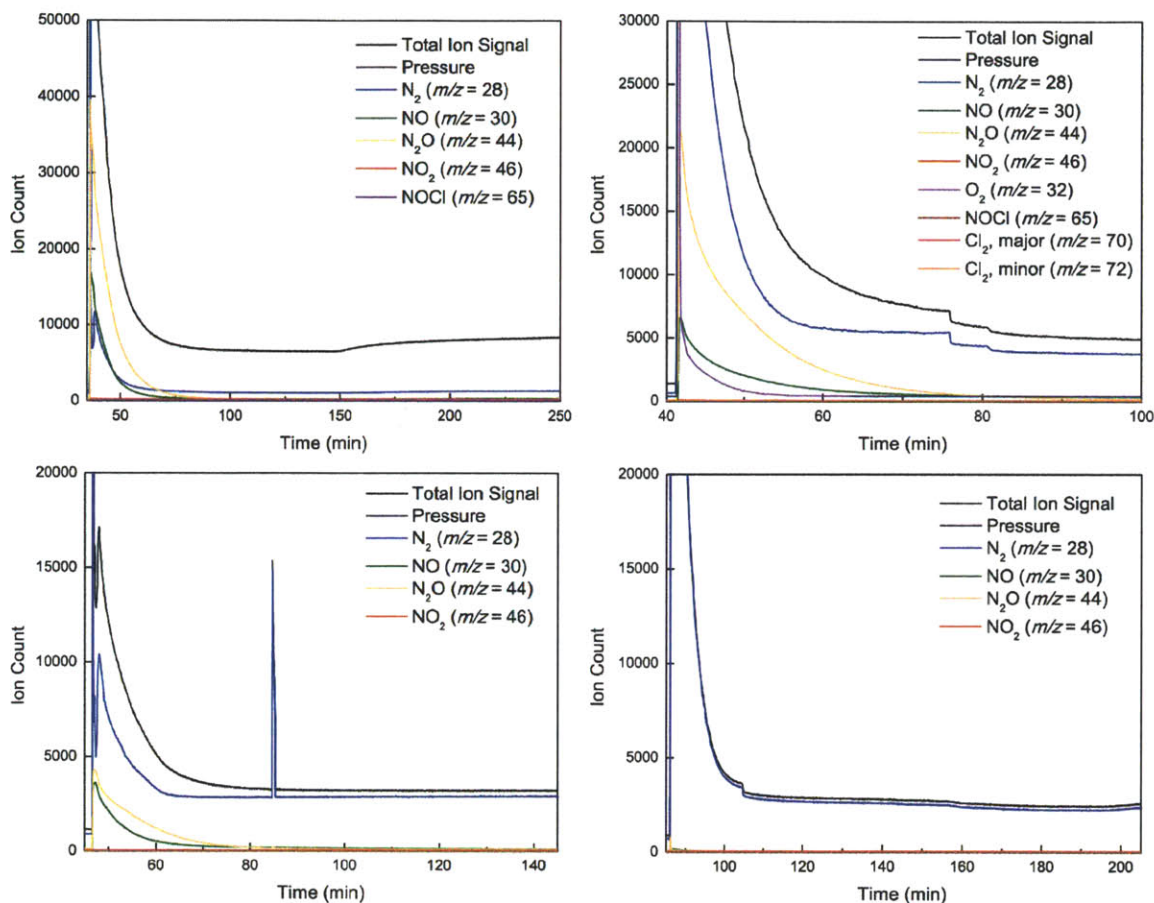


**Figure 2.13.** EI-MS analysis of the reaction headspace for  $[\text{ZnAPATHCl}]$  and  $\text{NOBF}_4$  in  $\text{CH}_3\text{CN}$  (*top left*); APATHNO and  $\text{ZnCl}_2$  in  $\text{CH}_3\text{CN}$  (*top right*); APATHNO and  $\text{Zn}(\text{OTf})_2$  in  $\text{CH}_3\text{CN}$  (*bottom left*); an APATHNO control experiment, in  $\text{CH}_3\text{CN}$  (*bottom right*).

in any redox chemistry. The headspace of a control solution of APATHNO was examined by EI-MS and neither  $\text{NO}$  nor  $\text{N}_2\text{O}$  were present (Fig. 2.13, *bottom right*). This control experiment confirms that  $\text{NO}$  and  $\text{N}_2\text{O}$  are true reaction products and not the result of *S*-nitrosothiol autodecomposition. A possible reaction pathway that accounts for  $\text{Zn}^{2+}$ -mediated decomposition of *S*-nitrosothiols with concomitant generation of  $\text{N}_2\text{O}$ , and not disulfide, involves thiolate

oxidation to generate a transient  $\text{RS}[\text{O}]^+$  species, which may undergo further decomposition. The existence of reactive  $\text{RS}[\text{O}]^+$  species is described in the literature.<sup>56</sup> Two equiv of *S*-nitrosothiol may react to form  $\text{N}_2\text{O}$ ,  $\text{RS}[\text{O}]^+$ , and  $\text{RS}^-$ . The resultant thiolate may coordinate  $\text{Zn}^{2+}$  to regenerate the starting complex. Equation 2.5 describes the proposed reaction. We also suggest that  $\text{Zn}^{2+}$ , by forming a stable complex with the resulting thiolate, may activate *S*-nitrosothiols to release  $\text{NO}^+$ , which may, in turn, lead to catalytic *S*-nitrosothiol decomposition and generation of  $\text{NO}$ .<sup>57</sup>



#### Reactions of Zinc PATH and APATH Complexes with $\text{NO}_2$ .

Exposure of  $[\text{ZnPATHCl}]$ ,  $[\text{ZnPATHOTf}]$ , and  $[\text{ZnAPATHCl}]$  to excess  $\text{NO}_2$  led to immediate appearance and subsequent decay of optical features attributed to *S*-nitrosothiols (Fig. 2.14). The decomposition of *S*-nitrosothiols in the presence of excess nitrogen dioxide has been

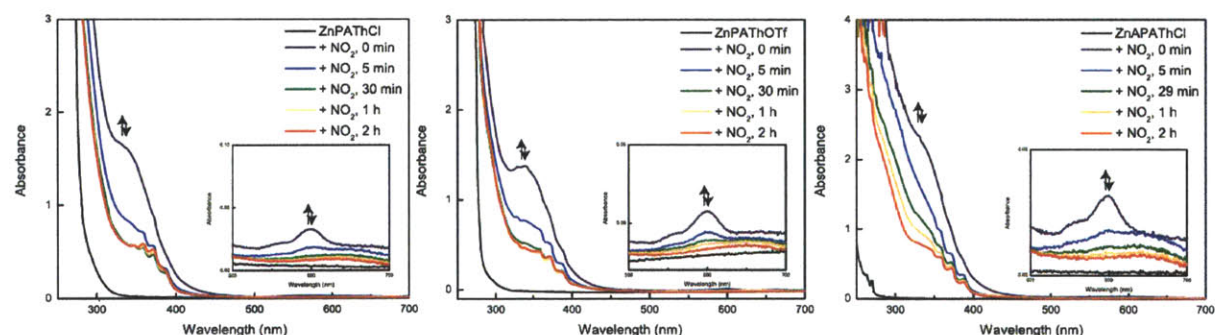
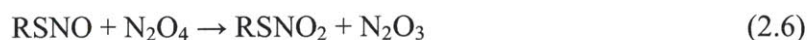


**Figure 2.14.** Acetonitrile solution spectra of  $\text{NO}_2$  reactions with 1.5 mM  $[\text{ZnPATHCl}]$  (left), 1.9 mM  $[\text{ZnPATHOTf}]$  (middle), and 1.5 mM  $[\text{ZnAPATHCl}]$  (right) reactions. The lower intensity peaks appearing in the 350 – 400 nm region of the spectrum are attributed to  $\text{NO}_2$ .

reported.<sup>58-59</sup>  $\text{N}_2\text{O}_4$  equilibrates with  $\text{NO}_2$  and oxidizes *S*-nitrosothiols to thionitrates (eq. 2.6), which lack the optical features of *S*-nitrosothiols.



### *Potential Biological Relevance.*

Consistent with prior results, we find that an isolated zinc thiolate bond is unreactive toward nitric oxide in the absence of an oxidizing agent. We propose, on the basis of spectral changes of *S*-nitrosothiols in the presence of  $\text{Zn}^{2+}$ , that zinc, in its role as a Lewis acid, activates the RSNO moiety, possibly stabilizing  $\text{RS}^-$  with release of  $\text{NO}^+$ . Biological consequences for nitric oxide synthase may be the need for zinc to dissociate from nitrosated thiolates in order to maintain physiological reversibility of the nitrosation reaction. Without such dissociation, interaction of  $\text{Zn}^{2+}$  with *S*-nitrosothiols could result in thiolate oxidation that would block conversion back to the biologically useful form of the enzyme.<sup>60-61</sup> Irreversible modification of zinc thiolates in transcription factors following oxidative stress provides a precedent for the biological irreversibility that we propose here.<sup>10,30</sup>

### **2.4. Summary and Conclusions**

Nitric oxide under anaerobic conditions is unreactive toward the zinc thiolates examined in this work, which implies that it is not NO itself, but an oxidized form thereof, that is the active species responsible for *S*-nitrosothiol formation and demetallation in NOS and metallothioneins in biology. Zinc thiolate reactivity with NO in the presence of dioxygen supports this hypothesis, and studies with  $\text{NO}_2$  indicate that nitrogen dioxide is a viable species for inducing zinc thiolate nitrosation in vivo. Exposure of  $[\text{ZnPATHCl}]$ ,  $[\text{ZnPATHOTf}]$ , and  $[\text{ZnAPATHCl}]$  to  $\text{NO}^+$  in the form of nitrosonium tetrafluoroborate also leads to thiolate nitrosation. Addition of  $\text{NOBF}_4$  to  $[\text{ZnPATHOTf}]$ , or of  $\text{Zn}(\text{OTf})_2$  to  $\text{PATHNO}$ , most likely generates a coordinated *S*-nitrosothiol as a transient species, but for both  $\text{PATHNO}$  and  $\text{APATHNO}$ , interaction of the  $-\text{SNO}$  moiety with  $\text{Zn}^{2+}$  promotes its decomposition. NO and  $\text{N}_2\text{O}$  were detected in the headspace of solutions containing  $\text{Zn}^{2+}$  and *S*-nitrosothiol, irrespective of whether the latter was prepared independently



or generated in situ. The absence of disulfide products from reaction mixtures is characteristic of heterolytic, not homolytic, cleavage of the S–N bond in the presence of  $Zn^{2+}$ , the role of which may be to activate the –SNO moiety toward heterolysis, possibly by stabilizing the thiolate formed in the reaction. Oxidized thiolates,  $RS[O]$ , may be the ultimate reaction products, as proposed in equation 2.5.

## 2.5. References

- (1) Moncada, S.; Palmer, R. M. J.; Higgs, E. A. *Pharmacol. Rev.* **1991**, *43*, 109-142.
- (2) Aravindakumar, C. T.; Ceulemans, J.; De Ley, M. *Biophys. Chem.* **2000**, *85*, 1-6.
- (3) Aravindakumar, C. T.; Ceulemans, J.; Ley, M. d. *Biochem. J.* **1999**, *344*
- (4) Bernal, P. J.; Leelavanichkul, K.; Bauer, E.; Cao, R.; Wilson, A.; Wasserloos, K. J.; Watkins, S. C.; Pitt, B. R.; St. Croix, C. M. *Circul. Res.* **2008**, *102*, 1575-1583.
- (5) Binet, M. R. B.; Cruz-Ramos, H.; Laver, J.; Hughes, M. N.; Poole, R. K. *FEMS Microbiol. Lett.* **2002**, *213*, 121-126.
- (6) Casero, E.; Martin-Gago, J. A.; Pariente, F.; Lorenzo, E. *Eur. Biophys. J.* **2004**, *33*, 726-731.
- (7) Chen, Y.; Irie, Y.; Keung, W. M.; Maret, W. *Biochemistry* **2002**, *41*, 8360-8367.
- (8) Gow, A.; Ischiropoulos, H. *Am. J. Physiol. Lung Cell. Mol. Physiol.* **2002**, *282*, L183-L184.
- (9) Khatai, L.; Goessler, W.; Lorencova, H.; Zangger, K. *Eur. J. Biochem.* **2004**, *271*, 2408-2416.
- (10) Kröncke, K. D. *Arch. Biochem. Biophys.* **2007**, *463*, 183-187.
- (11) Li, H.; Cao, R.; Wasserloos, K. J.; Bernal, P.; Liu, Z.-Q.; Pitt, B. R.; St. Croix, C. M. *Ann. N. Y. Acad. Sci.* **2010**, *1203*, 73-78.
- (12) Montoliu, C.; Monfort, P.; Carrasco, J.; Palacios, Ó.; Capdevila, M.; Hidalgo, J.; Felipo, V. *J. Neurochem.* **2000**, *75*, 266-273.
- (13) Pearce, L. L.; Gandley, R. E.; Han, W.; Wasserloos, K.; Stitt, M.; Kanai, A. J.; McLaughlin, M. K.; Pitt, B. R.; Levitan, E. S. *Proc. Natl. Acad. Sci. USA* **2000**, *97*, 477-482.
- (14) Pearce, L. L.; Wasserloos, K.; St. Croix, C. M.; Gandley, R.; Levitan, E. S.; Pitt, B. R. *J. Nutr.* **2000**, *130*, 1467S-1470S.
- (15) Spahl, D. U.; Berendji-Grün, D.; Suschek, C. V.; Kolb-Bachofen, V.; Kröncke, K.-D. *Proc. Natl. Acad. Sci. USA* **2003**, *100*, 13952-13957.
- (16) St. Croix, C. M.; Leelavaninchkul, K.; Watkins, S. C.; Kagan, V. E.; Pitt, B. R. *Proc. Am. Thorac. Soc.* **2005**, *2*, 236-242.
- (17) St. Croix, C. M.; Wasserloos, K. J.; Dineley, K. E.; Reynolds, I. J.; Levitan, E. S.; Pitt, B. R. *Am. J. Physiol. Lung Cell. Mol. Physiol.* **2002**, *282*, L185-L192.

- (18) Wang, H.; Li, H.; Cai, B.; Huang, Z. X.; Sun, H. *J. Biol. Inorg. Chem.* **2008**, *13*, 411-419.
- (19) Zangger, K.; Öz, G.; Haslinger, E.; Kunert, O.; Armitage, I. M. *FASEB J.* **2001**, *15*, 1303-1305.
- (20) Zhu, J.; Meeusen, J.; Krezoski, S.; Petering, D. H. *Chem. Res. Toxicol.* **2010**, *23*, 422-431.
- (21) Dudev, T.; Lin, D.; Dudev, M.; Lim, C. *J. Am. Chem. Soc.* **2003**, *125*, 3168-3180.
- (22) Karlin, S.; Zhu, Z.-Y. *Proc. Natl. Acad. Sci. USA* **1997**, *94*, 14231-14236.
- (23) Maret, W. *Antioxid. Redox Signal.* **2006**, *8*, 1419-1441.
- (24) Maret, W.; Li, Y. *Chem. Rev.* **2009**, *109*, 4682-4707.
- (25) Parkin, G. *Chem. Rev.* **2004**, *104*, 699-768.
- (26) Cuajungco, M. P.; Lees, G. J. *Brain Res.* **1998**, *799*, 118-129.
- (27) Kröncke, K. D.; Fehsel, K.; Schmidt, T.; Zenke, F. T.; Dasting, I.; Wesener, J. R.; Bettermann, H.; Breunig, K. D.; Kolb-Bachofen, V. *Biochem. Biophys. Res. Commun.* **1994**, *200*, 1105-1110.
- (28) Kröncke, K. D.; Kolb-Bachofen, V. In *Methods Enzymol.*; Lester, P., Ed.; Academic Press: 1999; Vol. 301, p 126-135.
- (29) Kröncke, K.-D.; Carlberg, C. *FASEB J.* **2000**, *14*, 166-173.
- (30) Kröncke, K.-D.; Klotz, L.-O.; Suschek, C. V.; Sies, H. *J. Biol. Chem.* **2002**, *277*, 13294-13301.
- (31) Ogra, Y.; Onishi, S.; Kajiwara, A.; Hara, A.; Suzuki, K. T. *J. Health Sci.* **2008**, *54*, 339-342.
- (32) Hemmens, B.; Goessler, W.; Schmidt, K.; Mayer, B. *J. Biol. Chem.* **2000**, *275*, 35786-35791.
- (33) Mitchell, D. A.; Erwin, P. A.; Michel, T.; Marletta, M. A. *Biochemistry* **2005**, *44*, 4636-4647.
- (34) Ravi, K.; Brennan, L. A.; Levic, S.; Ross, P. A.; Black, S. M. *Proc. Natl. Acad. Sci. USA* **2004**, *101*, 2619-2624.
- (35) Tummala, M.; Ryzhov, V.; Ravi, K.; Black, S. M. *DNA Cell Biol.* **2008**, *27*, 25-33.
- (36) Erwin, P. A.; Lin, A. J.; Golan, D. E.; Michel, T. *J. Biol. Chem.* **2005**, *280*, 19888-19894.
- (37) Erwin, P. A.; Mitchell, D. A.; Sartoretto, J.; Marletta, M. A.; Michel, T. *J. Biol. Chem.* **2006**, *281*, 151-157.
- (38) Smith, B. C.; Fernhoff, N. B.; Marletta, M. A. *Biochemistry* **2012**, *51*, 1028-1040.
- (39) Chang, S.; Karambelkar, V. V.; diTargiani, R. C.; Goldberg, D. P. *Inorg. Chem.* **2001**, *40*, 194-195.
- (40) Chang, S.; Karambelkar, V. V.; Sommer, R. D.; Rheingold, A. L.; Goldberg, D. P. *Inorg. Chem.* **2002**, *41*, 239-248.
- (41) diTargiani, R. C.; Chang, S.; Salter, M. H.; Hancock, R. D.; Goldberg, D. P. *Inorg. Chem.* **2003**, *42*, 5825-5836.
- (42) Szaciłowski, K.; Stasicka, Z. *Prog. React. Kinet. Mech.* **2001**, *26*, 1-58.
- (43) Andersen, R. J.; diTargiani, R. C.; Hancock, R. D.; Stern, C. L.; Goldberg, D. P.; Godwin, H. A. *Inorg. Chem.* **2006**, *45*, 6574-6576.
- (44) Mills, D. K.; Font, I.; Farmer, P. J.; Hsiao, Y.-M.; Tuntulani, T.; Buonomo, R. M.; Goodman, D. C.; Musie, G.; Grapperhaus, C. A.; Maguire, M. J.; Lai, C.-H.; Hatley, M. L.; Smee, J. J.; Bellefeuille, J. A.; Darensbourg, M. Y.; Hancock, R. D.; Eng, S.; Martell, A. E. In *Inorg. Synth.*; Darensbourg, M. Y., Ed. 2007, p 89-98.



- (45) Harrop, T. C.; Tonzetich, Z. J.; Reisner, E.; Lippard, S. J. *J. Am. Chem. Soc.* **2008**, *130*, 15602-15610.
- (46) Ji, M.; Vahrenkamp, H. *Eur. J. Inorg. Chem.* **2005**, *2005*, 1398-1405.
- (47) Lorković, I. M.; Ford, P. C. *Inorg. Chem.* **2000**, *39*, 632-633.
- (48) Noyes, W. A. *Org. Synth.* **1943**, *2*, 103.
- (49) Zhang, J.; Wang, H.; Xian, M. *Org. Lett.* **2009**, *11*, 477-480.
- (50) Zhang, J.; Wang, H.; Xian, M. *J. Am. Chem. Soc.* **2009**, *131*, 3854-3855.
- (51) Shaw, A. W.; Vosper, A. J. *J. Chem. Soc., Faraday Trans.* **1977**, *73*, 1239-1244.
- (52) Sander, R. *Surveys in Geophysics* **1999**, *20*, 1-31.
- (53) Tennyson, A. G.; Lippard, S. J., Unpublished work.
- (54) Hogg, N. *Annu. Rev. Pharmacol. Toxicol.* **2002**, *42*, 585-600.
- (55) Lawrance, G. A. *Chem. Rev.* **1986**, *86*, 17-33.
- (56) Derbesy, G.; Harpp, D. N. *J. Org. Chem.* **1995**, *60*, 1044-1052.
- (57) Zhao, Y.-L.; McCarren, P. R.; Houk, K. N.; Choi, B. Y.; Toone, E. J. *J. Am. Chem. Soc.* **2005**, *127*, 10917-10924.
- (58) Oae, S.; Shinhama, K. *Org. Prep. Proced. Int.* **1983**, *15*, 165 - 198.
- (59) Oae, S.; Shinhama, K.; Fujimori, K.; Kim, Y. H. *Bull. Chem. Soc. Jpn.* **1980**, *53*, 775-784.
- (60) Sengupta, R.; Ryter, S. W.; Zuckerbraun, B. S.; Tzeng, E.; Billiar, T. R.; Stoyanovsky, D. A. *Biochemistry* **2007**, *46*, 8472-8483.
- (61) Benhar, M.; Forrester, M. T.; Hess, D. T.; Stamler, J. S. *Science* **2008**, *320*, 1050-1054.

**Chapter 3. Reactions of Organozinc Thiolates with  
Nitrosonium Ion: C-Nitroso Formation by  
Intramolecular Transnitrosation**

### 3.1. Introduction

The importance of nitric oxide (NO) to the function of the immune, nervous, and circulatory systems has spurred interest in its chemistry<sup>1-4</sup> and that of related organic molecules, including *S*-nitrosothiols,<sup>5-6</sup> organic nitrites, *N*-nitrosamines, and *C*-nitroso species.<sup>7-11</sup> In Chapter 2, we described the reactivity of three bioinspired models of the tetracysteine-thiolate zinc site of nitric oxide synthase toward reactive nitrogen and oxygen species (Chart 3.1*a, b*).<sup>12</sup>

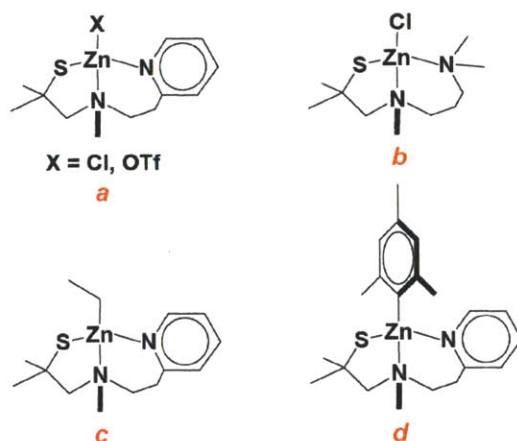


**Chart 3.1.** *N*<sub>2</sub>S-coordinated Zn<sup>2+</sup> species of interest. The molecules shown are *a*) [ZnPATHX] (X = Cl, OTf), *b*) [ZnAPATHCl], *c*) [ZnPATHEt], and *d*) [ZnPATHMes].

We demonstrated *S*-nitrosation of the ligand upon exposure of [ZnPATHCl], [ZnPATHOTf], and [ZnAPATHCl] to NO<sub>2</sub> (g), NOBF<sub>4</sub>, NO (g) and air, but not to anaerobic NO (g). We also examined the behavior of the independently synthesized *S*-nitrosothiols PATHNO and APATHNO in the presence of Zn<sup>2+</sup> (Chart 3.2). Building on this work, we were interested to extend our studies to include organometallic complexes, specifically [ZnPATHEt] and [ZnPATHMes] (Chart 1X*c, d*), and in this chapter we report their chemistry with NOBF<sub>4</sub>.

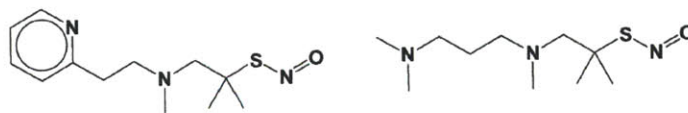


**Chart 3.2.** PATHNO (*left*) and APATHNO (*right*).

Earlier reports and reviews<sup>13</sup> describe chemistry of nitrosonium ion with organometallic complexes of mercury,<sup>14-18</sup> magnesium,<sup>19-22</sup> tin,<sup>23-24</sup> cadmium,<sup>25</sup> lithium,<sup>26-27</sup> thallium,<sup>28-29</sup> silicon,<sup>30</sup> aluminum,<sup>31</sup> molybdenum,<sup>32</sup> and chromium.<sup>33</sup> The coordination chemistry of *C*-nitroso species has also been explored,<sup>34-46</sup> and the reactions of alkylzinc complexes with nitric oxide have been exploited for nitrogen doping of ZnO films.<sup>47-50</sup> Additionally, the chemistry of organozinc complexes with dioxygen, alcohols, and water has been examined,<sup>51-53</sup> as well as with alkyl nitro and nitroso species.<sup>54-57</sup> Our search of the literature did not uncover any work regarding the chemistry of organozinc and nitrosonium ion, however, and contributed in part to the motivation for the studies described in this Chapter. Largely, we were inspired to conduct the experiments described herein by the possibility that *C*-nitroso compounds formed in the reaction of [ZnPAThR] (R = Et, Mes) with NO<sup>+</sup> through a transient *S*-nitrosothiol intermediate. That is, we wished to determine whether NO<sup>+</sup> attack on [ZnPAThR] (R = Et, Mes) occurs initially at the sulfur atom of the PATh ligand, with subsequent *C*-nitroso formation via intramolecular transnitrosation chemistry involving PAThNO.

### 3.2. Experimental Methods

**General Procedures and Starting Materials.** Air- and moisture-sensitive materials were handled in an MBraun glovebox under an inert nitrogen atmosphere. The compound 2-(2-methylaminoethyl)-pyridine was purchased from Sigma-Aldrich and used without further purification. Nitrosonium tetrafluoroborate (97%) was purchased from Strem and used as received. Isobutylene sulfide was prepared according to published methods.<sup>58</sup> PAThH was prepared as described<sup>59-60</sup> and purified by Al<sub>2</sub>O<sub>3</sub> column chromatography using 2:1 ethyl acetate:pentane to give the desired product as a colorless oil. [ZnPAThCl] was prepared as

described<sup>61</sup> and purified by recrystallization. A 1 M solution of ZnEt<sub>2</sub> in hexanes was purchased from Sigma-Aldrich and used without further purification. ZnMes<sub>2</sub> was prepared from zinc bromide and mesityl Grignard in a manner analogous to the published procedure.<sup>62</sup> Acetonitrile (MeCN), tetrahydrofuran (THF), methylene chloride, and pentane were saturated with argon, purified by passage through activated alumina, and stored over 4 Å molecular sieves under an inert nitrogen atmosphere prior to use. Deuterated NMR solvents were obtained from Cambridge Isotope Laboratories and used without further purification. Methylene chloride-*d*<sub>2</sub> and acetonitrile-*d*<sub>3</sub> were brought into the glovebox and stored over 4 Å molecular sieves under inert nitrogen atmosphere. CHN analyses were performed by Intertek-QTI (Whitehouse, NJ, USA) and Midwest Microlab, LLC (Indianapolis, IN, USA).

**Synthesis of [ZnPATHet].** To a stirring solution of PATHH (1.0 g, 4.46 mmol) in dry pentane (~10 mL) was added 1 M ZnEt<sub>2</sub> (4.46 mL, 4.46 mmol) under an inert nitrogen atmosphere. A white precipitate formed immediately. The suspension was left to stir for 1 h. The solid was isolated by filtration and washed with dry ether, giving the desired product (0.978 g, 69%) as a white solid. X-ray quality crystals were obtained by CH<sub>2</sub>Cl<sub>2</sub>/pentane vapor diffusion. <sup>1</sup>H NMR (CD<sub>3</sub>CN) δ -0.04 – 0.00 (m, 2H, CH<sub>2</sub>), 1.00 (t, *J* = 8.0 Hz, 3H, Et-CH<sub>3</sub>), 1.32 (s, 3H, CH<sub>3</sub>), 2.39 (d, *J* = 13.0 Hz, 1H, CH<sub>2</sub>), 2.60 (s, 3H, NCH<sub>3</sub>), 2.75 (d, *J* = 13.0 Hz, 1H, CH<sub>2</sub>), 2.79 – 2.84 (m, 1H, CH<sub>2</sub>), 3.02 – 2.99 (m, 2H, CH<sub>2</sub>), 3.10 – 3.19 (m, 1H, CH<sub>2</sub>), 7.36 (d, *J* = 7.6 Hz, 1H, py-*H*<sub>β</sub>), 7.40 – 7.43 (m, 1H, py-*H*<sub>δ</sub>), 7.87 (td, *J* = 7.6, 1.6 Hz, 1H, py-*H*<sub>γ</sub>), 8.50 (d, *J* = 4.4 Hz, 1H, py-*H*<sub>ε</sub>); <sup>13</sup>C NMR (CD<sub>3</sub>CN) δ 0.40, 13.78, 33.75, 34.59, 36.11, 46.62, 48.53, 60.08, 75.58, 123.88, 125.75, 140.25, 149.36, 161.63. Anal. Calc'd. for C<sub>14</sub>H<sub>24</sub>N<sub>2</sub>SZn: C, 52.91; H, 7.61; N, 8.81. Found: C, 52.93; H, 7.22; N, 9.11.

**Synthesis of [ZnPAThMes].** To a solution of PAThH (1.0 g, 4.46 mmol) in dry THF (~15 mL) was added ZnMes<sub>2</sub> (1.35 g, 4.46 mmol) as a solid in two portions. The reaction mixture was allowed to stir overnight under inert nitrogen atmosphere, during which time a white precipitate formed. The solvent was removed in vacuo and the residue was washed with diethyl ether. The solid was dried under vacuum to give 1.5 g (82% yield) of the desired material as a white powder. X-ray quality crystals were obtained by CH<sub>2</sub>Cl<sub>2</sub>/pentane vapor diffusion. <sup>1</sup>H NMR (CD<sub>2</sub>Cl<sub>2</sub>) δ 1.31 (s, 3H, CH<sub>3</sub>), 1.55 (s, 3H, CH<sub>3</sub>), 2.19 (s, 3H, Mes-CH<sub>3</sub>), 2.32 (s, 6H, Mes-CH<sub>3</sub>), 2.46 (d, *J* = 12.8 Hz, 1H, CH<sub>2</sub>), 2.62 (s, 3H, N-CH<sub>3</sub>), 2.87 (d, *J* = 12.8 Hz, 1H, CH<sub>2</sub>), 2.95 – 3.06 (m, 3H, CH<sub>2</sub>), 3.81 – 3.85 (m, 1H, CH<sub>2</sub>), 6.72 (s, 2H, Mes-H), 7.26 – 7.29 (m, 1H, py-H<sub>β</sub>), 7.32 (d, *J* = 8 Hz, 1H, py-H<sub>δ</sub>), 7.80 (td, *J* = 7.6 Hz, 1.6 Hz, 1H, py-H<sub>γ</sub>), 8.35 (d, *J* = 1.2 Hz, 1H, py-H<sub>ε</sub>); <sup>13</sup>C NMR (CD<sub>2</sub>Cl<sub>2</sub>) δ 21.26, 27.68, 33.33, 34.39, 36.13, 46.11, 49.76, 59.88, 74.01, 123.46, 125.42, 126.46, 135.62, 139.68, 147.60, 149.38, 151.37, 160.73. Anal. Calc'd. for C<sub>21</sub>H<sub>30</sub>N<sub>2</sub>SZn: C, 61.83; H, 7.41; N, 6.87. Found: C, 60.59; H, 7.14; N, 7.08.

**Preparatory Scale Reaction of [ZnPAThMes] with NOBF<sub>4</sub>.** To a stirring suspension of [ZnPAThMes] (0.4 g, 0.98 mmol) in acetonitrile under an inert nitrogen atmosphere was added NOBF<sub>4</sub> (0.114 g, 0.98 mmol) as a solid. The reaction was allowed to stir for 2 h, after which time the reaction vial was removed from the glovebox and the reaction was quenched by addition to water. A white solid formed immediately. The suspension was extracted into diethyl ether and the organic layer was dried (MgSO<sub>4</sub>) and evaporated to dryness to yield 92.1 mg (63%) of *C*-nitrosomesitylene. X-ray quality crystals of [MesNO]<sub>2</sub> were grown by slow evaporation of a diethyl ether solution of *C*-nitrosomesitylene. The analogous reaction was also performed in 2:1 MeCN:CH<sub>2</sub>Cl<sub>2</sub>, quenched with water, and extracted into methylene chloride. The organic layer

was dried ( $\text{MgSO}_4$ ) and concentrated in vacuo. The resultant residue was dissolved in  $\text{CH}_2\text{Cl}_2$ , and X-ray quality crystals of  $[\text{ZnPAThCl}]$  were grown by slow evaporation of this solution.

**Physical Measurements.**  $^1\text{H}$  and  $^{13}\text{C}$  NMR spectra were recorded on a 400 MHz Bruker Avance spectrometer. Optical spectra were measured on a Varian Cary 50 Bio UV-Visible Spectrophotometer in 6SQ Starna cells. The Cary WinUV scanning kinetics software was used to record optical time-dependent spectra. An Agilent Technologies 5975C mass selective detector running in electron impact ionization mode was used for EI-MS studies of the reaction headspace. An Argon matrix was used for EI-MS studies.

**UV-Vis Studies.** All solutions were prepared under an inert nitrogen atmosphere. Optical spectra were recorded at 25 °C. Stock solutions of  $\text{NOBF}_4$  in acetonitrile were prepared at 1.1 times the desired reaction concentration. Solutions of  $[\text{ZnPAThR}]$  ( $\text{R} = \text{Et}, \text{Mes}$ ) were prepared at 10 times the desired reaction concentration. A 2.7 mL portion of the  $\text{NOBF}_4$  solution was transferred into a cuvette and the cuvette was sealed with an air-tight Teflon cap containing a septum. A 300  $\mu\text{L}$  portion of zinc thiolate solution was withdrawn by a gas-tight syringe and the needle was covered by a septum. The cuvette was transferred to the UV-Vis spectrophotometer. After one optical scan of the nitrosonium tetrafluoroborate solution, the  $[\text{ZnPAThR}]$  solution was quickly injected. The cuvette was shaken to mix the reagents and returned to the spectrophotometer. Optical spectra were recorded at regular intervals.

**EI-MS Studies.** All solutions were prepared under a nitrogen atmosphere.  $\text{NOBF}_4$  (0.184 g, 1.57 mmol) was dissolved in  $\sim 3$  mL methylene chloride contained in a custom-made gas-tight cell. The cell was prepared in an MBraun glovebox under an inert nitrogen atmosphere. The cell was removed from the glovebox and exposed to an argon purge.  $[\text{ZnPAThMes}]$  (0.50 g, 1.57 mmol) was dissolved in  $\sim 1$  mL methylene chloride under a nitrogen atmosphere and was transferred by

gas-tight syringe to the reaction cell under an argon flow. The cell was sealed and the reaction mixture was allowed to stir for 1.5 h prior to analysis. The cell was connected to an Ar gas flow and then to the mass spectrometer. The connecting copper tubing was purged thoroughly prior to analysis of the reaction headspace. Headspace analysis was undertaken with the mass spectrometer operating in the selective ion mode. All reactions were carried out in the dark to prevent photodecomposition of light-sensitive species.

**Spectroscopic Yield Experiment.** [ZnPAThMes] (100 mg, 0.24 mmol) was dissolved in ~9 mL of 2:1  $CD_3CN:CD_2Cl_2$  and an aliquot of the solution was collected for later analysis by  $^1H$  NMR spectroscopy. Solid  $NOBF_4$  (29 mg, 0.24 mmol) was added to the stirring solution. The reaction mixture was observed to turn green briefly, before fading to yellow. The reaction was left to stir for 1.5 h under an inert nitrogen atmosphere, at which point an aliquot was collected and analyzed by  $^1H$  NMR spectroscopy. Aliquots were subsequently analyzed after 4 h and 1 day of reaction time. An additional aliquot, collected at the 1 day time point, was spiked with independently prepared [ZnPAThCl] and analyzed by  $^1H$  NMR spectroscopy for comparison with reaction spectra. This spiking experiment confirmed the presence of [ZnPAThCl] in reaction mixtures.

**X-Ray Crystallography.** Crystals were mounted in Paratone N oil and frozen at 100 K ([ZnPAThEt]) or 110 K ([ZnPAThMes], [MesNO] $_2$ ) under a cold nitrogen stream controlled by a Cryopad low-temperature apparatus. Data were collected on a Bruker APEX CCD X-ray diffractometer with graphite-monochromated Mo- $K_\alpha$  radiation ( $\lambda = 0.71073 \text{ \AA}$ ) controlled by the APEX2 ([ZnPAThEt]) or SMART ([ZnPAThMes], [MesNO] $_2$ ) software packages.<sup>63-64</sup> Empirical absorption correction was performed with SADABS.<sup>65</sup> The structure was solved by direct methods using SHELXS-97 and refined by full-matrix least-squares on  $F^2$  using the SHELXL-97



program incorporated into the SHELXTL software package.<sup>66</sup> Possible higher symmetries were evaluated by PLATON.<sup>67</sup> Non-hydrogen atoms were located and their positions refined anisotropically. Hydrogen atoms were assigned idealized positions and given thermal parameters 1.2 (non-methyl hydrogen atoms) or 1.5 (methyl hydrogen atoms) times the thermal parameters of the atoms to which they are attached. Thermal ellipsoid plots were generated using ORTEP-III.<sup>68</sup>

**Theoretical Calculations.**<sup>†</sup> Geometry optimizations, frequency calculations, and molecular orbital calculations were performed in Gaussian 03<sup>69</sup> or Gaussian 09.<sup>70</sup> Geometries were optimized using the B3LYP functional<sup>71-73</sup> and the 6-31G(d,p)<sup>74-75</sup> basis set over all atoms. All calculations were performed in the gas phase and only positive frequencies were found for all geometry optimized structures in the ground state. A single imaginary frequency was determined for the transition state of NO<sup>+</sup> attack on [ZnPAThEt]. Molecular orbitals were visualized with VMD software.<sup>76</sup> Isosurfaces are depicted at isovalues of 0.06. Intrinsic reaction coordinate (IRC) calculations were performed according to the method introduced by Fukui,<sup>77</sup> which connects the first-order saddle point, or transition state, and two minima, which correspond to the reactant and product, continuously along the potential energy surface.

### 3.3. Results

Exposure of the PThH<sup>59-60</sup> ligand to ZnEt<sub>2</sub> and ZnMes<sub>2</sub> afforded the desired organometallic species [ZnPAThEt] and [ZnPAThMes], respectively, in satisfactory yields (Fig. 3.1). Crystallographic parameters, and bond distances and angles of interest are tabulated in Tables 3.1 – 3.3.

---

<sup>†</sup> The author thanks Prof. Hélio F. Dos Santos, at Universidade Federal de Juiz de Fora, Brazil, who kindly provided computer time for Gaussian 09 calculations.

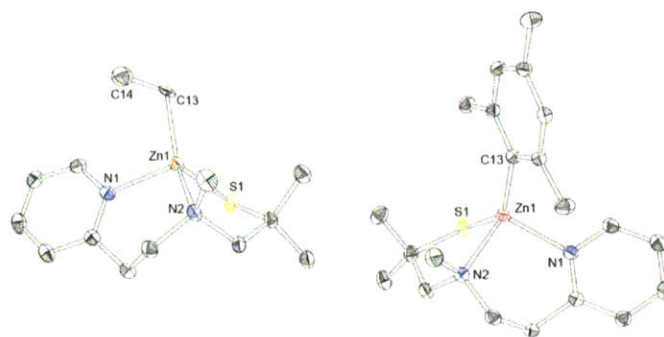


**Figure 3.1.** Thermal ellipsoid plots for [ZnPAThEt] (*left*) and [ZnPAThMes] (*right*), shown at 50% probability. Hydrogen atoms are omitted for clarity, and only one of the two molecules in the asymmetric unit of [ZnPAThMes] is shown.

**Table 3.1.** Crystallographic parameters for [ZnPAThEt] and [ZnPAThMes].

	[ZnPAThEt]	[ZnPAThMes]
<b>Empirical formula</b>	C <sub>14</sub> H <sub>24</sub> N <sub>2</sub> SZn	C <sub>21</sub> H <sub>30</sub> N <sub>2</sub> SZn
<b>Formula weight</b>	317.78	407.90
<b>Crystal system</b>	Monoclinic	Monoclinic
<b>Space group</b>	<i>P</i> 2 <sub>1</sub> / <i>n</i>	<i>P</i> 2 <sub>1</sub> / <i>c</i>
<b>a (Å)</b>	8.0009(10)	16.1505(11)
<b>b (Å)</b>	15.3847(19)	8.1973(6)
<b>c (Å)</b>	12.2845(15)	30.792(2)
<b>β (deg)</b>	92.387(2)	93.191(1)
<b>V (Å<sup>3</sup>)</b>	1510.8(3)	4070.3(5)
<b>Z</b>	4	8
<b>ρ<sub>calc</sub> (g/cm<sup>3</sup>)</b>	1.397	1.331
<b>Temperature (K)</b>	100 (2)	110 (2)
<b>μ (Mo Kα), (mm<sup>-1</sup>)</b>	1.749	1.315
<b>θ range (deg)</b>	2.12 to 25.55	1.26 to 28.61
<b>Crystal size (mm<sup>3</sup>)</b>	0.22 x 0.13 x 0.02	0.4 x 0.2 x 0.1
<b>Completeness to θ (%)</b>	99.5	99.7
<b>Max, min peaks (e/Å<sup>3</sup>)</b>	0.501 and -0.460	0.424 and -0.355
<b>Goodness-of-fit<sup>a</sup></b>	1.044	1.043
<b>Total no. of data</b>	23193	82984
<b>No. unique data</b>	2802	10375
<b>R<sub>1</sub> (%)<sup>b</sup></b>	3.67	2.72
<b>wR<sub>2</sub> (%)<sup>c</sup></b>	6.69	6.52

<sup>a</sup>GOF =  $[\sum w(F_o^2 - F_c^2)^2 / (n - p)]^{1/2}$  where *n* is the number of data and *p* is the number of refined parameters.

<sup>b</sup> $R_1 = \sum ||F_o| - |F_c|| / \sum |F_o|$

<sup>c</sup> $wR_2 = \{\sum [w(F_o^2 - F_c^2)^2] / \sum [w(F_o^2)^2]\}^{1/2}$

**Table 3.2.** Summary of bond lengths (Å) and angles (deg) of interest for [ZnPAThEt].

Zn – N <sub>pyridyl</sub>	2.125(2)	N <sub>pyridyl</sub> – Zn – N <sub>alkyl</sub>	95.28(9)
Zn – N <sub>alkyl</sub>	2.171(3)	N <sub>pyridyl</sub> – Zn – S	112.35(7)
Zn – S	2.2937(9)	N <sub>alkyl</sub> – Zn – S	89.62(7)
Zn – C <sub>ethyl</sub>	2.014(3)	C <sub>ethyl</sub> – Zn – N <sub>pyridyl</sub>	105.52(11)
		C <sub>ethyl</sub> – Zn – N <sub>alkyl</sub>	116.41(11)
		C <sub>ethyl</sub> – Zn – S	131.44(9)

**Table 3.3.** Summary of bond lengths (Å) and angles (deg) of interest for [ZnPAThMes]. [ZnPAThMes] crystallizes with two molecules in the asymmetric unit. Bond length and angle values are tabulated for both molecules.

Zn(1) – N <sub>pyridyl</sub>	2.1309(13)	N <sub>pyridyl</sub> – Zn(1) – N <sub>alkyl</sub>	96.00(5)
Zn(1) – N <sub>alkyl</sub>	2.2015(13)	N <sub>pyridyl</sub> – Zn(1) – S	107.60(4)
Zn(1) – S	2.2817(4)	N <sub>alkyl</sub> – Zn(1) – S	90.15(4)
Zn(1) – C <sub>ethyl</sub>	2.0161(15)	C <sub>ethyl</sub> – Zn(1) – N <sub>pyridyl</sub>	108.13(6)
		C <sub>ethyl</sub> – Zn(1) – N <sub>alkyl</sub>	113.25(5)
		C <sub>ethyl</sub> – Zn(1) – S	134.33(5)
Zn(2) – N <sub>pyridyl</sub>	2.1221(13)	N <sub>pyridyl</sub> – Zn(2) – N <sub>alkyl</sub>	96.09(5)
Zn(2) – N <sub>alkyl</sub>	2.2063(13)	N <sub>pyridyl</sub> – Zn(2) – S	106.56(4)
Zn(2) – S	2.3010(4)	N <sub>alkyl</sub> – Zn(2) – S	88.41(4)
Zn(2) – C <sub>ethyl</sub>	2.0196(15)	C <sub>ethyl</sub> – Zn(2) – N <sub>pyridyl</sub>	110.39(6)
		C <sub>ethyl</sub> – Zn(2) – N <sub>alkyl</sub>	115.16(6)
		C <sub>ethyl</sub> – Zn(2) – S	132.83(4)

The bond lengths and angles in [ZnPAThEt] and [ZnPAThMes] are comparable to those reported for [ZnPAThMe].<sup>78</sup> The metal centers of all three complexes have distorted tetrahedral geometries.<sup>78</sup> The N<sub>pyr</sub>-Zn-S angle in [ZnPAThMes] is smaller than in the alkyl zinc species. This contraction may be necessary to accommodate the sterically more bulky mesityl substituent. Metal-carbon distances are similar among the organozinc complexes, with bond lengths of 1.986 Å for [ZnPAThMe],<sup>78</sup> 2.014 Å for [ZnPAThEt], and 2.016 Å for [ZnPAThMes]. Unlike [ZnPAThMe]<sup>78</sup> and [ZnPAThEt], [ZnPAThMes] crystallizes with two molecules in the asymmetric unit.

Exposure of [ZnPAThEt] to 1 equiv of NOBF<sub>4</sub> resulted in little change in the optical spectrum (Fig. 3.2, *left*). Similarly, little optical change was observed upon exposure of [ZnPAThMes] to 1 equiv NOBF<sub>4</sub> (Fig. 3.2, *right*).

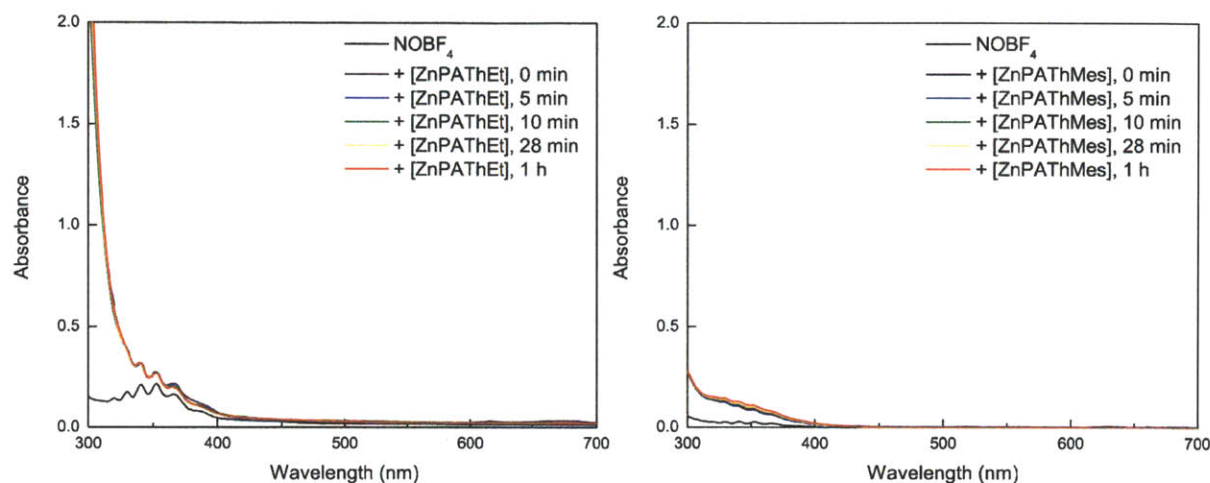


**Figure 3.2.** Optical spectra of 7.5 mM [ZnPAThEt] + 1 equiv NOBF<sub>4</sub> (*left*), and 2.5 mM [ZnPAThMes] + 1 equiv NOBF<sub>4</sub> (*right*). Spectra were recorded in 1:9 CH<sub>2</sub>Cl<sub>2</sub>:MeCN at 25 °C. Optical features in the 350 nm region of the NOBF<sub>4</sub> starting spectrum are attributed to NO<sub>2</sub>BF<sub>4</sub> contamination in the commercially available NOBF<sub>4</sub> starting material.

The headspace of the reaction mixture containing [ZnPAThEt] and 1 equiv NOBF<sub>4</sub> was analyzed by EI-MS and was found to contain gaseous NO, butane, and NO<sub>2</sub> (Figure 3.3).

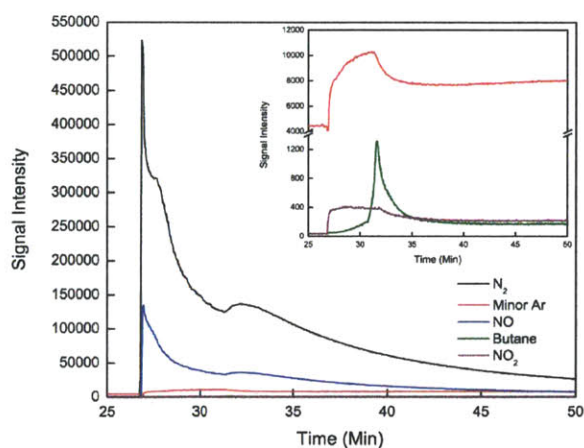


**Figure 3.3.** EI-MS analysis of the reaction headspace for the reaction between [ZnPAThEt] and 1 equiv NOBF<sub>4</sub> revealed the formation of NO, butane, and NO<sub>2</sub>.

The delay in the appearance of the butane signal (Fig. 3.3) may result from greater adsorption of butane to the reaction vessel or sampling lines compared with the other analytes. An increase in the intensity of the  $^{36}\text{Ar}$  signal occurs concomitantly with the appearance of the butane signal, and indicates an increase in flow rate. The increased flow rate may cause desorption of butane from the reaction cell and/or sampling lines. The detection of NO, butane, and  $\text{NO}_2$  suggests radical pathways for the decomposition of  $[\text{ZnPAThEt}]$  in the presence of nitrosonium (*vide infra*).

Difficulties in characterizing the non-gaseous products of the  $[\text{ZnPAThEt}]/\text{NOBF}_4$  reaction were alleviated once we turned to the  $[\text{ZnPAThMes}]/\text{NOBF}_4$  system. The *C*-nitrosomesitylene dimer,  $[\text{MesNO}]_2$ , was isolated when the  $[\text{ZnPAThMes}]/\text{NOBF}_4$  reaction was performed in acetonitrile, quenched with water, and extracted into diethyl ether (Fig. 3.4). Crystallographic parameters and bond distances and angles of interest are tabulated in Tables 3.4 and 3.5.

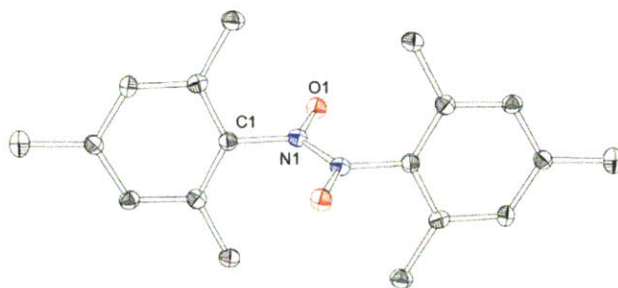


**Figure 3.4.** Thermal ellipsoid plot of the *C*-nitrosomesitylene dimer, shown at 50% probability. The major component of the disordered molecule is shown. Hydrogen atoms are omitted for clarity.

**Table 3.4.** Crystallographic parameters for [MesNO]<sub>2</sub>.

<b>Empirical formula</b>	C <sub>18</sub> H <sub>22</sub> N <sub>2</sub> O <sub>2</sub>
<b>Formula weight</b>	298.38
<b>Crystal system</b>	Orthorhombic
<b>Space group</b>	<i>Pbca</i>
<b>a (Å)</b>	8.7539(7)
<b>b (Å)</b>	10.3947(8)
<b>c (Å)</b>	17.2466(14)
<b>V (Å<sup>3</sup>)</b>	1569.3(2)
<b>Z</b>	4
<b><math>\rho_{calc}</math> (g/cm<sup>3</sup>)</b>	1.263
<b>Temperature (K)</b>	110
<b><math>\mu</math> (Mo K<math>\alpha</math>), (mm<sup>-1</sup>)</b>	0.083
<b><math>\theta</math> range (deg)</b>	2.36 to 31.72
<b>Crystal size (mm<sup>3</sup>)</b>	0.4 x 0.4 x 0.4
<b>Completeness to <math>\theta</math> (%)</b>	96.5
<b>Max, min peaks (e/Å<sup>3</sup>)</b>	0.403 and -0.183
<b>Goodness-of-fit<sup>a</sup></b>	1.052
<b>Total no. of data</b>	34785
<b>No. unique data</b>	2565
<b>R<sub>1</sub> (%)<sup>b</sup></b>	3.87
<b>wR<sub>2</sub> (%)<sup>c</sup></b>	10.89

<sup>a</sup>GOF =  $[\sum w(F_o^2 - F_c^2)^2 / (n - p)]^{1/2}$  where  $n$  is the number of data and  $p$  is the number of refined parameters.

<sup>b</sup> $R_1 = \sum ||F_o| - |F_c|| / \sum |F_o|$

<sup>c</sup> $wR_2 = \{\sum [w(F_o^2 - F_c^2)^2] / \sum [w(F_o^2)^2]\}^{1/2}$

**Table 3.5.** Summary of bond lengths (Å) and angles (deg) of interest for [MesNO]<sub>2</sub>.

O(1)-N(1)	1.263(3)	O(1)-N(1)-N(1#)	121.44(15)
N(1)-N(1#)	1.3248(15)	O(1)-N(1)-C(1)	119.82(14)
N(1)-C(1)	1.4615(12)	N(1#)-N(1)-C(1)	118.71(9)

C-nitrosomesitylene exists as a dimer in the solid state, with the two monomer units linked by an N–N bond. The bond distance between these symmetry-equivalent nitrogen atoms, N1-N1#, is 1.3248(15) Å. This value matches the 1.32 Å average N-N bond distance in dimeric C-nitrosoaryl compounds found in the Cambridge Structural Database (CSD).<sup>79-84</sup> The monomer units are crystallographically related by an inversion center, located at the center of the N1-N1# bond. The plane of the N(O)N(O) fragment in [MesNO]<sub>2</sub> makes a dihedral angle of 73.70° with



respect to the plane of the mesityl groups. The nearly perpendicular orientation of the two planes prevents unfavorable steric interactions of the N(O)N(O) fragment with the methyl groups of mesitylene. The nitrogen atom of the nitroso group has an idealized trigonal environment, with angles of  $121.44(15)^\circ$ ,  $119.82(14)^\circ$ , and  $118.71(9)^\circ$  about the nitrogen. The N1-C1 and N1-O1 distances are  $1.4615(12) \text{ \AA}$  and  $1.263(3) \text{ \AA}$ , respectively, and are comparable to the  $1.44 \text{ \AA}$  and  $1.26 \text{ \AA}$  for the N-C and N-O bond averages of *C*-nitrosoaryl species in the CSD.<sup>79-84</sup> The *C*-nitrosomesitylene dimer exhibits whole molecule disorder (Fig. 3.5), wherein the mesitylene moiety of the minor component lies at a  $10.78^\circ$  angle relative to the mesitylene moiety of the major component. The minor component accounts for  $\sim 15\%$  of electron density. The atomic displacement parameters for the atoms of the two components of the disorder were constrained to be equivalent, in order to facilitate solution of the structure.

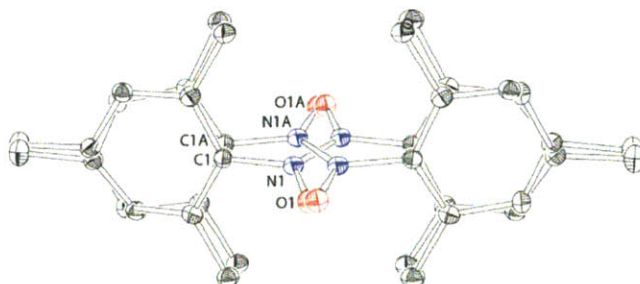


**Figure 3.5.** Thermal ellipsoid plot of  $[\text{MesNO}]_2$ , depicting the whole molecule disorder. Atoms C1A, N1A, and O1A belong to the minor component of the disorder. Thermal ellipsoids are shown at 50% probability, and hydrogen atoms are omitted for clarity.

Reaction of stoichiometric amounts of  $\text{NOBF}_4$  with  $[\text{ZnPAThMes}]$  in 2:1  $\text{MeCN}:\text{CH}_2\text{Cl}_2$  and subsequent workup led to the isolation of crystalline  $[\text{ZnPAThCl}]$  (Fig. 3.6). The isolated  $[\text{ZnPAThCl}]$  complex crystallized in space group  $P2_1/n$ , with unit cell parameters  $a = 8.2571(4) \text{ \AA}$ ,  $b = 15.1384(7) \text{ \AA}$ ,  $c = 11.7743(6) \text{ \AA}$ ,  $\beta = 92.682(1)^\circ$ , and a unit cell volume of  $1470.17 \text{ \AA}^3$ . These values are comparable to values reported previously for  $[\text{ZnPAThCl}]$ , which also crystallized in monoclinic space group  $P2_1/n$ .<sup>61</sup> Unit cell parameters for the previously reported

structure are  $a = 8.203(1) \text{ \AA}$ ,  $b = 14.979(2) \text{ \AA}$ ,  $c = 11.788(2) \text{ \AA}$ ,  $\beta = 93.436(2)^\circ$ .<sup>61</sup> The unit cell volume was calculated to be  $1445.8(4) \text{ \AA}^3$ .<sup>61</sup>

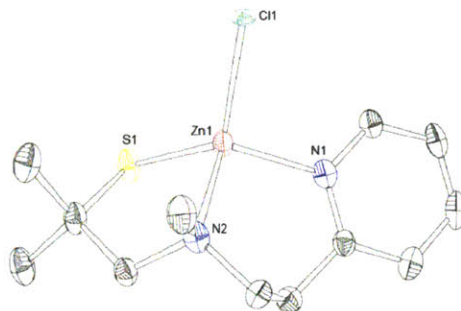


**Figure 3.6.** Thermal ellipsoid plot for [ZnPATHCl], shown at 50% probability. Unit cell parameters for this complex are  $a = 8.2571(4) \text{ \AA}$ ,  $b = 15.1384(7) \text{ \AA}$ ,  $c = 11.7743(6) \text{ \AA}$ ,  $V = 1470.17 \text{ \AA}^3$ . The compound crystallizes in the monoclinic space group  $P2_1/n$ , with  $\beta = 92.682(1)^\circ$ . Previously published values for [ZnPATHCl] in  $P2_1/n$  are  $a = 8.203(1) \text{ \AA}$ ,  $b = 14.979(2) \text{ \AA}$ ,  $c = 11.788(2) \text{ \AA}$ ,  $V = 1445.8(4) \text{ \AA}^3$ , and  $\beta = 93.436(2)^\circ$ .<sup>61</sup> Hydrogen atoms have been omitted for clarity.

A  $^1\text{H}$  NMR spectroscopic experiment revealed complete conversion of coordinated mesitylene anion to *C*-nitrosomesitylene and ~59% conversion to [ZnPATHCl] (Fig. 3.7). The percent conversion was computed by comparison of the integration values of [ZnPATHCl] pyridyl protons with integration values for pyridyl protons of other species in solution. The sums of pyridyl proton integration values for [ZnPATHCl] at 1.5 h, 4 h, and 1 day are 5.85, 5.29, and 4.96, respectively (Fig. 3.7, shown in red). Sums of pyridyl integration values for *all* pyridyl protons at 1.5 h, 4 h, and 1 day are 9.97, 8.98, and 8.37, respectively. The pyridyl protons of [ZnPATHCl] therefore constitute, on average, ~59% of all observed pyridyl protons in solution, corresponding to ~59% conversion of [ZnPATHMes] to [ZnPATHCl]. The presence of additional species in the reaction mixture precluded kinetic analyses and mechanistic studies of the [ZnPATHMes]/NOBF<sub>4</sub> reaction.



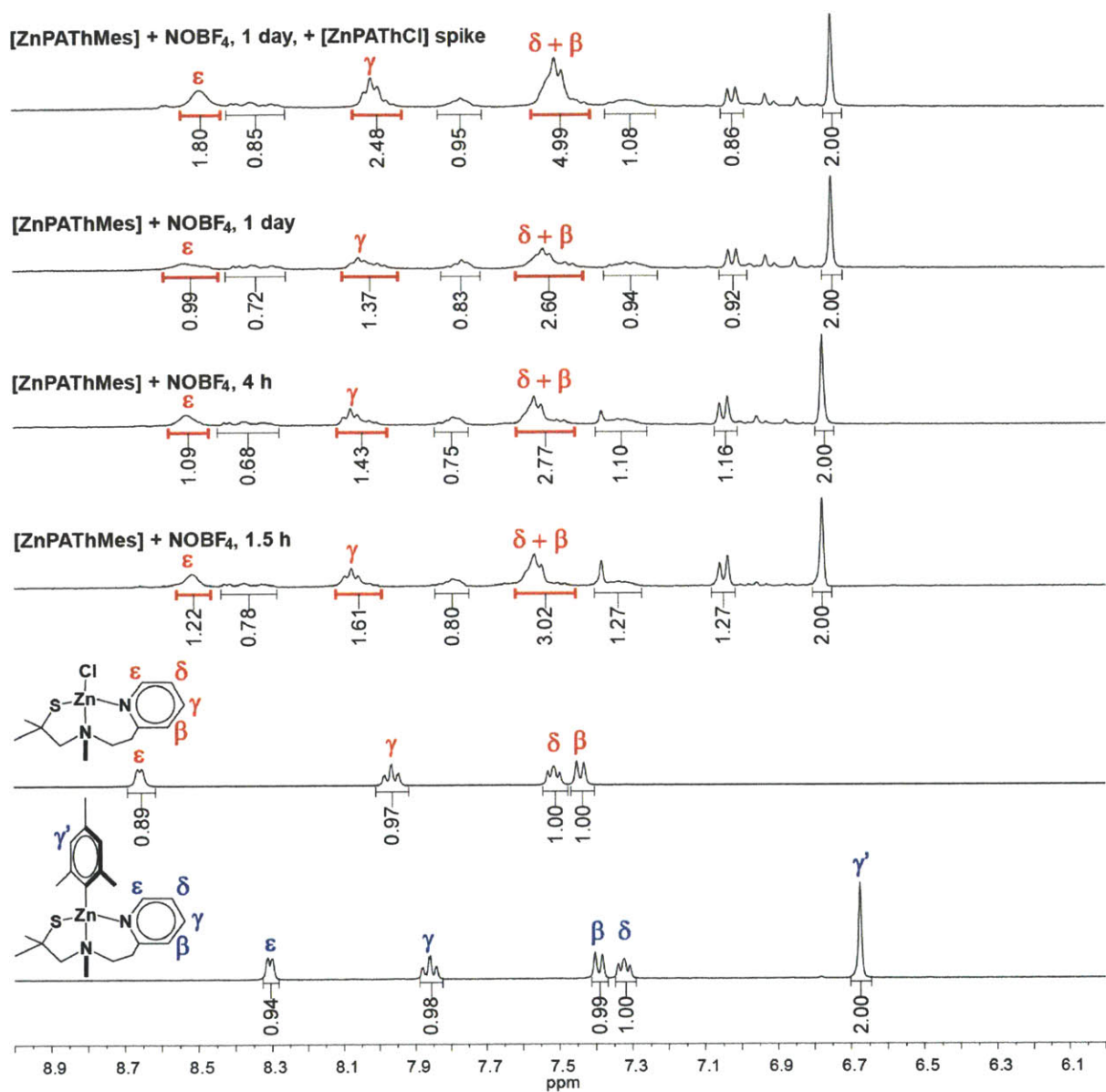


**Figure 3.7.** Spectroscopic analysis of the conversion of  $[\text{ZnPATHMes}]$  to independently prepared  $[\text{ZnPATHCl}]$  in the presence of 1 equiv of  $\text{NOBF}_4$ . An expanded view of the aryl region is shown for clarity. Peaks corresponding to aryl protons of  $[\text{ZnPATHCl}]$  are labeled in red. Peaks for the  $[\text{ZnPATHMes}]$  starting material are labeled in blue. The experiment was performed in 2:1  $\text{CD}_3\text{CN}:\text{CD}_2\text{Cl}_2$ .

Geometry optimizations and molecular orbital calculations were performed on  $[\text{ZnPATHEt}]$  and a qualitative assessment of atomic orbital contributions to the HOMO was undertaken. Greater contributions from the sulfur-based orbital as compared to the metal-bound

carbon orbital were observed at the B3LYP/6-31G(d,p) level in Gaussian 03 and Gaussian 09. The calculated geometric parameters for [ZnPAThEt] are comparable to those determined crystallographically (Table 3.6). The zinc center in the B3LYP optimized structure exists in a slightly distorted tetrahedral environment, with an S – Zn – N<sub>pyridyl</sub> angle of 106.5°, compared to the experimentally observed value of 112.35(7)°. Computationally and crystallographically determined bond distances are also similar, with Zn – S distances of 2.32 Å and 2.29 Å in the theoretical and experimental structures, respectively. Zn – N<sub>pyridyl</sub> and Zn – N<sub>alkyl</sub> distances are 2.16 Å and 2.21 Å in the computational model, and 2.12 Å and 2.17 Å in the X-ray structure. Theoretical and experimental Zn – C distances are 1.99 Å and 2.01 Å, respectively.

The [ZnPAThEt] complex has stereocenters at the Zn and N<sub>alkyl</sub> atoms, and crystallizes in the centrosymmetric space group  $P2_1/n$ . The compound therefore must exist as a racemic mixture of two enantiomers. The energy of [ZnPAThEt] in the (*S,R*) configuration was calculated and compared with the energy of the (*R,S*) stereoisomer of [ZnPAThEt], the structure of which was based on X-ray coordinates. The structures were optimized with different orientations of the coordinated ethyl group relative to the [PATh]<sup>-</sup> ligand. The (*R,S*) isomer was calculated with the ethyl substituent directed over the pyridyl ring of [PATh]<sup>-</sup>, whereas the ethyl group was oriented above the alkyl fragment of [PATh]<sup>-</sup> in the (*S,R*) isomer (Fig. 3.8). We found the (*S,R*) isomer to be 1.46 kcal/mol lower in energy than its enantiomer. The different orientations of the ethyl groups in the two calculated structures may account for this disparity in energies. A comparison of bond lengths for the X-ray structure and the structures of the theoretically determined enantiomers is provided in Table 3.6.

**Table 3.6.** Comparison of bond distances (Å) for experimentally and computationally characterized isomers of [ZnPATHet]. Stereochemistry is shown for the stereocenter at Zn followed by the stereocenter at N<sub>alkyl</sub>, *i.e.* (Zn, N<sub>alkyl</sub>).

	X-Ray Structure of ( <i>R,S</i> ) Isomer	B3LYP/6-31G(d,p) Structure of ( <i>R,S</i> ) Isomer	B3LYP/6-31G(d,p) Structure of ( <i>S,R</i> ) Isomer
Zn – S	2.2937(9)	2.317	2.305
Zn – N <sub>pyridyl</sub>	2.125(2)	2.163	2.155
Zn – N <sub>alkyl</sub>	2.171(3)	2.207	2.204
Zn – C	2.014(3)	1.994	1.992

Molecular orbital comparisons reveal similar atomic orbital distributions in the HOMOs of the (*S,R*) and (*R,S*) enantiomers. That is, atomic orbital contributions from the sulfur atoms qualitatively outweigh the contributions of the zinc-bound carbon-based orbitals, irrespective of the orientation of the ethyl substituent (Fig. 3.8).

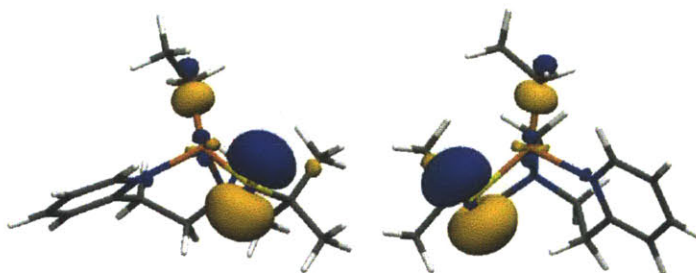


**Figure 3.8.** Highest occupied molecular orbitals for the geometry optimized (*S,R*) (*left*) and (*R,S*) (*right*) configurations of [ZnPATHet], calculated at the B3LYP/6-31G(d,p) level.

A transition state geometry was successfully calculated for the stereoisomer of [ZnPATHet] having *S* chirality at the zinc center and *R* chirality at the N<sub>alkyl</sub> atom, and with the zinc-bound ethyl group directed over the pyridyl ring of the [PATH]<sup>-</sup> ligand. The transition state was characterized by a unique imaginary frequency ( $\nu = 133.13i$ ), which we attribute to bond formation between the nitrogen atom of NO<sup>+</sup> and the sulfur atom of the [PATH]<sup>-</sup> ligand. This bond-forming reaction was supported by an intrinsic reaction coordinate (IRC) calculation, which connects the transition state with two minima continuously on the potential energy surface. The minima correspond to the reactant and product in the reaction. The reaction path

determined for [ZnPAThEt] interaction with  $\text{NO}^+$  is shown in Figure 3.9, clearly demonstrating attack by  $\text{NO}^+$  at the sulfur atom of the [PATh] ligand.

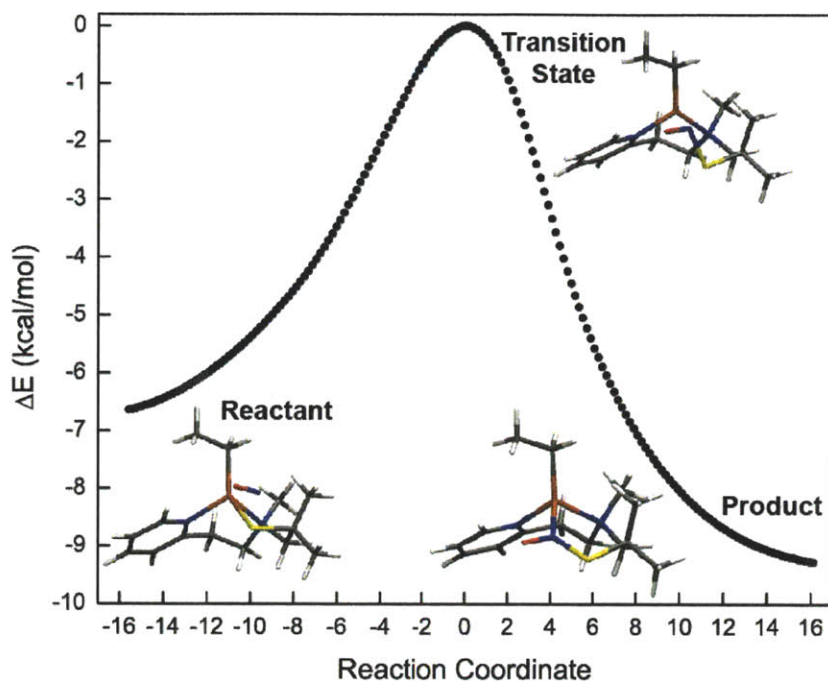


**Figure 3.9.** Intrinsic reaction coordinate for the interaction of [ZnPAThEt] with  $\text{NO}^+$ .

The calculated reactant was the [ZnPAThEt] complex in the presence of  $\text{NO}^+$ . The product was an *S*-nitrosothiol, coordinated by the  $\text{Zn}^{2+}$  center through its nitrogen atom. The reactant and product both represent stable minima along the reaction coordinate, and vibrational analyses revealed only positive vibrational frequencies for both species. Pertinent structural aspects for the reactant, transition state, and product are summarized in Table 3.7, and a comparison with experimental values is given where appropriate. XYZ matrices for all calculated species are provided in Tables 3.8 – 3.12 at the end of this chapter.

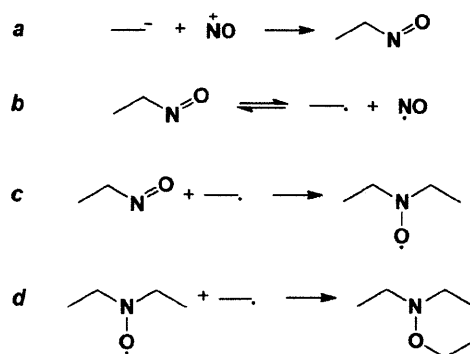
**Table 3.7.** Bond distances (Å) for species calculated from the IRC of the [ZnPAThEt]/NO<sup>+</sup> reaction, compared with X-ray structural data for [ZnPAThEt].

	Reactant	Transition State	Product	Experimental
Zn – S	2.573	3.158	3.485	2.2937(9)
Zn – N <sub>pyridyl</sub>	2.056	2.051	2.061	2.125(2)
Zn – N <sub>alkyl</sub>	2.133	2.115	2.143	2.171(3)
Zn – C	1.972	1.969	1.975	2.014(3)
Zn – N <sub>NO</sub>	3.497	2.552	2.143	
S – N <sub>NO</sub>	1.999	1.865	1.753	

### 3.4. Discussion

The studies with [ZnPAThEt] and [ZnPAThMes] described in this chapter complement our previous work on the reactivity of [ZnPAThCl] and [ZnPAThOTf] with reactive nitrogen species.<sup>12</sup> In the earlier work, we described *S*-nitrosothiol formation upon exposure of [ZnPAThCl] and [ZnPAThOTf] to aerobic NO (g), NO<sub>2</sub>, or NOBF<sub>4</sub>. *S*-nitrosothiols act as sources of ·NO and NO<sup>+</sup>,<sup>5-6</sup> and, with that in mind, we became interested in the ability of [ZnPAThNO]<sup>+</sup> systems to effect transnitrosation reaction chemistry.

Reactivity studies with [ZnPAThEt] showed negligible *S*-nitrosothiol formation upon exposure to stoichiometric amounts of NOBF<sub>4</sub>. This result indicates that 1 equiv of NO<sup>+</sup> is consumed by the [ZnPAThEt] complex prior to formation of a stable *S*-nitrosothiol. EI-MS analysis of the reaction headspace indirectly suggested EtNO formation. EtNO is an unstable species, and is prone to decomposition along the pathway outlined in Scheme 3.1.<sup>85</sup>



**Scheme 3.1.** Formation and autodecomposition pathway for EtNO, based on gas phase studies.<sup>85</sup>

According to Scheme 3.1, homolysis of the C-N bond in EtNO will result in formation of an ethyl radical and  $\cdot\text{NO}$ . The ethyl radical product of EtNO autodecomposition may react with intact EtNO to form more highly substituted nitrosoalkanes. Detection of  $\cdot\text{NO}$  in the EI-MS experiment supports the hypothesis that EtNO forms (Scheme 3.1.b). The hypothesis is similarly supported by the detection of butane, which can form by the combination of two ethyl radicals. The propensity of EtNO to effect the disproportionation of NO into  $\text{NO}_2$  and  $\text{N}_2$  accounts for the presence of  $\text{NO}_2$  in the reaction headspace.<sup>86</sup> Numerous radical recombination pathways are available to EtNO and its decomposition products in solution.  $\text{NO}_2$  formation is one of many such pathways, and consequently only small quantities of  $\text{NO}_2$  are formed. A low intensity signal for  $\text{NO}_2$  was detected by EI-MS as a result.

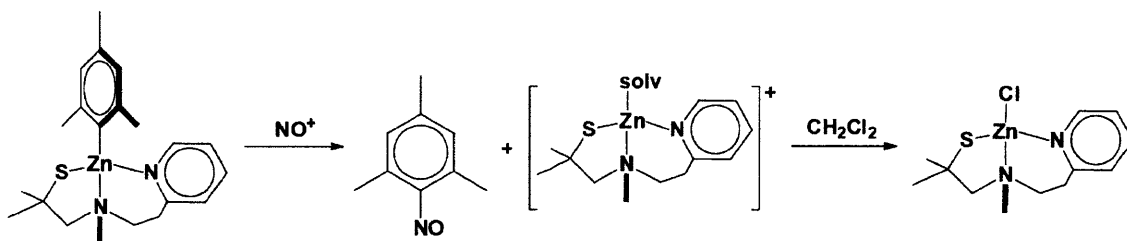
We investigated reactions of  $[\text{ZnPAThMes}]$  with  $\text{NOBF}_4$  in search of direct proof for C-nitroso formation. We rationalized that the expected C-nitroso product of the reaction, C-nitrosomesitylene, would be isolable as a crystalline solid and be amenable to structural characterization. As with  $[\text{ZnPAThEt}]$ , optical spectroscopy revealed little S-nitrosothiol formation upon exposure of  $[\text{ZnPAThMes}]$  to 1 equiv of  $\text{NOBF}_4$ . Crystalline material was obtained when the reaction was quenched with water and extracted into diethyl ether. The crystals were identified as the C-nitrosomesitylene dimer,  $[\text{MesNO}]_2$ .  $[\text{MesNO}]_2$  was isolated in

63% yield from the [ZnPAThMes]/NOBF<sub>4</sub> mixture after 2 h of reaction time. This yield is comparable to the reported 78% recovery of [MesNO]<sub>2</sub> from the direct nitrosation of mesitylene with NOBF<sub>4</sub>.<sup>87</sup> We conclude that nitrosation is indeed facilitated by mesitylene binding to Zn<sup>2+</sup>.

Long-standing discussions in the literature regarding the structural properties of *C*-nitrosomesitylene in the solid state<sup>88</sup> have been resolved with our determination of the [MesNO]<sub>2</sub> crystal structure. Historically, differences in color between *C*-nitroso compounds in solution and in the solid state generated interest in such compounds. The differences in color were attributed to monomer/dimer equilibria, which drew attention to the structural characteristics of *C*-nitroso species. In 1924, Ingold and Piggott proposed a ring structure for [MesNO]<sub>2</sub>.<sup>89</sup> This hypothesis was revised in the 1930's to describe [MesNO]<sub>2</sub> as the N-N bonded dimer that we have crystallographically characterized in the present work.<sup>88</sup> Charles P. Fenimore structurally characterized tribromonitrosobenzene in 1950, and he simultaneously reported the unit cell parameters of *C*-nitrosomesitylene.<sup>90</sup> He found that tribromonitrosobenzene exists as a dimer in the solid state, with the individual monomer units bound through their nitrogen atoms. No interaction between the oxygen atoms of the monomers existed. In 1956, Nakamoto and Rundle utilized IR spectroscopy to determine that nitrosomesitylene is a dimer in the solid state.<sup>91</sup> The structural characteristics of [MesNO]<sub>2</sub> described in this work conclusively confirm the dimeric structure of *C*-nitrosomesitylene in the solid state.

The zinc-containing products of the [ZnPAThMes]/NOBF<sub>4</sub> reaction could not be isolated when the reaction was performed in acetonitrile. Use of a 2:1 MeCN:CH<sub>2</sub>Cl<sub>2</sub> reaction solvent mixture enabled structural characterization of [ZnPAThCl]. We hypothesize that the nitrosation reaction takes place as outlined in Scheme 3.2, in which formation of MesNO generates an unstable [ZnPATh]<sup>+</sup> cation that abstracts chloride from methylene chloride. The presence of non-

coordinating tetrafluoroborate anion appears inadequate to stabilize  $[\text{ZnPATh}]^+$ . Similarly, previous attempts to recrystallize the triflate salt  $[\text{ZnPAThOTf}]$  from methylene chloride solutions resulted in the isolation of  $[\text{ZnPAThCl}]$ .<sup>92</sup>  $[\text{ZnPAThCl}]$  was analyzed by single crystal x-ray diffraction and was found to have analogous unit cell parameters to those previously reported for the compound.<sup>61</sup> The isolated  $[\text{ZnPAThCl}]$  complex crystallized in space group  $P2_1/n$ , with unit cell parameters  $a = 8.2571(4) \text{ \AA}$ ,  $b = 15.1384(7) \text{ \AA}$ ,  $c = 11.7743(6) \text{ \AA}$ ,  $\beta = 92.682(1)^\circ$ ,  $V = 1470.17 \text{ \AA}^3$ . Values reported previously for  $[\text{ZnPAThCl}]$  in  $P2_1/n$  are  $a = 8.203(1) \text{ \AA}$ ,  $b = 14.979(2) \text{ \AA}$ ,  $c = 11.788(2) \text{ \AA}$ ,  $\beta = 93.436(2)^\circ$ ,  $V = 1445.8(4) \text{ \AA}^3$ .<sup>61</sup>



**Scheme 3.2.** Proposed reaction pathway for the nitrosation of  $[\text{ZnPAThMes}]$ , resulting in formation of MesNO and  $[\text{ZnPAThCl}]$ .  $[\text{ZnPAThCl}]$  formation is proposed to occur via halide abstraction from methylene chloride.

Finally, we took advantage of theory to probe aspects of the nitrosation reaction. In particular, we were interested in determining whether the initial site of nitrosation in the organometallic  $[\text{ZnPAThR}]$  complexes would be the metal-bound carbon atom, or whether initial attack would occur at sulfur, with *C*-nitroso formation occurring via an intramolecular transnitrosation reaction. Theoretical calculations were performed in the gas phase to examine the atomic orbital distribution within the HOMO of  $[\text{ZnPAThEt}]$  (Fig. 3.10).



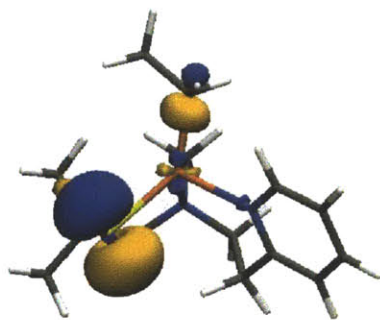
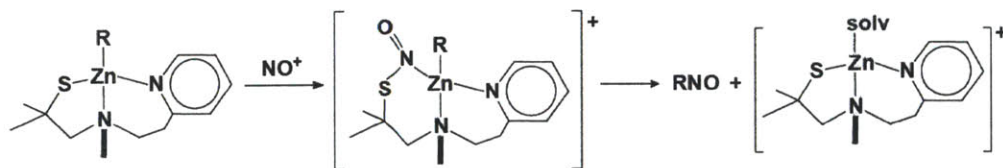


**Figure 3.10.** Highest occupied molecular orbital for [ZnPAThEt]. Calculations were performed at the B3LYP/6-31G(d,p) level, and orbitals were visualized at isovalues of 0.06.

The presence of greater electron density at the sulfur versus the coordinated carbon atom suggests that it would indeed be feasible for *C*-nitroso formation to take place by intramolecular transnitrosation. Such a reaction pathway is supported by transition state and intrinsic reaction coordinate (IRC) theoretical calculations (Fig. 3.8). A transition state for the attack of  $\text{NO}^+$  at the sulfur atom of [ZnPAThEt] was characterized by theoretical methods, and IRC analysis revealed that the formation of zinc-coordinated *S*-nitrosothiol constitutes a feasible reaction pathway. The observation of  $[\text{MesNO}]_2$  by crystallography suggests subsequent intramolecular transnitrosation.  $\text{NO}^+$  attacks [ZnPAThR] (R = Et, Mes) at the sulfur atom and forms an *S*-nitrosothiol. The *S*-nitrosothiol then transfers  $\text{NO}^+$  to the coordinated carbon to generate the *C*-nitroso products (Scheme 3.3).



**Scheme 3.3.** Proposed reaction pathway for *C*-nitroso formation via intramolecular transnitrosation in the reaction of [ZnPAThR] (R = Et, Mes) with  $\text{NO}^+$ .

### 3.5. Summary and Conclusions

Exposure of [ZnPAThEt] to NOBF<sub>4</sub> led to formation of EtNO. The gaseous products of EtNO decomposition were characterized by EI-MS. The analogous NOBF<sub>4</sub> reaction was performed with [ZnPAThMes] to trap C-nitrosomesitylene as a stable product. C-nitrosomesitylene was isolated and characterized as a dimer in the solid state. The zinc-containing product [ZnPAThCl] was isolated when the [ZnPAThMes]/NOBF<sub>4</sub> reaction was performed in the presence of the chlorinated solvent CH<sub>2</sub>Cl<sub>2</sub>, indicating that chloride atom abstraction may be effected by an unstable [ZnPATh]<sup>+</sup> cation. Theoretical calculations were performed to analyze the character of the [ZnPAThEt] HOMO. The results of these calculations suggest that attack by NO<sup>+</sup> on [ZnPAThR] (R = Et, Mes) may take place at the sulfur atom. C-nitroso formation may then occur by an intramolecular transnitrosation pathway.

### 3.6. Tables of XYZ Matrices for Computationally Determined Species

**Table 3.8.** XYZ coordinates, energy, and lowest calculated frequency for the geometry optimized structure of the (*S,R*) enantiomer of [ZnPAThEt].

E <sub>elec+nuc+ZPE</sub> (a.u.)		-2834.461804	
Lowest Frequency		21.8701	
Zn	-0.17048100	0.79818700	0.19274900
C	1.49438800	-1.65279800	1.38289700
H	1.35775300	-0.95002700	2.21372900
H	2.05517200	-2.50133900	1.78671400
C	0.12197800	-2.16194700	0.88462300
H	-0.18334400	-3.02590500	1.49596800
H	0.23583900	-2.51732900	-0.14184800
N	-0.95289700	-1.13724400	0.89895700
C	-1.44429600	-0.96342000	2.28187700
H	-2.24052800	-0.22221700	2.30474500
H	-0.64053200	-0.60289400	2.92696800
C	-2.06728100	-1.51312800	-0.02558300
H	-2.81191800	-2.10681600	0.52945500
H	-1.64561500	-2.16027800	-0.79742200
C	-2.77090000	-0.34794400	-0.76587600

C	-3.71335300	-0.99282100	-1.79870100
H	-3.15982500	-1.62361500	-2.50063000
H	-4.48036700	-1.60729000	-1.30682900
H	-4.22121000	-0.21628900	-2.37676900
C	-3.60869400	0.54568700	0.16779300
H	-4.16893500	1.27132200	-0.42756300
H	-4.32923600	-0.04710000	0.75012600
H	-2.98680800	1.12085100	0.85819800
S	-1.50919300	0.67394300	-1.67993500
C	2.32422200	-0.99519200	0.30373900
C	3.63048600	-1.40714400	0.02265000
C	2.42346200	0.59112600	-1.38805200
C	4.34319600	-0.77824800	-0.99633700
H	4.07619600	-2.21295900	0.59710300
C	3.72756300	0.24059400	-1.72183900
H	1.89222700	1.36932700	-1.92855200
H	5.35986000	-1.08449700	-1.22431200
H	4.23963600	0.75157200	-2.52975800
N	1.74241100	-0.00110500	-0.39491600
C	0.19895200	2.11702500	1.63974500
H	-0.74884400	2.43205700	2.09926000
H	0.76575400	1.65501100	2.46465300
H	-1.83059600	-1.91109200	2.68790700
C	0.95827700	3.37013900	1.17344800
H	1.15418800	4.08608300	1.98618200
H	1.93509200	3.11712900	0.73887700
H	0.40294800	3.91446500	0.39969900

**Table 3.9.** XYZ coordinates, energy, and lowest calculated frequency for the geometry optimized structure of the (*R,S*) enantiomer of [ZnPA<sub>4</sub>ThEt]. Crystallographic coordinates were used for the initial guess.

$E_{\text{elec+nuc+ZPE}}$ (a.u.)	-2834.463763		
Lowest Frequency	39.0041		
Zn	0.12850400	0.84298200	-0.20949700
S	1.21662300	-0.43391800	-1.80789700
C	2.54048400	-0.92060500	-0.59265300
N	-1.92502500	0.16471500	-0.17489300
N	0.82315300	-0.59922800	1.31001600
C	-4.20198900	0.67314300	-0.74454000
H	-4.92070700	1.39864800	-1.10946200
C	-0.31595700	-1.42752800	1.78255000
H	-0.93066900	-0.80296400	2.43903700
H	0.06888200	-2.25433500	2.39994500
C	0.04099700	2.76805100	0.30483900
H	-0.58376700	3.28347800	-0.44232000
H	-0.51781500	2.88947200	1.24702400

C	-2.28574200	-1.08624600	0.17273200
C	-1.19505500	-2.00905200	0.65473800
H	-0.56483600	-2.26332100	-0.20766500
H	-1.65110600	-2.93789000	1.01060800
C	-3.61680500	-1.50600700	0.07614800
H	-3.88242400	-2.51776400	0.36507900
C	-4.58429400	-0.62083600	-0.39253500
H	-5.62050600	-0.93489000	-0.47709000
C	1.36153200	0.16352700	2.45608800
H	2.24085600	0.72621100	2.14395700
H	1.64743600	-0.50047600	3.28645000
H	0.61106300	0.87461900	2.80954600
C	-2.86216300	1.02088600	-0.61397500
H	-2.50855400	2.01706600	-0.86176700
C	1.88031400	-1.46419400	0.69687100
H	1.42598700	-2.42468600	0.44420000
H	2.65013400	-1.67144900	1.45675800
C	1.36379700	3.54389500	0.41469700
H	1.94306600	3.48832600	-0.51444400
H	2.00908400	3.14661000	1.20969000
H	1.21968800	4.61167000	0.63912400
C	3.48542100	0.26117700	-0.30783300
H	3.97557300	0.57341900	-1.23369400
H	4.26491600	-0.02213000	0.41430000
H	2.95579000	1.13525900	0.07916900
C	3.36282600	-2.07078900	-1.20004900
H	2.72605900	-2.92575700	-1.44658500
H	4.14631600	-2.40800100	-0.50688100
H	3.84734900	-1.73885900	-2.12204200

**Table 3.10.** XYZ coordinates, energy, and lowest calculated frequency for the structure of the reactant that was determined from the IRC.

E <sub>elec+nuc+ZPE</sub> (a.u.)		-2964.142664	
Lowest Frequency		10.2764	
Zn	0.06917200	0.28661300	0.68412800
C	2.08901700	-2.08789800	0.53263900
H	2.00706400	-1.90227100	1.61138900
H	2.78789900	-2.92253000	0.43187900
C	0.73481700	-2.53642600	-0.05056300
H	0.58299300	-3.60325000	0.16059500
H	0.77086100	-2.42087600	-1.13633600
N	-0.45163700	-1.76964900	0.45553700
C	-0.78442400	-2.23969400	1.83061700
H	-1.64262200	-1.69253000	2.21647000
H	0.05453800	-2.05880000	2.50449200

C	-1.61723600	-1.98814800	-0.46540700
H	-2.21013100	-2.84102900	-0.10867200
H	-1.21894800	-2.27078300	-1.44283600
C	-2.58623000	-0.79926800	-0.68729800
C	-3.57174800	-1.20094100	-1.79864200
H	-3.05591800	-1.47280400	-2.72377200
H	-4.17208300	-2.05804000	-1.47273000
H	-4.25694400	-0.37913300	-2.01989400
C	-3.35952600	-0.37919400	0.57238400
H	-4.09958100	0.38770300	0.33738300
H	-3.89942200	-1.24857400	0.96334600
H	-2.71310300	0.01459100	1.35927400
S	-1.50444600	0.59810700	-1.32793800
N	-2.51928400	2.19669300	-0.68684500
O	-1.98132900	3.19763100	-0.91055300
C	2.68386600	-0.87607400	-0.14886800
C	3.97396400	-0.88855700	-0.68200800
C	2.40066700	1.33970200	-0.81901300
C	4.47670600	0.25738200	-1.29598300
H	4.57495700	-1.78886200	-0.61274800
C	3.67461900	1.39616000	-1.36749300
H	1.74258100	2.20278000	-0.84237300
H	5.47924000	0.26029100	-1.71196400
H	4.02526100	2.30962700	-1.83394800
N	1.91339200	0.23271400	-0.22386200
C	-0.23849700	1.40115100	2.28202000
H	-1.30831200	1.61706800	2.39958800
H	0.02958600	0.81934600	3.17460800
H	-1.01223500	-3.31317500	1.82987900
C	0.54471900	2.72648700	2.29755500
H	0.37708800	3.29067400	3.22327100
H	1.62659100	2.56762600	2.21625400
H	0.25567000	3.38742000	1.47100000

**Table 3.11.** XYZ coordinates, energy, and lowest calculated frequency for the structure of the transition state for NO<sup>+</sup> attack at the sulfur atom of [ZnPAThEt].

E <sub>elec+nuc+ZPE</sub> (a.u.)	-2964.131991		
Lowest Frequency	-133.1328		
Zn	0.09859500	0.36728300	0.80795600
C	1.68001900	-2.23804500	0.70417700
H	1.65403300	-1.96809300	1.76826800
H	2.23993400	-3.17576300	0.65815200
C	0.26221900	-2.51242100	0.16631000
H	-0.04721100	-3.52598500	0.45243900
H	0.29467400	-2.47295700	-0.92462700

N	-0.79146400	-1.54287300	0.62343700
C	-1.15018500	-1.83710900	2.04476700
H	-1.91985700	-1.14285500	2.38129900
H	-0.28138300	-1.71247500	2.69368700
C	-2.01278400	-1.71283700	-0.24216600
H	-2.72717700	-2.35566000	0.28686600
H	-1.71371400	-2.25518100	-1.14156300
C	-2.76580900	-0.44124000	-0.69389100
C	-3.93200700	-0.89665100	-1.59569000
H	-3.58525500	-1.46391100	-2.46487600
H	-4.61379800	-1.53507200	-1.02291800
H	-4.49706900	-0.03398000	-1.95521800
C	-3.31116400	0.40142100	0.46721400
H	-3.85153400	1.27459900	0.09420400
H	-4.01928200	-0.21161900	1.03602800
H	-2.53795700	0.75750400	1.14856500
S	-1.63606900	0.54192900	-1.82519400
N	-1.18232000	1.96778300	-0.71136300
O	-0.53654300	2.81762900	-1.23362300
C	2.43456500	-1.18649800	-0.07727700
C	3.69254600	-1.43359200	-0.62710000
C	2.46216600	0.99071500	-0.91986200
C	4.34164300	-0.42645500	-1.33966900
H	4.15523400	-2.40564300	-0.49475900
C	3.71412300	0.80957100	-1.49202300
H	1.93986500	1.93774200	-1.00665900
H	5.32202200	-0.60530800	-1.76975900
H	4.18179500	1.62068800	-2.03814100
N	1.83361600	0.01714100	-0.22810000
C	-0.01507100	1.62737100	2.31639400
H	-1.05813100	1.92122800	2.47685900
H	0.28740300	1.08748600	3.22443300
H	-1.51997200	-2.86433300	2.14742300
C	0.85559600	2.88143700	2.14957000
H	0.77557400	3.54429600	3.01987800
H	1.91794300	2.63471400	2.03686000
H	0.56150500	3.47184300	1.27461100

**Table 3.12.** XYZ coordinates, energy, and lowest calculated frequency for the structure of the product that was determined from the IRC.

$E_{\text{elec+nuc+ZPE}}$ (a.u.)	-2964.145584		
Lowest Frequency	18.5337		
Zn	0.16865500	0.50978500	0.67998900
C	1.67892100	-2.20944200	0.73131800
H	1.63729400	-1.92663300	1.79052800
H	2.19937800	-3.17049000	0.70673600

C	0.26373300	-2.43279200	0.16392200
H	-0.08954700	-3.43149700	0.45395000
H	0.32046200	-2.41112200	-0.92731200
N	-0.76022900	-1.41960400	0.59157000
C	-1.12434700	-1.68540000	2.01455400
H	-1.85703400	-0.95997900	2.35958800
H	-0.24582800	-1.59108400	2.65331300
C	-1.96953100	-1.59495400	-0.27951600
H	-2.56409500	-2.42428500	0.13053600
H	-1.62426600	-1.91654000	-1.26423800
C	-2.94886400	-0.41540500	-0.50587700
C	-4.17238400	-0.99738800	-1.25345100
H	-3.88310500	-1.56135900	-2.14492500
H	-4.71460600	-1.67019200	-0.58191600
H	-4.86506500	-0.20668700	-1.55457200
C	-3.42021700	0.33247600	0.75002500
H	-4.16790800	1.08257000	0.48021100
H	-3.89321100	-0.37153600	1.44346700
H	-2.60881800	0.84542700	1.27087600
S	-2.30048100	0.81778600	-1.75998800
N	-0.75593900	1.29910100	-1.08426100
O	-0.18105000	2.17771400	-1.68591900
C	2.50095500	-1.19792300	-0.03350200
C	3.76017300	-1.51282000	-0.54537300
C	2.66643200	0.96912200	-0.88284100
C	4.48217000	-0.54532700	-1.24236200
H	4.16668900	-2.50732000	-0.39623800
C	3.92471600	0.72063000	-1.41554900
H	2.18801200	1.93530100	-0.99750400
H	5.46351300	-0.77791100	-1.64364800
H	4.44957700	1.50416700	-1.94995200
N	1.96668000	0.03324800	-0.20749700
C	0.07162900	1.62877000	2.30510400
H	-0.97216300	1.81028900	2.59069600
H	0.49875500	1.05424300	3.13827400
H	-1.53572700	-2.69712300	2.12485800
C	0.80786300	2.97426500	2.19003400
H	0.74988100	3.55104300	3.12149500
H	1.87320400	2.84132100	1.96697900
H	0.38997500	3.60746100	1.39869300

---

### 3.7. References

- (1) Brecht, D. S.; Snyder, S. H. *Annu. Rev. Biochem* **1994**, *63*, 175-195.
- (2) Moncada, S.; Palmer, R. M. J.; Higgs, E. A. *Pharmacol. Rev.* **1991**, *43*, 109-142.
- (3) Richter-Addo, G. B.; Legzdins, P.; Burstyn, J. *Chem. Rev.* **2002**, *102*, 857-860.
- (4) Stamler, J.; Singel, D.; Loscalzo, J. *Science* **1992**, *258*, 1898-1902.
- (5) Hogg, N. *Annu. Rev. Pharmacol. Toxicol.* **2002**, *42*, 585-600.
- (6) Szaciłowski, K.; Stasicka, Z. *Prog. React. Kinet. Mech.* **2001**, *26*, 1-58.
- (7) Granik, V. G.; Grigoriev, N. B. *Russ. Chem. Rev.* **2011**, *80*, 171.
- (8) Granik, V. G.; Ryabova, S. Y.; Grigoriev, N. B. *Russ. Chem. Rev.* **1997**, *66*, 717.
- (9) King, S. B. *Free Radical Biol. Med.* **2004**, *37*, 735-736.
- (10) Napoli, C.; Ignarro, L. J. *Annu. Rev. Pharmacol. Toxicol.* **2003**, *43*, 97-123.
- (11) Wang, P. G.; Xian, M.; Tang, X.; Wu, X.; Wen, Z.; Cai, T.; Janczuk, A. J. *Chem. Rev.* **2002**, *102*, 1091-1134.
- (12) Kozhukh, J.; Lippard, S. J., Manuscript in preparation.
- (13) Gowenlock, B. G.; Richter-Addo, G. B. *Chem. Rev.* **2004**, *104*, 3315-3340.
- (14) Baeyer, A. *Berichte* **1874**, *7*, 1638-1640.
- (15) Robson, E.; Tedder, J. M.; Woodcock, D. J. *J. Chem. Soc. C* **1968**, 1324-1328.
- (16) Smith, L. I.; Taylor, F. L. *J. Am. Chem. Soc.* **1935**, *57*, 2460-2463.
- (17) Tarrant, P.; O'Connor, D. E. *J. Org. Chem.* **1964**, *29*, 2012-2013.
- (18) Motte, J.-C.; Viehe, H. G. *Chimia* **1975**, *29*, 515-516.
- (19) Waters, W. L.; Marsh, P. G. *J. Org. Chem.* **1975**, *40*, 3344-3349.
- (20) Waters, W. L.; Marsh, P. G. *J. Org. Chem.* **1975**, *40*, 3349-3351.
- (21) Oddo, B. *Gazz. Chim. Ital.* **1911**, *39*, 659-661.
- (22) Prickett, J. E., Duquesne University, 1975.
- (23) Bartlett, E. H.; Eaborn, C.; Walton, D. R. M. *J. Chem. Soc. C* **1970**, 1717-1718.
- (24) Volker, J.; Motte, J.-C.; Viehe, H. G. *Chimia* **1975**, *29*, 516-517.
- (25) Ludovici, K.; Naumann, D.; Siegemund, G.; Tyrra, W.; Varbelow, H. G.; Wrubel, H. J. *Fluorine Chem.* **1995**, *73*, 273-274.
- (26) Herberhold, M.; Haumaier, L. *Angew. Chem. Int. Ed.* **1984**, *23*, 521-522.
- (27) Kauffman, J. M.; Green, J.; Cohen, M. S.; Fein, M. M.; Cottrill, E. L. *J. Am. Chem. Soc.* **1964**, *86*, 4210-4211.
- (28) Taylor, E. C.; Danforth, R. H.; McKillop, A. *J. Org. Chem.* **1973**, *38*, 2088-2089.
- (29) Uemura, S.; Toshimitsu, A.; Okano, M. *J. Chem. Soc., Perkin Trans. 1* **1978**, 1076-1079.
- (30) Birkofer, L.; Franz, M. *Chem. Ber.* **1971**, *104*, 3062-3068.
- (31) Flanagan, P. W. K. Preparation of Nitrosoalkanes. U.S. Patent 3,205,273, September 7, 1965.
- (32) Lin, S.-H.; Peng, S.-M.; Liu, R.-S. *J. Chem. Soc., Chem. Commun.* **1992**, 615-617.
- (33) Legzdins, P.; Richter-Addo, G. B.; Wassink, B.; Einstein, F. W. B.; Jones, R. H.; Willis, A. C. *J. Am. Chem. Soc.* **1989**, *111*, 2097-2104.
- (34) Cameron, M.; Gowenlock, B. G.; Vasapollo, G. *Chem. Soc. Rev.* **1990**, *19*, 355-379.
- (35) Chan, S.-C.; Pat, P.-K.; Lau, T.-C.; Wong, C.-Y. *Organometallics* **2011**, *30*, 1311-1314.
- (36) Goldhaber, A.; Vollhardt, K. P. C.; Walborsky, E. C.; Wolfgruber, M. *J. Am. Chem. Soc.* **1986**, *108*, 516-518.
- (37) Krinninger, C.; Högg, C.; Nöth, H.; Gálvez Ruiz, J. C.; Mayer, P.; Burkacky, O.; Zumbusch, A.; Lorenz, I.-P. *Chem. Eur. J.* **2005**, *11*, 7228-7236.



- (38) Krinninger, C.; Wirth, S.; Klüfers, P.; Mayer, P.; Lorenz, I. P. *Eur. J. Inorg. Chem.* **2006**, 2006, 1060-1066.
- (39) Krinninger, C.; Wirth, S.; Ruiz, J. C. G.; Klüfers, P.; Nöth, H.; Lorenz, I.-P. *Eur. J. Inorg. Chem.* **2005**, 2005, 4094-4098.
- (40) Puiu, S. C.; Warren, T. H. *Organometallics* **2003**, 22, 3974-3976.
- (41) Wiese, S.; Kapoor, P.; Williams, K. D.; Warren, T. H. *J. Am. Chem. Soc.* **2009**, 131, 18105-18111.
- (42) Wilberger, R.; Krinninger, C.; Piotrowski, H.; Mayer, P.; Lorenz, I.-P. *Eur. J. Inorg. Chem.* **2004**, 2004, 2488-2492.
- (43) Doctorovich, F.; Di Salvo, F. *Acc. Chem. Res.* **2007**, 40, 985-993.
- (44) Escola, N.; Di Salvo, F.; Haddad, R.; Perissinotti, L.; Eberlin, M. N.; Doctorovich, F. *Inorg. Chem.* **2007**, 46, 4827-4834.
- (45) Escola, N.; Llebaría, A.; Leitus, G.; Doctorovich, F. *Organometallics* **2006**, 25, 3799-3801.
- (46) Richter-Addo, G. B. *Acc. Chem. Res.* **1999**, 32, 529-536.
- (47) Barnes, T. M.; Leaf, J.; Hand, S.; Fry, C.; Wolden, C. A. *J. Appl. Phys.* **2004**, 96, 7036-7044.
- (48) Li, X.; Asher, S. E.; Keyes, B. M.; Moutinho, H. R.; Luther, J.; Coutts, T. J. In *Photovoltaic Specialists Conference, 31st IEEE 2005*, p 152-154.
- (49) Li, X.; Yan, Y.; Gessert, T. A.; DeHart, C.; Perkins, C. L.; Young, D.; Coutts, T. J. *Electrochem. Solid-State Lett.* **2003**, 6, C56-C58.
- (50) Sun, S.; Tompa, G.; Hoerman, B.; Look, D.; Clafin, B.; Rice, C.; Masaun, P. *J. Electron. Mater.* **2006**, 35, 766-770.
- (51) Coates, G. E.; Ridley, D. *Journal of the Chemical Society A: Inorganic, Physical, Theoretical* **1966**, 1064-1069.
- (52) Jana, S.; Berger, R. J. F.; Fröhlich, R.; Pape, T.; Mitzel, N. W. *Inorg. Chem.* **2007**, 46, 4293-4297.
- (53) Lewiński, J.; Śliwiński, W.; Dranka, M.; Justyniak, I.; Lipkowski, J. *Angew. Chem. Int. Ed.* **2006**, 45, 4826-4829.
- (54) Bewad, I. *Journal für Praktische Chemie* **1901**, 63, 94-110.
- (55) Bewad, I. I. *Zhurnal Russkago Fiziko-Khimicheskago Obshchestva* **1900**, 32, 420-454.
- (56) Bewad, I. I. *Zhurnal Russkago Fiziko-Khimicheskago Obshchestva* **1907**, 39, 457-459.
- (57) Lachman, A. *J. Am. Chem. Soc.* **1901**, 23, 897-902.
- (58) Daniel, K. M.; Ivan, F.; Patrick, J. F.; Yui-May, H.; Thawatchai, T.; Rizalia, M. B.; Dawn, C. G.; Ghezai, M.; Craig, A. G.; Michael, J. M.; Chia-Huei, L.; Michelle, L. H.; Jason, J. S.; John, A. B.; Marcetta, Y. D.; Robert, D. H.; Sheila, E.; Arthur, E. M. In *Inorg. Synth.*; Marcetta, Y. D., Ed. 2007, p 89-98.
- (59) Chang, S.; Karambelkar, V. V.; diTargiani, R. C.; Goldberg, D. P. *Inorg. Chem.* **2001**, 40, 194-195.
- (60) Chang, S.; Karambelkar, V. V.; Sommer, R. D.; Rheingold, A. L.; Goldberg, D. P. *Inorg. Chem.* **2002**, 41, 239-248.
- (61) Ji, M.; Vahrenkamp, H. *Eur. J. Inorg. Chem.* **2005**, 2005, 1398-1405.
- (62) Seidel, W.; Bürger, I. *Z. Anorg. Allg. Chem.* **1981**, 473, 166-170.
- (63) APEX2, 4.0. Bruker AXS, Inc.: Madison, WI, 2008.
- (64) SMART, Software for the CCD Detector System, 5.6. Bruker AXS, Inc.: Madison, WI, 2000.

- (65) Sheldrick, G. M. *SADABS: Area-Detector Absorption Correction*, University of Göttingen: Göttingen, Germany, 2001.
- (66) Sheldrick, G. *Acta Crystallogr. Sect. A: Found. Crystallogr.* **2008**, *64*, 112-122.
- (67) Speck, A. L. *PLATON, A Multipurpose Crystallographic Tool*, Utrecht University: Utrecht, The Netherlands, 2001.
- (68) Burnett, M. N.; Johnson, C. K. *ORTEP-III: Oak Ridge Thermal Ellipsoid Plot Program for Crystal Structure Illustrations*, Oak Ridge National Laboratory Report ORNL-6895: 1996.
- (69) Frisch, M. J. T., G. W.; Schlegel, H. B.; Scuseria, G. E.; Robb, M. A.; Cheeseman, J. R.; Montgomery, Jr., J. A.; Vreven, T.; Kudin, K. N.; Burant, J. C.; Millam, J. M.; Iyengar, S. S.; Tomasi, J.; Barone, V.; Mennucci, B.; Cossi, M.; Scalmani, G.; Rega, N.; Petersson, G. A.; Nakatsuji, H.; Hada, M.; Ehara, M.; Toyota, K.; Fukuda, R.; Hasegawa, J.; Ishida, M.; Nakajima, T.; Honda, Y.; Kitao, O.; Nakai, H.; Klene, M.; Li, X.; Knox, J. E.; Hratchian, H. P.; Cross, J. B.; Bakken, V.; Adamo, C.; Jaramillo, J.; Gomperts, R.; Stratmann, R. E.; Yazyev, O.; Austin, A. J.; Cammi, R.; Pomelli, C.; Ochterski, J. W.; Ayala, P. Y.; Morokuma, K.; Voth, G. A.; Salvador, P.; Dannenberg, J. J.; Zakrzewski, V. G.; Dapprich, S.; Daniels, A. D.; Strain, M. C.; Farkas, O.; Malick, D. K.; Rabuck, A. D.; Raghavachari, K.; Foresman, J. B.; Ortiz, J. V.; Cui, Q.; Baboul, A. G.; Clifford, S.; Cioslowski, J.; Stefanov, B. B.; Liu, G.; Liashenko, A.; Piskorz, P.; Komaromi, I.; Martin, R. L.; Fox, D. J.; Keith, T.; Al-Laham, M. A.; Peng, C. Y.; Nanayakkara, A.; Challacombe, M.; Gill, P. M. W.; Johnson, B.; Chen, W.; Wong, M. W.; Gonzalez, C.; and Pople, J. A. *Gaussian 03, Revision C.02*, Gaussian, Inc.: Wallingford, CT, 2004.
- (70) Frisch, M. J. T., G. W.; Schlegel, H. B.; Scuseria, G. E.; Robb, M. A.; Cheeseman, J. R.; Scalmani, G.; Barone, V.; Mennucci, B.; Petersson, G. A.; Nakatsuji, H.; Caricato, M.; Li, X.; Hratchian, H. P.; Izmaylov, A. F.; Bloino, J.; Zheng, G.; Sonnenberg, J. L.; Hada, M.; Ehara, M.; Toyota, K.; Fukuda, R.; Hasegawa, J.; Ishida, M.; Nakajima, T.; Honda, Y.; Kitao, O.; Nakai, H.; Vreven, T.; Montgomery, Jr., J. A.; Peralta, J. E.; Ogliaro, F.; Bearpark, M.; Heyd, J. J.; Brothers, E.; Kudin, K. N.; Staroverov, V. N.; Kobayashi, R.; Normand, J.; Raghavachari, K.; Rendell, A.; Burant, J. C.; Iyengar, S. S.; Tomasi, J.; Cossi, M.; Rega, N.; Millam, N. J.; Klene, M.; Knox, J. E.; Cross, J. B.; Bakken, V.; Adamo, C.; Jaramillo, J.; Gomperts, R.; Stratmann, R. E.; Yazyev, O.; Austin, A. J.; Cammi, R.; Pomelli, C.; Ochterski, J. W.; Martin, R. L.; Morokuma, K.; Zakrzewski, V. G.; Voth, G. A.; Salvador, P.; Dannenberg, J. J.; Dapprich, S.; Daniels, A. D.; Farkas, Ö.; Foresman, J. B.; Ortiz, J. V.; Cioslowski, J.; Fox, D. J. *Gaussian 09, Revision A.1*, Gaussian, Inc.: Wallingford, CT, 2009.
- (71) Becke, A. D. *Phys. Rev. A* **1988**, *38*, 3098-3100.
- (72) Becke, A. D. *J. Chem. Phys.* **1993**, *98*, 5648-5652.
- (73) Lee, C.; Yang, W.; Parr, R. G. *Phys. Rev. B* **1988**, *37*, 785-789.
- (74) Ditchfield, R.; Hehre, W. J.; Pople, J. A. *J. Chem. Phys.* **1971**, *54*, 724-728.
- (75) Hehre, W. J.; Ditchfield, R.; Pople, J. A. *J. Chem. Phys.* **1972**, *56*, 2257-2261.
- (76) Humphrey, W.; Dalke, A.; Schulten, K. *J. Mol. Graphics* **1996**, *14*, 33-38.
- (77) Fukui, K. *Acc. Chem. Res.* **1981**, *14*, 363-368.
- (78) Chang, S.; Sommer, R. D.; Rheingold, A. L.; Goldberg, D. P. *Chem. Commun.* **2001**, 2396-2397.
- (79) Janbon, S.; Davey, R. J.; Shankland, K. *CrystEngComm* **2008**, *10*, 279-282.

- (80) Pritchard, R. G.; Banks, R. E.; Tipping, A. E.; Haider, P. *Acta Crystallogr. Sect. C: Cryst. Struct. Commun.* **1991**, *47*, 229-230.
- (81) Prout, C. K.; Cameron, T. S.; Dunn, R. M. A.; Hodder, O. J. R.; Viterbo, D. *Acta Crystallogr. Sect. B: Struct. Sci.* **1971**, *27*, 1310-1314.
- (82) Prout, C. K.; Coda, A.; Forder, R. A.; Kamenar, B. *Cryst. Struct. Commun.* **1974**, *3*, 39-42.
- (83) Whittleton, S. N.; Dunitz, J. D. *Acta Crystallogr. Sect. B: Struct. Sci.* **1982**, *38*, 2052-2053.
- (84) Thomas, I. R.; Bruno, I. J.; Cole, J. C.; Macrae, C. F.; Pidcock, E.; Wood, P. A. *J. Appl. Crystallogr.* **2010**, *43*, 362-366.
- (85) Tan, H.-S.; Lampe, F. W. *J. Phys. Chem.* **1972**, *76*, 3303-3311.
- (86) Christie, M. I.; Frost, J. S.; Voisey, M. A. *Trans. Faraday Soc.* **1965**, *61*, 674-680.
- (87) Bosch, E.; Kochi, J. K. *J. Org. Chem.* **1994**, *59*, 5573-5586.
- (88) Gowenlock, B. G.; Richter-Addo, G. B. *J. Chem. Educ.* **2008**, *85*, 1243.
- (89) Ingold, C. K.; Piggott, H. A. *J. Chem. Soc.* **1924**, *125*, 168 - 176.
- (90) Fenimore, C. P. *J. Am. Chem. Soc.* **1950**, *72*, 3226-3231.
- (91) Nakamoto, K.; Rundle, R. E. *J. Am. Chem. Soc.* **1956**, *78*, 1113-1118.
- (92) Kozhukh, J.; Lippard, S. J., Unpublished work.

**Chapter 4. Influence of Ligand Constraints on the  
Reactivity of Co(II) Complexes of  
Tetraazamacrocyclic Tropocoronand Ligands with  
Nitric Oxide**

*The work presented in this Chapter has been submitted for publication:*

Kozhukh, J.; Lippard, S.J. *J. Am. Chem. Soc.* Submitted.

## 4.1. Introduction

The tropocoronand ligands provide a tunable scaffold for the syntheses of metal complexes with widely varying geometries. The tetraazamacrocyclic ligand architecture can support metal complexes in square-planar, tetrahedral, square pyramidal, trigonal bipyramidal, and octahedral coordination environments without any change in the nature of the aminotroponeiminate donor atoms.<sup>1-21</sup> The tropocoronand scaffold (Fig. 4.1) allows tuning of the steric and electronic properties of the coordinated metal center through variations in the lengths of the polymethylene

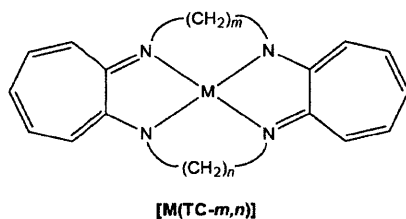


**Chart 4.1.** The tropocoronand scaffold binds metals in a variety of geometries, which may be tuned by changing the length of the methylene linker chains connecting the aminotroponeiminate units.

linker chains. A twist from square-planar toward increasingly more tetrahedral geometries can be induced by increasing the lengths of the connecting polymethylene chains. Structural profiles for metal complexes with chain lengths ranging from 3 to 6 methylene units have been established for cobalt(II)<sup>8</sup> and nickel(II),<sup>2,7,21</sup> and for chain lengths of 3 to 5 methylene units for copper(II).<sup>3</sup>

In separate studies, nitric oxide (NO) chemistry was explored for the divalent metal tropocoronand complexes [Co(TC-3,3)],<sup>4</sup> [Co(TC-4,4)],<sup>4</sup> [Mn(THF)(TC-5,5)],<sup>5,22</sup> and [Fe(TC-5,5)].<sup>6,22</sup> Metal mononitrosyl products were characterized from reaction mixtures.<sup>4-6,22</sup> These species are best described as {MNO}<sup>x</sup> adducts in the Enemark-Feltham notation, which circumvents the assignment of oxidation states in metal nitrosyl units, and instead characterizes metal nitrosyl fragment by the total number of electrons contributed by ·NO and the metal center.<sup>23</sup>

A thorough spectroscopic and computational study of nitrosyl complexes of first-row late transition metals was reported recently.<sup>24</sup> This report describes the electronic configurations of {CoNO}<sup>9</sup>, {NiNO}<sup>10</sup>, and {CuNO}<sup>11</sup> adducts and elucidates the nature of the metal-nitrosyl bonding interaction for {MNO}<sup>9/10/11</sup> fragments in otherwise three-coordinate environments with  $\sigma$ -donor ligands.<sup>24</sup> Although both the undertaking and outcome of the study are impressive, the authors note that further work is required to characterize the M-NO interaction in complexes with other geometries and coordination numbers.<sup>24</sup> In the absence of a report specifically addresses the nature of tropocoronand ligands and the corresponding metal nitrosyl complexes, we will utilize the Enemark-Feltham notation to describe metal-nitrosyl species in this work.

Cobalt mononitrosyls were observed when [Co(TC-*n,n*)] (*n* = 3, 4) was exposed to NO (g).<sup>4</sup> The Mn<sup>2+</sup> and Fe<sup>2+</sup> tropocoronands formed {MnNO}<sup>6</sup> and {FeNO}<sup>7</sup> adducts, respectively, in the presence of stoichiometric quantities of NO (g).<sup>5-6,22</sup> Both Mn<sup>2+</sup> and Fe<sup>2+</sup> species promoted NO disproportionation in the presence of excess nitric oxide.<sup>5-6</sup>

We became interested in exploring the NO reactivity of cobalt(II) coordinated by larger tropocoronand ligands. Specifically, we sought to characterize the reactivity of nitric oxide with [Co(TC-5,5)] and [Co(TC-6,6)], to determine whether tropocoronand ring size affects the NO reaction at the metal center. The results of our investigation are described in this Chapter.

## 4.2. Experimental Methods

**General Considerations.** Handling of air- and moisture-sensitive materials was conducted in an MBraun glovebox under a nitrogen atmosphere. Reagents were used as purchased, without further purification, with the exception of nitric oxide. Nitric oxide obtained from Airgas was purified according to published methods.<sup>25</sup> The NO was passed through an Ascarite column and a 6

ft coil containing silica gel at -78 °C to remove impurities and it was collected and stored under a nitrogen atmosphere in a gas storage bulb.  $^{15}\text{NO}$  was purchased from Cambridge Isotope Laboratories and purified similarly. All gas transfers were performed using gas-tight syringes under a nitrogen atmosphere. Methylene chloride and tetrahydrofuran (THF) were purified by passage through activated alumina and stored over 4 Å molecular sieves under an inert nitrogen atmosphere prior to use. Deuterated NMR solvents were obtained from Cambridge Isotope Laboratories, stored under a nitrogen atmosphere, and used without further purification. The syntheses of  $\text{H}_2\text{TC-6,6}$ ;<sup>7,21</sup>  $[\text{Co}(\text{TC-5,5})]$ ,<sup>8</sup>  $[\text{Co}(\text{TC-6,6})]$ ,<sup>8</sup> and  $[\text{Co}(\mu\text{-Cl})(\text{NO})_2]_2$ <sup>26</sup> are described elsewhere. CHN analyses were performed by Intertek-QTI (Whitehouse, NJ, USA) and Midwest Microlab, LLC (Indianapolis, IN, USA).

**Synthesis of  $[\text{Co}(\text{NO})(\text{TC-5,5})]$ .** To the headspace of a methylene chloride solution of  $[\text{Co}(\text{TC-5,5})]$  (59 mg, 0.136 mmol) was added NO (g) (5 mL, 0.204 mmol). The reaction mixture was left to stir for 2 h. The solvent was removed in vacuo to give the desired compound as a brown powder. X-ray quality crystals were obtained from  $\text{CH}_2\text{Cl}_2/\text{Et}_2\text{O}$  at -30 °C (20.3 mg, 32.2% yield).  $^1\text{H}$  NMR ( $\text{CD}_2\text{Cl}_2$ )  $\delta$  1.51 – 1.61 (m, 12H,  $\text{CH}_2$ ), 3.48 (m, 4H,  $\text{CH}_2$ ), 3.63 (m, 4H,  $\text{CH}_2$ ), 6.07 (t,  $J$  = 9.2 Hz, 2H, Ar- $H_\delta$ ), 6.51 (d,  $J$  = 11.2 Hz, 4H, Ar- $H_\beta$ ), 6.86 (t,  $J$  = 10.2 Hz, 4H, Ar- $H_\gamma$ ); IR (KBr)  $\nu_{\text{NO}}$  1622  $\text{cm}^{-1}$ ; UV-Vis ( $\text{CH}_2\text{Cl}_2$ ) ( $\epsilon$ ,  $\text{M}^{-1} \text{cm}^{-1}$ ) 281 nm (37 025), 329 nm (20 266), 394 nm (24 261), 414 nm (25 685), 490 nm (sh), 589 nm (sh), 892 nm (1069); Anal. Calc'd. for  $\text{C}_{24}\text{H}_{30}\text{N}_5\text{Co}$ : C, 62.20; H, 6.52; N, 15.11. Found: C, 61.49; H, 6.44; N, 14.54.

**Synthesis of  $[\text{Co}_2(\text{NO})_4(\text{TC-6,6})]$ .** To a stirring solution of  $\text{H}_2\text{TC-6,6}$  (100 mg, 0.247 mmol) in dry THF was added *n*-butyllithium (1.6 M in hexanes, 310  $\mu\text{L}$ , 0.494 mmol) under an inert nitrogen atmosphere. The dry ice/acetone cold bath was removed and the mixture was allowed to stir for 1 h at RT. The reaction flask was brought into a dry glovebox and  $[\text{Co}(\mu\text{-Cl})(\text{NO})_2]_2$  (76 mg,

0.247 mmol) was added to the solution under an inert nitrogen atmosphere. The reaction was left to stir 3 h, after which time the solvent was removed in vacuo. The resultant residue was suspended in methylene chloride and filtered through Celite. The filtrate was evaporated to dryness and the resultant solid washed with pentane and dried in vacuo. The desired product was obtained as a brown microcrystalline powder (94 mg, 59% yield). X-ray quality crystals were obtained from CH<sub>2</sub>Cl<sub>2</sub>/pentane at -30 °C. <sup>1</sup>H NMR (C<sub>6</sub>D<sub>6</sub>) δ 1.10 (m, 8H, CH<sub>2</sub>), 1.43 (m, 8H, CH<sub>2</sub>), 3.31 (m, 8H, CH<sub>2</sub>), 6.20 (t, *J* = 9.2 Hz, 2H, Ar-*H*<sub>δ</sub>), 6.40 (d, *J* = 11.2 Hz, 4H, Ar- *H*<sub>β</sub>), 6.81 (t, *J* = 10.2 Hz, 4H, Ar- *H*<sub>γ</sub>); IR (KBr) ν<sub>NO</sub> 1799 cm<sup>-1</sup>, 1722 cm<sup>-1</sup>; UV-Vis (toluene) (ε, M<sup>-1</sup> cm<sup>-1</sup>) 382 nm (31 796), 454 nm (20 324), 619 nm (sh); Anal. Calc'd. for C<sub>26</sub>H<sub>34</sub>N<sub>8</sub>O<sub>4</sub>Co<sub>2</sub>: C, 48.76; H, 5.35; N, 17.50. Found: C, 47.21; H, 5.18; N, 16.71.

**Physical Measurements.** <sup>1</sup>H NMR spectra were collected on a 400 MHz Bruker Avance spectrometer. Optical spectra were recorded on a Varian Cary 50 Bio UV-Visible Spectrophotometer in 6SQ Starna cells. Solutions were prepared under a nitrogen atmosphere. FT-IR spectra were recorded on a Thermo Nicolet Avatar 360 spectrometer running the OMNIC software package. An Agilent Technologies 5975C Mass Selective Detector running in electron impact ionization mode was used for EI-MS studies of the reaction headspace.

**X-ray Crystallography.** Crystals were mounted in Paratone N oil and frozen at 100 K under a cold nitrogen stream controlled by a Cryopad low-temperature apparatus. Data were collected on a Bruker APEX CCD X-ray diffractometer with graphite-monochromated Mo-K<sub>α</sub> radiation (λ = 0.71073 Å) controlled by the APEX2 software package.<sup>27</sup> Empirical absorption corrections were performed with SADABS.<sup>28</sup> The structure was solved by direct methods using SHELXS-97 and refined by full-matrix least-squares on *F*<sup>2</sup> using the SHELXL-97 program incorporated into the SHELXTL software package.<sup>29</sup> Possible higher symmetries were sought by PLATON<sup>30</sup> and none



were found. Non-hydrogen atoms were located and their positions refined anisotropically. Hydrogen atoms were assigned idealized positions and given thermal parameters 1.2 times the thermal parameters of the atoms to which they are attached. Thermal ellipsoid plots were generated using ORTEP-III.<sup>31</sup>

**NO Reactions.** Methylene chloride solutions of [Co(TC-*n,n*)] (*n* = 4 – 6) (59 – 200 mg, 0.14 – 0.49 mmol) or [Co<sub>2</sub>(NO)<sub>4</sub>(TC-6,6)] (20 mg, 0.031 mmol) were set up and allowed to stir under a nitrogen atmosphere in a septum-capped vial. A gas-tight syringe was used to remove a 5 mL volume of headspace from the vials, and subsequently excess NO or <sup>15</sup>NO (1.5 – 2.5 equiv) was injected into the headspace. The reaction mixtures were left to stir overnight, after which time they were evaporated to dryness in vacuo and KBr pellets were prepared from the resultant solid material for IR analysis. A solution IR timecourse was conducted in an analogous manner, except that aliquots were taken from the reaction solution by gas-tight syringe and injected into a CaF<sub>2</sub> solution IR cell. The cell was sealed and removed from the glovebox, and the solution was analyzed by infrared spectroscopy.

**NO<sub>2</sub> Reaction.** The reaction between [Co(TC-6,6)] (50 mg, 0.11 mmol) and NO<sub>2</sub> (2.7 mL, 0.11 mmol) was conducted in a manner analogous to that reported for the reactions described above, except that the reaction was concentrated to dryness in vacuo after 3 h, at which time the resultant residue was dissolved in CD<sub>2</sub>Cl<sub>2</sub> and analyzed by <sup>1</sup>H NMR spectroscopy. The sample was brought back into the glovebox after analysis, spiked with independently prepared [Co(NO<sub>2</sub>)(TC-6,6)],<sup>32</sup> and was examined again by <sup>1</sup>H NMR spectroscopy.

**EI-MS Studies.** All solutions were prepared under a nitrogen atmosphere. [Co(TC-6,6)] (30 mg, 0.065 mmol) was dissolved in ~3 mL of methylene chloride in a custom-made gas-tight cell in a glovebox under a nitrogen atmosphere. The cell was sealed, and a septum was fitted snugly over

one of the ports. The stopcock to the port was opened, and ~10 mL headspace was removed from the cell by a gas-tight syringe.  $^{15}\text{NO}$  (g) (11 mL, 0.46 mmol) was injected into the headspace of the cell through the septum by a gas-tight syringe. The cell was sealed and the reaction mixture was allowed to stir overnight prior to analysis. The cell was then connected to a He gas flow and to the mass spectrometer, and the connecting copper tubing was purged thoroughly prior to analysis of the reaction headspace. Headspace analysis was undertaken with the mass spectrometer operating in the selective ion mode. Analogous conditions were used for the control experiment, except that 3 mL of  $^{15}\text{NO}$  (g) (0.12 mmol) were injected into an empty cell. EI-MS analysis was performed the next day.

### 4.3. Results and Discussion

In this work we have discovered an unprecedented dependence on linker chain length of the reactions of cobalt(II) tropocoronands with NO (g). Specifically, we find preferential formation of  $\{\text{CoNO}\}^8$  species from the reaction of  $[\text{Co}(\text{TC-5,5})]$  and NO (g), whereas exposure of  $[\text{Co}(\text{TC-6,6})]$  to NO (g) results in a  $\{\text{Co}(\text{NO})_2\}^{10}$  compound. The cobalt(III) nitrite complex  $[\text{Co}(\text{NO}_2)(\text{TC-6,6})]$  was subsequently isolated from the reaction mixture.

Addition of excess NO (g) to the headspace of  $[\text{Co}(\text{TC-5,5})]$  in methylene chloride solution led to the formation of  $[\text{Co}(\text{NO})(\text{TC-5,5})]$  (Fig. 4.1, Tables 4.1 and 4.2).

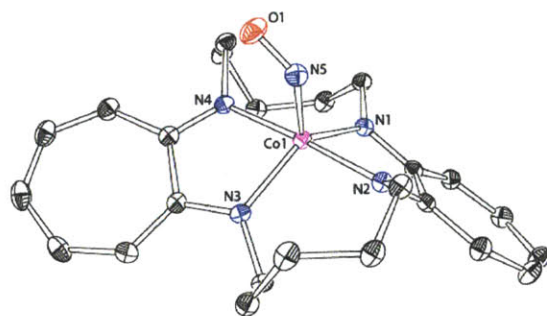


**Figure 4.1.** Thermal ellipsoid plot for [Co(NO)(TC-5,5)], depicted at 50% probability. Hydrogen atoms are omitted for clarity.

**Table 4.1.** Crystallographic parameters for [Co(NO)(TC-5,5)], 2 [Co(TC-6,6)] · [Co(NO<sub>2</sub>)(TC-6,6)], and [Co<sub>2</sub>(NO)<sub>2</sub>(TC-6,6)].

	[Co(NO)(TC-5,5)]	2 [Co(TC-6,6)] · [Co(NO <sub>2</sub> )(TC-6,6)]	[Co <sub>2</sub> (NO) <sub>2</sub> (TC-6,6)]
<b>Empirical formula</b>	C <sub>24</sub> H <sub>30</sub> CoN <sub>5</sub> O	C <sub>78</sub> H <sub>102</sub> Co <sub>3</sub> N <sub>13</sub> O <sub>2</sub>	C <sub>26</sub> H <sub>34</sub> Co <sub>2</sub> N <sub>8</sub> O <sub>4</sub>
<b>Formula weight</b>	463.46	1430.52	640.47
<b>Crystal system</b>	Triclinic	Orthorhombic	Monoclinic
<b>Space group</b>	<i>P</i> $\bar{1}$	Aba2	<i>P</i> 2 <sub>1</sub> / <i>c</i>
<b>a (Å)</b>	9.846(2)	29.641(5)	7.9786(7)
<b>b (Å)</b>	11.129(2)	22.626(4)	12.0151(11)
<b>c (Å)</b>	11.284(2)	10.566(2)	14.8237(13)
<b><math>\alpha</math> (deg)</b>	66.923(3)		
<b><math>\beta</math> (deg)</b>	69.839(3)		104.2330(10)
<b><math>\gamma</math> (deg)</b>	74.740(4)		
<b>V (Å<sup>3</sup>)</b>	1056.0(4)	7086(2)	1377.4(2)
<b>Z</b>	2	4	2
<b><math>\rho_{calc}</math> (g/cm<sup>3</sup>)</b>	1.458	1.341	1.544
<b>Temperature (K)</b>	100 (2)	100 (2)	100 (2)
<b><math>\mu</math> (Mo K<math>\alpha</math>), (mm<sup>-1</sup>)</b>	0.840	0.751	1.253
<b><math>\theta</math> range (deg)</b>	2.01 to 28.28	1.37 to 26.37	2.21 to 28.71
<b>Crystal size (mm<sup>3</sup>)</b>	0.40 x 0.1 x 0.06	0.40 x 0.25 x 0.20	0.40 x 0.40 x 0.08
<b>Completeness to <math>\theta</math> (%)</b>	99.1	100.0	99.9
<b>Max, min peaks (e/Å<sup>3</sup>)</b>	0.432 and -0.557	0.345 and -0.254	0.457 and -0.170
<b>Goodness-of-fit<sup>c</sup></b>	1.035	1.117	1.043
<b>Total no. of data</b>	18379	60694	21239
<b>No. unique data</b>	5195	7275	3551
<b>Flack parameter</b>		-0.005(10)	
<b>R<sub>1</sub> (%)<sup>a</sup></b>	3.60	3.03	2.31
<b>wR<sub>2</sub> (%)<sup>b</sup></b>	7.58	7.12	5.95

$$^a R_1 = \frac{\sum ||F_o| - |F_c||}{\sum |F_o|}$$

$$^b wR_2 = \left\{ \frac{\sum [w(F_o^2 - F_c^2)^2]}{\sum [w(F_o^2)]} \right\}^{1/2}$$

<sup>c</sup>GOF =  $[\sum w(F_o^2 - F_c^2)^2 / (n - p)]^{1/2}$  where  $n$  is the number of data and  $p$  is the number of refined parameters.

**Table 4.2.** Summary of bond lengths (Å) and angles (deg) of interest for [Co(NO)(TC-5,5)].

Co(1)-N(5)	1.7856(17)	N(5)-Co(1)-N(2)	92.50(7)	N(5)-Co(1)-N(1)	119.70(7)
Co(1)-N(2)	1.9129(15)	N(5)-Co(1)-N(4)	90.03(7)	N(2)-Co(1)-N(1)	80.65(6)
Co(1)-N(4)	1.9176(15)	N(2)-Co(1)-N(4)	176.48(7)	N(4)-Co(1)-N(1)	100.20(6)
Co(1)-N(3)	1.9183(15)	N(5)-Co(1)-N(3)	109.83(7)	N(3)-Co(1)-N(1)	130.44(7)
Co(1)-N(1)	1.9504(16)	N(2)-Co(1)-N(3)	96.12(6)	O(1)-N(5)-Co(1)	129.48(13)
N(5)-O(1)	1.177(2)	N(4)-Co(1)-N(3)	80.71(6)		

As with [Co(NO)(TC-4,4)], reported previously,<sup>4</sup> the nitrosyl ligand in [Co(NO)(TC-5,5)] lies in the equatorial plane of an idealized trigonal bipyramid. The Co – N – O angle is bent at 129.48(13)°. The degree of nitrosyl bending in [Co(NO)(TC-5,5)] is comparable to the 128.9(6)° and 134.9(9)° bend angles of the disordered nitrosyl in the [Co(NO)(TC-4,4)] crystal structure.<sup>4</sup> In contrast, the nitrosyls of [Fe(NO)(TC-5,5)]<sup>6</sup> and [Mn(NO)(TC-5,5)],<sup>5</sup> also bound in the equatorial positions of idealized trigonal bipyramids, have bend angles of 174.3(4)° and 174.1(3)°, respectively. Density functional theory calculations on [Fe(NO)(TC-5,5)]<sup>33</sup> and [Mn(NO)(TC-5,5)]<sup>34</sup> suggest that the nature of the HOMO (SOMO) regulates the bend angle at the metal nitrosyl. The SOMO is best characterized as a primarily  $d_{x^2-z^2}$ -based orbital for both {FeNO}<sup>7</sup> and {MnNO}<sup>6</sup> tropocoronand complexes, wherein the *z*-axis is oriented along the M-N<sub>NO</sub> vector.<sup>33-34</sup> The authors suggest that the  $\pi$ -bonding interaction between the metal  $d_{x^2-z^2}$  orbital and the NO( $\pi^*$ ) orbital accounts for the linear conformation of the metal nitrosyls.<sup>33-34</sup> This logic crumbles when applied to the *bent* nitrosyl in [Co(NO)(TC-5,5)]. Preliminary DFT calculations (not shown) suggest that the HOMO of [Co(NO)(TC-5,5)] is also best characterized as a primarily  $d_{x^2-z^2}$ -based orbital that  $\pi$ -bonds with the NO( $\pi^*$ ) orbital. The discrepancy between the nature of the HOMO and the Co – N – O angle in [Co(NO)(TC-5,5)] cannot be accounted for at this time.

The infrared spectrum of [Co(NO)(TC-5,5)] reveals a  $\nu_{\text{NO}}$  stretch at 1622 cm<sup>-1</sup>, which shifts to 1585 cm<sup>-1</sup> upon use of <sup>15</sup>NO in the synthesis (Fig. 4.2, *right*). The calculated value, based on the simple harmonic oscillator approximation, is 1592 cm<sup>-1</sup>. As occurs in the infrared

spectrum of the product of the reaction of  $[\text{Co}(\text{TC-4,4})]$  with  $\text{NO}(\text{g})$  (Fig. 4.2, *left*), low intensity bands appear at higher energy, possibly the result of a small quantity of the  $\{\text{Co}(\text{NO})_2\}^{10}$  adduct, which may form in the  $[\text{Co}(\text{TC-5,5})]/\text{NO}$  reaction mixture.

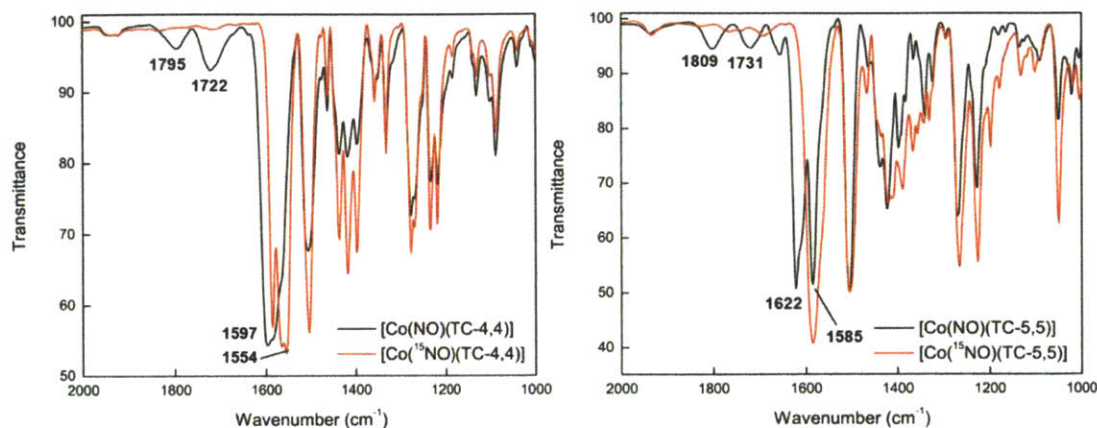


**Figure 4.2.** *Left:* Infrared spectroscopic comparison of  $[\text{Co}(\text{TC-4,4})] + \text{NO}(\text{g})$  (*black*) and  $[\text{Co}(\text{TC-4,4})] + {}^{15}\text{NO}(\text{g})$  (*red*). The strong band at  $1597\text{ cm}^{-1}$  corresponds to  $\nu_{\text{NO}}$  of  $[\text{Co}(\text{NO})(\text{TC-4,4})]$ , and the band at  $1554\text{ cm}^{-1}$  to  $\nu_{\text{NO}}$  of  $[\text{Co}({}^{15}\text{NO})(\text{TC-4,4})]$ . *Right:* Infrared spectroscopic comparison of  $[\text{Co}(\text{TC-5,5})] + \text{NO}(\text{g})$  (*black*) and  $[\text{Co}(\text{TC-5,5})] + {}^{15}\text{NO}(\text{g})$  (*red*). Bands at  $1622\text{ cm}^{-1}$  and  $1585\text{ cm}^{-1}$  correspond to  $\nu_{\text{NO}}$  stretches of  $[\text{Co}(\text{NO})(\text{TC-5,5})]$  and  $[\text{Co}({}^{15}\text{NO})(\text{TC-5,5})]$ , respectively. Infrared spectra were recorded in the solid state (KBr).

$\text{N}_2\text{O}$  was not observed by EI-MS analysis of the headspace of the  $[\text{Co}(\text{TC-5,5})]$  reaction with  ${}^{15}\text{NO}(\text{g})$  (Fig. 4.3). The cobalt mononitrosyl is the only species that we were able to isolate from the reaction of  $[\text{Co}(\text{TC-5,5})]$  with  $\text{NO}(\text{g})$ .

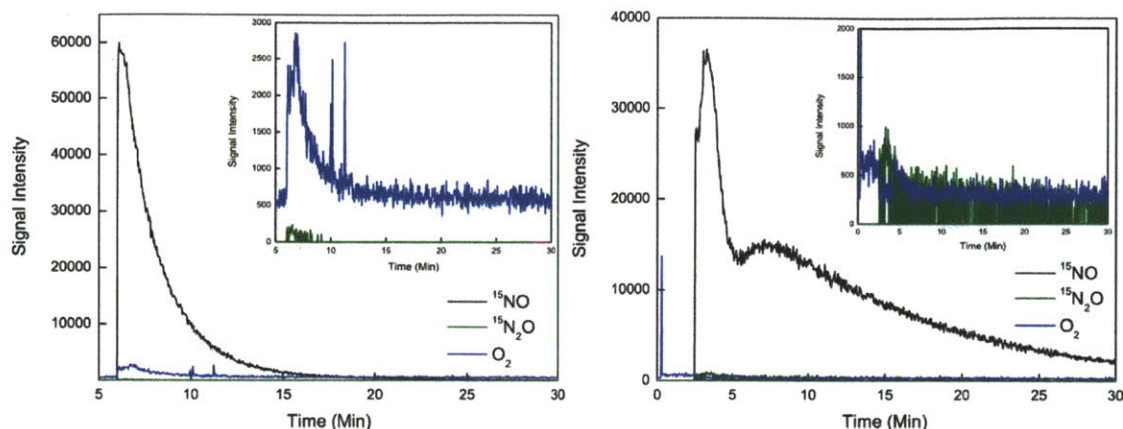


**Figure 4.3.** *Left:* EI-MS analysis of  $^{15}\text{NO}$  (g). *Right:* EI-MS analysis of the headspace of the reaction between  $[\text{Co}(\text{TC-5,5})]$  and  $^{15}\text{NO}$  (g) in  $\text{CH}_2\text{Cl}_2$ . The headspaces were monitored for  $^{15}\text{NO}$  ( $m/z = 31$ ),  $^{15}\text{N}_2\text{O}$  ( $m/z = 46$ ), and  $\text{O}_2$  ( $m/z = 32$ ). The detected dioxygen is residual after purging the connection lines of the instrument.

In light of the NO reactivity of  $[\text{Co}(\text{TC-}n,n)]$  ( $n = 3, 4, 5$ ), we were interested to discover that a stable  $[\text{Co}(\text{NO})(\text{TC-6,6})]$  species does not form when  $[\text{Co}(\text{TC-6,6})]$  is exposed to nitric oxide. Only crystals of the starting material could be isolated when  $[\text{Co}(\text{TC-6,6})]$  was allowed to react with 1 equiv of NO for 3 h. Recrystallization after exposure of  $[\text{Co}(\text{TC-6,6})]$  to 2.5 equiv of NO (g) for 2 h led to the formation of brown blocks, the composition of which was crystallographically determined to be a 2:1 mixture of  $[\text{Co}(\text{TC-6,6})]$  and  $[\text{Co}(\text{NO}_2)(\text{TC-6,6})]$  (Fig. 4.4, Tables 4.1 and 4.3).

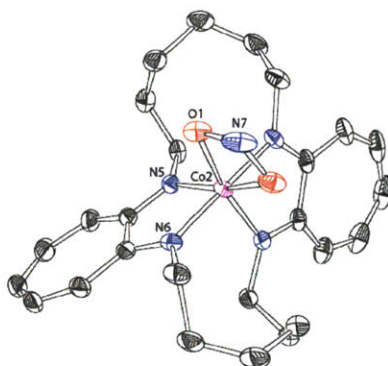


**Figure 4.4.** Plot for  $[\text{Co}(\text{NO}_2)(\text{TC-6,6})]$ , depicting the 50% probability thermal ellipsoids. Hydrogen atoms are omitted for clarity.

**Table 4.3.** Summary of bond lengths (Å) and angles (deg) of interest for 2 [Co(TC-6,6)]·[Co(NO<sub>2</sub>)(TC-6,6)].

Co(2)-N(5)	1.882(2)	N(5A)-Co(2)-N(5)	91.66(12)
Co(2)-N(6)	1.9247(18)	N(5)-Co(2)-N(6A)	97.53(8)
Co(2)-O(1)	2.0027(17)	N(5)-Co(2)-N(6)	82.13(9)
		N(6A)-Co(2)-N(6)	179.51(13)
		N(5A)-Co(2)-O(1)	165.57(8)
		N(5)-Co(2)-O(1)	102.64(8)
		N(6A)-Co(2)-O(1)	94.04(8)
		N(6)-Co(2)-O(1)	86.38(8)
		O(1)-Co(2)-O(1A)	63.13(11)
		N(5)-Co(2)-N(7)	134.17(6)
		N(6)-Co(2)-N(7)	90.24(6)
		O(1)-Co(2)-N(7)	31.56(5)

The nitrite ion is bound in a bidentate manner through its oxygen atoms to cobalt in the structurally characterized [Co(NO<sub>2</sub>)(TC-6,6)] complex, and the tropocoronand ligand folds back to accommodate an octahedral geometry at the cobalt(III) center. A crystallographically required C<sub>2</sub> symmetry axis passes through the nitrite nitrogen atom (N7) and the cobalt center (Co2). The asymmetric unit contains one complete [Co(TC-6,6)] molecule and one half [Co(NO<sub>2</sub>)(TC-6,6)]. The Co – O distance in [Co(NO<sub>2</sub>)(TC-6,6)] is 2.0027(17) Å, and the average distance between the cobalt center and the tropocoronand nitrogen atoms is 1.90 Å. The O1 – N7 – O1A angle is 110.5(3)°, and the O1 – Co2 – O1A four-membered chelate ring angle is 63.13(11)°.

Infrared spectroscopic analysis of a reaction mixture containing [Co(TC-6,6)] and NO revealed bands at 1799 cm<sup>-1</sup> and 1720 cm<sup>-1</sup>, corresponding to ν<sub>NO</sub> stretches of a putative dinitrosyl species (Fig. 4.5). These bands shifted to 1762 cm<sup>-1</sup> and 1687 cm<sup>-1</sup>, respectively, upon isotopic



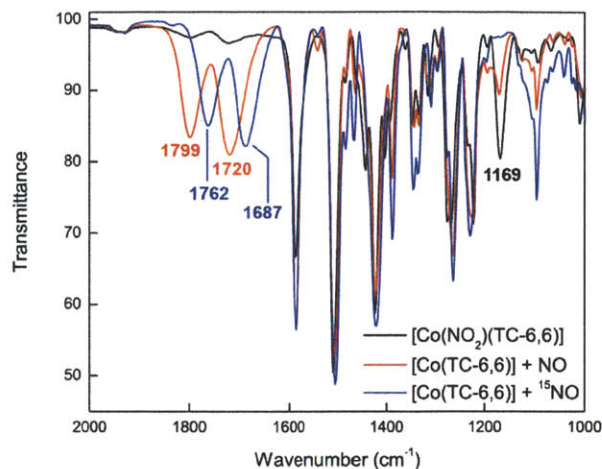


**Figure 4.5.** Infrared spectroscopic comparison of  $[\text{Co}(\text{NO}_2)(\text{TC-6,6})]$  (*black*);  $[\text{Co}(\text{TC-6,6})] + \text{NO}$  (g) (*red*); and  $[\text{Co}(\text{TC-6,6})] + {}^{15}\text{NO}$  (g) (*blue*). The strong band at  $1585\text{ cm}^{-1}$  is attributed to stretching modes of the aromatic region of the tropocoronand ligand. Infrared spectra were recorded in the solid state (KBr).

labeling with  ${}^{15}\text{NO}$ . By comparison with independently prepared  $[\text{Co}(\text{NO}_2)(\text{TC-6,6})]$ ,<sup>32</sup> we can assign the band at  $1169\text{ cm}^{-1}$  in the natural abundance NO reaction spectrum to the asymmetric N – O stretch of the nitrite ion.<sup>35</sup> This band shifts to the  $1140\text{ cm}^{-1}$  region in the  ${}^{15}\text{NO}$  reaction spectrum, where it is obscured by other bands.

A timecourse study in methylene chloride solution by IR spectroscopy revealed that the reaction between  $[\text{Co}(\text{TC-6,6})]$  and 3 equiv of NO (g) proceeds through what is likely to be a metastable  $[\text{Co}(\text{NO})(\text{TC-6,6})]$  intermediate (Fig. 4.6), with  $\nu_{\text{NO}}$  at  $1621\text{ cm}^{-1}$ , a band that increases in intensity over  $\sim 20$  min and then begins to disappear. The bands assigned to  $\nu_{\text{NO}}$  stretches of the dinitrosyl do not appear immediately, but instead increase in intensity over time, concomitant with the disappearance of the  $\nu_{\text{NO}}$  stretch of the putative  $[\text{Co}(\text{NO})(\text{TC-6,6})]$  species. Any nitrite stretches of  $[\text{Co}(\text{NO}_2)(\text{TC-6,6})]$  that may be present are obscured by methylene chloride.



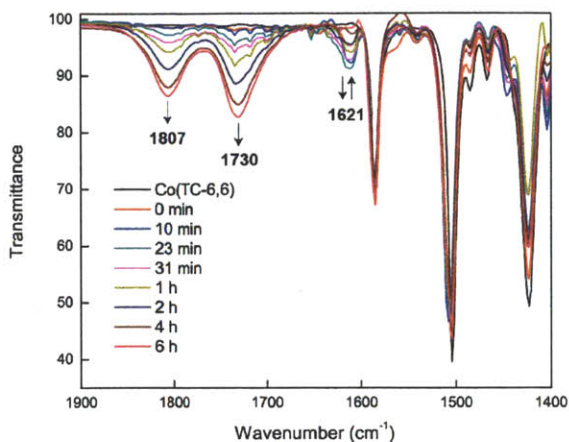


**Figure 4.6.** Solution IR timecourse for the reaction between  $[\text{Co}(\text{TC-6,6})]$  and 3 equiv of NO, recorded in methylene chloride. A band at  $1621\text{ cm}^{-1}$ , assigned to  $\nu_{\text{NO}}$  of a putative  $[\text{Co}(\text{NO})(\text{TC-6,6})]$  complex, grows in over 23 min and subsequently decreases in intensity over time. Bands at  $1730\text{ cm}^{-1}$  and  $1807\text{ cm}^{-1}$  increase in intensity over the course of the experiment and are assigned to  $\nu_{\text{NO}}$  of an overall neutral  $\{\text{Co}(\text{NO})_2\}^{10}$  fragment.

We sought to confirm that a neutral coordination complex containing a  $\{\text{Co}(\text{NO})_2\}^{10}$  core is accessible utilizing the  $[\text{TC-6,6}]^{2-}$  coordination environment. We prepared the dicobalt tetranitrosyl complex  $[\text{Co}_2(\text{NO})_4(\text{TC-6,6})]$  and compared its infrared spectroscopic features with those of the  $[\text{Co}(\text{TC-6,6})]/\text{NO}$  reaction mixture (Fig. 4.7).

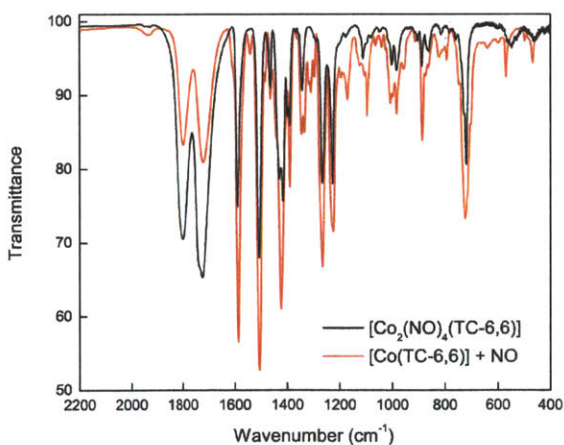


**Figure 4.7.** Infrared spectroscopic comparison of  $[\text{Co}_2(\text{NO})_4(\text{TC-6,6})]$  (black) and the  $[\text{Co}(\text{TC-6,6})]/\text{NO}$  reaction mixture (red). Infrared spectra were recorded in the solid state (KBr). The  $\nu_{\text{NO}}$  stretches of  $[\text{Co}_2(\text{NO})_4(\text{TC-6,6})]$  at  $1799\text{ cm}^{-1}$  and  $1722\text{ cm}^{-1}$  match well with  $\nu_{\text{NO}}$  stretches at  $1799\text{ cm}^{-1}$  and  $1720\text{ cm}^{-1}$  in the  $[\text{Co}(\text{TC-6,6})]/\text{NO}$  reaction spectrum.

Structural analysis of  $[\text{Co}_2(\text{NO})_4(\text{TC-6,6})]$  (Fig. 4.8, Tables 4.1 and 4.4) reveals pseudo-tetrahedral symmetry about both cobalt centers, and  $\text{Co} - \text{N}_{\text{NO}}$  bond distances of 1.6575(11) Å and 1.6897(12) Å for the linear and bent nitrosyls of the  $\{\text{Co}(\text{NO})_2\}^{10}$  fragment, respectively. The  $\text{N}_{\text{NO}} - \text{Co} - \text{N}_{\text{NO}}$  angle is  $114.40(6)^\circ$ , distorted significantly from the  $90^\circ$  angle predicted by Enemark and Feltham for first-row transition metals with good  $\pi$ -acceptor ligands.<sup>23</sup>

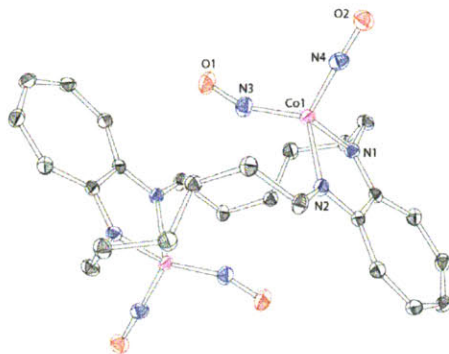


**Figure 4.8.** Thermal ellipsoid plot for  $[\text{Co}_2(\text{NO})_4(\text{TC-6,6})]$ , depicted at 50% probability. Hydrogen atoms are omitted for clarity.

**Table 4.4.** Summary of bond lengths (Å) and angles (deg) of interest for  $[\text{Co}_2(\text{NO})_2(\text{TC-6,6})]$ .

Co(1)-N(1)	1.9397(10)	N(4)-Co(1)-N(3)	114.40(6)
Co(1)-N(2)	1.9640(10)	N(4)-Co(1)-N(1)	110.21(5)
Co(1)-N(3)	1.6897(12)	N(3)-Co(1)-N(1)	114.93(5)
Co(1)-N(4)	1.6575(11)	N(4)-Co(1)-N(2)	116.18(5)
O(1)-N(3)	1.1589(15)	N(3)-Co(1)-N(2)	115.95(5)
O(2)-N(4)	1.1643(14)	N(1)-Co(1)-N(2)	80.69(4)
		O(1)-N(3)-Co(1)	156.84(11)
		O(2)-N(4)-Co(1)	174.76(10)

The reaction between  $[\text{Co}(\text{TC-5,5})]$  and  $\text{NO}$  (g), and the resultant formation of the  $\{\text{CoNO}\}^8$  species  $[\text{Co}(\text{NO})(\text{TC-5,5})]$ , are analogous to the chemistry of  $[\text{Co}(\text{TC-3,3})]$  and  $[\text{Co}(\text{TC-4,4})]$  with nitric oxide. The binding of nitric oxide to the cobalt(II) center of  $[\text{Co}(\text{TC-5,5})]$  leads to a stable arrangement of the tropocoronand ligand. In contrast, the putative cobalt mononitrosyl that is formed from  $[\text{Co}(\text{TC-6,6})]$  and  $\text{NO}$  (g) would be metastable, and if formed,

would readily convert to the dinitrosyl adduct. We surmise that the [TC-6,6]<sup>2-</sup> ligand must fold back about the metal center once the cobalt mononitrosyl is formed in order to minimize steric interactions among atoms within the polymethylene chains. This conformational change may expose an additional binding site for NO and enable dinitrosyl formation.

We hypothesize that the dinitrosyl formed in the reaction of [Co(TC-6,6)] with NO (g) corresponds to a neutral {Co(NO)<sub>2</sub>}<sup>10</sup> species. This inference is based on a comparison of the infrared spectroscopic features of independently synthesized [Co<sub>2</sub>(NO)<sub>4</sub>(TC-6,6)] with those of the [Co(TC-6,6)]/NO reaction mixture. Additionally, we draw comparisons between the infrared spectrum of the [Co(TC-6,6)]/NO reaction mixture and the infrared spectroscopic features of previously reported {Co(NO)<sub>2</sub>}<sup>10</sup> species that are bound to β-diketiminato and substituted aminotroponoiminate ligands. [Co<sub>2</sub>(NO)<sub>4</sub>(TC-6,6)] is characterized by ν<sub>NO</sub> stretches at 1799 cm<sup>-1</sup> and 1722 cm<sup>-1</sup> in the infrared spectrum, the energies of which compare very well with bands at 1799 cm<sup>-1</sup> and 1720 cm<sup>-1</sup> in the [Co(TC-6,6)]/NO spectrum. Nitrosyl stretches at comparable energies were previously reported for other nitrogen-bound {Co(NO)<sub>2</sub>}<sup>10</sup> fragments. The ν<sub>NO</sub> stretches for [Co(NO)<sub>2</sub>(Ar-nacnac)], where Ar-nacnac is a bulky β-diketiminato ligand, appear at 1801 cm<sup>-1</sup> and 1706 cm<sup>-1</sup> in benzene-*d*<sub>6</sub> solution.<sup>36</sup> The ν<sub>NO</sub> stretching frequencies for [Co(NO)<sub>2</sub>(*i*-Pr<sub>2</sub>ATI)] are 1809 cm<sup>-1</sup> and 1730 cm<sup>-1</sup>,<sup>37-39</sup> and bands in the ranges 1833 – 1838 cm<sup>-1</sup> and 1755 – 1760 cm<sup>-1</sup> are observed in spectra of the related [Co(NO)<sub>2</sub>(<sup>R</sup>DATI)] complexes.<sup>37-39</sup> The authors attribute the shift to higher energy in the DATI species to the electron-withdrawing nature of the sulfonamide-substituted ligands.<sup>37-39</sup> As in the reaction between [Co(TC-6,6)] and NO, cobalt mononitrosyl formation and subsequent decay are observed spectroscopically upon exposure of [Co(<sup>R</sup>DATI)] to nitric oxide.<sup>37-39</sup>

We were unable to obtain crystalline material of the putative tropocoronand-bound  $\{\text{Co}(\text{NO})_2\}^{10}$  complex in  $[\text{Co}(\text{TC-6,6})]/\text{NO}$  reaction mixtures, and instead we isolated crystals of the  $[\text{Co}(\text{TC-6,6})]$  starting material and the cobalt(III) nitrite  $[\text{Co}(\text{NO}_2)(\text{TC-6,6})]$ . We eliminated the possibility that the tropocoronand-bound  $\{\text{Co}(\text{NO})_2\}^{10}$  adduct is inherently unstable by the successful isolation and characterization of  $[\text{Co}_2(\text{NO})_4(\text{TC-6,6})]$ . The formation of a  $\{\text{Co}(\text{NO})_2\}^{10}$  species from  $[\text{Co}(\text{TC-6,6})]$  and  $\text{NO}$  (g) must occur by reductive nitrosylation, and oxidized species must therefore arise by virtue of the redox reaction. We suggest that the difficulty in isolating and structurally characterizing the putative  $\{\text{Co}(\text{NO})_2\}^{10}$  species from  $[\text{Co}(\text{TC-6,6})]/\text{NO}$  reaction mixtures may result from degradation of the cobalt dinitrosyl in the presence of reactive nitrogen and oxygen species generated in the reaction. We propose that nitrite may be generated in the reaction by attack of free  $\text{NO}$  on the coordinated nitrosyl of a metastable  $[\text{Co}(\text{NO})(\text{TC-6,6})]$  adduct, with concomitant release of  $\text{N}_2\text{O}$  (g). Attack of free  $\text{NO}$  (g) on coordinated  $\text{NO}$  has been described in the literature, and a mechanism for this transformation is discussed.<sup>40-45</sup>  $^{15}\text{N}_2\text{O}$  was indeed detected in the headspace gas of the reaction between  $[\text{Co}(\text{TC-6,6})]$  and  $^{15}\text{NO}$  (g) when the reaction headspace was analyzed by EI-MS (Fig. 4.9). This result gives credence to the proposed pathway for nitrite formation. Mechanistic studies to probe the  $[\text{Co}(\text{TC-6,6})]/\text{NO}$  reaction were precluded by the complexity of the reductive nitrosylation pathway and the difficulty in fully characterizing the products of the reaction.

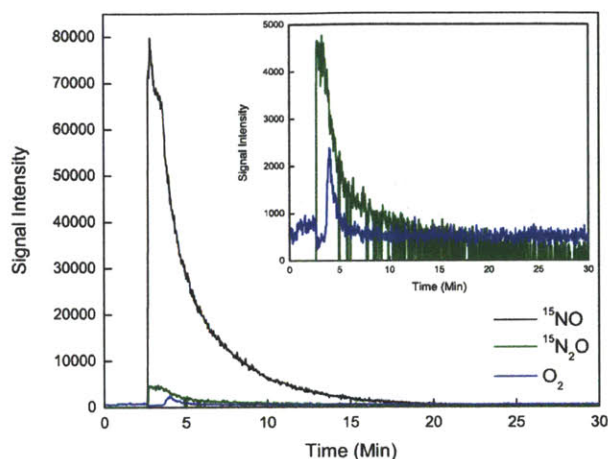


**Figure 4.9.** EI-MS analysis of the headspace of the reaction between [Co(TC-6,6)] and  $^{15}\text{NO}$  (g) in  $\text{CH}_2\text{Cl}_2$ . The headspace was monitored for  $^{15}\text{NO}$  ( $m/z = 31$ ),  $^{15}\text{N}_2\text{O}$  ( $m/z = 46$ ), and  $\text{O}_2$  ( $m/z = 32$ ). The detected dioxygen is residual after purging the connection lines of the instrument.

Finally, we wish to emphasize the differences in reactivity between [Co(TC-5,5)] and [Co(TC-6,6)] with NO (g). Cobalt(III) nitrite is absent from the [Co(TC-5,5)]/NO reaction, and we note a proclivity toward cobalt *mononitrosyl* formation. In contrast, nitrite,  $\text{N}_2\text{O}$ , and a cobalt *dinitrosyl* adduct are observed in the reaction of [Co(TC-6,6)] with NO. This example is the first to demonstrate a true size-dependent reactivity of cobalt(II) tropocoronands, and it reveals the preference for the smaller [Co(TC- $n,n$ )] ( $n = 3, 4, 5$ ) complexes to form mononitrosyl adducts upon exposure to NO (g). A dinitrosyl species can form in reactions of [Co(TC-6,6)], which contains a larger tropocoronand ligand.

#### 4.4. Summary and Conclusions

Size-dependent reactivity of cobalt(II) tropocoronands with NO (g) was demonstrated for [Co(TC- $n,n$ )] ( $n = 3 - 6$ ). Mononitrosyl formation was previously reported for the reactions of [Co(TC-3,3)] and [Co(TC-4,4)] with NO (g),<sup>4</sup> and demonstrated for the [Co(TC-5,5)]/NO reaction in the present work. In contrast, a neutral  $\{\text{Co}(\text{NO})_2\}^{10}$  adduct forms when NO (g) was add-

ed to solutions of [Co(TC-6,6)]. [Co(NO<sub>2</sub>)(TC-6,6)] was isolated by recrystallization from reaction mixtures. [Co<sub>2</sub>(NO)<sub>4</sub>(TC-6,6)] was prepared by independent synthesis and characterized structurally and spectroscopically. Comparable features in the infrared spectrum of [Co<sub>2</sub>(NO)<sub>4</sub>(TC-6,6)] and that of the reaction between [Co(TC-6,6)] and NO (g) suggest that a neutral {Co(NO)<sub>2</sub>}<sup>10</sup> species may be a reaction product of [Co(TC-6,6)] exposure to NO (g).

#### 4.5. References

- (1) Davis, W. M.; Lippard, S. J. *Inorg. Chem.* **1985**, *24*, 3688-3691.
- (2) Davis, W. M.; Roberts, M. M.; Zask, A.; Nakanishi, K.; Nozoe, T.; Lippard, S. J. *J. Am. Chem. Soc.* **1985**, *107*, 3864-3870.
- (3) Davis, W. M.; Zask, A.; Nakanishi, K.; Lippard, S. J. *Inorg. Chem.* **1985**, *24*, 3737-3743.
- (4) Franz, K. J.; Doerrer, L. H.; Spingler, B.; Lippard, S. J. *Inorg. Chem.* **2001**, *40*, 3774-3780.
- (5) Franz, K. J.; Lippard, S. J. *J. Am. Chem. Soc.* **1998**, *120*, 9034-9040.
- (6) Franz, K. J.; Lippard, S. J. *J. Am. Chem. Soc.* **1999**, *121*, 10504-10512.
- (7) Imajo, S.; Nakanishi, K.; Roberts, M.; Lippard, S. J.; Nozoe, T. *J. Am. Chem. Soc.* **1983**, *105*, 2071-2073.
- (8) Jaynes, B. S.; Doerrer, L. H.; Liu, S.; Lippard, S. J. *Inorg. Chem.* **1995**, *34*, 5735-5744.
- (9) Jaynes, B. S.; Ren, T.; Masschelein, A.; Lippard, S. J. *J. Am. Chem. Soc.* **1993**, *115*, 5589-5599.
- (10) Scott, M. J.; Lippard, S. J. *J. Am. Chem. Soc.* **1997**, *119*, 3411-3412.
- (11) Scott, M. J.; Lippard, S. J. *Organometallics* **1997**, *16*, 5857-5868.
- (12) Scott, M. J.; Lippard, S. J. *Inorg. Chim. Acta* **1997**, *263*, 287-299.
- (13) Scott, M. J.; Lippard, S. J. *Organometallics* **1998**, *17*, 1769-1773.
- (14) Scott, M. J.; Lippard, S. J. *Organometallics* **1998**, *17*, 466-474.
- (15) Villacorta, G. M.; Gibson, D.; Williams, I. D.; Lippard, S. J. *J. Am. Chem. Soc.* **1985**, *107*, 6732-6734.
- (16) Villacorta, G. M.; Gibson, D.; Williams, I. D.; Whang, E.; Lippard, S. J. *Organometallics* **1987**, *6*, 2426-2431.
- (17) Villacorta, G. M.; Lippard, S. J. *Pure Appl. Chem.* **1986**, *58*, 1474 - 1477.
- (18) Villacorta, G. M.; Lippard, S. J. *Inorg. Chem.* **1987**, *26*, 3672-3676.
- (19) Villacorta, G. M.; Lippard, S. J. *Inorg. Chem.* **1988**, *27*, 144-149.
- (20) Villacorta, G. M.; Rao, C. P.; Lippard, S. J. *J. Am. Chem. Soc.* **1988**, *110*, 3175-3182.
- (21) Zask, A.; Gonnella, N.; Nakanishi, K.; Turner, C. J.; Imajo, S.; Nozoe, T. *Inorg. Chem.* **1986**, *25*, 3400-3407.
- (22) Franz, K. J.; Lippard, S. J. *Inorg. Chem.* **2000**, *39*, 3722-3723.
- (23) Enemark, J. H.; Feltham, R. D. *Coord. Chem. Rev.* **1974**, *13*, 339-406.

- (24) Tomson, N. C.; Crimmin, M. R.; Petrenko, T.; Rosebrugh, L. E.; Sproules, S.; Boyd, W. C.; Bergman, R. G.; DeBeer, S.; Toste, F. D.; Wieghardt, K. *J. Am. Chem. Soc.* **2011**, *133*, 18785-18801.
- (25) Lorković, I. M.; Ford, P. C. *Inorg. Chem.* **2000**, *39*, 632-633.
- (26) Sacco, A.; Rossi, M.; Nobile, C. F. *Ann. Chim. (Rome)* **1967**, *57*, 499-507.
- (27) *APEX2*, 4.0. Bruker AXS, Inc.: Madison, WI, 2008.
- (28) Sheldrick, G. M. *SADABS: Area-Detector Absorption Correction*, University of Göttingen: Göttingen, Germany, 2001.
- (29) Sheldrick, G. *Acta Crystallogr. Sect. A: Found. Crystallogr.* **2008**, *64*, 112-122.
- (30) Speck, A. L. *PLATON, A Multipurpose Crystallographic Tool*, Utrecht University: Utrecht, The Netherlands, 2001.
- (31) Burnett, M. N.; Johnson, C. K. *ORTEP-III: Oak Ridge Thermal Ellipsoid Plot Program for Crystal Structure Illustrations*, Oak Ridge National Laboratory Report ORNL-6895: 1996.
- (32) Kozhukh, J.; Lippard, S. J., Manuscript in preparation.
- (33) Tangen, E.; Conradie, J.; Ghosh, A. *Inorg. Chem.* **2005**, *44*, 8699-8706.
- (34) Tangen, E.; Conradie, J.; Franz, K.; Friedle, S.; Telsler, J.; Lippard, S. J.; Ghosh, A. *Inorg. Chem.* **2010**, *49*, 2701-2705.
- (35) Nakamoto, K. In *Infrared and Raman Spectra of Inorganic and Coordination Compounds, Part B: Applications in Coordination, Organometallic, and Bioinorganic Chemistry*; 5 ed. 1998.
- (36) Tonzetich, Z. J.; Héroguel, F.; Do, L. H.; Lippard, S. J. *Inorg. Chem.* **2011**, *50*, 1570-1579.
- (37) Franz, K. J.; Singh, N.; Lippard, S. J. *Angew. Chem. Int. Ed.* **2000**, *39*, 2120-2122.
- (38) Franz, K. J.; Singh, N.; Spingler, B.; Lippard, S. J. *Inorg. Chem.* **2000**, *39*, 4081-4092.
- (39) Lim, M. H.; Kuang, C.; Lippard, S. J. *ChemBioChem* **2006**, *7*, 1571-1576.
- (40) Bau, R.; Sabherwal, I. H.; Burg, A. B. *J. Am. Chem. Soc.* **1971**, *93*, 4926-4928.
- (41) Gwost, D.; Caulton, K. G. *Inorg. Chem.* **1974**, *13*, 414-417.
- (42) McCleverty, J. A. *Chem. Rev.* **1979**, *79*, 53-76.
- (43) Rossi, M.; Sacco, A. *J. Chem. Soc., Chem. Commun.* **1971**, 694-694.
- (44) Strouse, C. E.; Swanson, B. I. *J. Chem. Soc., Chem. Commun.* **1971**, 55-56.
- (45) Gargano, M.; Giannoccaro, P.; Rossi, M.; Sacco, A.; Vasapollo, G. *Gazz. Chim. Ital.* **1975**, *105*, 1279-1290.

**Chapter 5. Reactivity of Tropocoronand-Bound  
Cobalt(III) Nitrite with Nitric Oxide as a Function of  
Polymethylene Linker Chain Length**



## 5.1. Introduction

The many functions of physiological nitric oxide (NO) have stimulated research into the chemistry of nitrogen oxides to gain insight into their biological roles. Studies of the biological chemistry of nitrite, for example, have implicated  $\text{NO}_2^-$  in storage and transport pathways for biological NO in the cardiovascular system.<sup>1-3</sup> Plasma nitrite concentrations correlate well with constitutive NO synthesis, and nitrite has been proposed to donate NO selectively to hypoxic sites, where deoxyhemoglobin can reduce  $\text{NO}_2^-$  to NO.<sup>1</sup> Hemoglobin (Hb) can reduce nitrite ion to NO and has therefore been implicated in blood flow regulation as well as oxygen sensing.<sup>1-7</sup> These associations have made Hb a potential target for nitrite-based therapies to treat hypertension and cyanide poisoning.<sup>1</sup> Nitrite reductases with heme iron or copper active sites occur in both eukaryotes and bacteria.<sup>1,4,8-11</sup> The preservation of nitrite reductase activity in such a broad range of organisms is an indicator of the ubiquity of the relationship between  $\text{NO}_2^-$  and NO in biology.

In the previous chapter we described the ability of cobalt(II) tropocoronand  $[\text{Co}(\text{TC-}n,n)]$  ( $n = 4 - 6$ ) linker chain length to tune the reactivity of these complexes with nitric oxide (NO).<sup>12</sup> We observed that  $[\text{Co}(\text{TC-}n,n)]$  complexes with shorter linker chains ( $n = 4, 5$ ) form  $\{\text{CoNO}\}$ <sup>8</sup> mononitrosyl adducts<sup>13</sup> upon exposure to NO (g). A  $[\text{Co}(\text{TC-}n,n)]$  complex with larger linkers,  $[\text{Co}(\text{TC-}6,6)]$ , favors formation of the  $\{\text{Co}(\text{NO})_2\}$ <sup>10</sup> neutral cobalt dinitrosyl, which ultimately converts to a cobalt(III) nitrite complex.<sup>12</sup> The discovery of nitrite formation spurred our interest in the potential interconversion between cobalt nitrosyls and cobalt nitrites, and we therefore examined the dependence of the reactivity of  $[\text{Co}(\text{NO}_2)(\text{TC-}n,n)]$  ( $n = 4 - 6$ ) complexes with NO (g) on the choice of tropocoronand ligand.

## 5.2. Experimental methods

**General Considerations.** Handling of air- and moisture-sensitive materials was conducted in an MBraun glovebox under an inert nitrogen atmosphere. Reagents were used as purchased, without further purification, with the exception of nitric oxide. Nitric oxide was obtained from Airgas and purified according to published methods.<sup>14</sup> The NO was passed through an Ascarite column and a 6 ft coil containing silica gel at -78 °C to remove impurities, and was collected and stored under an inert nitrogen atmosphere in a gas storage bulb. <sup>15</sup>NO was purchased from Cambridge Isotope Laboratories and purified similarly. All gas transfers were performed using gas-tight syringes under an inert nitrogen atmosphere. Methylene chloride and tetrahydrofuran (THF) were purified by passage through activated alumina and stored over 4 Å molecular sieves under an inert nitrogen atmosphere prior to use. Deuterated NMR solvents were obtained from Cambridge Isotope Laboratories, stored under an inert nitrogen atmosphere, and used without further purification. The syntheses of H<sub>2</sub>TC-6,6,<sup>15-16</sup> [Co(TC-4,4)];<sup>17</sup> [Co(TC-5,5)];<sup>17</sup> and [Co(TC-6,6)]<sup>17</sup> are described elsewhere. CHN analyses were performed by Intertek-QTI (Whitehouse, NJ, USA) and Midwest Microlab, LLC (Indianapolis, IN, USA).

**Synthesis of [Co(NO<sub>2</sub>)(TC-4,4)].** To a solution of [Co(TC-4,4)] (100 mg, 0.247 mmol) in methylene chloride was added AgNO<sub>2</sub> (42 mg, 0.271 mmol) in the dark. The reaction was left to stir overnight, resulting in a color change to brown and the formation of precipitate. The solution was filtered through Celite and the precipitate was washed with methylene chloride. The filtrate was collected and the solvent was removed in vacuo to give the desired product as a brown powder. X-ray quality crystals were obtained by recrystallization from CH<sub>2</sub>Cl<sub>2</sub>/Et<sub>2</sub>O at -30 °C (15.7 mg, 14.1 % yield). <sup>1</sup>H NMR (CD<sub>2</sub>Cl<sub>2</sub>) δ 1.59 (m, 4H, CH<sub>2</sub>), 1.77 (m, 4H, CH<sub>2</sub>), 3.53 (t, *J* = 9.2, 4H, CH<sub>2</sub>), 3.79 (d, *J* = 11.2, 4H, CH<sub>2</sub>), 6.12 (t, *J* = 10.4, 2H, Ar-H<sub>δ</sub>), 6.59 (d, *J* = , 4H, Ar-H<sub>β</sub>), 6.86 (t, *J* = , 4H, Ar-H<sub>γ</sub>); IR (KBr) ν<sub>NO</sub> 1172 cm<sup>-1</sup>; UV-Vis (CH<sub>2</sub>Cl<sub>2</sub>) (ε, M<sup>-1</sup> cm<sup>-1</sup>) 288 nm

(71 400), 299 nm (sh), 412 nm (49 678), 482 nm (sh), 519 nm (sh), 813 nm (1311); Anal. Calc'd. for  $C_{22}H_{26}N_5O_2Co$ : C, 58.54; H, 5.81; N, 15.51. Found: C, 57.17; H, 5.48; N, 14.83.

**Synthesis of [Co(NO<sub>2</sub>)(TC-5,5)].** To [Co(TC-5,5)] (50 mg, 0.115 mmol) in ~ 7 mL of methylene chloride was added silver nitrite (18 mg, 0.115 mmol). The solution was allowed to stir for 8 h and was then filtered through Celite to remove Ag<sup>0</sup>. The filtrate was layered with pentane left to crystallize at -30 °C. The desired product was isolated as brown crystals (34.3 mg, 62.2 % yield). <sup>1</sup>H NMR (CD<sub>2</sub>Cl<sub>2</sub>) δ 1.12 – 1.18 (m, 2H, CH<sub>2</sub>), 1.77 – 2.05 (m, 10H, CH<sub>2</sub>), 2.17 – 2.22 (m, 2H, CH<sub>2</sub>), 2.76 (d, *J* = 14 Hz, 2H, CH<sub>2</sub>), 3.53 – 3.60 (m, 2H, CH<sub>2</sub>), 3.79 (dd, *J* = 14.6 Hz, 3 Hz, 2H, CH<sub>2</sub>), 6.00 (t, *J* = 9 Hz, 2H, Ar-*H*<sub>δ</sub>), 6.56 (d, *J* = 11.2 Hz, 2H, Ar-*H*<sub>β</sub>), 6.72 (t, *J* = 10.2 Hz, 2H, Ar-*H*<sub>γ</sub>), 6.95 (t, *J* = 10.2 Hz, 2H, Ar-*H*<sub>γ</sub>), 7.04 (d, *J* = 11.6 Hz, 2H, Ar-*H*<sub>β</sub>); IR (KBr) ν<sub>NO</sub> 1176 cm<sup>-1</sup>; UV-Vis (CH<sub>2</sub>Cl<sub>2</sub>) (ε, M<sup>-1</sup> cm<sup>-1</sup>) 283 nm (38 296), 406 nm (23 268), 475 nm (sh), 497 nm (sh), 745 nm (sh), 949 nm (1111); Anal. Calc'd. for  $C_{24}H_{30}N_5O_2Co$ : C, 60.12; H, 6.31; N, 14.61. Found: C, 60.41; H, 6.08; N, 14.74.

**Synthesis of [Co(NO<sub>2</sub>)(TC-6,6)].** To a solution of [Co(TC-6,6)] (50 mg, 0.108 mmol) in methylene chloride was added silver nitrite (17 mg, 0.110 mmol). The suspension was allowed to stir overnight and then filtered through Celite to remove Ag<sup>0</sup>. The filtrate was concentrated, layered with diethyl ether, and placed at -30 °C to crystallize. The desired product was obtained as brown crystals (36 mg, 65.6% yield). <sup>1</sup>H NMR (CD<sub>2</sub>Cl<sub>2</sub>) δ 1.10 – 1.17 (m, 2H, CH<sub>2</sub>), 1.50 – 1.54 (m, 4H, CH<sub>2</sub>), 1.70 – 1.72 (m, 2H, CH<sub>2</sub>), 1.95 – 1.98 (m, 2H, CH<sub>2</sub>), 2.10 – 2.13 (m, 6H, CH<sub>2</sub>), 2.31 – 2.34 (m, 2H, CH<sub>2</sub>), 2.91 – 2.93 (m, 2H, CH<sub>2</sub>), 3.74 – 3.76 (m, 2H, CH<sub>2</sub>), 3.83 – 3.85 (m, 2H, CH<sub>2</sub>), 6.06 (t, *J* = 9 Hz, 2H, Ar-*H*<sub>δ</sub>), 6.54 (d, *J* = 11.2 Hz, 2H, Ar-*H*<sub>β</sub>), 6.69 (t, *J* = 10 Hz, 2H, Ar-*H*<sub>γ</sub>), 6.85 – 6.93 (m, 4H, Ar-*H*<sub>γ</sub> + Ar-*H*<sub>β</sub>); IR (KBr) ν<sub>NO</sub> 1169 cm<sup>-1</sup>; UV-Vis (CH<sub>2</sub>Cl<sub>2</sub>) (ε, M<sup>-1</sup> cm<sup>-1</sup>) 280 nm (44 450), 396 nm (28 325), 473 nm (14 442), 585 nm (sh), 938 nm (1742).

Anal. Calc'd. for  $C_{26}H_{34}N_5O_2Co$ : C, 61.53; H, 6.75; N, 13.80. Found: C, 60.91; H, 6.77; N, 13.22.

**Physical Measurements.**  $^1H$  NMR spectra were collected on a 400 MHz Bruker Avance spectrometer. Optical spectra were recorded on a Varian Cary 50 Bio UV-Visible Spectrophotometer in 6SQ Starna cells. Solutions were prepared under a nitrogen atmosphere. FT-IR spectra were recorded on a Thermo Nicolet Avatar 360 spectrometer running the OMNIC software package.

**X-ray Crystallography.** Crystals were mounted in Paratone N oil and frozen at 100 K under a cold nitrogen stream controlled by a Cryopad low-temperature apparatus. Data were collected on a Bruker APEX CCD X-ray diffractometer with graphite-monochromated  $Mo-K_{\alpha}$  radiation ( $\lambda = 0.71073 \text{ \AA}$ ), controlled by the APEX2 software package.<sup>18</sup> Empirical absorption correction was performed with SADABS.<sup>19</sup> The structure was solved by direct methods using SHELXS-97 and refined by full-matrix least-squares on  $F^2$  using the SHELXL-97 program incorporated into the SHELXTL software package.<sup>20</sup> Possible higher symmetry was evaluated by PLATON.<sup>21</sup> Non-hydrogen atoms were located and their positions refined anisotropically. Hydrogen atoms were assigned idealized positions and given thermal parameters 1.2 times the thermal parameters of the atoms to which they are attached. Thermal ellipsoid plots were generated in ORTEP-III<sup>22</sup> and space filling models were prepared using Raster3D.<sup>23</sup>

**NO Reactions.** Methylene chloride solutions of  $[Co(NO_2)(TC-n,n)]$  ( $n = 4, 5, 6$ ) (13 – 15 mg, 0.028 – 0.030 mmol) were set up to stir under a nitrogen atmosphere in a septum-capped vial. A gas-tight syringe was used to remove a 5 mL volume of headspace from the vials, and subsequently excess NO or  $^{15}NO$  (5 mL, 0.20 mmol) was injected in to the headspace. The reactions were allowed to stir overnight, after which time they were evaporated to dryness in vacuo, and KBr pellets for infrared, or  $CD_2Cl_2$  samples for  $^1H$  NMR, spectral analysis were

prepared from the resultant solid material. A solution IR timecourse was conducted in an analogous manner, except that aliquots were removed from the reaction solution by gas-tight syringe and injected into a CaF<sub>2</sub> solution IR cell. The cell was sealed, removed from the glovebox, and the solution was analyzed by infrared spectroscopy.

### 5.3. Results

[Co(NO<sub>2</sub>)(TC-*n,n*)] (*n* = 4 – 6) complexes were prepared by oxidation of the cobalt(II) [Co(TC-*n,n*)] (*n* = 4 – 6) compounds with AgNO<sub>2</sub> (Fig. 5.1, Tables 5.1 – 5.4). X-ray quality crystals of the [Co(NO<sub>2</sub>)(TC-*n,n*)] complexes were isolated in 14.1%, 62.2%, and 65.6% yields for the *n* = 4, 5, and 6 derivatives, respectively. All three complexes contain octahedral cobalt(III)

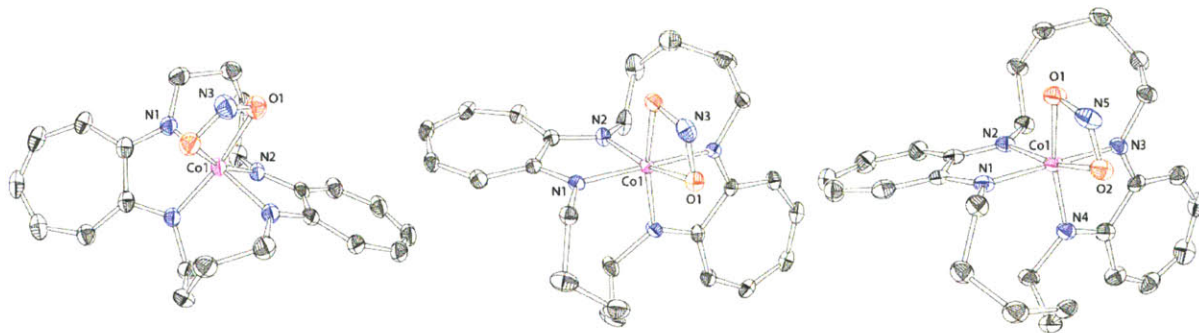


**Figure 5.1.** Thermal ellipsoid plots for [Co(NO<sub>2</sub>)(TC-4,4)] (*left*), [Co(NO<sub>2</sub>)(TC-5,5)] (*middle*), and [Co(NO<sub>2</sub>)(TC-6,6)] (*right*), depicted at 50% probability. Hydrogen atoms are omitted for clarity.

centers, and the nitrite ligands are bound in a bidentate manner through the oxygen atoms. [Co(NO<sub>2</sub>)(TC-4,4)] and [Co(NO<sub>2</sub>)(TC-5,5)] crystallize in the monoclinic space group *C*<sub>2</sub>/*c*. A crystallographically required *C*<sub>2</sub> symmetry axis passes through the cobalt center and the nitrogen atom of the nitrite ligand in both complexes. The asymmetric units of [Co(NO<sub>2</sub>)(TC-4,4)] and [Co(NO<sub>2</sub>)(TC-5,5)] each contain one half of the molecule as a result. [Co(NO<sub>2</sub>)(TC-6,6)] crystallizes in *P*<sub>2</sub><sub>1</sub>/*c* with two molecules of the cobalt(III) nitrite complex and a disordered

diethyl ether molecule in the asymmetric unit. The cobalt(III) centers of the three  $[\text{Co}(\text{NO}_2)(\text{TC-}n,n)]$  ( $n = 4 - 6$ ) complexes exist in similar coordination environments. The Co – O distances are 2.019(3) Å and 2.0237(17) Å for  $[\text{Co}(\text{NO}_2)(\text{TC-}4,4)]$  and  $[\text{Co}(\text{NO}_2)(\text{TC-}5,5)]$ , respectively. Average distances of 2.006(3) Å and 2.012(3) Å are observed for the Co – O bonds in the two crystallographically distinct  $[\text{Co}(\text{NO}_2)(\text{TC-}6,6)]$  molecules. Average distances between the cobalt center and the tropocoronand nitrogen atoms are 1.88 Å, 1.89 Å, and 1.90 Å for  $[\text{Co}(\text{NO}_2)(\text{TC-}n,n)]$  ( $n = 4 - 6$ ), respectively. The Co – N<sub>TC</sub> bond distances in  $[\text{Co}(\text{NO}_2)(\text{TC-}n,n)]$  ( $n = 4 - 6$ ) are shorter by an average 0.037 Å for tropocoronand nitrogen atoms located *trans* to oxygen atoms of the nitrite ligands. The disparity between Co – N<sub>TC</sub> bond lengths within individual molecules is attributed to the weaker *trans* effect of coordinated nitrite ion than of aminotroponeiminate. The geometric parameters of the  $[\text{Co}(\text{NO}_2)(\text{TC-}6,6)]$  complex presented in this work are comparable to those observed for the cobalt(III) nitrite complex that was isolated from  $[\text{Co}(\text{TC-}6,6)]/\text{NO}$  reaction mixtures, which is described in Chapter 4 of this thesis.

**Table 5.1.** Crystallographic parameters for [Co(NO<sub>2</sub>)(TC-4,4)] , [Co(NO<sub>2</sub>)(TC-5,5)], and [Co(NO<sub>2</sub>)(TC-6,6)].

	[Co(NO <sub>2</sub> )(TC-4,4)]	[Co(NO <sub>2</sub> )(TC-5,5)]	[Co(NO <sub>2</sub> )(TC-6,6)]
<b>Empirical formula</b>	C <sub>22</sub> H <sub>26</sub> CoN <sub>5</sub> O <sub>2</sub>	C <sub>24</sub> H <sub>30</sub> CoN <sub>5</sub> O <sub>2</sub>	C <sub>56</sub> H <sub>76</sub> Co <sub>2</sub> N <sub>10</sub> O <sub>5</sub>
<b>Formula weight</b>	451.41	479.46	1087.13
<b>Crystal system</b>	Monoclinic	Monoclinic	Monoclinic
<b>Space group</b>	<i>C2/c</i>	<i>C2/c</i>	<i>P2<sub>1</sub>/c</i>
<b>a (Å)</b>	13.186(6)	15.9717(17)	14.5809(14)
<b>b (Å)</b>	15.794(7)	13.0636(14)	12.7705(12)
<b>c (Å)</b>	9.718(4)	10.3826(11)	28.256(3)
<b>β (deg)</b>	102.575(7)	90.910(2)	93.057(2)
<b>V (Å<sup>3</sup>)</b>	1975.1(15)	2166.0(4)	5254.0(9)
<b>Z</b>	4	4	4
<b>ρ<sub>calc</sub> (g/cm<sup>3</sup>)</b>	1.518	1.470	1.374
<b>Temperature (K)</b>	100 (2)	100 (2)	100 (2)
<b>μ (Mo Kα), (mm<sup>-1</sup>)</b>	0.900	0.825	0.691
<b>θ range (deg)</b>	2.04 to 26.37	2.01 to 26.78	1.40 to 26.43
<b>Crystal size (mm<sup>3</sup>)</b>	0.40 x 0.05 x 0.05	0.14 x 0.08 x 0.03	0.35 x 0.10 x 0.05
<b>Completeness to θ (%)</b>	100.0	100.0	99.8
<b>Max, min peaks (e/Å<sup>3</sup>)</b>	0.764 and -0.381	0.603 and -0.375	0.741 and -0.532
<b>Goodness-of-fit<sup>a</sup></b>	1.086	1.053	1.026
<b>Total no. of data</b>	16194	19369	90211
<b>No. unique data</b>	2022	2319	10787
<b>R<sub>1</sub> (%)<sup>b</sup></b>	5.03	3.85	5.88
<b>wR<sub>2</sub> (%)<sup>c</sup></b>	9.46	7.38	11.67

<sup>a</sup>GOF =  $[\sum w(F_o^2 - F_c^2)^2 / (n - p)]^{1/2}$  where *n* is the number of data and *p* is the number of refined parameters.

<sup>b</sup>R<sub>1</sub> =  $\sum ||F_o| - |F_c|| / \sum |F_o|$

<sup>c</sup>wR<sub>2</sub> =  $\{\sum [w(F_o^2 - F_c^2)^2] / \sum [w(F_o^2)^2]\}^{1/2}$

**Table 5.2.** Summary of bond lengths (Å) and angles (deg) of interest for [Co(NO<sub>2</sub>)(TC-4,4)].

Co(1)-N(2)	1.861(3)	N(2A)-Co(1)-N(2)	96.31(17)
Co(1)-N(1)	1.904(3)	N(2A)-Co(1)-N(1)	82.17(12)
Co(1)-O(1)	2.019(3)	N(2)-Co(1)-N(1)	94.60(12)
		N(1)-Co(1)-N(1A)	175.18(18)
		N(2A)-Co(1)-O(1)	162.65(11)
		N(2)-Co(1)-O(1)	101.00(11)
		N(1)-Co(1)-O(1)	95.22(11)
		N(1A)-Co(1)-O(1)	88.92(11)
		O(1)-Co(1)-O(1A)	61.73(14)

**Table 5.3.** Summary of bond lengths (Å) and angles (deg) of interest for [Co(NO<sub>2</sub>)(TC-5,5)].

Co(1)-N(2)	1.8728(19)	N(2A)-Co(1)-N(2)	92.22(12)
Co(1)-N(1)	1.9107(18)	N(2)-Co(1)-N(1A)	97.19(8)
Co(1)-O(1)	2.0237(17)	N(1A)-Co(1)-N(1)	179.05(12)
		N(2)-Co(1)-N(1)	82.14(8)
		N(2)-Co(1)-O(1A)	102.89(8)
		N(1)-Co(1)-O(1)	94.63(7)
		N(2)-Co(1)-O(1)	164.84(8)
		N(1)-Co(1)-O(1A)	86.19(7)
		O(1A)-Co(1)-O(1)	62.03(10)

**Table 5.4.** Summary of bond lengths (Å) and angles (deg) of interest for [Co(NO<sub>2</sub>)(TC-6,6)], shown for both crystallographically independent molecules.

Co(1)-N(4)	1.880(3)	N(4)-Co(1)-N(2)	91.83(14)	N(6)-Co(2)-N(8)	92.79(14)
Co(1)-N(2)	1.888(3)	N(4)-Co(1)-N(1)	97.08(14)	N(6)-Co(2)-N(9)	97.53(15)
Co(1)-N(1)	1.914(3)	N(2)-Co(1)-N(1)	81.60(14)	N(8)-Co(2)-N(9)	82.09(14)
Co(1)-N(3)	1.917(3)	N(4)-Co(1)-N(3)	81.67(14)	N(6)-Co(2)-N(7)	81.93(15)
Co(1)-O(2)	1.995(3)	N(2)-Co(1)-N(3)	96.87(14)	N(8)-Co(2)-N(7)	98.17(15)
Co(1)-O(1)	2.017(3)	N(1)-Co(1)-N(3)	178.01(14)	N(9)-Co(2)-N(7)	179.42(16)
		N(4)-Co(1)-O(2)	102.29(13)	N(6)-Co(2)-O(3)	102.33(14)
		N(2)-Co(1)-O(2)	165.69(13)	N(8)-Co(2)-O(3)	164.72(14)
		N(1)-Co(1)-O(2)	94.23(13)	N(9)-Co(2)-O(3)	93.60(13)
Co(2)-N(6)	1.888(3)	N(3)-Co(1)-O(2)	87.55(13)	N(7)-Co(2)-O(3)	86.29(13)
Co(2)-N(8)	1.899(3)	N(4)-Co(1)-O(1)	164.84(13)	N(6)-Co(2)-O(4)	164.33(14)
Co(2)-N(9)	1.908(3)	N(2)-Co(1)-O(1)	103.31(13)	N(8)-Co(2)-O(4)	102.71(14)
Co(2)-N(7)	1.920(3)	N(1)-Co(1)-O(1)	85.99(13)	N(9)-Co(2)-O(4)	86.96(13)
Co(2)-O(3)	2.010(3)	N(3)-Co(1)-O(1)	95.62(13)	N(7)-Co(2)-O(4)	93.49(14)
Co(2)-O(4)	2.014(3)	O(2)-Co(1)-O(1)	62.61(12)	O(3)-Co(2)-O(4)	62.29(13)
		N(4)-Co(1)-N(5)	133.70(14)	N(6)-Co(2)-N(10)	133.20(15)
		N(2)-Co(1)-N(5)	134.42(14)	N(8)-Co(2)-N(10)	134.01(15)
		N(1)-Co(1)-N(5)	89.53(13)	N(9)-Co(2)-N(10)	90.57(13)
		N(3)-Co(1)-N(5)	92.46(13)	N(7)-Co(2)-N(10)	89.62(14)
		O(2)-Co(1)-N(5)	31.41(11)	O(3)-Co(2)-N(10)	30.95(12)
		O(1)-Co(1)-N(5)	31.21(11)	O(4)-Co(2)-N(10)	31.35(13)

We used vibrational spectroscopy to probe the effect of tropocoronand ring size in the [Co(NO<sub>2</sub>)(TC-*n,n*)] (*n* = 4 – 6) complexes on their reactivity with NO (g). Exposure of [Co(NO<sub>2</sub>)(TC-4,4)] to NO (g) resulted in the appearance of a strong band at 1592 cm<sup>-1</sup> in the infrared spectrum, characteristic of the  $\nu_{\text{NO}}$  stretching band in [Co(NO)(TC-4,4)] (Fig. 5.2, *left*).<sup>24</sup> The analogous reaction with <sup>15</sup>NO shifted this band to 1571 cm<sup>-1</sup> (Fig. 5.2, *right*).



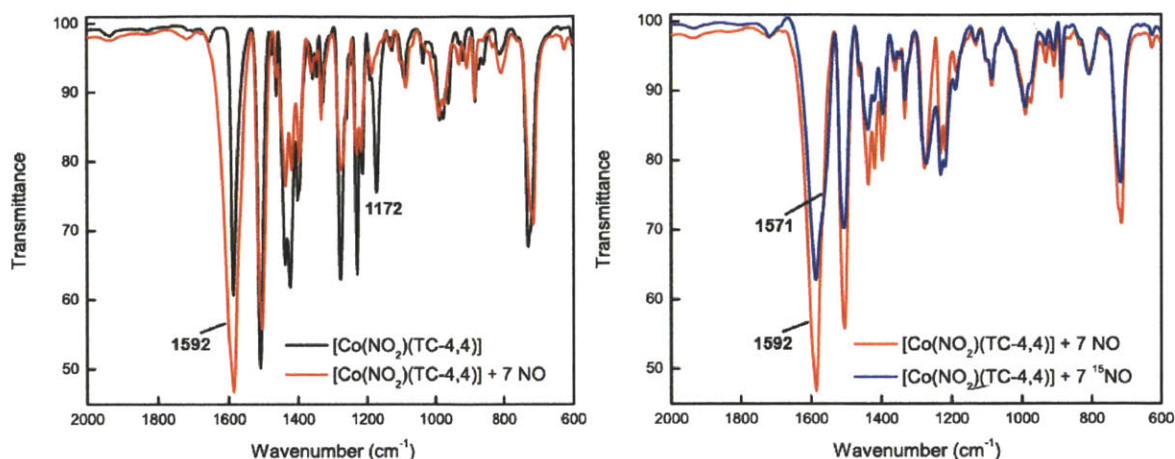


**Figure 5.2.** Infrared spectroscopic comparisons of the reactions of [Co(NO<sub>2</sub>)(TC-4,4)] with NO (g) (left) and <sup>15</sup>NO (g) (right). Stretches for  $\nu_{\text{NO}}$  are labeled.

From the expected isotope shift, based on the simple harmonic oscillator model, the frequency is computed to be 1563 cm<sup>-1</sup>. Complete consumption of [Co(NO<sub>2</sub>)(TC-4,4)] occurred during the reaction, as determined by the disappearance of the  $\nu_{\text{NO}}$  stretching band of the nitrite ligand in {Co(NO<sub>2</sub>)} at 1172 cm<sup>-1</sup>. There was no spectroscopic evidence that a {Co(NO)<sub>2</sub>} species had formed. The reaction mixture was also examined by <sup>1</sup>H NMR spectroscopy, but because the <sup>1</sup>H NMR spectra of [Co(NO<sub>2</sub>)(TC-4,4)] and [Co(NO)(TC-4,4)] are identical, the results were inconclusive (Fig. 5.3). We grew crystals from the [Co(NO<sub>2</sub>)(TC-4,4)]/NO reaction mixture to confirm conversion to the {CoNO}<sup>8</sup> species and were able to crystallographically characterize the cobalt mononitrosyl [Co(NO)(TC-4,4)]. The resultant crystallographic and structural parameters for [Co(NO)(TC-4,4)] are analogous to those previously reported.<sup>24</sup>

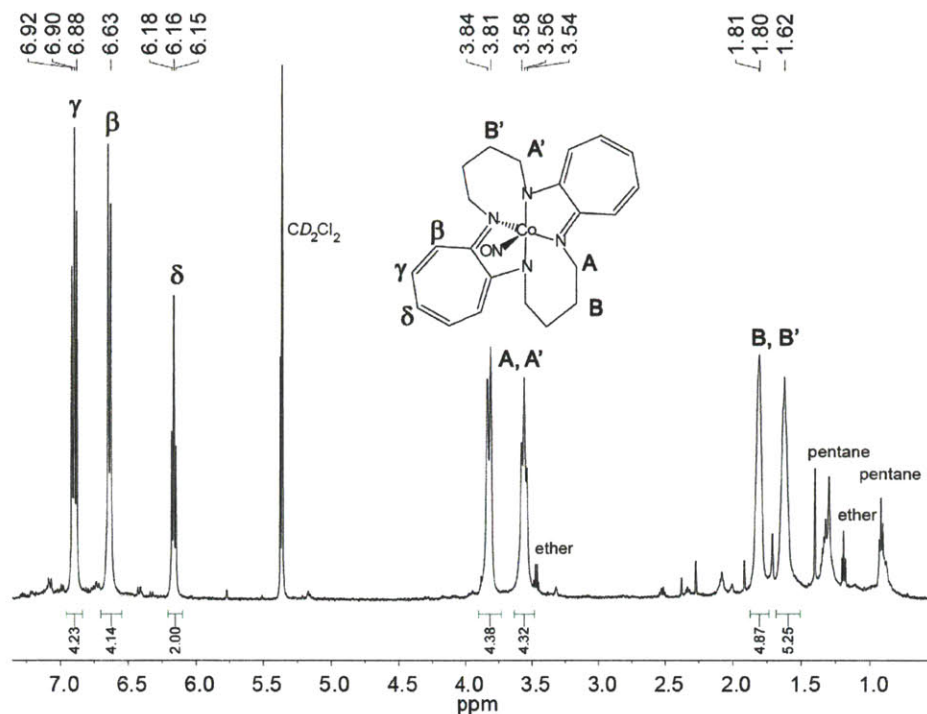


**Figure 5.3.**  $^1\text{H}$  NMR spectrum of the reaction of  $[\text{Co}(\text{NO}_2)(\text{TC-4,4})]$  with  $\text{NO}$  (g).

We next exposed  $[\text{Co}(\text{NO}_2)(\text{TC-5,5})]$  to  $\text{NO}$  (g) and observed the formation of both  $\{\text{CoNO}\}^8$  and  $\{\text{Co}(\text{NO})_2\}^{10}$  species (Fig. 5.4). The  $\{\text{CoNO}\}^8$  complex is characterized by

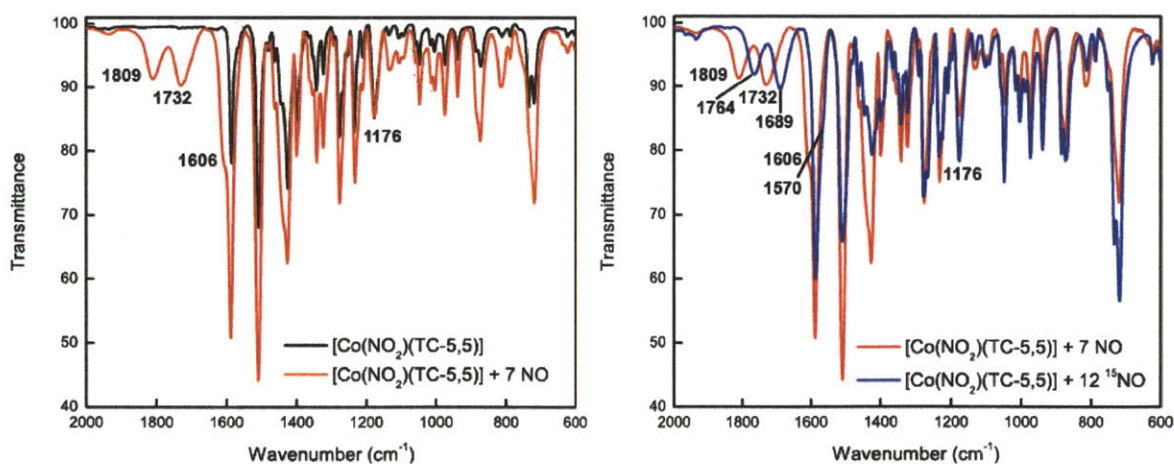


**Figure 5.4.** Infrared spectroscopic comparisons of the reactions of  $[\text{Co}(\text{NO}_2)(\text{TC-5,5})]$  with  $\text{NO}$  (g) (left) and  $^{15}\text{NO}$  (g) (right). Stretches for  $\nu_{\text{NO}}$  are labeled.

a strong band corresponding to the  $\nu_{\text{NO}}$  stretch at  $1606\text{ cm}^{-1}$  in the infrared spectrum of the reaction mixture. This band shifted to  $1570\text{ cm}^{-1}$  upon use of  $^{15}\text{NO}$  (g). The  $\{\text{Co}(\text{NO})_2\}^{10}$  species was identified by its  $\nu_{\text{NO}}$  stretches at  $1809\text{ cm}^{-1}$  and  $1732\text{ cm}^{-1}$ , which shifted to  $1764\text{ cm}^{-1}$  and  $1689\text{ cm}^{-1}$  upon  $^{15}\text{NO}$  isotopic labeling. The persistence of the band at  $1176\text{ cm}^{-1}$  in the  $[\text{Co}(\text{NO}_2)(\text{TC-5,5})]/\text{NO}$  and  $^{15}\text{NO}$  (g) reaction spectra leads us to conclude that  $[\text{Co}(\text{NO}_2)(\text{TC-5,5})]$  is incompletely consumed in the reaction.  $^1\text{H}$  NMR spectroscopic analysis of the reaction mixture revealed peaks corresponding only to the  $[\text{Co}(\text{NO}_2)(\text{TC-5,5})]$  starting material and indicated that consumption of this cobalt(III) nitrite is incomplete in the presence of  $\text{NO}$  (g) (Fig. 5.5).

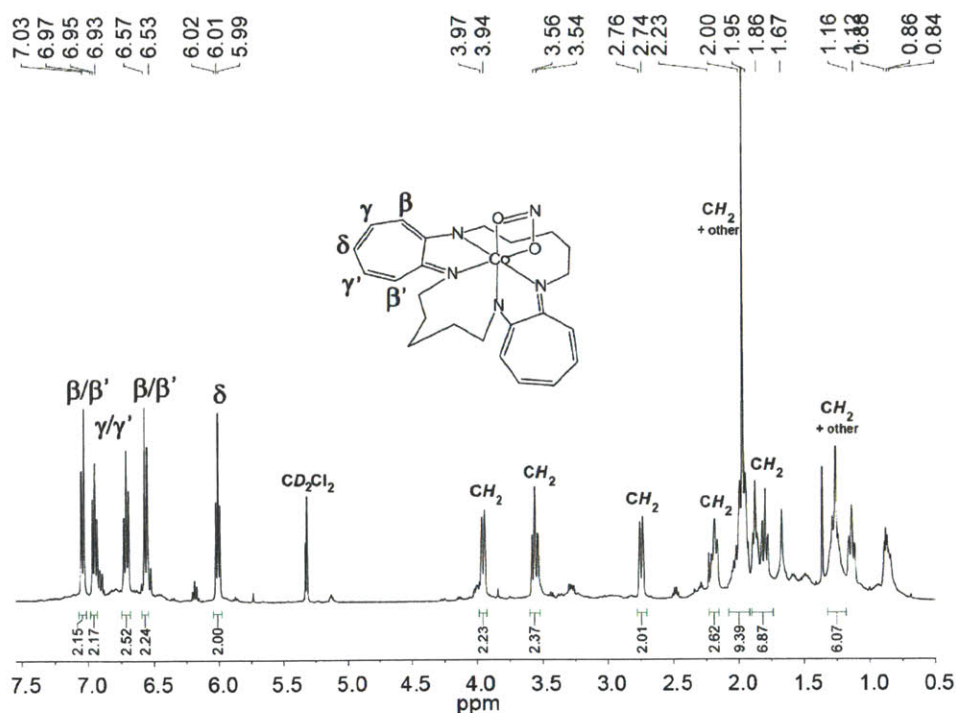


**Figure 5.5.**  $^1\text{H}$  NMR spectrum of the reaction of  $[\text{Co}(\text{NO}_2)(\text{TC-5,5})]$  with  $\text{NO}$  (g).

As for the  $[\text{Co}(\text{NO}_2)(\text{TC-5,5})]/\text{NO}$  reaction, reaction of  $[\text{Co}(\text{NO}_2)(\text{TC-6,6})]$  with  $\text{NO}$  (g) also produced a  $\{\text{Co}(\text{NO})_2\}^{10}$  complex (Fig. 5.6). The  $\nu_{\text{NO}}$  stretching frequencies for the

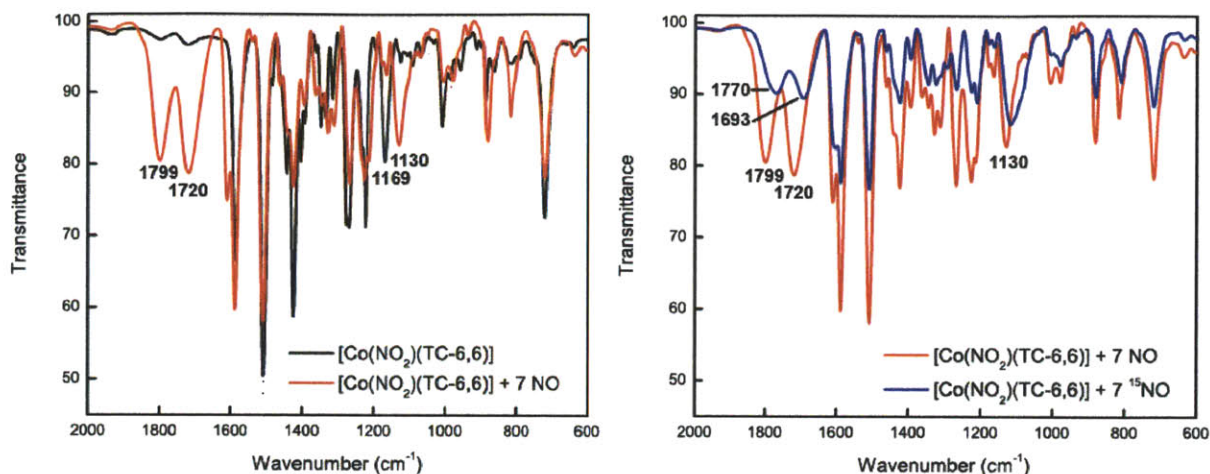


**Figure 5.6.** Infrared spectroscopic comparisons of the reactions of  $[\text{Co}(\text{NO}_2)(\text{TC-6,6})]$  with  $\text{NO}$  (g) (*left*) and  $^{15}\text{NO}$  (g) (*right*). Stretches for  $\nu_{\text{NO}}$  are labeled.

cobalt dinitrosyl product appeared at  $1799\text{ cm}^{-1}$  and  $1720\text{ cm}^{-1}$ . The bands shifted to  $1770\text{ cm}^{-1}$  and  $1693\text{ cm}^{-1}$  when  $^{15}\text{NO}$  was used. Additionally, the band assigned to  $\nu_{\text{NO}}$  of  $\{\text{Co}(\text{NO}_2)\}$  in the  $[\text{Co}(\text{NO}_2)(\text{TC-6,6})]$  starting material shifted from  $1169\text{ cm}^{-1}$  to  $1130\text{ cm}^{-1}$  upon reaction with natural abundance  $\text{NO}$  (g). Analysis of the  $[\text{Co}(\text{NO}_2)(\text{TC-6,6})]/\text{NO}$  reaction mixture by  $^1\text{H}$  NMR spectroscopy revealed a spectrum with peaks corresponding only to the  $[\text{Co}(\text{NO}_2)(\text{TC-6,6})]$  starting material (Fig. 5.7).



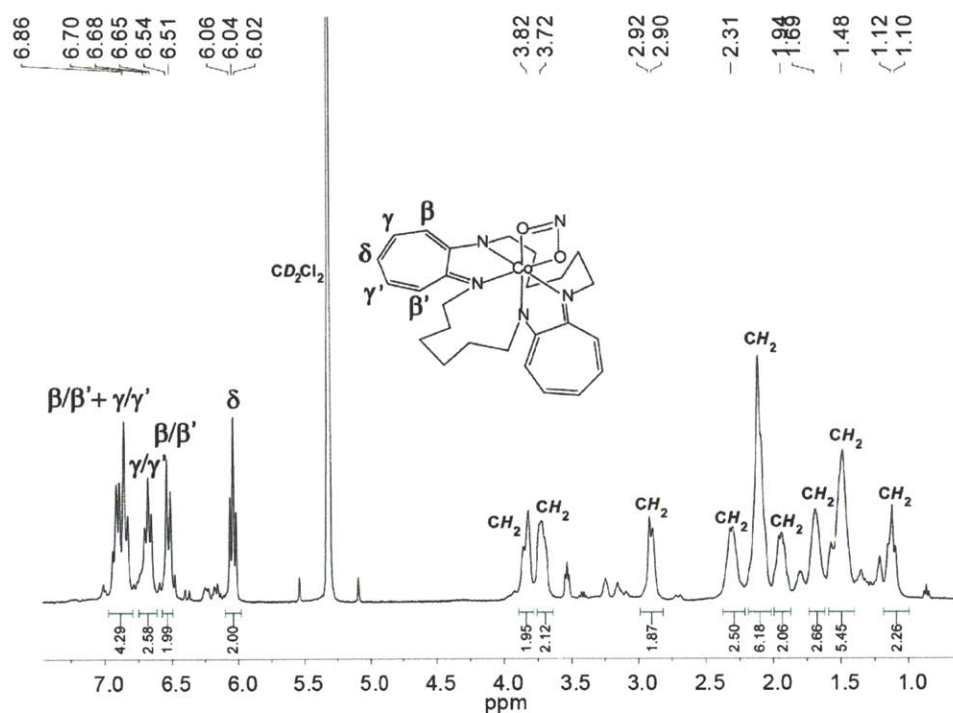


**Figure 5.7.**  $^1\text{H}$  NMR spectrum of the reaction of  $[\text{Co}(\text{NO}_2)(\text{TC-6,6})]$  with  $\text{NO}$  (g).

#### 5.4. Discussion

$[\text{Co}(\text{NO}_2)(\text{TC-}n,n)]$  ( $n = 4, 5, 6$ ) species react with  $\text{NO}$  (g) in a manner that reflects the size of the tropocoronand ring. Exclusive *mononitrosyl* formation occurs for the  $[\text{Co}(\text{NO}_2)(\text{TC-4,4})]$  complex. Both mono- and dinitrosyl adducts formed in the reaction of  $[\text{Co}(\text{NO}_2)(\text{TC-5,5})]$  with  $\text{NO}$  (g), and exposure of  $[\text{Co}(\text{NO}_2)(\text{TC-6,6})]$  to  $\text{NO}$  (g) led to cobalt *dinitrosyl* formation. An increased preference toward *dinitrosyl* formation with increasing tropocoronand ligand size was described in Chapter 4 for the chemistry of cobalt(II) tropocoronands with  $\text{NO}$  (g).  $^{15}\text{NO}$  isotope labeling studies support the assignment of the mono- and dinitrosyl species. Complete conversion of  $[\text{Co}(\text{NO}_2)(\text{TC-4,4})]$  to the nitrosyl product in the presence of  $\text{NO}$  (g) is unique by comparison with the chemistry of  $[\text{Co}(\text{NO}_2)(\text{TC-5,5})]$  and  $[\text{Co}(\text{NO}_2)(\text{TC-6,6})]$ , which showed little reactivity toward nitric oxide. These differences in conversion may be a consequence of

greater steric accessibility of NO to the cobalt(III) center in  $[\text{Co}(\text{NO}_2)(\text{TC-4,4})]$  as compared to that in  $[\text{Co}(\text{NO}_2)(\text{TC-5,5})]$  and  $[\text{Co}(\text{NO}_2)(\text{TC-6,6})]$  (Fig. 5.8).

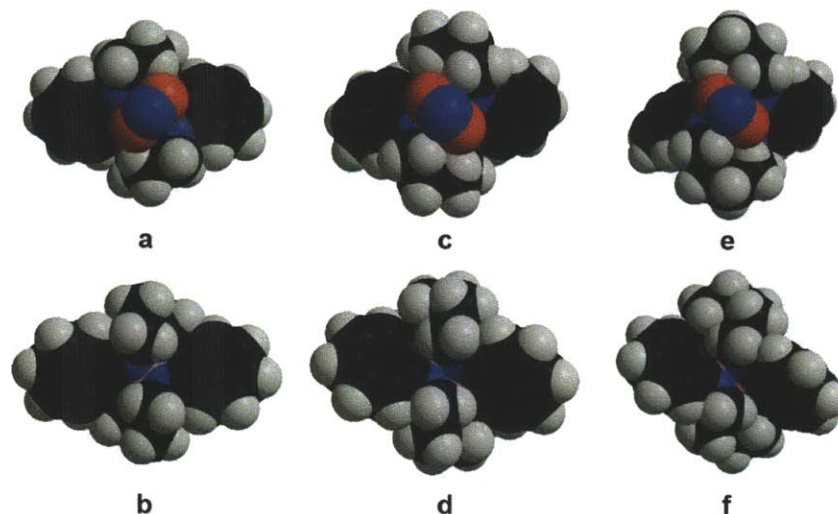


**Figure 5.8.** Space filling models of  $[\text{Co}(\text{NO}_2)(\text{TC-4,4})]$  (*a, b*);  $[\text{Co}(\text{NO}_2)(\text{TC-5,5})]$  (*c, d*); and  $[\text{Co}(\text{NO}_2)(\text{TC-6,6})]$  (*e, f*). The view down the  $\text{Co} - \text{N}_{\text{NO}_2}$  vector is shown in the top row, and the bottom row shows the view up the  $\text{Co} - \text{N}_{\text{NO}_2}$  vector. Access to the cobalt center (*magenta*) is reduced with increasing tropocoronand linker chain length.

A dependence of cobalt(III) tropocoronand reactivity on linker chain length was shown previously for the metal-carbon bond homolysis reactions of the alkyl species  $[\text{CoMe}(\text{TC-3,3})]$  and  $[\text{CoMe}(\text{TC-4,4})]$ .<sup>25</sup> Bond homolysis occurred more than 13 times faster in  $[\text{CoMe}(\text{TC-4,4})]$  than in  $[\text{CoMe}(\text{TC-3,3})]$ , likely due to the greater ring strain in the larger of the two square-pyramidal tropocoronand complexes.<sup>25</sup> A size dependence was also observed in the reactivities of  $[\text{CoEt}(\text{TC-4,4})]$  and  $[\text{CoMe}(\text{TC-4,4})]$  with carbon dioxide. The CO insertion product  $[\text{Co}(\text{COMe})(\text{TC-4,4})]$  formed readily from  $[\text{CoMe}(\text{TC-4,4})]$ , whereas  $[\text{CoEt}(\text{TC-3,3})]$  did not react under similar conditions.<sup>25</sup> The authors attribute this difference in reactivity to the flexibility of  $[\text{TC-4,4}]^{2-}$ , which allows CO to bind the cobalt center *cis* to the coordinated methyl group.<sup>25</sup>

We must note an important aspect of the nitrite-to-nitrosyl interconversion described herein.  $^{15}\text{NO}$  labeling studies indicate that the source of the nitrosyl atoms in the newly formed  $\{\text{CoNO}\}^8$  and  $\{\text{Co}(\text{NO})_2\}^{10}$  complexes must be exogenous  $\text{NO}$  (g), and that nitrite is not directly converted to  $\text{NO}$  in these reactions. Direct conversion of nitrite to nitrosyl would lead to the appearance of bands corresponding to natural abundance  $\{\text{CoNO}\}^8$  and  $\{\text{Co}(\text{NO})_2\}^{10}$  in the infrared spectra of the  $^{15}\text{NO}$  (g) reactions with  $[\text{Co}(\text{NO}_2)(\text{TC-}n,n)]$ . The absence of such natural abundance nitrosyl stretching bands in  $^{15}\text{NO}$  (g) reaction spectra is indicative of exogenous  $\text{NO}$  acting as the nitrosyl source.

Previous reports detailing reactions of cobalt(III) centers with  $\text{NO}$  (g) describe reductive nitrosylation pathways, whereby cobalt(III) reacts with  $\text{NO}$  to form species that are formally  $\{\text{Co}^{\text{III}}\text{-NO}^{\cdot-}\}^8$  adducts.<sup>26-33</sup> An external reductant such as butylamine is sometimes utilized in these reactions.<sup>26-27,30</sup> We hypothesize that in the reductive nitrosylation reactions between  $[\text{Co}(\text{NO}_2)(\text{TC-}n,n)]$  ( $n = 4 - 6$ ) and  $\text{NO}$  (g), nitrite provides electrons for  $\{\text{CoNO}\}^8$  formation and generates  $\cdot\text{NO}_2$  as a byproduct.

We note that the bands assigned to  $\nu_{\text{NO}}$  stretches of  $\{\text{Co}(\text{NO})_2\}^{10}$  species throughout this discussion correspond well with the infrared spectroscopic features of the  $\{\text{Co}(\text{NO})_2\}^{10}$  species  $[\text{Co}_2(\text{NO})_4(\text{TC-}6,6)]$ , crystallographically characterized in Chapter 4 of this thesis. Comparable infrared spectroscopic features are reported for the products of  $[\text{Co}(i\text{-Pr}_2\text{ATI})]$  and  $[\text{Co}(\text{R}^{\text{D}}\text{ATI})]$  reactions with  $\text{NO}$  (g),<sup>34-36</sup> as well as for  $[\text{Co}(\text{NO})_2(\text{Ar-nacnac})]$ , where Ar-nacnac is a bulky  $\beta$ -diketiminato ligand.<sup>37</sup> We conclude from these similarities that the species generated in the reactions of  $[\text{Co}(\text{NO}_2)(\text{TC-}5,5)]$  and  $[\text{Co}(\text{NO}_2)(\text{TC-}6,6)]$  with  $\text{NO}$  (g) are indeed  $\{\text{Co}(\text{NO})_2\}^{10}$  adducts.

## 5.5. Conclusions

We established the tropocoronand ring size-dependent reactivity of  $[\text{Co}(\text{NO}_2)(\text{TC-}n,n)]$  ( $n = 4, 5, 6$ ) with NO (g), analogous to the NO (g) reactivity of  $[\text{Co}(\text{TC-}n,n)]$  ( $n = 4, 5, 6$ ).<sup>12,24</sup> Mononitrosyl formation is favored for the  $[\text{Co}(\text{NO}_2)(\text{TC-}4,4)]/\text{NO}$  reaction, whereas  $[\text{Co}(\text{NO}_2)(\text{TC-}5,5)]$  forms both mono- and dinitrosyl species in the presence of NO (g). Only dinitrosyl formation occurs in the NO chemistry of  $[\text{Co}(\text{NO}_2)(\text{TC-}6,6)]$ . Greater conversion of cobalt(III) nitrite to the cobalt nitrosyl is observed for  $[\text{Co}(\text{NO}_2)(\text{TC-}4,4)]$  relative to  $[\text{Co}(\text{NO}_2)(\text{TC-}5,5)]$  and  $[\text{Co}(\text{NO}_2)(\text{TC-}6,6)]$ . We hypothesize that this dissimilarity arises from differences in the accessibility of the metal site to NO, which is influenced by the steric bulk of the ligand.

## 5.6. References

- (1) Dejam, A.; Hunter, C. J.; Schechter, A. N.; Gladwin, M. T. *Blood Cell. Mol. Dis.* **2004**, *32*, 423-429.
- (2) Gladwin, M. T.; Crawford, J. H.; Patel, R. P. *Free Radical Biol. Med.* **2004**, *36*, 707-717.
- (3) Tota, B.; Quintieri, A. M.; Angelone, T. *Curr. Med. Chem.* **2010**, *17*, 1915-1925.
- (4) Basu, S.; Grubina, R.; Huang, J.; Conradie, J.; Huang, Z.; Jeffers, A.; Jiang, A.; He, X.; Azarov, I.; Seibert, R.; Mehta, A.; Patel, R.; King, S. B.; Hogg, N.; Ghosh, A.; Gladwin, M. T.; Kim-Shapiro, D. B. *Nat. Chem. Biol.* **2007**, *3*, 785-794.
- (5) Gladwin, M. T.; Grubina, R.; Doyle, M. P. *Acc. Chem. Res.* **2008**, *42*, 157-167.
- (6) Gladwin, M. T.; Kim-Shapiro, D. B. *Blood* **2008**, *112*, 2636-2647.
- (7) Jensen, F. B. *BBA Bioenergetics* **2009**, *1787*, 841-848.
- (8) Averill, B. A. *Chem. Rev.* **1996**, *96*, 2951-2964.
- (9) Cutruzzolà, F.; Rinaldo, S.; Castiglione, N.; Giardina, G.; Pecht, I.; Brunori, M. *Bioessays* **2009**, *31*, 885-891.
- (10) Suzuki, S.; Kataoka, K.; Yamaguchi, K. *Acc. Chem. Res.* **2000**, *33*, 728-735.
- (11) Suzuki, S.; Kataoka, K.; Yamaguchi, K.; Inoue, T.; Kai, Y. *Coord. Chem. Rev.* **1999**, *190-192*, 245-265.
- (12) Kozhukh, J.; Lippard, S. J., Manuscript in preparation.
- (13) Enemark, J. H.; Feltham, R. D. *Coord. Chem. Rev.* **1974**, *13*, 339-406.
- (14) Lorković, I. M.; Ford, P. C. *Inorg. Chem.* **2000**, *39*, 632-633.
- (15) Zask, A.; Gonnella, N.; Nakanishi, K.; Turner, C. J.; Imajo, S.; Nozoe, T. *Inorg. Chem.* **1986**, *25*, 3400-3407.



- (16) Imajo, S.; Nakanishi, K.; Roberts, M.; Lippard, S. J.; Nozoe, T. *J. Am. Chem. Soc.* **1983**, *105*, 2071-2073.
- (17) Jaynes, B. S.; Doerrler, L. H.; Liu, S.; Lippard, S. J. *Inorg. Chem.* **1995**, *34*, 5735-5744.
- (18) APEX2, 4.0. Bruker AXS, Inc.: Madison, WI, 2008.
- (19) Sheldrick, G. M. *SADABS: Area-Detector Absorption Correction*, University of Göttingen: Göttingen, Germany, 2001.
- (20) Sheldrick, G. *Acta Crystallogr. Sect. A: Found. Crystallogr.* **2008**, *64*, 112-122.
- (21) Speck, A. L. *PLATON, A Multipurpose Crystallographic Tool*, Utrecht University: Utrecht, The Netherlands, 2001.
- (22) Burnett, M. N.; Johnson, C. K. *ORTEP-III: Oak Ridge Thermal Ellipsoid Plot Program for Crystal Structure Illustrations*, Oak Ridge National Laboratory Report ORNL-6895: 1996.
- (23) Merritt, E. A.; Bacon, D. J. *Methods Enzymol.* **1997**, *277*, 505-524.
- (24) Franz, K. J.; Doerrler, L. H.; Spingler, B.; Lippard, S. J. *Inorg. Chem.* **2001**, *40*, 3774-3780.
- (25) Jaynes, B. S.; Ren, T.; Masschelein, A.; Lippard, S. J. *J. Am. Chem. Soc.* **1993**, *115*, 5589-5599.
- (26) Naito, S. *J. Chem. Soc., Chem. Commun.* **1978**, 175-176.
- (27) Naito, S.; Tamaru, K. *J. Chem. Soc., Faraday Trans.* **1982**, *78*, 735-745.
- (28) Franke, A.; Roncaroli, F.; van Eldik, R. *Eur. J. Inorg. Chem.* **2007**, *2007*, 773-798.
- (29) Cheng, S.-H.; Su, Y. O. *Inorg. Chem.* **1994**, *33*, 5847-5854.
- (30) Dózsa, L.; Pénezeli, P. *React. Kinet. Catal. Lett.* **1995**, *55*, 121-126.
- (31) Pukhovskaya, S.; Guseva, L.; Golubchikov, O. *Russ. Chem. Bull.* **2007**, *56*, 743-747.
- (32) Roncaroli, F.; van Eldik, R. *J. Am. Chem. Soc.* **2006**, *128*, 8042-8053.
- (33) Zhu, X.-Q.; Li, Q.; Hao, W.-F.; Cheng, J.-P. *J. Am. Chem. Soc.* **2002**, *124*, 9887-9893.
- (34) Lim, M. H.; Kuang, C.; Lippard, S. J. *ChemBioChem* **2006**, *7*, 1571-1576.
- (35) Franz, K. J.; Singh, N.; Lippard, S. J. *Angew. Chem. Int. Ed.* **2000**, *39*, 2120-2122.
- (36) Franz, K. J.; Singh, N.; Spingler, B.; Lippard, S. J. *Inorg. Chem.* **2000**, *39*, 4081-4092.
- (37) Tonzetich, Z. J.; Héroguel, F.; Do, L. H.; Lippard, S. J. *Inorg. Chem.* **2011**, *50*, 1570-1579.

## **Chapter 6. Nitric Oxide Reactivity of Cobalt(III)**

Triflate and Cobalt(III) Thiolate Tropocoronand

Complexes

## 6.1. Introduction

The chemistry of nitric oxide with cobalamins (Cbls) isolated in the  $\text{Co}^{2+}$  and  $\text{Co}^{3+}$  states has been explored during studies of the transformations of Cbl-containing enzymes in biology. Nitrosylcobalamin is readily characterized as the product of Cbl(II) exposure to  $\text{NO (g)}$ ,<sup>1-7</sup> but controversy surrounds the  $\text{NO}$  chemistry of the Cbl(III) form.<sup>4-5,7-12</sup> Reductive nitrosylation pathways to form nitrosylcobalamin (Cbl-NO) may be at play, but the reaction course appears to depend heavily on conditions.

Other cobalt(III) species react with  $\text{NO (g)}$  to form cobalt mononitrosyl complexes by reductive nitrosylation. Three water-soluble cobalt(III) porphyrins,  $[\text{Co(P)(H}_2\text{O)}_2]$ , each consumed 2 equiv of  $\text{NO (g)}$  to form  $[\text{Co(P)(NO)(H}_2\text{O)}]$  complexes.<sup>13</sup> Cobalt(III) alkyldiamines exposed to  $\text{NO (g)}$  react through a putative cobalt mononitrosyl intermediate to disproportionate  $\text{NO}$  to  $\text{N}_2\text{O}$  and  $\text{N}_2$ .<sup>14-16</sup> Glutathionylcobalamin forms Cbl-NO and glutathionyl disulfide, GSSG, in the presence of nitric oxide.<sup>17</sup> The mechanism of this conversion is unreported, but is almost certainly mediated by the readily accessible radical character of the glutathionyl substituent.

The structural relationship between tetraazamacrocyclic tropocoronands and the cobalamin scaffold, as well as the varied reactivity of Cbl(III) complexes with  $\text{NO (g)}$ , inspired us to examine the  $\text{NO}$  chemistry of cobalt(III) tropocoronands. Specifically, we examined the behavior of  $[\text{Co(TC-4,4)}]^+$  and  $[\text{Co(SC}_6\text{F}_5\text{)(TC-4,4)}]$  in order to compare the results with those of Cbl(III) analogs.

## 6.2. Experimental Methods

**General Considerations.** Reactants and reagents were handled as described in previous chapters of this thesis. Handling of air- and moisture-sensitive materials was conducted in an MBraun

glovebox under an inert nitrogen atmosphere. Reagents were used as purchased, without further purification, with the exception of nitric oxide, which was purified as follows. Nitric oxide was obtained from Airgas and purified according to published methods.<sup>18</sup> The NO was passed through an Ascarite column and a 6 ft coil containing silica gel at -78 °C to remove impurities and was collected and stored under an inert atmosphere in a gas storage bulb. <sup>15</sup>NO was purchased from Cambridge Isotope Laboratories and purified similarly. All gas transfers were performed using gas-tight syringes under inert nitrogen atmosphere. Acetonitrile and methylene chloride were purified by passage through activated alumina and stored over 4 Å molecular sieves under an inert nitrogen atmosphere prior to use. Deuterated NMR solvents were obtained from Cambridge Isotope Laboratories and used without further purification. Acetonitrile-*d*<sub>3</sub>, methylene chloride-*d*<sub>2</sub>, and 2-methyltetrahydrofuran (2-MeTHF) were brought into the glovebox and stored over 4 Å molecular sieves under inert nitrogen atmosphere. Tropicoronand species H<sub>2</sub>TC-4,4,<sup>19-20</sup> [Co(TC-4,4)],<sup>21</sup> [Co(SC<sub>6</sub>F<sub>5</sub>)(TC-4,4)],<sup>22</sup> and [Co(NO)(TC-4,4)],<sup>22</sup> and the substituted tropolones,<sup>23-25</sup> were prepared according to published procedures. Spectroscopic properties of these compounds matched those reported previously. CHN analyses were performed by Intertek-QTI (Whitehouse, NJ, USA) and Midwest Microlab, LLC (Indianapolis, IN, USA).

**Synthesis of [Co(TC-4,4)](OTf).** To a solution of [Co(TC-4,4)] (230 mg, 567 μmol) in methylene chloride was added AgOTf (146 mg, 567 μmol) in the dark. The reaction was left to stir overnight, resulting in a color change to deep pink and the formation of a precipitate. The solution was filtered through Celite and the precipitate was washed with methylene chloride. The filtrate was collected and the solvent was removed in vacuo. Recrystallization from DCM/Et<sub>2</sub>O at -30 °C yielded X-ray quality crystals (268 mg, 85.2 % yield). UV-Vis (MeCN) λ (ε) 210

(24625), 277 (44115), 363 (21051), 429 (15422), 548 (6980), 794 (5282); IR (KBr)  $\nu_{\text{CN}}$  1580  $\text{cm}^{-1}$ ; Anal. Calc'd. for  $[\text{Co}(\text{TC-4,4})](\text{OTf}) \cdot 0.21 \text{CH}_2\text{Cl}_2$ : C, 48.71; H, 4.65; N, 9.79. Observed: C, 48.75; H, 4.81; N, 9.56. The presence of residual methylene chloride was confirmed by the  $^1\text{H}$  NMR spectrum and the quantity used for the computed elemental composition was adjusted for the best fit to the results.

**Synthesis of  $\text{H}_2\text{TC-4,4}^{2\text{Br}}$ .** To 8 mL of a stirring methylene chloride solution of  $\text{H}_2\text{TC-4,4}$  (300 mg, 0.861 mmol) on dry ice/acetone was added  $\text{Br}_2$  (97  $\mu\text{L}$ , 1.89 mmol) in 1 mL  $\text{CH}_2\text{Cl}_2$  dropwise. The solution was allowed to stir for 30 min, after which time the cooling bath was removed and the reaction was allowed to proceed at room temperature for 1 h. The suspension was then washed with 2 M NaOH, dried ( $\text{MgSO}_4$ ), and evaporated to dryness. The crude material was purified using basic  $\text{Al}_2\text{O}_3$  chromatography (2:1 hexanes:  $\text{CH}_2\text{Cl}_2$ ) and the product was isolated as an orange solid (0.28 g, 64%). X-ray quality crystals were obtained by slow evaporation of  $\text{CDCl}_3$ .  $^1\text{H}$  NMR ( $\text{CD}_2\text{Cl}_2$ )  $\delta$  1.98 (m, 4H,  $\text{CH}_2$ ), 3.30 (m, 4H,  $\text{CH}_2$ ), 6.08 (d, 4H, Ar- $H_\alpha$ ), 7.04 (d, 4H, Ar- $H_\beta$ ), 8.07 (bs, 2H, NH); ESI-MS  $[\text{M}+\text{H}]^+$   $m/z$  507.0 (Calc'd 507.0).

**Synthesis of  $[\text{Co}(\text{TC-4,4}^{2\text{Br}})]$ .** To a solution of  $\text{H}_2\text{TC-4,4}^{2\text{Br}}$  (55 mg, 0.11 mmol) in THF was added NaHMDS (44 mg, 0.24 mmol) and the deprotonation reaction was left to stir for 30 min.  $\text{CoCl}_2$  (17 mg, 0.13 mmol) was added to the reaction as a solid and the reaction was allowed to stir overnight. The mixture was concentrated to dryness, the solid was suspended in methylene chloride, and the suspension was filtered through Celite. The filtrate was concentrated to dryness in vacuo.  $[\text{Co}(\text{TC-4,4}^{2\text{Br}})]$  was isolated in 24% yield (15 mg). The poor solubility of  $[\text{Co}(\text{TC-4,4}^{2\text{Br}})]$  in organic solvents may account for the low isolated yield. X-ray quality crystals were grown from  $\text{CH}_2\text{Cl}_2$ /pentane. EPR (2-MeTHF, 77 K)  $g = 2.09, 2.64$ ; Anal. Calc'd. for  $[\text{Co}(\text{TC-4,4}^{2\text{Br}})] \cdot 0.15 \text{C}_5\text{H}_{12}$ : C, 47.62; H, 4.54; N, 9.75. Observed: C, 47.73; H, 4.14; N, 9.62.

**Physical Measurements.**  $^1\text{H}$ ,  $^{13}\text{C}$ , and  $^{19}\text{F}$  NMR spectra were collected on a 400 MHz Bruker Avance spectrometer. Optical spectra were recorded with a Varian Cary 50 Bio UV-Visible Spectrophotometer in 6SQ Starna cells. Solutions were prepared under nitrogen and spectra were recorded at 25 °C. Cary WinUV Scanning Kinetics software was used to record optical timecourse spectra. FT-IR spectra were recorded on a Thermo Nicolet Avatar 360 spectrometer running the OMNIC software package. A  $\text{CaF}_2$  cell was utilized for solution IR spectra. ESI-MS analyses were performed on the Agilent 1100 Series LC/MSD Trap spectrometer. An Agilent Technologies 5975C Mass Selective Detector running in electron impact ionization mode was used for EI-MS studies of reaction headspace. Samples were analyzed on a helium gas matrix. EPR samples were prepared in 2-MeTHF under inert nitrogen atmosphere. EPR spectra were recorded at 77 K on a Bruker EMX spectrometer with an ER 4199HS cavity and Gunn diode microwave source which produces X-band radiation. The EPR spectrometer is controlled by the Bruker Win-EPR software package.

#### **Reactivity Studies with Nitric Oxide.**

*Reaction between [Co(TC-4,4)](OTf) and NO (g).* To the headspace of a solution of [Co(TC-4,4)](OTf) (50 mg, 0.09 mmol) in  $\text{CD}_2\text{Cl}_2$  was added NO (g) (2.2 mL, 0.09 mmol) by gas-tight syringe. The reaction was left to stir 30 min, after which time an aliquot of the reaction mixture was removed and analyzed by solution infrared spectroscopy. Nitric oxide (2.2 mL, 0.09 mmol) was injected into the reaction headspace to achieve a total stoichiometry of 2 equiv with respect to [Co(TC-4,4)](OTf) and the solution was again analyzed by infrared spectroscopy after 30 min. NO (g) addition and infrared spectroscopic analysis were repeated with 4 equiv and 6 equiv NO (g) relative to [Co(TC-4,4)](OTf) in solution. After addition of 6 equiv and 30 min of reaction time, the solution was also analyzed by  $^1\text{H}$  NMR spectroscopy.

*Reaction of [Co(TC-4,4)](OTf) with NO (g) and Proton Sponge with and without 1,2-Dimethoxybenzene.* A solution of [Co(TC-4,4)](OTf) (50 mg, 0.09 mmol), 1,2-dimethoxybenzene (28 mg, 0.20 mmol), and *N,N,N',N'*-tetramethyl-1,8-naphthalenediamine, also called proton sponge, (22 mg, 0.10 mmol) was prepared in CD<sub>3</sub>CN and capped with a septum. A portion of NO (g) (9 mL, 0.36 mmol) was injected into the reaction headspace by gas-tight syringe. The reaction was allowed to stir 1 h, placed briefly under vacuum to remove unreacted NO (g), and filtered to remove a precipitate that had formed. The resultant filtrate was analyzed by <sup>1</sup>H NMR spectroscopy. The experiment was repeated in an analogous manner without the 1,2-dimethoxybenzene.

*Titration of Proton Sponge into Solutions of [Co(TC-4,4)](OTf) and NO (g).* To solutions of [Co(TC-4,4)](OTf) (10 mg, 0.018 mmol) in CD<sub>2</sub>Cl<sub>2</sub> was added proton sponge (4, 8, 12, or 40 mg, corresponding to 0.018 mmol, 0.036 mmol, 0.048 mmol, 0.18 mmol). Hexamethylbenzene (0.002 mmol) was added as a standard. The reaction vials were capped with septa, and NO (g) (1.8 mL, 4 equiv) was injected into the headspaces of the reaction solutions. The reactions were left for 1 h, exposed briefly to vacuum to remove unreacted NO (g), and analyzed by <sup>1</sup>H NMR spectroscopy.

*Reaction of [Co(TC-4,4)](OTf) with NO (g) and Cs<sub>2</sub>CO<sub>3</sub>.* [Co(TC-4,4)](OTf) (50 mg, 0.09 mmol) and cesium carbonate (294 mg, 0.9 mmol) were combined in acetonitrile in a septum-capped vial. Headspace gas (~10 mL) was removed by gas-tight syringe, and NO (g) (9 mL, 0.36 mmol) was injected into the headspace of the reaction mixture. The reaction was concentrated to dryness after 1 h and the residue was suspended in CD<sub>2</sub>Cl<sub>2</sub>, filtered through Celite, and analyzed by <sup>1</sup>H NMR spectroscopy.

*[Co(NO)(TC-4,4)] Spiking Study.* Three solutions of [Co(TC-4,4)](OTf) (50 mg, 0.09 mmol) and proton sponge (19 mg, 0.09 mmol) were prepared in CD<sub>2</sub>Cl<sub>2</sub>. To one solution was added independently prepared [Co(NO)(TC-4,4)] (20 mg, 0.046 mmol). The vials were capped with septa and NO (g) (9 mL, 0.36 mmol) was injected into the headspace of each reaction. After 1 h, the headspace of the reactions was exposed briefly to vacuum to remove unreacted NO (g). [Co(NO)(TC-4,4)] (20 mg, 0.046 mmol) was added to another solution. The remaining solution, without [Co(NO)(TC-4,4)], was used as a control experiment. All three reaction mixtures were analyzed by <sup>1</sup>H NMR spectroscopy to test for [Co(NO)(TC-4,4)] formed in the reaction.

*Titration of Nitric Oxide into Solutions of [Co(TC-4,4)](OTf) and Proton Sponge.* Solutions of [Co(TC-4,4)](OTf) (10 mg, 0.018 mmol) and proton sponge (3.9 mg, 0.018 mmol) were prepared in methylene chloride. A portion of NO (g) (0.5 mL, 1 mL, or 2 mL, corresponding to 0.018 mmol, 0.036 mmol, or 0.072 mmol) was injected into the reaction headspace and the reactions were left to stir. The solutions were concentrated to dryness in vacuo after 35 min and analyzed by <sup>1</sup>H NMR spectroscopy with a hexamethylbenzene standard.

*Ligand Recovery Experiment for the Reaction of [Co(TC-4,4)](OTf) with NO (g) and Proton Sponge.* A solution of [Co(TC-4,4)](OTf) (10 mg, 0.018 mmol) and proton sponge (4 mg, 0.018 mmol) in acetonitrile was exposed to NO (g) (2 mL, 0.072 mmol) for 2 h. The reaction was removed from the glove box and acidified with conc. HCl. An aliquot was diluted with acetonitrile and analyzed by ESI-MS. Ligand substitution was not observed by mass spectrometry. Mass spectrometric peaks were only observed for salts of unsubstituted H<sub>2</sub>TC-4,4.

*COSY NMR Spectroscopic Study of the Reaction of [Co(SC<sub>6</sub>F<sub>5</sub>)(TC-4,4)] with NO (g).* To the headspace of a solution of [Co(SC<sub>6</sub>F<sub>5</sub>)(TC-4,4)] (50 mg, 0.083 mmol) in methylene chloride was added NO (g) (2 mL, 0.083 mmol) and the reaction was allowed to stir for 50 min. The



mixture was concentrated to dryness, after which the solid was washed with pentane and dried in vacuo. The residue was suspended in  $CD_2Cl_2$ , filtered, and analyzed by NMR spectroscopy.

*NMR Spectroscopic Timecourse Study of a Small Scale Reaction of [Co(SC<sub>6</sub>F<sub>5</sub>)(TC-4,4)] with NO (g).* [Co(SC<sub>6</sub>F<sub>5</sub>)(TC-4,4)] was prepared by previously reported methods and recrystallized from fluorobenzene. Approximately 10 mg (~ 0.02 mmol) of the cobalt(III) thiolate complex was placed into an NMR tube and the spectrum was recorded in  $CD_2Cl_2$ . The NMR tube containing the sample was cycled into the glove box and NO (g) (1 mL, 0.06 mmol) was injected through a septum cap. The sample was shaken vigorously and analyzed by <sup>1</sup>H and <sup>19</sup>F NMR spectroscopy after 10 min. The sample was similarly analyzed again the following day.

**EI-MS Studies.** EI-MS experiments were performed in a custom made gas-tight double-chamber cell, in which the two chambers can be connected by opening a joint. The volume of each chamber was determined by filling with water and weighing the water. All manipulations were performed under inert nitrogen atmosphere. The atmosphere of the whole cell was pumped down under vacuum for 1 h. After pumping, the cell was closed off from the vacuum and nitric oxide was injected. The amount of NO in each chamber was 4.5 equiv relative to the cobalt complex employed. One NO-containing chamber was sealed off, and the other chamber was evacuated and refilled with N<sub>2</sub> to remove remaining nitric oxide. This evacuation/refill procedure was repeated three times. [Co(TC-4,4)](OTf) (50 mg, 0.09 mmol) was placed into the empty chamber in ~4 mL acetonitrile, the chamber was sealed, and the cell was connected to the instrument for analysis. The solution headspace was analyzed for NO<sub>2</sub> and N<sub>2</sub>O and the cell was sealed off from the instrument. The joint between the two chambers was opened and the complex was allowed to react with NO for 1 h. The NO chamber was sealed, and the reaction headspace was analyzed. A control experiment was performed to ensure that the N<sub>2</sub>O detected in the reaction was not a

contaminant in the nitric oxide. For the control experiment, the cell was prepared as above, with the exception that the chamber containing acetonitrile was lacking [Co(TC-4,4)](OTf). The control sample was analyzed in a manner similar to that employed for the cobalt complex, using the procedure described here.

**X-ray Crystallography.** Crystals were mounted in Paratone N oil and frozen at 100 K under a cold nitrogen stream controlled by a Cryopad low-temperature apparatus. Data were collected on a Bruker APEX CCD X-ray diffractometer with graphite-monochromated Mo- $K_{\alpha}$  radiation ( $\lambda = 0.71073 \text{ \AA}$ ) controlled by the APEX2 software package.<sup>26</sup> Empirical absorption correction was performed with SADABS.<sup>27</sup> The structure was solved by direct methods using SHELXS-97 and refined by full-matrix least-squares on  $F^2$  using the SHELXL-97 program incorporated into the SHELXTL software package.<sup>28</sup> Possible higher symmetries were evaluated by PLATON.<sup>29</sup> Non-hydrogen atoms were located and their positions refined anisotropically. Hydrogen atoms were assigned idealized positions and given thermal parameters either 1.2 (non-methyl hydrogen atoms) or 1.5 (methyl hydrogen atoms) times the thermal parameters of the atoms to which they are attached. Thermal ellipsoid plots were generated using ORTEP-III.<sup>30</sup>

**Theoretical Calculations.** Theoretical calculations were performed in Gaussian 03,<sup>31</sup> using the B3LYP<sup>32-34</sup> functional and 6-311+G(d,p)<sup>35-36</sup> basis set over all atoms. Molecular orbitals were visualized using VMD software, version 1.8.7.<sup>37</sup>

### 6.3. Results and Discussion

We began our studies of the chemistry of cobalt(III) tropocoronands with a preliminary examination of the chemistry of cobalt(III) species bound only by the tropocoronand ligand. In particular, we investigated the reactivity of [Co(TC-4,4)](OTf) with nitric oxide. We then

extended our work to include a redox-active thiolate ligand bound to cobalt. We prepared [Co(TC-4,4)](OTf) from [Co(TC-4,4)] and silver triflate. Structural characterization revealed that the triflate anion is not coordinated to the cobalt center (Fig. 6.1, Tables 6.1 – 6.2).



**Figure 6.1.** Thermal ellipsoid plot for [Co(TC-4,4)](OTf) depicting 50% probability. Hydrogen atoms are omitted for clarity.

**Table 6.1.** Summary of crystallographic parameters for [Co(TC-4,4)](OTf).

<b>Empirical formula</b>	C <sub>23</sub> H <sub>26</sub> CoF <sub>3</sub> N <sub>4</sub> O <sub>3</sub> S
<b>Formula weight</b>	554.47
<b>Crystal system</b>	Triclinic
<b>Space group</b>	<i>P</i> 1̄
<b>a (Å)</b>	8.2000(16)
<b>b (Å)</b>	9.6700(19)
<b>c (Å)</b>	15.050(3)
<b>α (deg)</b>	105.56(3)
<b>β (deg)</b>	91.92(3)
<b>γ (deg)</b>	96.23(3)
<b>V (Å<sup>3</sup>)</b>	1140.4(4)
<b>Z</b>	2
<b>ρ<sub>calc</sub> (g/cm<sup>3</sup>)</b>	1.615
<b>Temperature (K)</b>	100 (2)
<b>μ (Mo Kα), (mm<sup>-1</sup>)</b>	0.904
<b>θ range (deg)</b>	1.41 to 29.13
<b>Crystal size (mm<sup>3</sup>)</b>	0.40 x 0.10 x 0.03
<b>Completeness to θ (%)</b>	98.9
<b>Max, min peaks (e/Å<sup>3</sup>)</b>	0.688 and -0.296
<b>Goodness-of-fit<sup>a</sup></b>	1.043
<b>Total no. of data</b>	23909
<b>No. unique data</b>	6075
<b>R<sub>1</sub> (%)<sup>b</sup></b>	3.54
<b>wR<sub>2</sub> (%)<sup>c</sup></b>	8.87

<sup>a</sup>GOF =  $[\sum w(F_o^2 - F_c^2)^2 / (n - p)]^{1/2}$  where *n* is the number of data and *p* is the number of refined parameters.

<sup>b</sup> $R_1 = \sum ||F_o| - |F_c|| / \sum |F_o|$

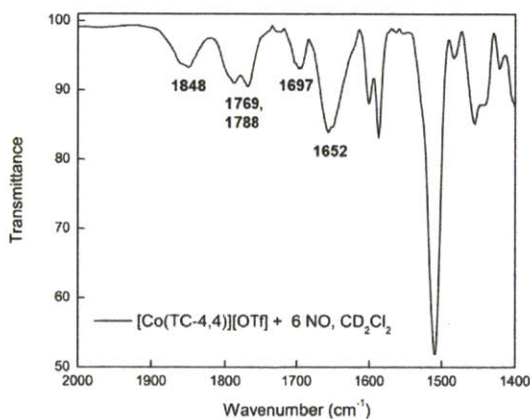
<sup>c</sup> $wR_2 = \{\sum [w(F_o^2 - F_c^2)^2] / \sum [w(F_o^2)^2]\}^{1/2}$

**Table 6.2.** Summary of bond lengths (Å) and angles (deg) of interest for [Co(TC-4,4)](OTf).

Co(1)-N(1)	1.8568(16)	N(1)-Co(1)-N(3)	151.31(7)
Co(1)-N(2)	1.8852(15)	N(1)-Co(1)-N(2)	84.20(7)
Co(1)-N(3)	1.8603(16)	N(3)-Co(1)-N(2)	101.80(7)
Co(1)-N(4)	1.8869(15)	N(1)-Co(1)-N(4)	101.31(7)
		N(3)-Co(1)-N(4)	84.28(7)
		N(2)-Co(1)-N(4)	156.71(7)

The coordination environment at cobalt is similar to that in previously reported cobalt(III) tropocoronands.<sup>38</sup> The twist angle at the metal center is 39°, falling into the reported range for known [Co(TC-4,4)]<sup>+</sup> complexes.<sup>38</sup> We assign a band at 1580 cm<sup>-1</sup> in the infrared spectrum of [Co(TC-4,4)](OTf) to C=C stretches of the aminotroponimine rings. Neither a room temperature <sup>1</sup>H NMR spectrum nor a liquid nitrogen temperature EPR spectrum could be recorded for the cobalt(III) complex, suggesting a probable *S* = 1 electronic configuration at the metal center, in agreement with results for previously reported [Co(TC-4,4)]<sup>+</sup> complexes.<sup>38</sup>

With [Co(TC-4,4)](OTf) in hand, we next investigated its reaction with nitric oxide. Addition of excess NO (g) to the headspace of a methylene chloride solution of [Co(TC-4,4)](OTf) led to the appearance of infrared spectral bands at 1650 cm<sup>-1</sup>, 1697 cm<sup>-1</sup>, 1769 cm<sup>-1</sup>, 1788 cm<sup>-1</sup>, and 1848 cm<sup>-1</sup> (Fig. 6.2).

**Figure 6.2.** Solution infrared spectrum of the reaction between [Co(TC-4,4)](OTf) and 6 equiv of NO (g), recorded in CD<sub>2</sub>Cl<sub>2</sub>.

Previously reported reactIR studies of the reaction of NO with [Co(TC-4,4)] revealed the appearance of a band at  $1640\text{ cm}^{-1}$  that was attributed to the nitrosyl stretch of a {Co(NO)(NO<sub>2</sub>)} species.<sup>22</sup> The band at  $1650\text{ cm}^{-1}$  in the present study may arise from a similar species. The bands appearing at  $1697\text{ cm}^{-1}$ ,  $1769\text{ cm}^{-1}$ ,  $1788\text{ cm}^{-1}$ , and  $1848\text{ cm}^{-1}$  may correspond to nitrosyl stretches of {Co(NO)<sub>2</sub>}<sup>10</sup> species, a hypothesis derived from comparison with the spectral bands of the neutral {Co(NO)<sub>2</sub>}<sup>10</sup> adduct that forms upon exposure of [Co(TC-6,6)] to NO (g), described in Chapter 4 of this thesis. The <sup>1</sup>H NMR spectrum of the reaction mixture after addition of 6 equiv NO similarly revealed the presence of multiple products (Fig. 6.3).

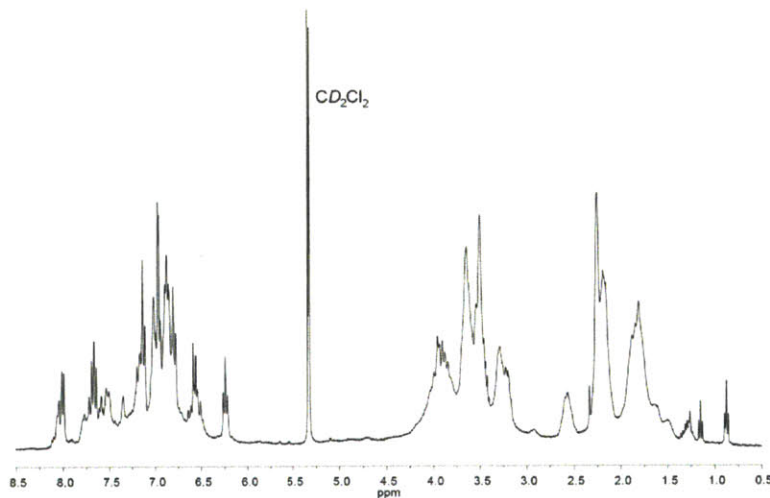


**Figure 6.3.** <sup>1</sup>H NMR spectrum of the reaction of [Co(TC-4,4)](OTf) with 6 equiv NO (g), recorded in CD<sub>2</sub>Cl<sub>2</sub>.

Previous reports describe reactions of cobalt(III) complexes with NO (g) that result in formation of {CoNO}<sup>8</sup> species, a reductive nitrosylation process that concomitantly generates N<sub>2</sub>O.<sup>13-16</sup> EI-MS studies of the headspace of the reaction between [Co(TC-4,4)](OTf) and NO (g) confirmed the presence of N<sub>2</sub>O (Fig. 6.4).

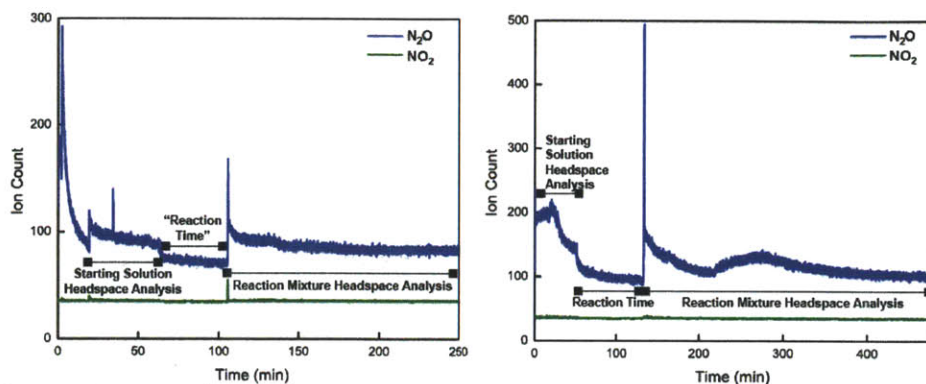
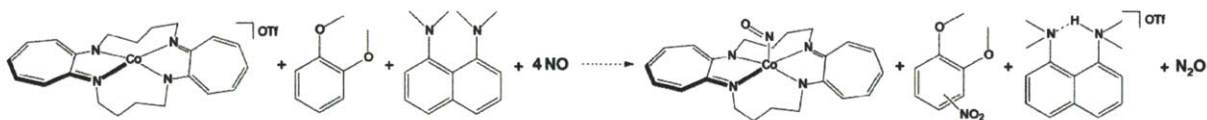


**Figure 6.4.** EI-MS control experiment: analysis of NO (g) (*left*). The headspace of the reaction of [Co(TC-4,4)](OTf) with NO (g) was analyzed by EI-MS, and N<sub>2</sub>O was observed (*right*).

One possible scheme for the reaction between [Co(TC-4,4)](OTf) and NO (g) is described in equation 6.1.



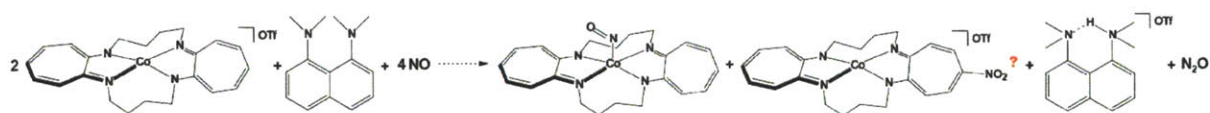
The formation of [Co(NO)(TC-4,4)] is expected from previously reported reactivity studies of cobalt(III) species with nitric oxide,<sup>13-16</sup> and the generation of N<sub>2</sub>O has been demonstrated. We were unable to observe a cobalt mononitrosyl by <sup>1</sup>H NMR spectroscopy, however, and considered its decomposition in the presence of reactive nitrogen and oxygen species such as NO<sub>2</sub><sup>+</sup> to be a possible cause. We attempted to trap the RNOS by reaction with an electron rich aromatic species, choosing 1,2-dimethoxybenzene for this purpose. We carried out the [Co(TC-4,4)](OTf)/NO reaction in the presence of the aromatic nucleophile, as well as a base to quench protons that would be released upon nucleophilic aromatic substitution (Scheme 6.1).



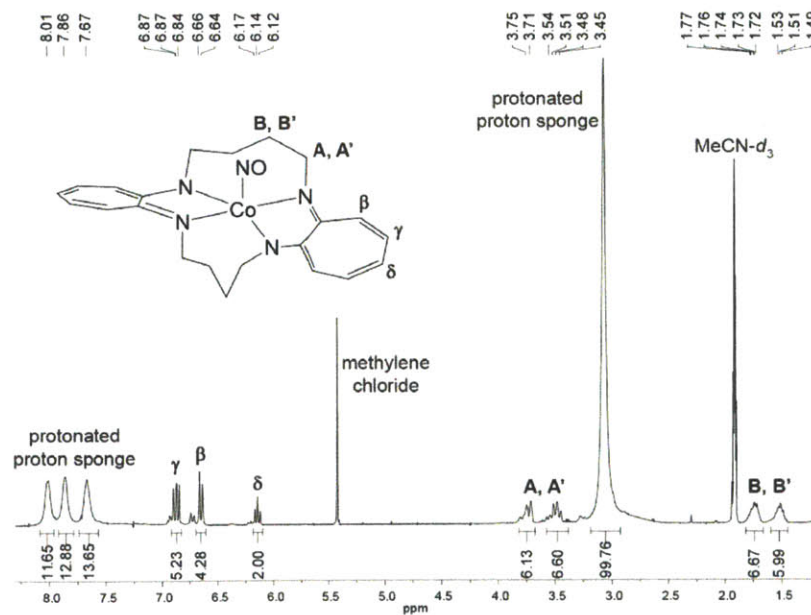
**Scheme 6.1.** The [Co(TC-4,4)](OTf)/NO reaction was carried out in the presence of 1,2-dimethoxybenzene and proton sponge, with the intention of trapping RNOS and characterizing the [Co(NO)(TC-4,4)] reaction product spectroscopically.



$^1\text{H}$  NMR spectroscopic analysis of the reaction mixture revealed that 1,2-dimethoxybenzene is unreactive toward any RNOS that may have formed. We also discovered that proton sponge becomes protonated in the reaction. Slow evaporation of the reaction mixture resulted in the formation of colorless crystals, confirmed to be the triflate salt of protonated proton sponge by X-ray crystallography. Formation of  $[\text{Co}(\text{NO})(\text{TC-4,4})]$  was evident by  $^1\text{H}$  NMR spectroscopy. The reaction was repeated in the absence of 1,2-dimethoxybenzene (Scheme 6.2) and protonation of the proton sponge was similarly observed (Fig. 6.5). Precipitation of a brown solid occurred during the reaction and most likely accounts for the low integration values of  $[\text{Co}(\text{NO})(\text{TC-4,4})]$  peaks relative to those for the protonated base.

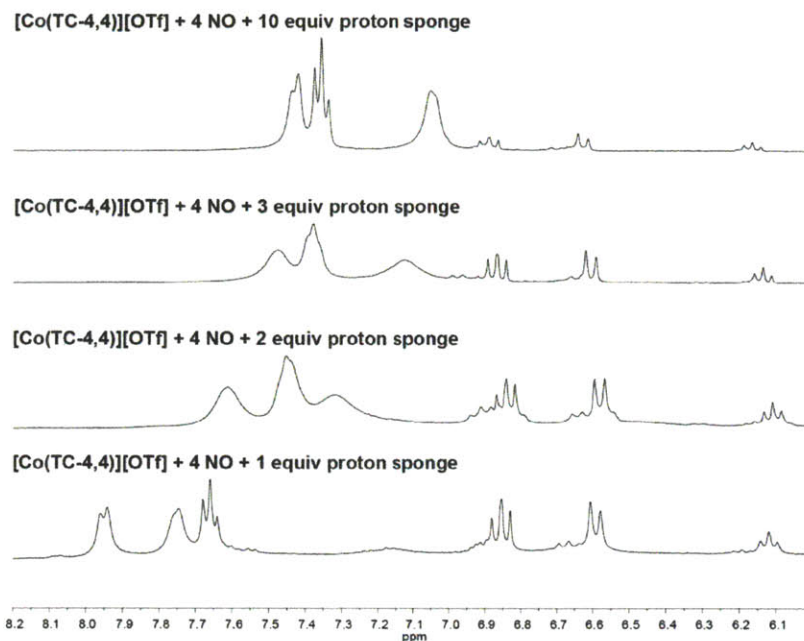


**Scheme 6.2.** The  $[\text{Co}(\text{TC-4,4})](\text{OTf})/\text{NO}$  reaction, in the presence of proton sponge.



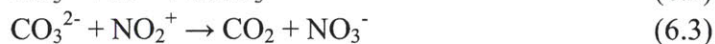
**Figure 6.5.** Reaction of  $[\text{Co}(\text{TC-4,4})](\text{OTf})$  and 4 NO (g) in the presence of 1 equiv of proton sponge. Peaks corresponding to the formation of  $[\text{Co}(\text{NO})(\text{TC-4,4})]$  are readily identified. Recorded in  $\text{CD}_3\text{CN}$ .

Titration of proton sponge into [Co(TC-4,4)](OTf)/NO reaction mixtures revealed that 1 equiv of the former is consumed per equivalent of the cobalt complex in solution (Fig. 6.6).



**Figure 6.6.** Titration of proton sponge into [Co(TC-4,4)](OTf)/NO reaction mixtures and analysis by  $^1\text{H}$  NMR spectroscopy. Peaks corresponding to unprotonated proton sponge appear in increasing intensity with addition of increasing amounts of base. The stoichiometry appears to be 1 equiv proton sponge: 1 equiv [Co(TC-4,4)](OTf) consumed in the reaction with NO (g).

The use of cesium carbonate instead of basic proton sponge enabled us to stabilize [Co(NO)(TC-4,4)] in the reaction mixture (Fig. 6.7). Introduction of carbonate as a base was intended to facilitate isolation of [Co(NO)(TC-4,4)] from reaction mixtures. The quenching of reactive species by carbonate would promote to the formation of organic-insoluble salts and readily removable gases (eq 6.2 – 6.3),<sup>39</sup> rather than species with excellent solubility in organic solvents, as is the case for protonated proton sponge. We did not attempt to isolate the cobalt mononitrosyl from [Co(TC-4,4)](OTf)/NO reaction mixtures.





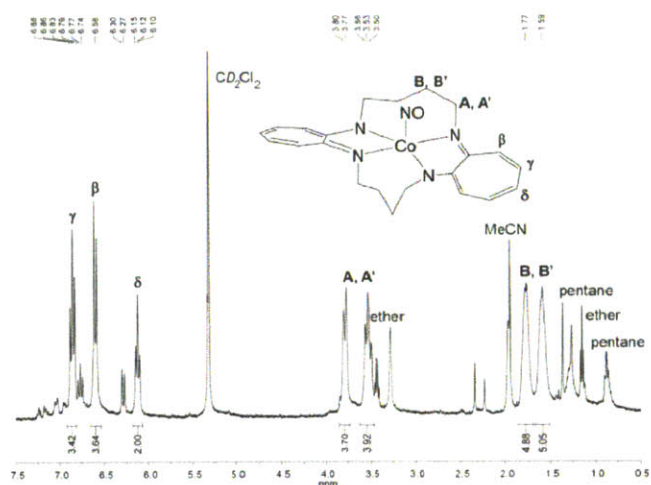


**Figure 6.7.**  $^1\text{H}$  NMR spectrum of the reaction between  $[\text{Co}(\text{TC-4,4})](\text{OTf})$  and NO in the presence of  $\text{Cs}_2\text{CO}_3$ .

A spiking study was performed to confirm that  $[\text{Co}(\text{NO})(\text{TC-4,4})]$  forms during the reaction of  $[\text{Co}(\text{TC-4,4})](\text{OTf})$  with NO (Fig. 6.8).  $^1\text{H}$  NMR spectral peaks in an independently prepared sample of  $[\text{Co}(\text{NO})(\text{TC-4,4})]$  overlap those of  $[\text{Co}(\text{NO})(\text{TC-4,4})]$  formed in the reaction mixture. Additionally, the study indicates that  $[\text{Co}(\text{NO})(\text{TC-4,4})]$  is stable to the reaction conditions, supporting the assignment that a cobalt mononitrosyl forms as a reaction product.

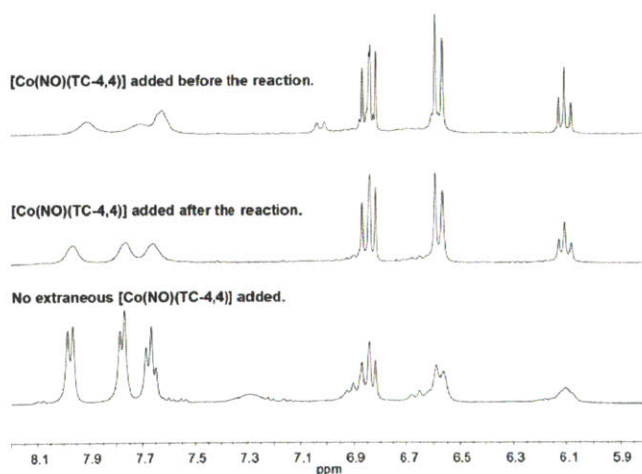


**Figure 6.8.**  $[\text{Co}(\text{NO})(\text{TC-4,4})]$  spiking experiment, examined by  $^1\text{H}$  NMR spectroscopy. Spectra are shown for the  $[\text{Co}(\text{TC-4,4})](\text{OTf})/\text{NO}/\text{proton sponge}$  reaction mixture (*bottom*), the reaction mixture with  $[\text{Co}(\text{NO})(\text{TC-4,4})]$  added after completion of the reaction (*middle*), and the reaction mixture with  $[\text{Co}(\text{NO})(\text{TC-4,4})]$  added prior to initiation of the reaction (*top*). The aromatic region of the  $^1\text{H}$  NMR spectrum is shown for clarity.

A  $^1\text{H}$  NMR spectroscopic investigation of changes that occur following titration of NO into solutions of  $[\text{Co}(\text{TC-4,4})](\text{OTf})$  suggested that 2 equiv of NO (g) are required per equivalent of  $[\text{Co}(\text{TC-4,4})](\text{OTf})$  to form the maximum amount of  $[\text{Co}(\text{NO})(\text{TC-4,4})]$  (Fig. 6.9). We make this determination based on the relative integration of peaks in the  $^1\text{H}$  NMR spectra for protonated proton sponge and the cobalt mononitrosyl. That is, more  $[\text{Co}(\text{NO})(\text{TC-4,4})]$  forms relative to the amount of protonated base as the amount of NO (g) is increased from 1 equiv to 2 equiv relative to the starting cobalt(III) complex. Addition of 4 equiv of NO (g) leads to little increase in the integrated  $^1\text{H}$  NMR spectral peaks corresponding to  $[\text{Co}(\text{NO})(\text{TC-4,4})]$  compared to integration values for protonated proton sponge. We are unable to assign with certainty a 2:1 stoichiometry for the  $[\text{Co}(\text{TC-4,4})](\text{OTf})/\text{NO}$  reaction, however, due to the possible occurrence of reactions that do not produce  $[\text{Co}(\text{NO})(\text{TC-4,4})]$ . These side reactions may generate species that are poorly soluble and/or undetectable by  $^1\text{H}$  NMR spectroscopy. Indeed,  $^1\text{H}$  NMR spectroscopic studies imply the formation of approximately 0.4 equiv of  $[\text{Co}(\text{NO})(\text{TC-4,4})]$  per equiv of protonated base. This substoichiometric ratio of cobalt mononitrosyl formation suggests that additional tropocoronand-containing species have yet to be identified.

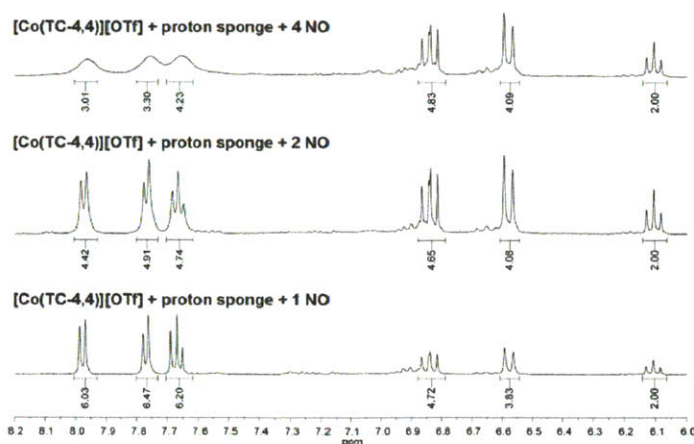


**Figure 6.9.**  $^1\text{H}$  NMR spectroscopic titration of NO (g) into the headspace of solutions of  $[\text{Co}(\text{TC-4,4})](\text{OTf})$ . Recorded in  $\text{CD}_2\text{Cl}_2$ . The aromatic region of the  $^1\text{H}$  NMR spectrum is shown for clarity.

We conclude from the work described in this Chapter thus far that  $[\text{Co}(\text{TC-4,4})](\text{OTf})$  undergoes reductive nitrosylation in the presence of nitric oxide, leading to the formation of  $\text{N}_2\text{O}$  and  $[\text{Co}(\text{NO})(\text{TC-4,4})]$ . An electron-releasing process occurs, whereby 1 equiv of  $\text{H}^+$  is released per equivalent of  $[\text{Co}(\text{TC-4,4})](\text{OTf})$  consumed. We propose that the source of this proton is an electron-rich aminotroponoiminate ring of the tropocoronand ligand, which can undergo attack by a reactive nitrogen or oxygen species. DFT calculations show electron density localized to the  $\delta$ -carbon atoms of the aromatic rings (Fig. 6.10), and synthetic work with aminotroponoiminates indicates that the ring is susceptible to substitution at this position.<sup>23-25,40-43</sup> A ligand recovery experiment was performed on the reaction mixture and the resultant material was analyzed by ESI-MS, but only unsubstituted  $\text{H}_2\text{TC-4,4}$  was observed by mass spectrometry.

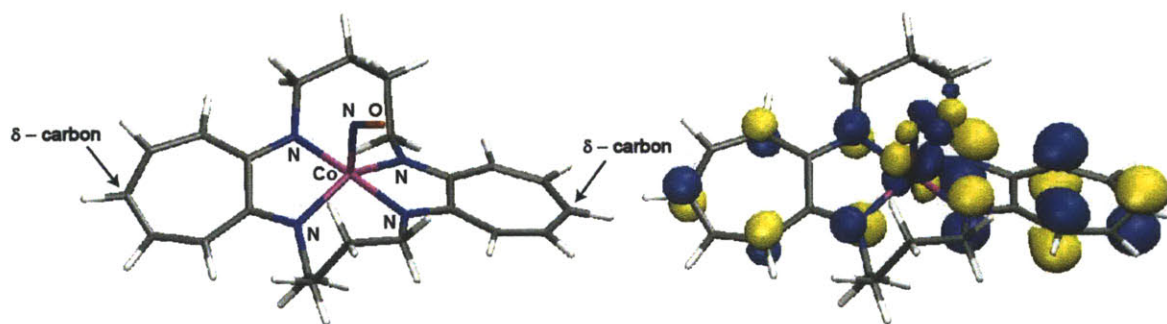


**Figure 6.10.** HOMO for  $[\text{Co}(\text{NO})(\text{TC-4,4})]$ , calculated at the B3LYP/6-311+G(d,p) level, represented at an isovalue of 0.04. Electron density at the  $\delta$ -carbon atoms may make the aminotroponoiminate rings susceptible to nucleophilic aromatic substitution.

After establishing basic reactivity patterns for  $[\text{Co}(\text{TC-4,4})]^+$  and  $\text{NO}$  (g), we next examined the reactivity of the cobalt(III) thiolate  $[\text{Co}(\text{SC}_6\text{F}_5)(\text{TC-4,4})]$  with nitric oxide. Previous studies of the reaction of glutathionylcobalamin with  $\text{NO}$  (g) revealed the formation of nitrosocobalamin and glutathionyl disulfide.<sup>17</sup> By analogy to this work, we expected  $[\text{Co}(\text{NO})(\text{TC-4,4})]$  and  $\text{F}_5\text{C}_6\text{SSC}_6\text{F}_5$  to form following exposure of  $[\text{Co}(\text{SC}_6\text{F}_5)(\text{TC-4,4})]$  to  $\text{NO}$  (g). Infrared spectroscopic studies supported the formation of  $[\text{Co}(\text{NO})(\text{TC-4,4})]$  from

[Co(SC<sub>6</sub>F<sub>5</sub>)(TC-4,4)] and 1 equiv of NO (g) (Fig. 6.11). A band corresponding to the  $\nu_{\text{NO}}$  stretch of [Co(NO)(TC-4,4)]<sup>22</sup> appears at 1587 cm<sup>-1</sup>, and shifts to 1570 cm<sup>-1</sup> with the use of isotopically labeled <sup>15</sup>NO.

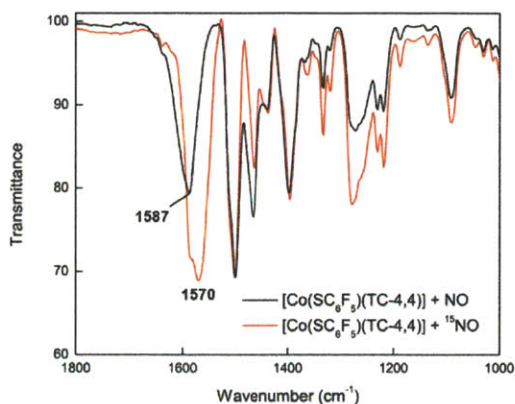


**Figure 6.11.** Isotope labeling comparison of the reactions of [Co(SC<sub>6</sub>F<sub>5</sub>)(TC-4,4)] with NO (g) or <sup>15</sup>NO (g). Infrared spectra recorded in the solid state (KBr).

The calculated N–O stretching band for [Co(<sup>15</sup>NO)(TC-4,4)], based on a simple harmonic oscillator model, is 1558 cm<sup>-1</sup>. <sup>1</sup>H NMR spectroscopic analysis of the reaction mixture confirmed the formation of [Co(NO)(TC-4,4)], but there were additional peaks in the aromatic region of the spectrum (Fig. 6.12).

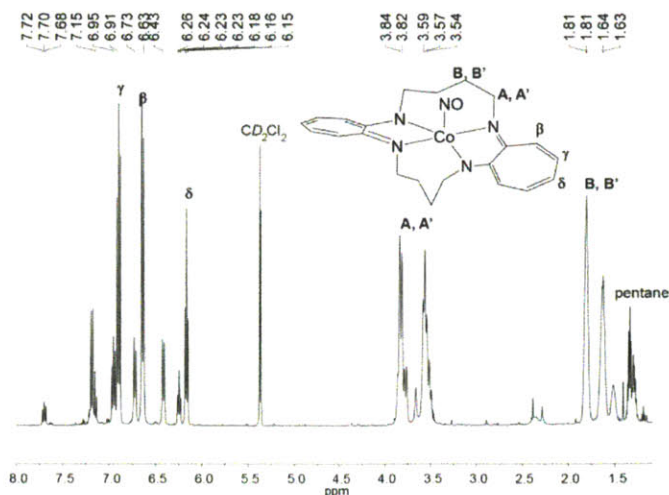


**Figure 6.12.** <sup>1</sup>H NMR spectroscopic analysis of the [Co(SC<sub>6</sub>F<sub>5</sub>)(TC-4,4)]/NO reaction mixture, recorded in CD<sub>2</sub>Cl<sub>2</sub>.



A COSY NMR experiment suggested that peaks in the aromatic region of the NMR spectrum arise from three major aminotroponeiminate species (Fig. 6.13).

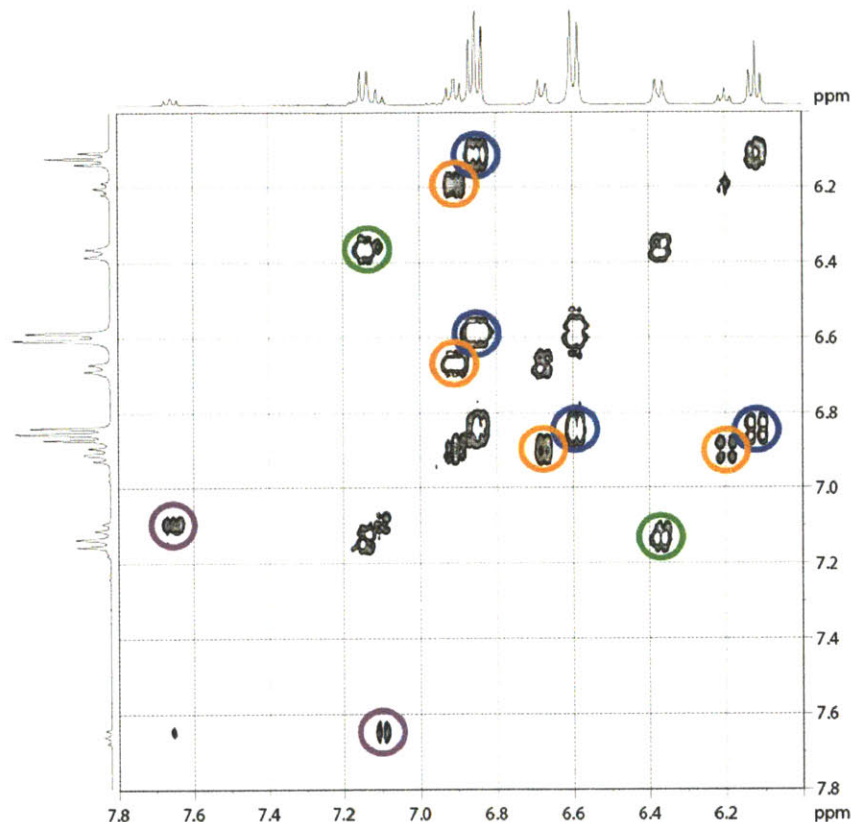


**Figure 6.13.** COSY spectrum of the  $[\text{Co}(\text{SC}_6\text{F}_5)(\text{TC-4,4})]/\text{NO}$  reaction mixture, recorded in  $\text{CD}_2\text{Cl}_2$ . Only the aromatic region is shown for clarity. Off-diagonal peaks for each of three aminotroponeiminate species are circled in blue, green, and orange, and violet. Peaks in blue correspond to aryl protons of the ligand in  $[\text{Co}(\text{NO})(\text{TC-4,4})]$ .

The  $[\text{Co}(\text{SC}_6\text{F}_5)(\text{TC-4,4})]/\text{NO}$  reaction was then carried out on an NMR spectroscopic scale, and the mixture was analyzed by  $^1\text{H}$  and  $^{19}\text{F}$  NMR spectroscopy after 10 min, and again after 1 day.  $^1\text{H}$  NMR spectroscopy revealed the presence of  $[\text{Co}(\text{NO})(\text{TC-4,4})]$  10 min after exposure of  $[\text{Co}(\text{SC}_6\text{F}_5)(\text{TC-4,4})]$  to nitric oxide (Fig. 6.14). The disulfide  $\text{F}_5\text{C}_6\text{SSC}_6\text{F}_5$  is observed by  $^{19}\text{F}$  NMR at the same time point (Fig. 6.15).<sup>44</sup> Additional peaks also appeared in the  $^{19}\text{F}$  NMR spectrum.

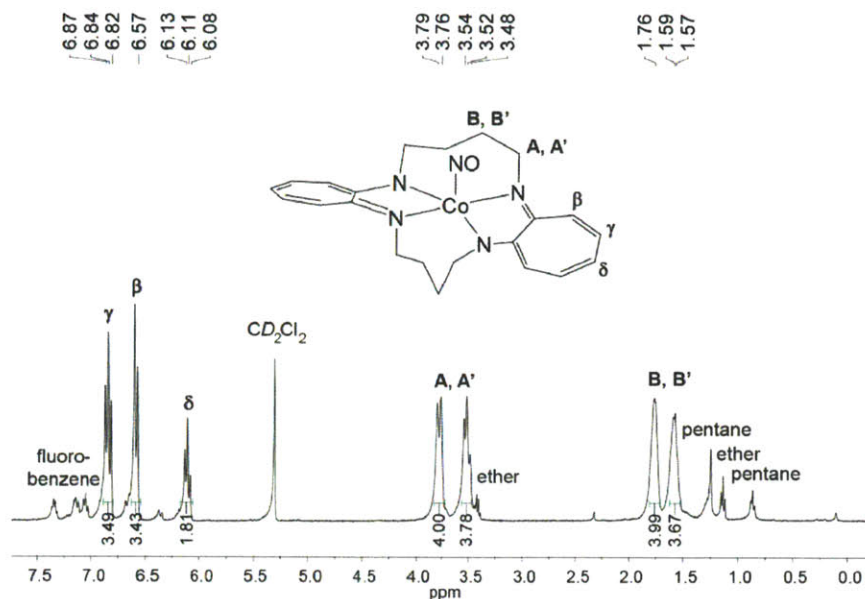


**Figure 6.14.**  $^1H$  NMR spectroscopic analysis of the  $[Co(SC_6F_5)(TC-4,4)]/NO$  reaction mixture, 10 min after injection of NO (g) into the headspace of a solution containing  $[Co(SC_6F_5)(TC-4,4)]$ . Recorded in  $CD_2Cl_2$ .

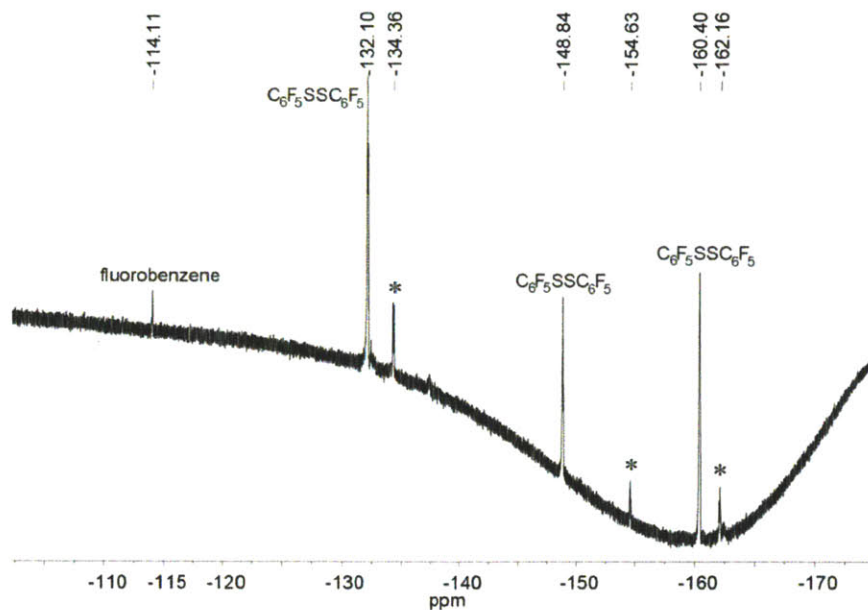


**Figure 6.15.**  $^{19}F$  NMR spectrum of NMR-scale reaction between  $[Co(SC_6F_5)(TC-4,4)]$  and  $\sim 100$  equiv NO, 10 min after NO injection. “\*” Indicates new peak growing in. Fluorobenzene was the recrystallization solvent for  $[Co(SC_6F_5)(TC-4,4)]$ . Difficulty in phasing the spectrum led to deep curvature in the baseline. Recorded in  $CD_2Cl_2$ .

Analysis of the same sample 1 day after initiation of the reaction revealed new peaks in the aromatic region of the  $^1\text{H}$  NMR spectrum (Fig. 6.16). Complete conversion of  $\text{F}_5\text{C}_6\text{SSC}_6\text{F}_5$  to a novel species was indicated in the  $^{19}\text{F}$  NMR spectrum (Fig. 6.17). The chemical shifts of these new peaks are different from the values reported for  $\text{F}_5\text{C}_6\text{SH}$ , as well as for the  $\text{NaSC}_6\text{F}_5$  starting material (data not shown).

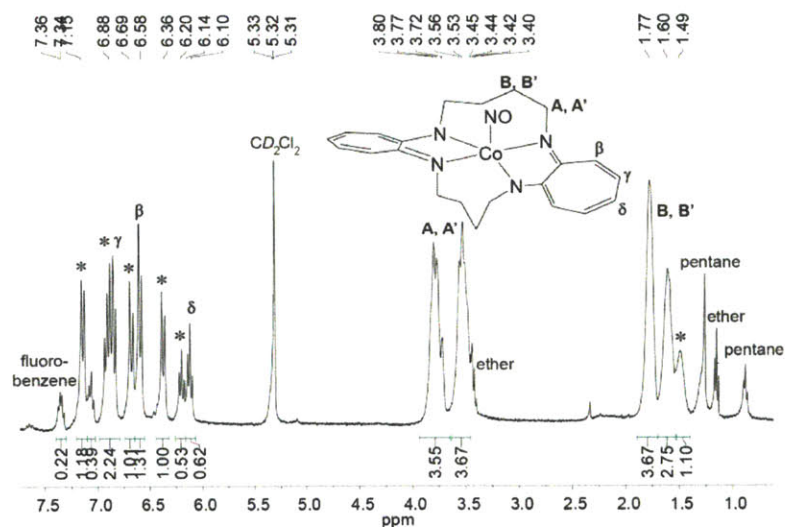


**Figure 6.16.**  $^1\text{H}$  NMR spectrum of NMR-scale reaction between  $[\text{Co}(\text{SC}_6\text{F}_5)(\text{TC-4,4})]$  and  $\sim 100$  equiv NO, 1 day after NO injection. “\*” Indicates new peaks in the  $^1\text{H}$  NMR spectrum.  $[\text{Co}(\text{SC}_6\text{F}_5)(\text{TC-4,4})]$  was recrystallized from fluorobenzene. Recorded in  $\text{CD}_2\text{Cl}_2$ .

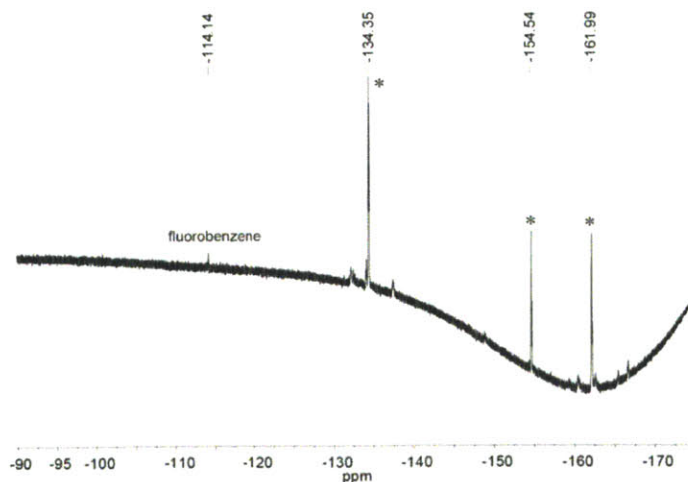


**Figure 6.17.**  $^{19}\text{F}$  NMR spectrum of NMR-scale reaction between  $[\text{Co}(\text{SC}_6\text{F}_5)(\text{TC-4,4})]$  and  $\sim 100$  equiv NO, 1 day after NO injection. “\*” Indicates new peaks in the  $^{19}\text{F}$  NMR spectrum.  $[\text{Co}(\text{SC}_6\text{F}_5)(\text{TC-4,4})]$  was recrystallized from fluorobenzene. Recorded in  $\text{CD}_2\text{Cl}_2$ .

Based on the  $^1\text{H}$  and  $^{19}\text{F}$  NMR spectroscopic data, and taking into account the electron-rich nature of the tropocoronand ligand in  $[\text{Co}(\text{NO})(\text{TC-4,4})]$  (*vide supra*), we propose that  $[\text{Co}(\text{SC}_6\text{F}_5)(\text{TC-4,4})]$  reacts with  $\text{NO}$  (g) to form  $[\text{Co}(\text{NO})(\text{TC-4,4})]$  and the disulfide  $\text{F}_5\text{C}_6\text{SSC}_6\text{F}_5$  (eq 6.4). The electron-rich tropocoronand may then attack electron-deficient  $\text{F}_5\text{C}_6\text{SSC}_6\text{F}_5$ , thereby undergoing nucleophilic aromatic substitution with concomitant formation of  $\text{F}_5\text{C}_6\text{SH}$  (eq 6.5). The acidic thiol  $\text{F}_5\text{C}_6\text{SH}$ , with  $\text{pK}_a$  2.68,<sup>45</sup> may promote partial decomposition of cobalt mononitrosyl adducts.



From the splitting patterns in the  $^1\text{H}$  NMR spectra, we propose that nucleophilic aromatic substitution takes place at the  $\delta$ -carbon atom of one aminotroponeiminate ring in  $[\text{Co}(\text{NO})(\text{TC-4,4})]$ , leaving the other ring unsubstituted (Chart 6.1). This regioselectivity of the substitution reaction would account for the observation of three major aminotroponeiminate species in the aryl region of the COSY NMR spectrum. That is, we observe aminotroponeiminate protons for  $[\text{Co}(\text{NO})(\text{TC-4,4})]$ , as well as one set of protons each for the substituted and unsubstituted rings of  $[\text{Co}(\text{NO})(\text{TC-4,4-SC}_6\text{F}_5)]$ .

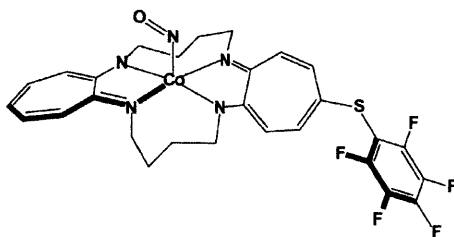


**Chart 6.1.**  $[\text{Co}(\text{NO})(\text{TC-4,4-SC}_6\text{F}_5)]$  is the proposed nucleophilic aromatic substitution product formed in the reaction of  $[\text{Co}(\text{SC}_6\text{F}_5)(\text{TC-4,4})]$  and  $\text{NO}$  (g).



The presence of  $[\text{Co}(\text{NO})(\text{TC-4,4-SC}_6\text{F}_5)]$  was supported by ESI-MS analysis of reaction mixtures, which led to the detection of low-intensity signal corresponding to  $[\text{H}_2\text{TC-4,4-SC}_6\text{F}_5 + \text{H}]^+$  and  $[\text{Co}(\text{TC-4,4-SC}_6\text{F}_5) - \text{H}]^+$  at  $m/z = 546.5$  and  $601.9$ , respectively (Fig. 6.18).

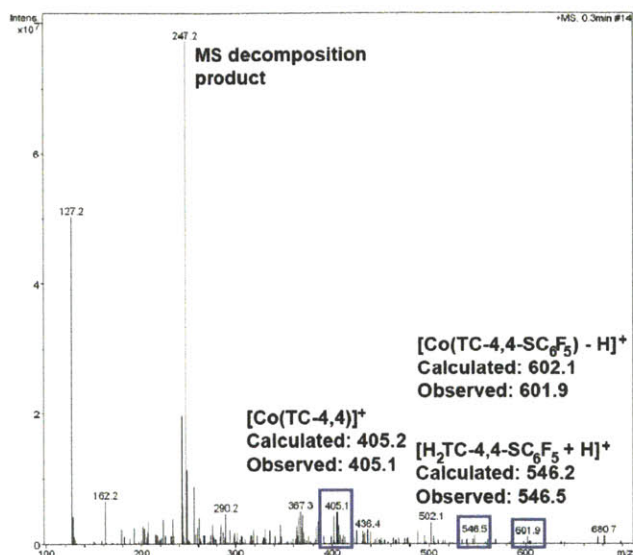


**Figure 6.18.** ESI-MS analysis of the  $[\text{Co}(\text{SC}_6\text{F}_5)(\text{TC-4,4})]/\text{NO}$  reaction mixture.

We sought to support the formation of  $[\text{Co}(\text{NO})(\text{TC-4,4-SC}_6\text{F}_5)]$  in the  $[\text{Co}(\text{SC}_6\text{F}_5)(\text{TC-4,4})]$  reaction with  $\text{NO}$  (g) through independent synthesis. Initial attempts were made to prepare the mono-substituted ligand  $\text{H}_2\text{TC-4,4-SC}_6\text{F}_5$  and, subsequently,  $[\text{Co}(\text{NO})(\text{TC-4,4-SC}_6\text{F}_5)]$ , for use in a  $^1\text{H}$  NMR spectroscopic comparison with the  $[\text{Co}(\text{SC}_6\text{F}_5)(\text{TC-4,4})]/\text{NO}$  reaction mixture. We were unable to obtain  $\text{H}_2\text{TC-4,4-SC}_6\text{F}_5$  through reaction of  $\text{H}_2\text{TC-4,4}$  and  $\text{F}_5\text{C}_6\text{SCl}$ , however. Instead, we observed a distribution of mono-, di-, and tri-substituted tropocoronands, in spite of slow addition of reagents under high dilution conditions and at cold reaction temperatures. A report<sup>23</sup> describing nucleophilic attack by thiols on bromo-substituted aminotroponeimines provided an encouraging route to the substituted ligand target, and we attempted isolation of the mono-brominated ligand  $\text{H}_2\text{TC-4,4}^{\text{Br}}$ . This ligand was not synthetically accessible, however, and

all attempted reaction conditions yielded the disubstituted derivative H<sub>2</sub>TC-4,4<sup>2Br</sup> (Fig. 6.19, Table 6.3). Nucleophilic substitution on H<sub>2</sub>TC-4,4<sup>2Br</sup> was attempted using pentafluorobenzene thiol and trityl thiol. Both reactions were unsuccessful, most likely due to the electron deficient nature of pentafluorobenzene thiol and the sterically hindered character of trityl thiol.

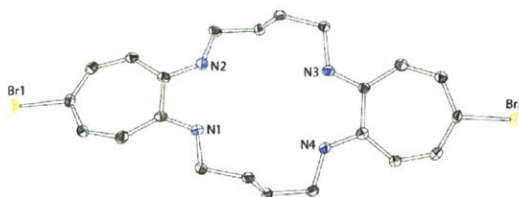


**Figure 6.19.** Thermal ellipsoid plot for H<sub>2</sub>TC-4,4<sup>2Br</sup>, depicted at 50% probability. Hydrogen atoms are omitted for clarity.

**Table 6.3.** Crystallographic parameters for H<sub>2</sub>TC-4,4<sup>2Br</sup> and [Co(TC-4,4<sup>2Br</sup>)].

	H <sub>2</sub> TC-4,4 <sup>2Br</sup>	[Co(TC-4,4 <sup>2Br</sup> )]
<b>Empirical formula</b>	C <sub>22</sub> H <sub>26</sub> Br <sub>2</sub> N <sub>4</sub>	C <sub>22</sub> H <sub>24</sub> Br <sub>2</sub> CoN <sub>4</sub>
<b>Formula weight</b>	506.29	563.20
<b>Crystal system</b>	Monoclinic	Orthorhombic
<b>Space group</b>	<i>P2</i> <sub>1</sub>	<i>Pna2</i> <sub>1</sub>
<b>a (Å)</b>	10.2293(7)	19.299(4)
<b>b (Å)</b>	7.7477(5)	13.105(2)
<b>c (Å)</b>	13.7910(9)	8.1995(17)
<b>β (deg)</b>	106.8500(10)	
<b>V (Å<sup>3</sup>)</b>	1046.06(12)	2073.7(7)
<b>Z</b>	2	4
<b>ρ<sub>calc</sub> (g/cm<sup>3</sup>)</b>	1.607	1.804
<b>Temperature (K)</b>	100 (2)	100 (2)
<b>μ (Mo Kα), (mm<sup>-1</sup>)</b>	3.890	4.698
<b>θ range (deg)</b>	1.54 to 28.78	1.88 to 26.37
<b>Crystal size (mm<sup>3</sup>)</b>	0.21 x 0.10 x 0.03	0.20 x 0.16 x 0.04
<b>Completeness to θ (%)</b>	99.9	100.0
<b>Max, min peaks (e/Å<sup>3</sup>)</b>	0.468 and -0.280	0.398 and -0.339
<b>Goodness-of-fit<sup>a</sup></b>	1.046	1.031
<b>Total no. of data</b>	21740	33976
<b>No. unique data</b>	5467	4243
<b>Flack parameter</b>	0.006(7)	0.054(7)
<b>R<sub>1</sub> (%)<sup>b</sup></b>	2.70	3.33
<b>wR<sub>2</sub> (%)<sup>c</sup></b>	5.43	5.28

<sup>a</sup>GOF = [Σ w(F<sub>o</sub><sup>2</sup>-F<sub>c</sub><sup>2</sup>)<sup>2</sup>/(n-p)]<sup>1/2</sup> where n is the number of data and p is the number of refined parameters.

<sup>b</sup>R<sub>1</sub> = Σ||F<sub>o</sub>|-|F<sub>c</sub>||/Σ|F<sub>o</sub>

<sup>c</sup>wR<sub>2</sub> = {Σ[w(F<sub>o</sub><sup>2</sup>-F<sub>c</sub><sup>2</sup>)<sup>2</sup>]/Σ[w(F<sub>o</sub><sup>2</sup>)<sup>2</sup>]}<sup>1/2</sup>

The inability to prepare H<sub>2</sub>TC-4,4-SC<sub>6</sub>F<sub>5</sub> led us to reconsider our strategy. We redirected our efforts to attempt substitution of electron-withdrawing groups at the  $\delta$ -carbon atoms of tropocoronand aminotroponimine rings. Subsequent coordination to cobalt(III) of the resulting disubstituted ligand, formation of the pentafluorobenzene thiolate complex, and reactivity studies with NO (g) has the potential to afford a cobalt mononitrosyl and the disulfide F<sub>5</sub>C<sub>6</sub>SSC<sub>6</sub>F<sub>5</sub>. Nucleophilic aromatic attack by the disulfide at the  $\delta$ -position of the aminotroponimine ring should be blocked, and the electron withdrawing nature of the pentafluorophenyl groups will remove electron density from the aromatic ring, possibly preventing attack at a different position.

Our first attempt to execute this strategy involved the dibrominated ligand, H<sub>2</sub>TC-4,4<sup>2Br</sup>, which we already had in hand. Deprotonation and metallation led to isolation of [Co(TC-4,4<sup>2Br</sup>)] (Fig. 6.20, Table 6.3 – 6.4), albeit in poor yield due to the poor solubility of [Co(TC-4,4<sup>2Br</sup>)] in organic solvents.

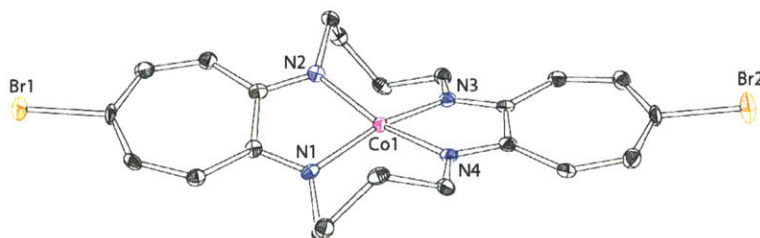


**Figure 6.20.** Thermal ellipsoid plot for [Co(TC-4,4<sup>2Br</sup>)], shown at 50% probability. Hydrogen atoms have been omitted for clarity.

**Table 6.4.** Summary of bond lengths (Å) and angles (deg) of interest for [Co(TC-4,4<sup>2Br</sup>)].

Co(1)-N(1)	1.873(3)	N(1)-Co(1)-N(3)	160.47(11)
Co(1)-N(2)	1.873(3)	N(1)-Co(1)-N(2)	81.51(11)
Co(1)-N(3)	1.900(3)	N(3)-Co(1)-N(2)	101.28(11)
Co(1)-N(4)	1.912(2)	N(1)-Co(1)-N(4)	101.50(11)
		N(3)-Co(1)-N(4)	82.68(10)
		N(2)-Co(1)-N(4)	159.65(11)

We attempted to prepare  $[\text{Co}(\text{TC-4,4}^{2\text{Br}})](\text{BF}_4)$  in a one-pot reaction, starting from  $\text{H}_2\text{TC-4,4}^{2\text{Br}}$ , in order to improve the yield by circumventing the solubility problem in the isolation of  $[\text{Co}(\text{TC-4,4}^{2\text{Br}})]$ . After metallation of the dibrominated tropocoronand, we added  $\text{FcBF}_4$  as an oxidant and recrystallized the product. We isolated crystals of  $[\text{Co}(\text{Br})(\text{TC-4,4}^{2\text{Br}})]$  from the reaction mixture (Fig. 6.21).

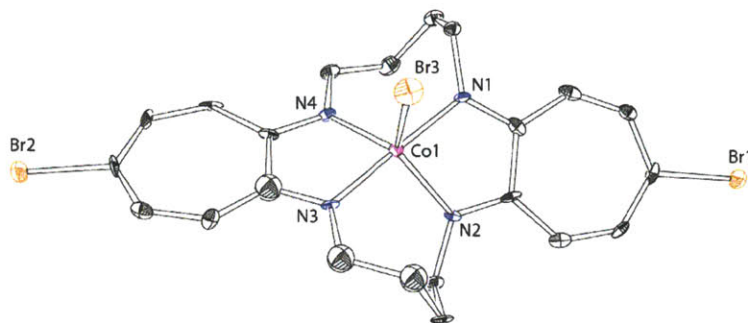
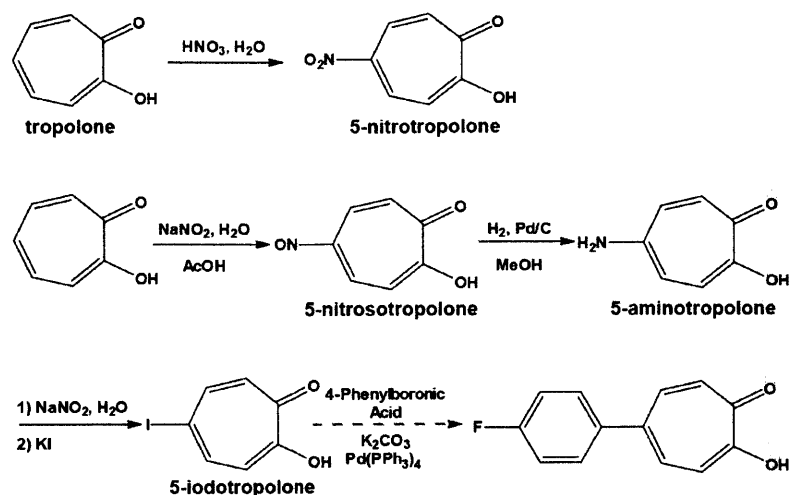


**Figure 6.21.** Thermal ellipsoid plot of  $[\text{Co}(\text{Br})(\text{TC-4,4}^{2\text{Br}})]$ , depicted at 50% probability. Hydrogen atoms are omitted for clarity. Poor quality crystals prevented high quality structure refinement.

The high reactivity of the dibrominated tropocoronand toward oxidation led us to seek other alternatives for ligand substitution. Suzuki coupling of  $\text{H}_2\text{TC-4,4}^{2\text{Br}}$  with phenylboronic acid was attempted, but was unsuccessful due to the irreversible coordination of palladium by the macrocyclic tropocoronand. Substitution of nitro groups directly onto the tropocoronand ring was also tried, but the reaction between  $\text{H}_2\text{TC-4,4}$  and  $\text{NO}_2\text{BF}_4$  proved difficult to control and, as in the substitution chemistry with  $\text{F}_5\text{C}_6\text{SCl}$ , a mixture of mono-, di-, and tri-substituted ligands formed. We next attempted to substitute tropolone, which appears early in the pathway for tropocoronand synthesis.

Tropolone was readily nitrated at the 5-position by nitric acid (Scheme 6.3),<sup>46</sup> but the subsequent tosylation step proved unusually difficult, possibly due to the presence of residual

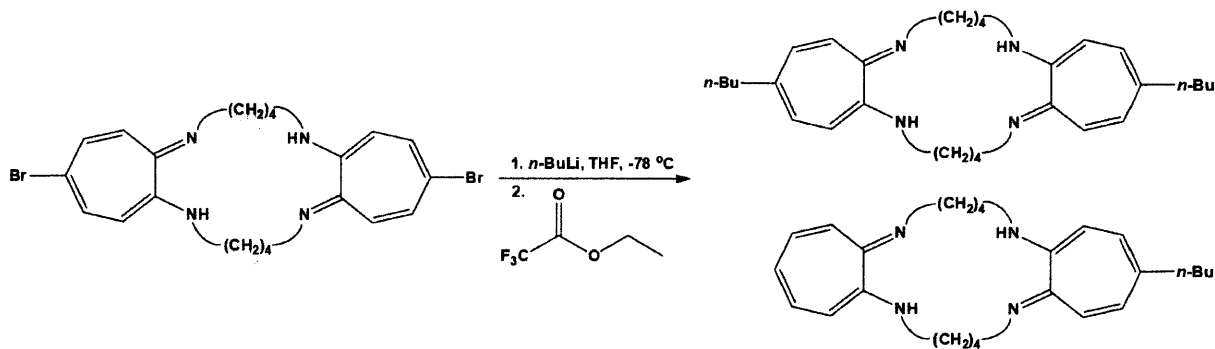


**Scheme 6.3.** Synthesis of substituted tropolone derivatives.

acid that could not be eliminated. 5-Nitrotropolone was readily prepared in good yield (Scheme 6.3),<sup>47</sup> but similarly could not be tosylated, possibly as a result of the nucleophilic character of the nitroso nitrogen atom.<sup>48-52</sup> Literature reports of Suzuki coupling reactions between 5-iodotropolone and a variety of boronic acids<sup>47,53</sup> spurred us to carry 5-nitrosotropolone through to the 5-iodo species. 5-Nitrosotropolone was reduced to 5-aminotropolone in excellent yield (Scheme 6.3).<sup>47</sup> Diazotization and substitution with potassium iodide gave 5-iodotropolone in moderate yield (Scheme 6.3).<sup>47</sup> Subsequent Suzuki coupling reactions of the 5-iodotropolone with 4-fluorophenylboronic acid were unsuccessful (Scheme 6.3).

We then returned to the dibrominated ligand,  $\text{H}_2\text{TC-4,4}^{2\text{Br}}$ , and pursued coupling via lithiation in a final effort to prepare the desired substituted tropocoronand. Addition of 4 equiv of *n*-butyllithium<sup>43</sup> to  $\text{H}_2\text{TC-4,4}^{2\text{Br}}$ , and subsequent exposure to ethyl trifluoroacetate, resulted in the formation of monobutyl and dibutyl tropocoronands (Scheme 6.4).





**Scheme 6.4.** Attempted substitution of trifluoroacetate onto the tropocoronand scaffold.

Dismayed by the reactivity of the butyl anion, we next exposed pentafluorobenzene to *n*-butyllithium and subsequently added H<sub>2</sub>TC-4,4<sup>2Br</sup>, in the hope of achieving the analogous substitution of the pentafluorobenzyl anion. The desired product, however, was not observed in the reaction mixture, and further attempts to substitute electron withdrawing substituents on H<sub>2</sub>TC-4,4 were abandoned.

#### 6.4. Summary and Conclusions

The reactions of [Co(TC-4,4)](OTf) and [Co(SC<sub>6</sub>F<sub>5</sub>)(TC-4,4)] with NO (g) were examined. Reductive nitrosylation of [Co(TC-4,4)](OTf) was demonstrated, with the formation of [Co(NO)(TC-4,4)], N<sub>2</sub>O, and the release of H<sup>+</sup>. The complexity of the reaction was prohibitive, and we were unable to further characterization the reaction products.

Exposure of [Co(SC<sub>6</sub>F<sub>5</sub>)(TC-4,4)] to nitric oxide also led to [Co(NO)(TC-4,4)] formation, as well as to generation of the disulfide F<sub>5</sub>C<sub>6</sub>SSC<sub>6</sub>F<sub>5</sub>. These species were unstable to the reaction conditions, and electrophilic aromatic substitution of F<sub>5</sub>C<sub>6</sub>S<sup>+</sup> onto the tropocoronand aromatic ring was deduced from spectroscopic and mass spectrometric experiments. Extensive attempts to synthesize tropocoronands with electron-withdrawing substituents that would block the

electrophilic aromatic substitution reaction were ultimately unsuccessful. No further efforts to characterize or isolate products of the [Co(SC<sub>6</sub>F<sub>5</sub>)(TC-4,4)]/NO reaction were pursued.

## 6.5. References

- (1) Zheng, D.; Birke, R. L. *J. Am. Chem. Soc.* **2001**, *123*, 4637-4638.
- (2) Wolak, M.; Stochel, G.; van Eldik, R. *Inorg. Chem.* **2005**, *45*, 1367-1379.
- (3) Hannibal, L.; Smith, C. A.; Jacobsen, D. W.; Brasch, N. E. *Angew. Chem. Int. Ed.* **2007**, *46*, 5140-5143.
- (4) Selçuki, C.; van Eldik, R.; Clark, T. *Inorg. Chem.* **2004**, *43*, 2828-2833.
- (5) Rochelle, L. G.; Morana, S. J.; Kruszyna, H.; Russell, M. A.; Wilcox, D. E.; Smith, R. P. *J. Pharmacol. Exp. Ther.* **1995**, *275*, 48-52.
- (6) Hassanin, H. A.; Hannibal, L.; Jacobsen, D. W.; Brown, K. L.; Marques, H. M.; Brasch, N. E. *Dalton Trans.* **2009**, 424-433.
- (7) Sharma, V. S.; Pilz, R. B.; Boss, G. R.; Magde, D. *Biochemistry* **2003**, *42*, 8900-8908.
- (8) Brown, K. L. *Chem. Rev.* **2005**, *105*, 2075-2150.
- (9) Vilakazi, S. L.; Nyokong, T. *Electrochim. Acta* **2000**, *46*, 453-461.
- (10) Wolak, M.; Stochel, G.; Hamza, M.; van Eldik, R. *Inorg. Chem.* **2000**, *39*, 2018-2019.
- (11) Franke, A.; Roncaroli, F.; van Eldik, R. *Eur. J. Inorg. Chem.* **2007**, *2007*, 773-798.
- (12) Zheng, D.; Yan, L.; Birke, R. L. *Inorg. Chem.* **2002**, *41*, 2548-2555.
- (13) Roncaroli, F.; van Eldik, R. *J. Am. Chem. Soc.* **2006**, *128*, 8042-8053.
- (14) Dózsa, L.; Pénzeli, P. *React. Kinet. Catal. Lett.* **1995**, *55*, 121-126.
- (15) Naito, S. *J. Chem. Soc., Chem. Commun.* **1978**, 175-176.
- (16) Naito, S.; Tamaru, K. *J. Chem. Soc., Faraday Trans.* **1982**, *78*, 735-745.
- (17) Zheng, D.; Birke, R. L. *J. Am. Chem. Soc.* **2002**, *124*, 9066-9067.
- (18) Lorković, I. M.; Ford, P. C. *Inorg. Chem.* **2000**, *39*, 632-633.
- (19) Imajo, S.; Nakanishi, K.; Roberts, M.; Lippard, S. J.; Nozoe, T. *J. Am. Chem. Soc.* **1983**, *105*, 2071-2073.
- (20) Zask, A.; Gonnella, N.; Nakanishi, K.; Turner, C. J.; Imajo, S.; Nozoe, T. *Inorg. Chem.* **1986**, *25*, 3400-3407.
- (21) Jaynes, B. S.; Doerrer, L. H.; Liu, S.; Lippard, S. J. *Inorg. Chem.* **1995**, *34*, 5735-5744.
- (22) Franz, K. J.; Doerrer, L. H.; Spingler, B.; Lippard, S. J. *Inorg. Chem.* **2001**, *40*, 3774-3780.
- (23) Dochnahl, M.; Löhnwitz, K.; Lühl, A.; Pissarek, J.-W.; Biyikal, M.; Roesky, P. W.; Blechert, S. *Organometallics* **2010**, *29*, 2637-2645.
- (24) Dochnahl, M.; Löhnwitz, K.; Pissarek, J.-W.; Roesky, P. W.; Blechert, S. *Dalton Trans.* **2008**, 2844-2848.
- (25) Eaton, D. R.; McClellan, W. R.; Weiher, J. F. *Inorg. Chem.* **1968**, *7*, 2040-2046.
- (26) APEX2, 4.0. Bruker AXS, Inc.: Madison, WI, 2008.
- (27) Sheldrick, G. M. *SADABS: Area-Detector Absorption Correction*, University of Göttingen: Göttingen, Germany, 2001.

- (28) Sheldrick, G. *Acta Crystallogr. Sect. A: Found. Crystallogr.* **2008**, *64*, 112-122.
- (29) Speck, A. L. *PLATON, A Multipurpose Crystallographic Tool*, Utrecht University: Utrecht, The Netherlands, 2001.
- (30) Burnett, M. N.; Johnson, C. K. *ORTEP-III: Oak Ridge Thermal Ellipsoid Plot Program for Crystal Structure Illustrations*, Oak Ridge National Laboratory Report ORNL-6895: 1996.
- (31) Frisch, M. J. T., G. W.; Schlegel, H. B.; Scuseria, G. E.; Robb, M. A.; Cheeseman, J. R.; Montgomery, Jr., J. A.; Vreven, T.; Kudin, K. N.; Burant, J. C.; Millam, J. M.; Iyengar, S. S.; Tomasi, J.; Barone, V.; Mennucci, B.; Cossi, M.; Scalmani, G.; Rega, N.; Petersson, G. A.; Nakatsuji, H.; Hada, M.; Ehara, M.; Toyota, K.; Fukuda, R.; Hasegawa, J.; Ishida, M.; Nakajima, T.; Honda, Y.; Kitao, O.; Nakai, H.; Klene, M.; Li, X.; Knox, J. E.; Hratchian, H. P.; Cross, J. B.; Bakken, V.; Adamo, C.; Jaramillo, J.; Gomperts, R.; Stratmann, R. E.; Yazyev, O.; Austin, A. J.; Cammi, R.; Pomelli, C.; Ochterski, J. W.; Ayala, P. Y.; Morokuma, K.; Voth, G. A.; Salvador, P.; Dannenberg, J. J.; Zakrzewski, V. G.; Dapprich, S.; Daniels, A. D.; Strain, M. C.; Farkas, O.; Malick, D. K.; Rabuck, A. D.; Raghavachari, K.; Foresman, J. B.; Ortiz, J. V.; Cui, Q.; Baboul, A. G.; Clifford, S.; Cioslowski, J.; Stefanov, B. B.; Liu, G.; Liashenko, A.; Piskorz, P.; Komaromi, I.; Martin, R. L.; Fox, D. J.; Keith, T.; Al-Laham, M. A.; Peng, C. Y.; Nanayakkara, A.; Challacombe, M.; Gill, P. M. W.; Johnson, B.; Chen, W.; Wong, M. W.; Gonzalez, C.; and Pople, J. A. *Gaussian 03, Revision C.02*, Gaussian, Inc.: Wallingford, CT, 2004.
- (32) Becke, A. D. *Phys. Rev. A* **1988**, *38*, 3098-3100.
- (33) Becke, A. D. *J. Chem. Phys.* **1993**, *98*, 5648-5652.
- (34) Lee, C.; Yang, W.; Parr, R. G. *Phys. Rev. B* **1988**, *37*, 785-789.
- (35) Ditchfield, R.; Hehre, W. J.; Pople, J. A. *J. Chem. Phys.* **1971**, *54*, 724-728.
- (36) Hehre, W. J.; Ditchfield, R.; Pople, J. A. *J. Chem. Phys.* **1972**, *56*, 2257-2261.
- (37) Humphrey, W.; Dalke, A.; Schulten, K. *J. Mol. Graphics* **1996**, *14*, 33-38.
- (38) Doerrler, L. H.; Bautista, M. T.; Lippard, S. J. *Inorg. Chem.* **1997**, *36*, 3578-3579.
- (39) Uppu, R. M.; Pryor, W. A. *Biochem. Biophys. Res. Commun.* **1996**, *229*, 764-769.
- (40) Eaton, D. R.; Benson, R. E.; Bottomley, C. G.; Josey, A. D. *J. Am. Chem. Soc.* **1972**, *94*, 5996-6004.
- (41) Eaton, D. R.; Josey, A. D.; Benson, R. E. *J. Am. Chem. Soc.* **1967**, *89*, 4040-4050.
- (42) Eaton, D. R.; Josey, A. D.; Benson, R. E.; Phillips, W. D.; Cairns, T. L. *J. Am. Chem. Soc.* **1962**, *84*, 4100-4106.
- (43) Eaton, D. R.; McClellan, W. R. *Inorg. Chem.* **1967**, *6*, 2134-2138.
- (44) Peach, M. E. *Can. J. Chem.* **1968**, *46*, 2699-2706.
- (45) Cros, E.; Planas, M.; Bardají, E. *Lett. Pept. Sci.* **2002**, *9*, 1-4.
- (46) Pauson, P. L. *Chem. Rev.* **1955**, *55*, 9-136.
- (47) Potenziano, J.; Spitale, R.; Janik, M. E. *Synth. Commun.* **2005**, *35*, 2005-2016.
- (48) Asao, T.; Imajo, S.; Nozoe, T. *Bull. Chem. Soc. Jpn.* **1990**, *63*, 3089-3095.
- (49) Baudisch, O.; Karzeff, N. *Ber. Dtsch. Chem. Ges.* **1917**, *50*, 328-330.
- (50) Ito, A.; Muratake, H.; Shudo, K. *J. Org. Chem.* **2008**, *74*, 1275-1281.
- (51) Nozoe, T.; Asao, T.; Kobayashi, M. *Bull. Chem. Soc. Jpn.* **1973**, *46*, 3161-3164.
- (52) Sato, O.; Tsurumaki, K.; Tamaru, S.; Tsunetsugu, J. *Heterocycles* **2004**, *62*, 535-542.
- (53) Nair, V.; Powell, D. W.; Suri, S. C. *Synth. Commun.* **1987**, *17*, 1897-1900.



## **Chapter 7. Synthesis and Characterization of Mononuclear, Pseudotetrahedral Cobalt(III) Compounds**

## 7.1. Introduction

The flexibility of the tropocoronand ligand scaffold allows it to accommodate varied coordination environments and stabilize unusual or otherwise unachievable geometries at transition metal centers. Such stabilization was demonstrated for tetrahedral nickel(II) complexes,<sup>1-3</sup> and, to some extent, the corresponding copper(II) species.<sup>4</sup> Related structural motifs and entatic interactions have been described for blue copper proteins, whereby the outer-sphere coordination environment of the protein stabilizes an unusual distorted tetrahedral geometry for coordinated copper(II).<sup>5-8</sup>

A survey of the tropocoronand literature revealed a truncated series for cobalt(III) in tetragonal environments, which was limited to distorted square planar [Co(TC-3,3)]<sup>+</sup> and [Co(TC-4,4)]<sup>+</sup> species.<sup>9</sup> The authors report reversible Co<sup>2+</sup>/Co<sup>3+</sup> electrochemical couples for the [TC-5,5]<sup>2-</sup> and [TC-6,6]<sup>2-</sup> cobalt complexes, but were unable to obtain bulk samples of the cobalt(III) species.<sup>9</sup> Small molecule cobalt(III) complexes in tetrahedral environments are extremely rare. A small number of mononuclear cobalt(III) imides have been prepared and characterized by X-ray crystallography.<sup>10-14</sup> The polyoxometallate [CoW<sub>12</sub>O<sub>40</sub>]<sup>5-</sup> has also been structurally characterized,<sup>15</sup> whereas the tetrahedral geometry of [Co(nor)<sub>4</sub>]<sup>-</sup> (nor = norbornyl anion) was determined by infrared spectroscopy.<sup>16-17</sup> During our studies of the tropocoronand ring size effect on the NO reactivity of the cobalt(II) and cobalt(III) complexes, reported in Chapters 4 – 6 of this thesis, we were able to extend the series of [Co(TC-*n,n*)]<sup>+</sup> species to include the [Co(TC-5,5)]<sup>+</sup> and [Co(TC-6,6)]<sup>+</sup> derivatives. These results are presented in this, the final chapter of the thesis.

## 7.2. Experimental Methods

**General Considerations.** Handling of air- and moisture-sensitive materials was conducted in an MBraun glovebox under a nitrogen atmosphere. Reagents were used as purchased, without further purification. Methylene chloride and tetrahydrofuran (THF) solvents were purified by passage through activated alumina and stored over 4 Å molecular sieves under a nitrogen atmosphere prior to use. Deuterated NMR solvents were obtained from Cambridge Isotope Laboratories, stored under an inert nitrogen atmosphere, and used without further purification. The syntheses of [Co(TC-5,5)],<sup>18</sup> and [Co(TC-6,6)],<sup>18</sup> [Zn(TC-5,5)],<sup>19</sup> and [Zn(TC-6,6)]<sup>19</sup> are described elsewhere. Fc(BPh<sub>4</sub>) was prepared according to previously published procedures.<sup>20-21</sup> CHN analyses were performed by Intertek-QTI (Whitehouse, NJ, USA) and Midwest Microlab, LLC (Indianapolis, IN, USA).

**Synthesis of [Co(TC-5,5)](BF<sub>4</sub>).** To a solution of [Co(TC-5,5)] (150 mg, 0.346 mmol) in methylene chloride was added Fc(BF<sub>4</sub>) (94.4 mg, 0.346 mmol). The reaction was left to stir overnight. The solution was evaporated to dryness and the resultant solid was washed with diethyl ether to remove ferrocene. The solid was dried in vacuo. Recrystallization from DCM/Et<sub>2</sub>O at -30 °C yielded X-ray quality crystals (174.5 mg, 96.9 % yield). UV-Vis-nIR (CDCl<sub>3</sub>) λ (ε) 349 (13652), 412 (15670), 757 (11418), 1166 (9183); IR (KBr) (cm<sup>-1</sup>) ν<sub>C=N</sub> 1501, ν<sub>C=C</sub> 1586. Anal. Calc'd. for C<sub>24</sub>H<sub>30</sub>BCoF<sub>4</sub>N<sub>4</sub>·0.32 CH<sub>2</sub>Cl<sub>2</sub>: C, 53.35; H, 5.64; N, 10.23. Found: C, 53.33; H, 5.89; N, 10.21.

**Synthesis of [Co(TC-6,6)](BPh<sub>4</sub>).** To a solution of [Co(TC-6,6)] (200 mg, 0.434 mmol) in methylene chloride was added Fc(BPh<sub>4</sub>) (218 mg, 0.434 mmol) in the dark. The reaction was allowed to stir overnight. The solution was evaporated to dryness and the resultant solid was washed with diethyl ether to remove ferrocene. The solid was dried in vacuo. Recrystallization from DCM/Et<sub>2</sub>O at -30 °C yielded X-ray quality crystals (327 mg, 96.6 % yield). *Note:* We found

methylene chloride solutions of Fc(BPh<sub>4</sub>) to be unstable, and attribute variations in product yield to this property. UV-Vis-nIR (CDCl<sub>3</sub>)  $\lambda$  ( $\epsilon$ ) 271 (60900), 349 (21467), 424 (34562), 702 (2362), 981 (561), 1240 (475); IR (KBr) (cm<sup>-1</sup>)  $\nu_{C=N}$  1504,  $\nu_{C=C}$  1595. Anal. Calc'd. for C<sub>50</sub>H<sub>54</sub>BCoN<sub>4</sub>: C, 76.92; H, 6.97; N, 7.18. Found: C, 76.68; H, 6.71; N, 7.33.

**Synthesis of [Ga(TC-5,5)](GaCl<sub>4</sub>).** To a solution of H<sub>2</sub>TC-5,5 (300 mg, 0.797 mmol) in THF was added NaHMDS (292 mg, 1.59 mmol) and the reaction was allowed to stir for 10 min. GaCl<sub>3</sub> (448 mg, 1.59 mmol) was added to the solution as a solid, and the reaction was left to stir overnight. The solution was evaporated to dryness, suspended in CH<sub>2</sub>Cl<sub>2</sub>, and filtered through Celite. The resultant solid was washed with diethyl ether and dried in vacuo. Recrystallization from CH<sub>2</sub>Cl<sub>2</sub>/Et<sub>2</sub>O at -30 °C yielded X-ray quality crystals (367 mg, 70% yield). <sup>1</sup>H NMR (CD<sub>2</sub>Cl<sub>2</sub>)  $\delta$  1.68 (m, 8H, CH<sub>2</sub>), 1.91 (m, 4H, CH<sub>2</sub>), 3.74, (m, 4H, CH<sub>2</sub>), 3.85 (m, 4H, CH<sub>2</sub>), 7.10 (t,  $J$  = 10 Hz, 2H, Ar- $H_\gamma$ ), 7.26 (d,  $J$  = 8 Hz, 2H, Ar- $H_\alpha$ ), 7.64 (t,  $J$  = 12 Hz, 2H, Ar- $H_\beta$ ); ESI-MS [M-GaCl<sub>4</sub>]<sup>+</sup>  $m/z$  433.1 (Calc'd 433.12); UV-Vis (CDCl<sub>3</sub>)  $\lambda$  ( $\epsilon$ ) 274 (sh, 63388), 280 (70812), 365 (40918), 416 (sh, 19478), 433 (27086); IR (KBr) (cm<sup>-1</sup>)  $\nu_{C=N}$  1512,  $\nu_{C=C}$  1513. Anal. Calc'd. for C<sub>24</sub>H<sub>30</sub>N<sub>4</sub>Ga<sub>2</sub>Cl<sub>4</sub>: C, 43.96; H, 4.61; N, 8.54. Found: C, 43.88; H, 4.44; N, 8.42.

**Synthesis of [Ga(TC-6,6)](GaCl<sub>4</sub>).** To a solution of H<sub>2</sub>TC-6,6 (54 mg, 0.133 mmol) in THF was added NaHMDS (45 mg, 0.267 mmol) and the reaction was allowed to stir 15 min. GaCl<sub>3</sub> (70 mg, 0.267 mmol) was added to the solution as a solid, and the reaction was left to stir overnight. The solution was evaporated to dryness, suspended in CH<sub>2</sub>Cl<sub>2</sub>, and filtered through Celite. The resultant solid was washed with diethyl ether and dried in vacuo. Recrystallization from CH<sub>2</sub>Cl<sub>2</sub>/Et<sub>2</sub>O at -30 °C yielded X-ray quality crystals (52 mg, 57 % yield). <sup>1</sup>H NMR (CD<sub>2</sub>Cl<sub>2</sub>)  $\delta$  1.13 – 1.26 (m, 8H, CH<sub>2</sub>), 1.44 (m, 4H, CH<sub>2</sub>), 2.19 – 2.26 (m, 4H, CH<sub>2</sub>), 3.64 – 3.71 (m, 4H, CH<sub>2</sub>), 3.97 – 4.02 (m, 4H, CH<sub>2</sub>), 7.12 (t,  $J$  = 8 Hz, 2H, Ar- $H_\gamma$ ), 7.35 (d,  $J$  = 8 Hz, 2H, Ar-

$H_\alpha$ ), 7.60 (t,  $J = 6$  Hz, 2H, Ar- $H_\beta$ ); ESI-MS  $[M-GaCl_4]^+$   $m/z$  471.1 (Calc'd 471.20); UV-Vis ( $CDCl_3$ )  $\lambda$  ( $\epsilon$ ) 272 (sh, 73753), 280 (83827), 363 (45724), 410 (sh, 22978), 422 (sh, 28929), 429 (37976); IR (KBr) ( $cm^{-1}$ )  $\nu_{C=N}$  1514,  $\nu_{C=C}$  1595. Anal. Calc'd. for  $C_{26}H_{34}N_4Ga_2Cl_4$ : C, 45.67; H, 5.01; N, 8.19. Found: C, 45.98; H, 4.93; N, 7.86.

**Physical Measurements.**  $^1H$  NMR spectra were collected on a 400 MHz Bruker Avance spectrometer. Optical spectra were recorded on a Varian Cary 5000 UV-Visible-nIR Spectrophotometer in 6SQ Starna cells. Solutions were prepared under a nitrogen atmosphere. FT-IR spectra were recorded on a Thermo Nicolet Avatar 360 spectrometer running the OMNIC software package. ESI-MS analyses were performed on the Agilent 1100 Series LC/MSD Trap spectrometer. Cyclic voltammograms were recorded under nitrogen using the VersaSTAT3 potentiostat (Princeton Applied Research) and the *V3 Studio* software. A glassy carbon working electrode, silver wire pseudo-reference electrode, and Pt wire auxiliary electrode were used. Samples were prepared as 3-5 mM solutions in methylene chloride with 0.1 M ( $n-Bu_4N$ )(PF<sub>6</sub>) as supporting electrolyte. Reported spectra were recorded at 50 mV/s scan rates. The reversible Fc/Fc<sup>+</sup> couple appeared at 0.57 V vs. Ag/Ag<sup>+</sup>.

**X-ray Crystallography.** Crystals were mounted in Paratone N oil and frozen at 100 K under a cold nitrogen stream controlled by a Cryopad low-temperature apparatus. Data were collected on a Bruker APEX CCD X-ray diffractometer with graphite-monochromated Mo- $K_\alpha$  radiation ( $\lambda = 0.71073$  Å) controlled by the APEX2 software package.<sup>22</sup> Empirical absorption correction was performed with SADABS.<sup>23</sup> The structure was solved by direct methods using SHELXS-97 and refined by full-matrix least-squares on  $F^2$  using the SHELXL-97 program incorporated into the SHELXTL software package.<sup>24</sup> Possible higher symmetries were evaluated by PLATON.<sup>25</sup> Non-hydrogen atoms were located and their positions refined anisotropically. Hydrogen atoms were

assigned idealized positions and given thermal parameters 1.2 times the thermal parameters of the atoms to which they are attached. The structure of  $[\text{Ga}(\text{TC-6,6})](\text{GaCl}_4)$  contained voids filled with heavily disordered solvent molecules. The program SQUEEZE<sup>26</sup> was used to remove the contributions of the disordered solvent to the structure factors. The electron density attributed to disordered solvent molecules created a channel along the  $6_5$  screw axis, and corresponded to 7 molecules of methylene chloride or diethyl ether. Thermal ellipsoid plots were generated using ORTEP-III.<sup>27</sup>

### 7.3. Results

$[\text{Co}(\text{TC-5,5})]$  was successfully oxidized to  $[\text{Co}(\text{TC-5,5})](\text{BF}_4)$  by reaction with ferrocenium tetrafluoroborate in dichloromethane (Fig. 7.1, *left*, Tables 7.1 and 7.2).

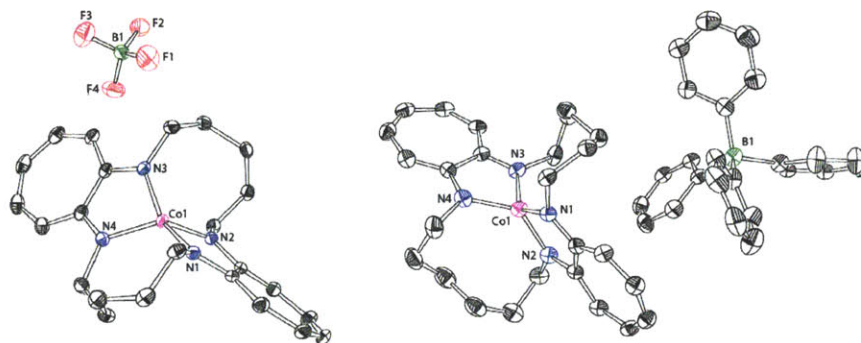


**Figure 7.1.** Thermal ellipsoid plots for  $[\text{Co}(\text{TC-5,5})](\text{BF}_4)$  (*left*) and  $[\text{Co}(\text{TC-6,6})](\text{BPh}_4)$  (*right*), shown at 50% probability. Hydrogen atoms have been omitted for clarity.

**Table 7.1.** Crystallographic parameters for [Co(TC-5,5)](BF<sub>4</sub>) and [Co(TC-6,6)](BPh<sub>4</sub>).

	[Co(TC-5,5)](BF <sub>4</sub> )	[Co(TC-6,6)](BPh <sub>4</sub> )
<b>Empirical formula</b>	C <sub>24</sub> H <sub>30</sub> BCoF <sub>4</sub> N <sub>4</sub>	C <sub>50</sub> H <sub>54</sub> BCoN <sub>4</sub>
<b>Formula weight</b>	520.26	780.71
<b>Crystal system</b>	Monoclinic	Triclinic
<b>Space group</b>	<i>P</i> 2 <sub>1</sub> / <i>c</i>	<i>P</i> $\bar{1}$
<b>a (Å)</b>	11.137(8)	10.824(3)
<b>b (Å)</b>	24.040(19)	13.521(4)
<b>c (Å)</b>	8.549(7)	14.593(4)
<b><math>\alpha</math> (deg)</b>	90	87.014(4)
<b><math>\beta</math> (deg)</b>	105.35(2)	84.962(4)
<b><math>\gamma</math> (deg)</b>	90	74.812(4)
<b>V (Å<sup>3</sup>)</b>	2207(3)	2052.3(10)
<b>Z</b>	4	2
<b><math>\rho_{calc}</math> (g/cm<sup>3</sup>)</b>	1.566	1.263
<b>Temperature (K)</b>	100 (2)	100 (2)
<b><math>\mu</math> (Mo K<math>\alpha</math>), (mm<sup>-1</sup>)</b>	0.833	0.458
<b><math>\theta</math> range (deg)</b>	1.69 to 26.76	1.40 to 26.33
<b>Crystal size (mm<sup>3</sup>)</b>	0.40 x 0.10 x 0.05	0.40 x 0.09 x 0.02
<b>Completeness to <math>\theta</math> (%)</b>	99.3	98.9
<b>Max, min peaks (e/Å<sup>3</sup>)</b>	0.406 and -0.364	0.692 and -0.622
<b>Goodness-of-fit<sup>a</sup></b>	1.042	1.051
<b>Total no. of data</b>	37590	33495
<b>No. unique data</b>	4665	8290
<b>R<sub>1</sub> (%)<sup>b</sup></b>	3.57	5.58
<b>wR<sub>2</sub> (%)<sup>c</sup></b>	7.59	12.26

<sup>a</sup>GOF =  $[\sum w(F_o^2 - F_c^2)^2 / (n - p)]^{1/2}$  where *n* is the number of data and *p* is the number of refined parameters.

<sup>b</sup>R<sub>1</sub> =  $\sum ||F_o| - |F_c|| / \sum |F_o|$

<sup>c</sup>wR<sub>2</sub> =  $\{\sum [w(F_o^2 - F_c^2)^2] / \sum [w(F_o^2)^2]\}^{1/2}$

**Table 7.2.** Summary of bond lengths (Å) and angles (deg) of interest for [Co(TC-5,5)](BF<sub>4</sub>).

Co(1)-N(1)	1.850(2)	N(2)-Co(1)-N(3)	103.34(9)
Co(1)-N(2)	1.832(2)	N(2)-Co(1)-N(1)	82.69(9)
Co(1)-N(3)	1.845(2)	N(3)-Co(1)-N(1)	151.43(8)
Co(1)-N(4)	1.857(2)	N(2)-Co(1)-N(4)	125.24(8)
		N(3)-Co(1)-N(4)	83.01(8)
		N(1)-Co(1)-N(4)	116.66(8)

Structural characterization of [Co(TC-5,5)](BF<sub>4</sub>) revealed the twist angle at the cobalt center of [Co(TC-5,5)]<sup>+</sup> to be 65°, computed as the angle between planes defined by the metal and the two sets of aminotroponeiminate nitrogen atoms.<sup>1</sup> The average bond distance between

the metal center and coordinating nitrogen atoms,  $\text{Co1} - \text{N}_{\text{ave}}$ , was 1.85 Å, which is comparable to the 1.86 Å and 1.87 Å of  $[\text{Co}(\text{TC-3,3})](\text{BPh}_4)$  and  $[\text{Co}(\text{TC-4,4})](\text{BAr}^{\text{F}}_4)$ , respectively.

We were able to oxidize  $[\text{Co}(\text{TC-6,6})]$  to  $[\text{Co}(\text{TC-6,6})](\text{BPh}_4)$  with ferrocenium tetraphenylborate and to structurally characterize the cobalt(III) product (Fig. 7.1, *right*, Tables 7.1 and 7.3).

**Table 7.3.** Summary of bond lengths (Å) and angles (deg) of interest for  $[\text{Co}(\text{TC-6,6})](\text{BPh}_4)$ .

Co(1)-N(1)	1.817(3)	N(1)-Co(1)-N(4)	116.97(13)
Co(1)-N(2)	1.834(3)	N(1)-Co(1)-N(3)	132.83(13)
Co(1)-N(3)	1.823(3)	N(4)-Co(1)-N(3)	82.15(13)
Co(1)-N(4)	1.823(3)	N(1)-Co(1)-N(2)	82.37(12)
		N(4)-Co(1)-N(2)	133.80(14)
		N(3)-Co(1)-N(2)	116.35(12)

The twist angle in  $[\text{Co}(\text{TC-6,6})]^+$  is  $74^\circ$ , the largest observed for cobalt(III) tropocoronands to date.<sup>9</sup> The  $\text{Co1}-\text{N}_{\text{ave}}$  bond distance is 1.82 Å, somewhat shorter than in previously reported cobalt(III) tropocoronand coordination compounds.<sup>9</sup> The aminotroponeiminate rings of the tropocoronand stack via  $\pi$ - $\pi$  interactions with phenyl groups of the tetraphenylborate counteranion in the crystal lattice (Fig. 7.2). A phenyl ring of  $(\text{BPh}_4)^-$  lies at  $71.9^\circ$  to each aminotroponeiminate ring of  $[\text{Co}(\text{TC-6,6})]^+$ . The phenyl group that participates in the  $\pi$ - $\pi$  interaction is 3.8 Å from the plane of the aminotroponeiminate. This  $\pi$ - $\pi$  interaction may contribute to the stability of the  $[\text{Co}(\text{TC-6,6})](\text{BPh}_4)$  complex.

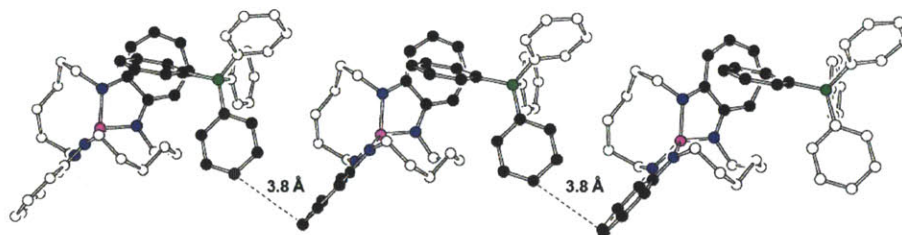


**Figure 7.2.** Crystal packing for  $[\text{Co}(\text{TC-6,6})](\text{BPh}_4)$ , emphasizing the  $\pi$ - $\pi$  interactions of the aminotroponeiminate rings of  $[\text{Co}(\text{TC-6,6})]^+$  with the phenyl rings of  $(\text{BPh}_4)^-$ . Carbon atoms depicted in black comprise the aryl groups that participate in  $\pi$ - $\pi$  interactions. Otherwise, the color scheme is: carbon, white; nitrogen, blue; cobalt, magenta; boron, lime green.



We also prepared the analogous gallium(III) tropocoronands,  $[\text{Ga}(\text{TC-5,5})]^+$  and  $[\text{Ga}(\text{TC-6,6})]^+$ , for comparison of structural and electrochemical properties (Fig. 7.3, Tables 7.4 – 7.6).

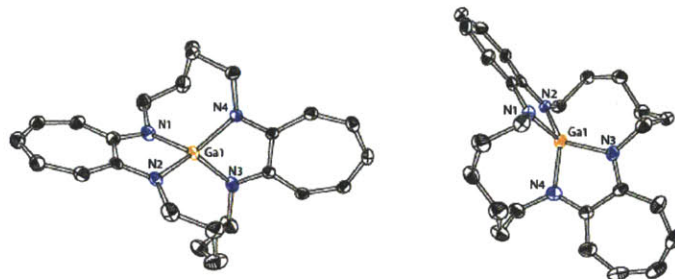


**Figure 7.3.** Thermal ellipsoid plots for  $[\text{Ga}(\text{TC-5,5})](\text{GaCl}_4)$  and  $[\text{Ga}(\text{TC-6,6})](\text{GaCl}_4)$ , depicted at 50% probability. Hydrogen atoms and the gallium tetrachloride anions are omitted for clarity.

**Table 7.4.** Crystallographic parameters for  $[\text{Ga}(\text{TC-5,5})](\text{GaCl}_4)$  and  $[\text{Ga}(\text{TC-6,6})](\text{GaCl}_4)$ .

	$[\text{Ga}(\text{TC-5,5})](\text{GaCl}_4)$	$[\text{Ga}(\text{TC-6,6})](\text{GaCl}_4)$
<b>Empirical formula</b>	$\text{C}_{24}\text{H}_{30}\text{Cl}_4\text{Ga}_2\text{N}_4$	$\text{C}_{26}\text{H}_{34}\text{Cl}_4\text{Ga}_2\text{N}_4$
<b>Formula weight</b>	655.76	683.80
<b>Crystal system</b>	Monoclinic	Hexagonal
<b>Space group</b>	$P2_1/c$	$P6_5$
<b>a (Å)</b>	15.6905(10)	21.9860(8)
<b>b (Å)</b>	12.8780(8)	
<b>c (Å)</b>	14.2525(9)	11.9576(8)
<b><math>\beta</math> (deg)</b>	109.8660(10)	
<b>V (Å<sup>3</sup>)</b>	2708.5(3)	5005.7(4)
<b>Z</b>	4	6
<b><math>\rho_{\text{calc}}</math> (g/cm<sup>3</sup>)</b>	1.608	1.357
<b>Temperature (K)</b>	100 (2)	100 (2)
<b><math>\mu</math> (Mo K<math>\alpha</math>), (mm<sup>-1</sup>)</b>	2.405	1.955
<b><math>\theta</math> range (deg)</b>	2.10 to 26.81	1.07 to 25.66
<b>Crystal size (mm<sup>3</sup>)</b>	0.40 x 0.20 x 0.20	0.20 x 0.07 x 0.03
<b>Completeness to <math>\theta</math> (%)</b>	99.9	100.0
<b>Max, min peaks (e/Å<sup>3</sup>)</b>	1.092 <sup>a</sup> and -0.810	0.467 and -0.339
<b>Goodness-of-fit<sup>b</sup></b>	1.407	1.094
<b>Total no. of data</b>	47316	83492
<b>No. unique data</b>	5798	6340
<b>Flack parameter</b>		0.41(7)
<b>R<sub>1</sub> (%)<sup>c</sup></b>	3.98	4.18
<b>wR<sub>2</sub> (%)<sup>d</sup></b>	9.33	8.13

<sup>a</sup>The maximum residual electron density peak appears near a carbon atom that is part of a disordered polymethylene chain in the tropocoronand ligand.

<sup>b</sup>GOF =  $[\sum w(F_o^2 - F_c^2)^2 / (n - p)]^{1/2}$  where  $n$  is the number of data and  $p$  is the number of refined parameters.

<sup>c</sup> $R_1 = \sum ||F_o| - |F_c|| / \sum |F_o|$

<sup>d</sup> $wR_2 = \{\sum [w(F_o^2 - F_c^2)^2] / \sum [w(F_o^2)^2]\}^{1/2}$

**Table 7.5.** Summary of bond lengths (Å) and angles (deg) of interest for [Ga(TC-5,5)](GaCl<sub>4</sub>).

Ga(1)-N(1)	1.859(11)	N(3)-Ga(1)-N(1)	125.2(7)
Ga(1)-N(2)	1.890(14)	N(3)-Ga(1)-N(2)	118.1(9)
Ga(1)-N(3)	1.858(12)	N(1)-Ga(1)-N(2)	85.9(4)
Ga(1)-N(4)	1.898(19)	N(3)-Ga(1)-N(4)	86.4(5)
		N(1)-Ga(1)-N(4)	117.0(8)
		N(2)-Ga(1)-N(4)	129.1(13)

**Table 7.6.** Summary of bond lengths (Å) and angles (deg) of interest for [Ga(TC-6,6)](GaCl<sub>4</sub>).

Ga(1)-N(1)	1.891(5)	N(1)-Ga(1)-N(2)	86.0(2)
Ga(1)-N(2)	1.891(5)	N(1)-Ga(1)-N(3)	123.4(2)
Ga(1)-N(3)	1.893(5)	N(2)-Ga(1)-N(3)	123.4(2)
Ga(1)-N(4)	1.903(5)	N(1)-Ga(1)-N(4)	121.1(2)
		N(2)-Ga(1)-N(4)	122.2(2)
		N(3)-Ga(1)-N(4)	85.4(2)

The [Ga(TC-5,5)](GaCl<sub>4</sub>) complex crystallizes in  $P2_1/c$  and exhibits crystallographic disorder over the entirety of the tropocoronand ligand. The  $N_4$ -coordinated gallium(III) center has a twist angle of 81°, displaying distorted tetrahedral geometry. The average gallium-nitrogen distance, Ga1-N<sub>ave</sub>, is 1.88 Å. [Ga(TC-6,6)](GaCl<sub>4</sub>) crystallizes in  $P6_5$  and exhibits nearly perfect tetrahedral coordination at the gallium(III) center. The twist angle in [Ga(TC-6,6)]<sup>+</sup> is 89° and Ga1-N<sub>ave</sub> is 1.89 Å.

We attempted to characterize [Co(TC-5,5)](BF<sub>4</sub>) by X-band EPR spectroscopy, but were unable to observe any signal at 77 K. Helium temperature EPR spectroscopic studies of [Co(TC-6,6)](BPh<sub>4</sub>) were equally unrevealing. The <sup>1</sup>H NMR spectrum of [Co(TC-5,5)](BF<sub>4</sub>) shows broad, low intensity peaks in the diamagnetic region of the spectrum, which may correspond to a tropocoronand-containing species. These features may be attributed to the ligand in [Co(TC-5,5)](BF<sub>4</sub>) or, more likely, considering the weak signal relative to sample concentration, may arise from the presence of an impurity. Peaks corresponding to protons of the tropocoronand ligand are absent in the <sup>1</sup>H NMR spectrum of [Co(TC-6,6)](BPh<sub>4</sub>), but peaks for the

tetraphenylborate counteranion are readily observed. We attempted to perform SQUID magnetic susceptibility measurements to characterize the electronic state of the cobalt(III) metal centers, but residual iron contamination, as suggested by X-ray fluorescence spectroscopy, prohibited acquisition of a satisfactory data set.

Optical features of [Co(TC-5,5)][BF<sub>4</sub>], [Co(TC-6,6)][BPh<sub>4</sub>], [Ga(TC-5,5)][GaCl<sub>4</sub>], and [Ga(TC-6,6)][GaCl<sub>4</sub>] are listed in Table 7.7, and compared with the previously reported optical bands of [Co(TC-5,5)] and [Co(TC-6,6)]. Typical tropocoronand ligand bands appeared in the infrared spectra of [Co(TC-5,5)][BF<sub>4</sub>], [Co(TC-6,6)][BPh<sub>4</sub>], [Ga(TC-5,5)][GaCl<sub>4</sub>], and [Ga(TC-6,6)][GaCl<sub>4</sub>]. Spectra of cobalt(III) complexes matched closely with IR spectra of the parent cobalt(II) species.

**Table 7.7.** Optical Properties of Co(III) and Ga(III) Tropocoronands.<sup>a</sup>

[Co(TC-5,5)] <sup>b</sup>	[Co(TC-6,6)] <sup>b</sup>	[Co(TC-5,5)] <sup>+</sup>	[Co(TC-6,6)] <sup>+</sup>	[Ga(TC-5,5)] <sup>+</sup>	[Ga(TC-6,6)] <sup>+</sup>
332 (19000)	336 (18800)		271 (60900)	274 (sh, 63388)	272 (sh, 73753)
<u>392 (34100)</u>	<u>387 (33500)</u>	349 (13652)	349 (21467)	280 (70812)	280 (83827)
<u>405 (sh, 32100)</u>	<u>413 (38600)</u>	412 (15670)	424 (34562)	365 (40918)	363 (45724)
				416 (sh, 19478)	410 (sh, 22978)
<i>490 (sh, 4800)</i>	<i>478 (sh, 3890)</i>			433 (27086)	422 (sh, 28929)
	<i>565 (sh, 1170)</i>				429 (37976)
<i>596 (sh, 820)</i>	<i>599 (sh, 950)</i>				
	<i>670 (sh, 100)</i>				
		757 (11418)	702 (2362)		
			981 (561)		
		1166 (9183)	1240 (475)		

<sup>a</sup> Absorption maxima are reported in nm. Molar extinction coefficients are in parentheses, in M<sup>-1</sup> cm<sup>-1</sup>.

<sup>b</sup> Ref. 18. Underlined values were previously assigned to charge transfers; italicized values were assigned to d-d transitions.

#### 7.4. Discussion

Tetrahedral geometry is rare for cobalt(III) and, to our knowledge, has been observed in mononuclear small molecules only for [Co(nor)<sub>4</sub>]<sup>-</sup> and a handful of cobalt(III) imido complexes to date.<sup>10-14,16-17,28</sup> The rarity of cobalt(III) in tetrahedral environments and the unusual geome-

tries of the metal centers in  $[\text{Co}(\text{TC-5,5})]^+$  and  $[\text{Co}(\text{TC-6,6})]^+$  raised the possibility that oxidation of the parent cobalt(II) compounds occurred at the ligand rather than the metal center. We therefore prepared and characterized  $[\text{Ga}(\text{TC-5,5})](\text{GaCl}_4)$  and  $[\text{Ga}(\text{TC-6,6})](\text{GaCl}_4)$ , and compared their structural and electrochemical properties with those of the cobalt complexes.

Comparison of analogous bond distances between the  $[\text{Co}(\text{TC-}n,n)]^+$  and  $[\text{Ga}(\text{TC-}n,n)]^+$  complexes provided insight into the electron distribution in the former species (Figs. 7.4 and 7.5).

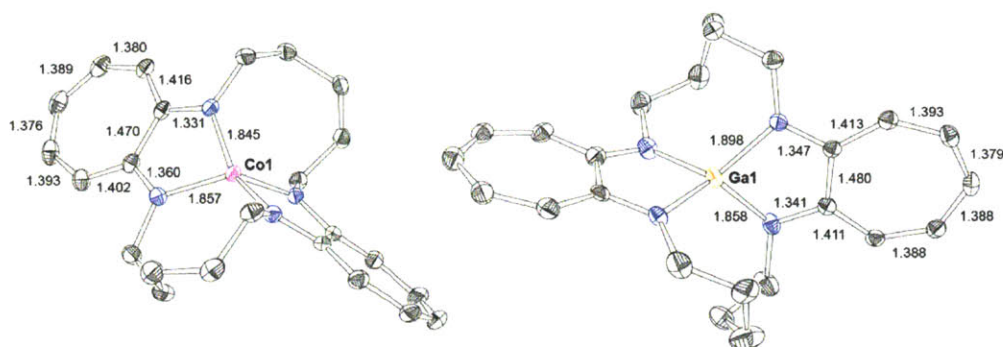


**Figure 7.4.** Comparison of structural parameters for  $[\text{Co}(\text{TC-5,5})](\text{BF}_4)$  (*left*) and  $[\text{Ga}(\text{TC-5,5})](\text{GaCl}_4)$  (*right*). Distances shown are representative of bond distances within the tropocoronand ligand.

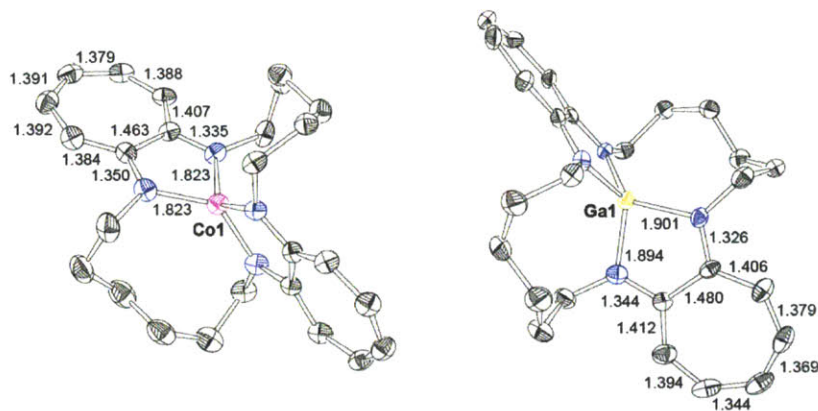


**Figure 7.5.** Comparison of structural parameters for  $[\text{Co}(\text{TC-6,6})](\text{BPh}_4)$  (*left*) and  $[\text{Ga}(\text{TC-6,6})](\text{GaCl}_4)$  (*right*). Distances shown are representative of bond distances within the tropocoronand ligand.

The metal-nitrogen bonds in both cobalt complexes are shorter than in the analogous gallium(III) tropocoronands. The elongation of the Ga-N bond relative to the Co-N bond is a consequence of the larger Shannon-Prewitt radius of gallium(III) compared to cobalt(III). This conclusion is plausible, although Shannon-Prewitt radii are reported for 6-coordinate, but not 4-coordinate, cobalt(III) species.<sup>29</sup> The more covalent character of the cobalt-tropocoronand bonds compared to the gallium-tropocoronand bonds may also contribute to the difference in metal-ligand bond lengths.<sup>30</sup> In a review of the experimental and theoretical properties of transition metal complexes bound to redox non-innocent ligands, Ray, *et al.* note difficulties in using X-ray structural parameters to draw conclusions regarding ligand- versus metal-based oxidation in delocalized systems, where the electron of a ligand radical is shared between two different ligands.<sup>31</sup> The tropocoronand complexes provide such a delocalized system, for if a ligand radical were to form, the free electron would be able to travel between the two aminotroponeiminate rings via the metal center. We are also aware of reports describing non-innocent ligands that undergo negligible structural rearrangement upon changes in redox state.<sup>31-38</sup> We therefore turned to electrochemical methods to confirm that oxidation of [Co(TC-5,5)] and [Co(TC-6,6)] results in cobalt(III) species.

Previously published cyclic voltammetry studies of [Co(TC-5,5)]<sup>9</sup> and [Co(TC-6,6)]<sup>9</sup> were repeated and compared to the results of analogous studies of [Ga(TC-5,5)](GaCl<sub>4</sub>) and [Ga(TC-6,6)](GaCl<sub>4</sub>) (Fig. 7.6). We observed reversible couples at -0.344 V vs. Fc/Fc<sup>+</sup> for [Co(TC-5,5)] and -0.367 V vs. Fc/Fc<sup>+</sup> for [Co(TC-6,6)].

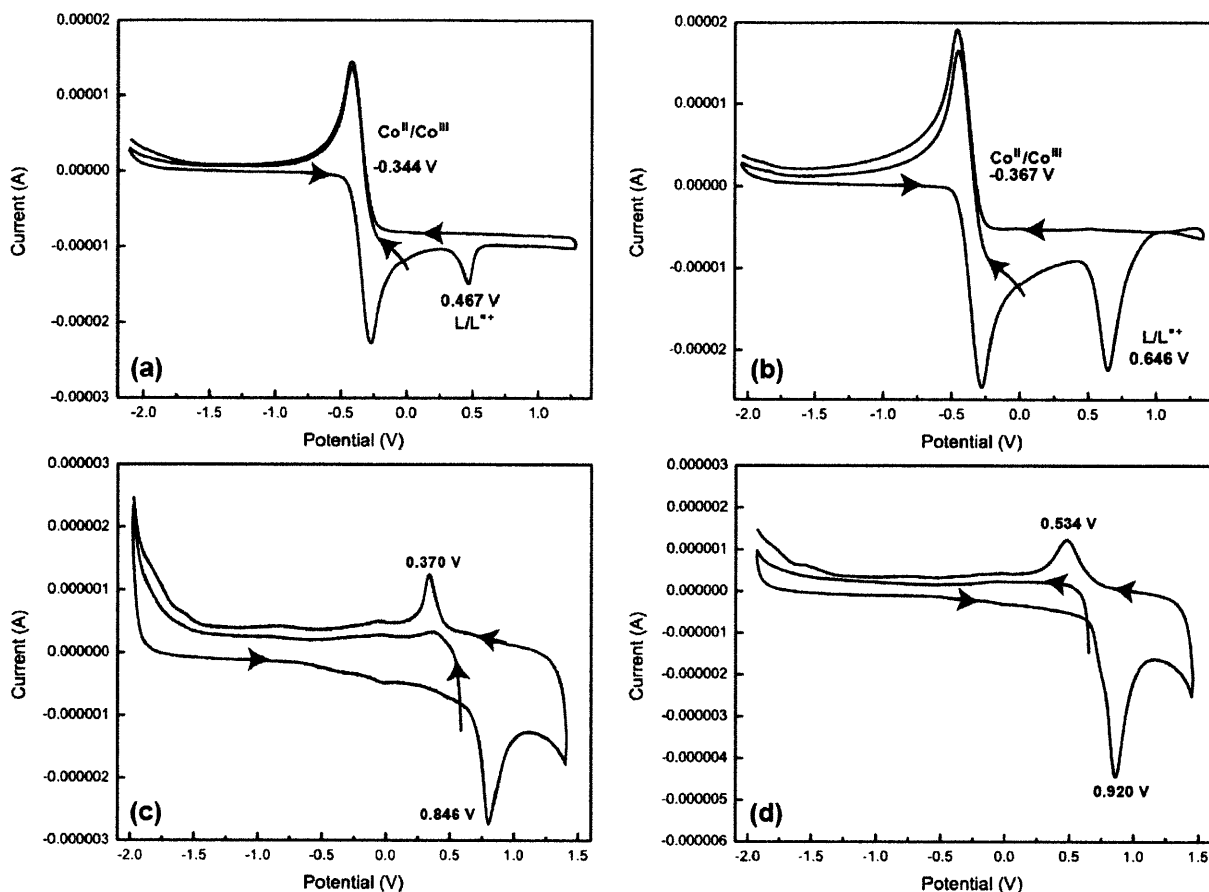


**Figure 7.6.** Cyclic voltammograms of (a) [Co(TC-5,5)]; (b) [Co(TC-6,6)]; (c) [Ga(TC-5,5)](GaCl<sub>4</sub>); and (d) [Ga(TC-6,6)](GaCl<sub>4</sub>). Traces are referenced to Fc/Fc<sup>+</sup>.

We assigned these processes to metal-based redox reactions by comparison with electrochemical studies of [Zn(TC-5,5)] and [Zn(TC-6,6)].<sup>19</sup> The absence of similar reversible processes in the voltammograms of the zinc complexes is consistent with these redox events being metal-based. Additionally, we assign the irreversible features at 0.467 V in the [Co(TC-5,5)] voltammogram and at 0.646 V in the [Co(TC-6,6)] voltammogram to ligand-based oxidations. The cobalt(II)/cobalt(III) couples observed in this work appeared at ~100 mV more negative potential than previously published.<sup>9</sup> The reason for this discrepancy is currently unknown. Cyclic voltammetry of [Ga(TC-5,5)](GaCl<sub>4</sub>) and [Ga(TC-6,6)](GaCl<sub>4</sub>) showed ligand-based oxidations at

0.846 V and 0.920 V vs.  $\text{Fc}/\text{Fc}^+$ , respectively. Metal-based redox processes were not observed. Ligand oxidation was observed at more positive potentials in the gallium(III) complexes than in the analogous zinc and cobalt compounds.<sup>19</sup> The shift to more positive potentials in the gallium(III) tropocoronands relative to the zinc(II) analogues is attributed to the higher oxidation state of the gallium center. Ligand oxidation in the gallium complexes may occur at more positive potentials than in the corresponding cobalt species because the cobalt center may be better able to stabilize the additional charge through covalent metal-ligand interactions than gallium.

Electronic spectral characterization indicates that oxidation of the cobalt(II) parent compounds to  $[\text{Co}(\text{TC-5,5})]^+$  and  $[\text{Co}(\text{TC-6,6})]^+$  produces a bathochromic shift in the reported d-d transitions. As expected, these bands are absent in spectra of the gallium(III) analogues.

The assignment of charge transfer bands, as per the literature report,<sup>18</sup> may need to be reconsidered in light of the gallium(III) optical data. Bands at 392 nm, 405 nm, and 490 nm in the optical spectrum of  $[\text{Co}(\text{TC-5,5})]$ , as well as bands at 387 nm, 413 nm, and 478 nm for  $[\text{Co}(\text{TC-6,6})]$  were previously assigned to charge transfer transitions between the metal and the tropocoronand ligand. Corresponding features at 365 nm, 416 nm, and 433 nm appear in the optical spectrum of  $[\text{Ga}(\text{TC-5,5})]^+$ , and at 363 nm, 410 nm, and 429 nm in the spectrum of  $[\text{Ga}(\text{TC-6,6})]^+$  (Table 7.7, *vide supra*). The presence of correlated optical features in the spectra of cobalt(II) and gallium(III) complexes suggests these features may be due to  $\pi - \pi^*$  transitions of the ligand, because MLCT and LMCT are unavailable to the gallium(III) complexes. Alternately, the transitions may be assigned to ligand – ligand charge transfer. Studies that examine the solvatochromic properties of these complexes would shed light on a possible ligand – ligand charge transfer mechanism.

## 7.5. Summary and Conclusions

Comparison of structural and electrochemical properties of the cobalt and gallium species  $[\text{Co}(\text{TC-5,5})]^+$ ,  $[\text{Co}(\text{TC-6,6})]^+$ ,  $[\text{Ga}(\text{TC-5,5})]^+$ , and  $[\text{Ga}(\text{TC-6,6})]^+$  confirmed the cobalt(III) character of the metal centers in  $[\text{Co}(\text{TC-5,5})](\text{BF}_4)$  and  $[\text{Co}(\text{TC-6,6})](\text{BPh}_4)$ . The characterization of  $[\text{Co}(\text{TC-5,5})](\text{BF}_4)$  and  $[\text{Co}(\text{TC-6,6})](\text{BPh}_4)$  augments the number of cobalt(III) species having the rare pseudotetrahedral geometry.

## 7.6. References

- (1) Imajo, S.; Nakanishi, K.; Roberts, M.; Lippard, S. J.; Nozoe, T. *J. Am. Chem. Soc.* **1983**, *105*, 2071-2073.
- (2) Davis, W. M.; Roberts, M. M.; Zask, A.; Nakanishi, K.; Nozoe, T.; Lippard, S. J. *J. Am. Chem. Soc.* **1985**, *107*, 3864-3870.
- (3) Zask, A.; Gonnella, N.; Nakanishi, K.; Turner, C. J.; Imajo, S.; Nozoe, T. *Inorg. Chem.* **1986**, *25*, 3400-3407.
- (4) Davis, W. M.; Zask, A.; Nakanishi, K.; Lippard, S. J. *Inorg. Chem.* **1985**, *24*, 3737-3743.
- (5) Lippard, S. J.; Berg, J. M. *Principles of Bioinorganic Chemistry*; University Science Books: Mill Valley, CA, 1994.
- (6) Comba, P. *Coord. Chem. Rev.* **2000**, *200-202*, 217-245.
- (7) Holm, R. H.; Kennepohl, P.; Solomon, E. I. *Chem. Rev.* **1996**, *96*, 2239-2314.
- (8) Solomon, E. I.; LaCroix, L. B.; Randall, D. W. *Pure Appl. Chem.* **1998**, *70*, 799-808.
- (9) Doerrer, L. H.; Bautista, M. T.; Lippard, S. J. *Inorg. Chem.* **1997**, *36*, 3578-3579.
- (10) Cowley, R. E.; Bontchev, R. P.; Sorrell, J.; Sarracino, O.; Feng, Y.; Wang, H.; Smith, J. M. *J. Am. Chem. Soc.* **2007**, *129*, 2424-2425.
- (11) Hu, X.; Meyer, K. *J. Am. Chem. Soc.* **2004**, *126*, 16322-16323.
- (12) Jenkins, D. M.; Betley, T. A.; Peters, J. C. *J. Am. Chem. Soc.* **2002**, *124*, 11238-11239.
- (13) Mehn, M. P.; Brown, S. D.; Jenkins, D. M.; Peters, J. C.; Que, L. *Inorg. Chem.* **2006**, *45*, 7417-7427.
- (14) Shay, D. T.; Yap, G. P. A.; Zakharov, L. N.; Rheingold, A. L.; Theopold, K. H. *Angew. Chem. Int. Ed.* **2005**, *44*, 1508-1510.
- (15) Greenwood, N. N.; Earnshaw, A. *Chemistry of the Elements*; Pergamon Press Ltd.: Oxford, England, 1984.
- (16) Byrne, E. K.; Theopold, K. H. *J. Am. Chem. Soc.* **1987**, *109*, 1282-1283.
- (17) Byrne, E. K.; Theopold, K. H. *J. Am. Chem. Soc.* **1989**, *111*, 3887-3896.
- (18) Jaynes, B. S.; Doerrer, L. H.; Liu, S.; Lippard, S. J. *Inorg. Chem.* **1995**, *34*, 5735-5744.
- (19) Doerrer, L. H.; Lippard, S. J. *Inorg. Chem.* **1997**, *36*, 2554-2563.



- (20) Calderazzo, F.; Pampaloni, G.; Rocchi, L.; Englert, U. *Organometallics* **1994**, *13*, 2592-2601.
- (21) Piglosiewicz, I. M.; Beckhaus, R.; Wittstock, G.; Saak, W.; Haase, D. *Inorg. Chem.* **2007**, *46*, 7610-7620.
- (22) APEX2, 4.0. Bruker AXS, Inc.: Madison, WI, 2008.
- (23) Sheldrick, G. M. *SADABS: Area-Detector Absorption Correction*, University of Göttingen: Göttingen, Germany, 2001.
- (24) Sheldrick, G. *Acta Crystallogr. Sect. A: Found. Crystallogr.* **2008**, *64*, 112-122.
- (25) Speck, A. L. *PLATON, A Multipurpose Crystallographic Tool*, Utrecht University: Utrecht, The Netherlands, 2001.
- (26) van der Sluis, P.; Spek, A. L. *Acta Crystallogr. Sect. A: Found. Crystallogr.* **1990**, *A46*, 194-201.
- (27) Burnett, M. N.; Johnson, C. K. *ORTEP-III: Oak Ridge Thermal Ellipsoid Plot Program for Crystal Structure Illustrations*, Oak Ridge National Laboratory Report ORNL-6895: 1996.
- (28) Wasbotten, I. H.; Ghosh, A. *Inorg. Chem.* **2007**, *46*, 7890-7898.
- (29) Shannon, R. *Acta Crystallogr. Sect. A: Found. Crystallogr.* **1976**, *32*, 751-767.
- (30) Miessler, G. L.; Tarr, D. A. *Inorganic Chemistry*; 3rd ed.; Prentice Hall, 2003.
- (31) Ray, K.; Petrenko, T.; Wieghardt, K.; Neese, F. *Dalton Trans.* **2007**, 1552-1566.
- (32) Bill, E.; Bothe, E.; Chaudhuri, P.; Chlopek, K.; Herebian, D.; Kokatam, S.; Ray, K.; Weyhermüller, T.; Neese, F.; Wieghardt, K. *Chemistry – A European Journal* **2005**, *11*, 204-224.
- (33) Kapre, R.; Ray, K.; Sylvestre, I.; Weyhermüller, T.; DeBeer George, S.; Neese, F.; Wieghardt, K. *Inorg. Chem.* **2006**, *45*, 3499-3509.
- (34) Petrenko, T.; Ray, K.; Wieghardt, K. E.; Neese, F. *J. Am. Chem. Soc.* **2006**, *128*, 4422-4436.
- (35) Ray, K.; Begum, A.; Weyhermüller, T.; Piligkos, S.; van Slageren, J.; Neese, F.; Wieghardt, K. *J. Am. Chem. Soc.* **2005**, *127*, 4403-4415.
- (36) Ray, K.; Bill, E.; Weyhermüller, T.; Wieghardt, K. *J. Am. Chem. Soc.* **2005**, *127*, 5641-5654.
- (37) Ray, K.; Weyhermüller, T.; Goossens, A.; Crajé, M. W. J.; Wieghardt, K. *Inorg. Chem.* **2003**, *42*, 4082-4087.
- (38) Ray, K.; Weyhermüller, T.; Neese, F.; Wieghardt, K. *Inorg. Chem.* **2005**, *44*, 5345-5360.

### **Biographical Note**

The author was born on February 15, 1985, in Gatchina, Russia, to Raisa Pavlyuchkova and Michael Kozhukh. She immigrated to the United States with her family and grew up in Ohio, Florida, and California. Julia graduated from Palo Alto Senior High School in 2003, and pursued her undergraduate degree at the University of California, Berkeley. At Berkeley the author worked in Professor David Schaffer's lab studying the effect of microenvironment on neural stem cell proliferation and differentiation, and in Professor Kenneth Raymond's group, tuning ligands for gadolinium(III) contrast agents for MRI. The author graduated from Berkeley with a B.S. in Chemistry in 2007, and commenced graduate studies in Professor Stephen Lippard's laboratory at MIT, where she studied the nitric oxide reactivity of bio-inspired zinc and cobalt complexes. After completing her graduate studies, the author will pursue a career in industry with Dow Chemical Company in Marlborough, MA.

## Curriculum Vitae

### Education

**Massachusetts Institute of Technology**, Cambridge, MA June 2012

#### Ph.D. Inorganic Chemistry

Thesis Topic: Nitric Oxide Reactions of Bio-Inspired Zinc and Cobalt Complexes

Thesis Advisor: Professor Stephen J. Lippard

**University of California, Berkeley**, Berkeley, CA May 2007

#### B.S. Chemistry

### Publications

**Kozhukh, J.**; Lippard, S.J. Zinc Thiolate Reactivity toward Nitrogen Oxides: Insights into the Interaction of  $Zn^{2+}$  with S-Nitrosothiols and Implications for Nitric Oxide Synthase. *Inorg. Chem.* Submitted.

Rosenthal, J.; Nepomnyashchii, A.B.; **Kozhukh, J.**; Bard A.J.; Lippard, S.J. Synthesis, Photophysics, Electrochemistry, and Electrogenerated Chemiluminescence of a Homologous Set of BODIPY-Appended Bipyridine Derivatives. *J. Phys. Chem. C* **2011** 115(36), 17993 – 18001.

Werner, E.J.; **Kozhukh, J.**; Botta, M.; Moore, E.G.; Avedano, S.; Aime, S.; Raymond, K.N. 1,2-Hydroxypyridonate/Terephthalamide Complexes of Gadolinium(III): Synthesis, Stability, Relaxivity, and Water Exchange Properties. *Inorg. Chem.* **2009** 48(1), 277 – 286.

Saha, K.; Irwin, E.F.; **Kozhukh, J.**; Schaffer, D.V.; K.E. Healy. Biomimetic Interfacial Interpenetrating Polymer Networks Control Neural Stem Cell Behavior. *J. Biomed. Mater. Res., Part A* **2007** 81A(1), 240 – 249.

### Presentations

**Kozhukh, J.** Insights into the Interaction of Zinc and Cobalt Coordination Compounds with Reactive Nitrogen Species. MIT Department of Chemistry Inorganic Seminar Series; Cambridge, MA; January 26, 2011.

**Kozhukh, J.**, Lippard, S.J. Insights into the Interaction of Thiolate-Bound  $Zn^{2+}$  with Nitric Oxide and S-nitrosothiols. 240<sup>th</sup> American Chemical Society National Meeting, Boston, MA; August 22 –26, 2010; INOR-16.

**Awards**

Lorry I. Lokey Supporting Foundation Scholarship (2005, 2006)

Merck Undergraduate Summer Research Award (2005)

Stanley and Alice Thompson Summer Research Award (2004)

Gill Foundation of Texas Scholarship (2003-6)

California Alumni Association Scholarship (2003)

American Association of University Women Education and Equity Award in Mathematics (2003)